THE SEMICLASSICAL FEW-BODY PROBLEM

by

JAMAL SAKHR

A Thesis
Submitted to the School of Graduate Studies
in Partial Fulfilment of the Requirements
for the Degree
Doctor of Philosophy

McMaster University

THE SEMICLASSICAL FEW-BODY PROBLEM

DOCTOR OF PHILOSOPHY (2003)
(Physics)

McMaster University
Hamilton, Ontario

TITLE: The Semiclassical Few-Body Problem

AUTHOR: Jamal Sakhr, B.Sc. (UWO), M.Sc. (McMaster)

SUPERVISOR: Professor Emeritus Rajat K. Bhaduri

NUMBER OF PAGES: xv, 168

for dad

Abstract

The few-body problem has not been studied in a general context from the point of view of semiclassical periodic orbit theory. The purpose of this thesis is to give a periodic orbit analysis of the quantum mechanical few-body problem. In particular, the goal is to study two important special cases: noninteracting and weakly-interacting few-body systems. The standard Gutzwiller theory does not apply to the case of noninteracting many-body systems since the single-particle energies are conserved causing the periodic orbits to occur in continuous families in phase space. The unsymmetrized few-body problem is analyzed using the formalism of Creagh and Littlejohn [33], who have studied semiclassical dynamics in the presence of continuous symmetries. The symmetrized few-body problem further requires using the formalism of Robbins [30], and it is shown how the various exchange terms of symmetrized densities of states can be understood in terms of pseudoperiodic orbits. Numerical studies of two- and three-particle systems in a fully chaotic cardioid billiard are used throughout to illustrate and test the results of the theory.

For weak interactions, the Gutzwiller theory also fails. Although the continuous families are destroyed, the periodic orbits are not sufficiently isolated for the standard theory to apply. The interaction can be thought of as a symmetry-breaking perturbation, and then it is possible to apply the results of semiclassical perturbation theory as developed by Creagh [38]. The periodic orbit structure is affected by the symmetry breaking, and this can be understood through asymptotic analysis. An approximate quantization of a two-body nonscaling nonintegrable system is achieved, although explicit quantization of nonintegrable systems is generally not possible. Issues related to the convergence of periodic orbit expansions arise in several places. The convergence of a two-particle system in a disk billiard is explored using an amplitude ordering of the sum. Problems related to truncation and ordering are further explored using two other expansions from number theory.

Acknowledgements

The research problem studied in this thesis was inspired by Niall Whelan. I began working on my Master's research project under his supervision in the Summer of 1998. Unfortunately, he left McMaster at about the same time I was starting my doctoral studies in the Fall of 2000. Nevertheless, he taught me a lot before he left. He also provided me with the conceptual framework from which to begin working on the problem. We have continued to have occasional correspondence through email, and I would like to acknowledge him for taking the time to give succinct comments to questions I had about various aspects of semiclassics. He also worked out the calculation given in Appendix B.4 of the thesis.

I wish to thank my supervisor Rajat Bhaduri for useful physics discussions throughout my graduate studies. But, I would also want to thank him for much more...for supporting me financially during the course of my studies, for granting me the independence to work on this project (although it came with much responsibility), for helping me prepare for the comprehensive examination, for teaching me QED, ... etc. He is a physicist's physicist.

Randy Dumont should also be acknowledged for useful discussions and for providing the quantum spectrum used for numerical comparisons in Chapter 5. Finally, I would like to thank Donald Sprung (one of my thesis readers) for diligently reading my thesis, detecting typographical errors, and providing me with a valuable list of comments, which I used to clarify several points in the thesis.

Preface

This thesis is essentially one long research paper. As such, it conforms to a style typical of research papers in physics journals. It is assumed the reader has some background in semiclassics. Therefore, I have included very little introductory/background material. Some readers may think this is inappropriate for a thesis, but I feel that the addition of such material would be a redundant effort since there are now good books available on the subject. For example, the interested reader may consult the excellent monograph/textbook *Semiclassical Physics* by M. Brack and R. K. Bhaduri (Ref. [7]).

Neither have I included lengthy algebraic derivations. Such details are uninteresting to the general reader. As a result, there is a considerable amount of algebra "between the lines". For example, the discussion in Secs. 4.4.3 - 4.4.5 is very concise, and the serious reader will require pencil and paper to verify many of the statements. I have described the important logical steps so that the reader (if he/she so wishes) could reproduce all of the results with little hardship. Sec. 2.3 is of general interest, and for this reason that section is written in a more tutorial style with detailed explanations.

Furthermore, I have not described the numerical procedures used or included script codes in an appendix since I think this distracts from communicating the most important aspect (i.e. the physics). Much information on the classical, semiclassical, and quantum mechanics of the two-dimensional disk and cardioid billiards can be found in my M.Sc. thesis (Ref. [93]). Details on computing the monodromy matrix and Maslov indices for one-particle orbits in the full and fundamental domains of the cardioid billiard can also be found there.

In several places, I refer to a previously published paper (Ref. [35]), which I have not included here since this research was mostly completed for the M.Sc. degree. Much of the material in Chapters 2 - 4 is already published [Phys. Rev. A **64**, 044102 (2001); Phys. Rev. E **67**, 066213 (2003); Phys. Rev. E **68**, 026206 (2003).]. Nevertheless, the writing of this thesis gave me the opportunity to revise some of the exposition that I thought needed improvement, and so in some sense what is given here is more definitive than what has appeared in the journals.

Some of the notation used in the published papers have been changed for the writing of this thesis. I would like to point out these notational changes here:

Description	Chapter	Symbol in Paper	Symbol in Thesis
Real part of a Riemann Zero	2	γ	η
Number of Evolving Particles	3	M	D
Cycle	4	k	$\Bbbk$
Number of Evolving Cycles	4	e	$n_{\mathfrak{e}}$
Number of Stationary Cycles	4	s	$n_{\mathfrak{s}}$
Number of Cycles in τ	4	m_τ	n_τ
Number of 2-Particle Exchanges for τ	4	n_τ	s_τ

The terse appendixes contain material of a more technical nature. Appendix A discusses the symmetrization of the average density of states. This is relevant for the numerical work, but not for the main theoretical developments. Appendix B elaborates on some points regarding the monodromy matrix which are only mentioned in the main discussion. I thought these explanations disrupted the continuity of the arguments, and so I opted to defer these to an appendix. Finally, Appendix C on the convolution formalism is complementary to Chapter 3. I included it since I think it is conceptually useful to see how the results of Chapter 3 can be obtained from a very distinct point of view. Originally, I thought the material in Appendix C should be a chapter in itself, but since the discussion is mostly technical, I decided to include it as an appendix. It is not necessary reading to understand the rest of the thesis.

Hamilton, ON
October 2003 J.S.

Contents

List of Figures

List of Tables

Chapter 1

Introduction

Semiclassical theory emerged at the advent of quantum mechanics and has evolved into a powerful tool for performing analytical calculations and for developing our intuition on new problems. The most important energy domain[1] semiclassical theory is periodic orbit theory (POT), which extracts spectral information from knowledge of the classical periodic orbits. In the semiclassical limit of quantum mechanics, the periodic orbits of the corresponding classical system play a special role in determining the spectral properties of the quantum system. This fundamental fact has been a dominant theme in modern semiclassical mechanics ("semiclassics"), and was pioneered by Gutzwiller [2], Balian and Bloch [3], Strutinsky and Magner [4], and Berry and Tabor [5]. One of the central results that emerged from these pioneering works is the representation of the density of states in terms of classical periodic orbits. Such representations are now referred to as trace formulas (see Sec. 1.2.1 for a brief review). Semiclassical analysis based on the use of trace formulas is now common in many areas of physics [6, 7, 8]. Besides providing a natural framework for studying the quantum manifestations of classical chaos [6, 9, 10], such analysis has been used in the study of nuclei [4, 11, 12], atoms [13, 14], metal clusters [15, 16], molecules [17], chemical systems [18], spins [19], Casimir effects [20], and tunneling [21]. Trace formulas have also become a prominent analytical tool in the study of mesoscopic systems [22]. New directions continue to be explored [23].

[1] In this thesis, all semiclassical formulations are in the energy domain rather than the time domain. In the energy domain, the most important quantity is the energy Green function, whereas in the time domain, the van Vleck Green function (i.e. the semiclassical time Green function obtained from the semiclassical time propagator) is the fundamental quantity. The latter can be evaluated and is often quite accurate (see, for example, Refs. [1]). The time propagator and the energy Green function are related by a one-sided (i.e. $t \geq 0$) Fourier transformation.

1.1 The Semiclassical Few- and Many-Body Problem

Despite the vast utility of trace formulas, their general use in few- or many-body systems has received almost no attention[2]. Although trace formulas are applicable to interacting many-body systems, more effort has gone into developing semiclassical descriptions of single-particle dynamics in an appropriate mean field. (One impressive exception is the application of the Gutzwiller trace formula to the study of two-electron atoms and related three-body systems [26, 27].) The main difficulty of applying the theory is that periodic orbits must be found for the interacting many-body system. One approach to this problem was proposed in Ref. [28], which develops a particle number expansion of the trace formula.

The few-body problem has not been studied from the point of view of periodic orbit theory. The purpose of this thesis is to give a periodic orbit analysis of the quantum mechanical few-body problem. In particular, the goal is to study two important special cases: noninteracting and weakly-interacting few-body systems. At first, these two situations might seem trivial or uninteresting. However, as discussed below and examined in the following chapters, in both cases, the standard Gutzwiller theory fails. Therefore, a semiclassical framework must be developed for these two cases before a more ambitious theory can be developed that can accurately describe the entire range of behaviors between the noninteracting and strongly-interacting limits.

Noninteracting systems cannot be described by the standard Gutzwiller theory, that is, there is no Gutzwiller trace formula for a system of noninteracting particles[3]. The Gutzwiller theory is, in principle, applicable to an interacting many-body system (albeit impossible to apply in practice). For this reason, it is easy to overlook a subtle point to be mentioned shortly and naively conclude that the Gutzwiller formula is applicable in all cases. The subtle point is that all one-particle energies are constants of motion, and so noninteracting systems possess continuous (time-translational) symmetries. (Discrete symmetries in semiclassical trace formulas are discussed in Refs. [29, 30, 31, 32], and continuous symmetries in Refs. [4, 33, 34].) These symmetries have a profound consequence;

[2]The semiclassical mechanics of many-body systems has been studied in other contexts; for example, the work on semiclassical response functions for many-body systems [24, 25].

[3]This is not completely true. As explained in Chapter 3, the Gutzwiller formula can be used to obtain *one* of the periodic orbit contributions to the semiclassical many-body density of states. However, this contribution is (in general) not significant since it is a high-order correction. The Gutzwiller theory does apply to one nongeneric integrable noninteracting many-body system: nonidentical particles with incommensurate masses in a harmonic oscillator potential.

we cannot simply apply the Gutzwiller trace formula since the presence of continuous symmetries implies the periodic orbits of the full phase space are not isolated, but rather occur in continuous families. Fortunately, Creagh and Littlejohn [33] have developed a general formalism for systems that possess continuous Abelian symmetries. This general theory is applicable to the specific problem of interest here, namely, the noninteracting many-body problem. In Chapter 3, the formalism of Ref. [33] is used to derive semiclassical many-body trace formulas (analogous to Gutzwiller) that are applicable to noninteracting particles in a chaotic potential.

The trace formulas derived in Chapter 3 can also be obtained from a different point of view. If the particles are noninteracting, the many-body density of states can be written as a multiple convolution of the one-body density of states. If each one-body density is decomposed as in Eq. (1.1), the total density of states is a sum of mixed or unmixed multiple convolutions of smooth and oscillating one-body densities of states. Each of the various convolution integrals can be evaluated using asymptotics to obtain the various periodic orbit contributions. This technique was introduced for two-particle systems in Ref. [35], and it is extended to three-particle systems in Appendix C. However, the formalism developed in Chapter 3 (which uses the full classical phase space) is more fundamental and ultimately more useful than the convolution formalism (which uses the individual phase spaces of each particle). Nevertheless, it is still conceptually useful to see how the same structure emerges from these two distinct points of view.

The semiclassical many-body problem can be understood as a special case of the more general class of problems for which there is a breaking of a continuous symmetry caused by the variation of a continuous parameter in the full Hamiltonian [36, 37, 38, 39, 40]. If there are no interactions, each of the particle energies is separately conserved. Thus, as mentioned above, there are (continuous) time-translational symmetries and consequently the periodic orbits of the classical system occur in degenerate families that exist on higher-dimensional tori in phase space. This is discussed in detail in Chapter 3. Interactions destroy the continuous symmetry and therefore break up the periodic orbit families into a discrete set of isolated orbits. This transition happens discontinuously as soon as the interaction is turned on. By contrast, the actual quantum behavior is smooth and continuous. Therefore, we seek a semiclassical picture which captures this smooth behavior. We can use the standard Gutzwiller theory *if the interaction is sufficiently strong.* For weak interactions, the Gutzwiller theory fails and a different analysis is required. In the latter case, we

can think of the interaction as a symmetry-breaking perturbation and apply the ideas of Ref. [38], which describe the effect of symmetry-breaking on trace formulas using classical perturbation theory (see Sec. 1.2.2 for a brief review). This procedure is explored in Chapter 5. The essential idea is that a calculation to first order in perturbation theory of the actions should be adequate to describe the regime where the periodic orbits are not isolated enough so that the standard Gutzwiller trace formula applies. It is important to emphasize here that this analysis makes use of the full Hamiltonian and does not imply the use of any mean-field approximations.

If the interactions are sufficiently weak, the only modification to the noninteracting many-body trace formulas (which are derived in Chapter 3) occur in the amplitude which gets modulated by a factor which is (in principle) straightforward to calculate. If the interactions are sufficiently strong, we should use the Gutzwiller formula for isolated orbits, and for interaction strengths in the intermediate regime, we expect the perturbative analysis mentioned above and the Gutzwiller theory to yield consistent results. It is also of fundamental interest to develop uniform semiclassical calculations to continuously interpolate between the noninteracting and strongly-interacting limits. In this thesis, uniform calculations for the transition from noninteracting $\rightarrow$ strongly-interacting identical particles are not considered; the focus is rather on how the first-order perturbation theory can be used to study the initial part of the transition when the interaction is first turned on. This regime is physically relevant; for example, it applies to a high-density two-dimensional electron gas in which the particles interact weakly through the short-range screened Coulomb interaction.

Most realistic few- or many-body quantum systems consist of identical particles. The role of symmetries and the influence of particle symmetry on trace formulas is an important problem in its own right and is an essential part of any semiclassical many-body theory. In fact, this problem was included in a list of "open challenges" for the future of periodic orbit theory first given by P. Cvitanović in Ref. [41]. The trace formula for the special case of interacting fermions in one dimension was briefly considered in Ref. [42]. However, the derivation assumed the periodic orbits to be isolated which (as discussed above) is the case relevant to strongly-interacting identical particles. There is also a brief discussion on noninteracting fermions in which the many-body level density is written as a convolution integral involving one-body level densities. This is similar to what was described above for the total (rather than symmetrized) density of states. Although the convolution

formula in Ref. [42] explicitly takes into account the symmetry operations of the permutation group, there are no explicit trace formulas given for the symmetrized densities of states.

The convolution method for noninteracting systems is purely formal. A comprehensive theory of the semiclassical many-body problem requires an analysis in the full phase space. This is necessary to understand weak interactions and to then develop uniform approximations for the symmetrized many-body problem. So it is crucial to first understand the symmetry decomposition of the noninteracting problem from an analysis in the full phase space. The point of view adopted here is that particle symmetry is a discrete symmetry, and so the ideas of Robbins [30] and Lauritzen [31] (who have studied the effect of discrete symmetries in semiclassics) can be exploited to derive trace formulas for the various exchange terms of the symmetrized densities of states. Each trace formula will involve a sum over pseudoperiodic orbits, which are structures in phase space that are periodic under time evolution and the symmetry operations of the group responsible for the discrete symmetry. For systems of identical particles, these operations are the particle exchange operations of the permutation group. The symmetry decomposition is further complicated by the fact that there are also continuous symmetries for noninteracting systems, and so the pseudo-orbits themselves will also occur in families. Thus, the mixture of continuous time-translational symmetries and the discrete particle symmetry requires a nontrivial revision of the Weidenmüller theory for identical particles [42]. This is studied in Chapter 4.

Naturally, the next step would be to examine the symmetry decomposition in the presence of weak interactions. This is not done in this thesis, but is a problem for future study. The idea is that the interaction breaks the continuous symmetries (at least some of them), but leaves the discrete symmetry intact. In phase space, this would imply that the families of pseudo-orbits are broken up into discrete sets of isolated pseudo-orbits. Thus, in principle, the formulas obtained in Chapter 4 for the noninteracting system would still apply, but with appropriate amplitude modulations. (However, there are complications that require further study.) For strongly-interacting identical particles, a generalization of the Weidenmüller formalism [42] would apply, and in the intermediate regime, the analysis of the pseudo-orbits under perturbation and a generalized Weidenmüller formalism should give consistent results.

To conclude this introduction to the semiclassical few- and many-body problem, it is relevant to make some comments regarding the enumeration, truncation, and order-

ing of periodic orbit contributions, and the overall convergence of few-body trace formulas. Generally speaking, the extraction of individual eigenvalues for a generic system is an unsettled problem in semiclassics, and we can only hope to acquire low-resolution spectra from classical information alone. However, the situation is different for integrable systems. The coarse-grained level density of a one-body integrable system is relatively simple to reproduce numerically from periodic orbit quantization. The quantization of a few-body system, on the other hand, is a computationally intensive task due to the enormous proliferation of periodic orbits with increasing action. Furthermore, a noninteracting few-body integrable system will have many near degeneracies even at low energies. Resolving such near-degenerate levels is a precision test of any few-body trace formula. These issues are explored in the first part of Chapter 2 using the example of a two-dimensional disk billiard. This example is sufficient to illustrate the general problem; even if a multibody trace formula is available, the convergence of standard Fourier truncation will be inadequate, and if the interest is in full quantization, then alternative truncation strategies must be explored. In the second part of Chapter 2, there is a brief digression unrelated to the few-body problem, but nevertheless related to issues associated with the truncation of Fourier-type sums. The main discussion begins in Chapter 3.

1.2 Review of Semiclassical Formulations

1.2.1 Semiclassical density of states

The quantum density of states can be exactly decomposed into smooth and oscillatory components, and in particular, for a one-particle density,

$$\rho_1(\varepsilon) = \bar{\rho}_1(\varepsilon) + \tilde{\rho}_1(\varepsilon), \tag{1.1}$$

where $\bar{\rho}$ and $\tilde{\rho}$ denote the smooth and oscillating components, respectively. There is an extensive literature on this decomposition [7]. In this thesis, the conventional point of view that it is sufficient to use the first few terms of each component is adopted. The subtle issues related to the asymptotic nature of this decomposition are considered elsewhere (see, for example, Refs. [43, 44, 45]). For analytic potentials in d dimensions, the leading-order term of the smooth density of states (i.e. the Thomas-Fermi term) is

$$\bar{\rho}_1(\varepsilon) \approx \frac{1}{(2\pi\hbar)^d} \int \delta\left[\varepsilon - h(\mathbf{z})\right] \mathrm{d}\mathbf{z}, \tag{1.2}$$

where $\mathbf{z}$ collectively denotes the $2d$ classical phase space coordinates, and $h(\mathbf{z})$ is the classical Hamiltonian (for an exception to this general result, see Refs. [46, 47]). There are corrections to Eq. (1.2) involving derivatives of the δ-function in the integrand. The first correction is $O(\hbar^2)$. For a two-dimensional billiard, the smooth component is given by the Weyl expansion [48]

$$\bar{\rho}_1(\varepsilon) = \frac{\alpha\mathcal{A}}{4\pi} \pm \frac{\sqrt{\alpha}\mathcal{L}}{8\pi\sqrt{\varepsilon}} + \mathcal{K}\delta(\varepsilon) + \ldots, \tag{1.3}$$

where $\alpha = 2m/\hbar^2$, $\mathcal{A}$ and $\mathcal{L}$ refer to the area and perimeter, respectively, and the $\pm$ refers to Neumann and Dirichlet boundary conditions, respectively. The third term

$$\mathcal{K} = \frac{1}{12\pi}\oint \mathcal{C}(l)\mathrm{d}l + \frac{1}{24\pi}\sum_j \frac{\pi^2 - \theta_j^2}{\theta_j}, \tag{1.4}$$

is the average curvature integrated along the boundary with corrections due to corners that have angles θ_j. It does not actually contribute to the density of states, but rather to its first integral. (The curvature term will be included for various calculations in Chapters 3 and 4.) There are also corrections involving powers and derivatives of the curvature (see Refs. [43, 44]). Similar results hold for higher-dimensional billiards (see Ref. [7]).

The leading-order term of the oscillating component can be written as [2]

$$\tilde{\rho}_1(\varepsilon) \approx -\frac{1}{\pi}\mathrm{Im}\left\{\sum_\gamma A_\gamma(\varepsilon)\exp\left[i\left(\frac{S_\gamma(\varepsilon)}{\hbar} - \sigma_\gamma\frac{\pi}{2}\right)\right]\right\}, \tag{1.5}$$

where γ labels the isolated periodic orbits of the system, S_γ is the classical action integral along the orbit, σ_γ is a topological index [49] counting the caustics in phase space encountered by the orbit, and the amplitude of the periodic orbit

$$A_\gamma(\varepsilon) = \frac{1}{i\hbar}\frac{T_\gamma^0(\varepsilon)}{\sqrt{\left|\det\left(\tilde{M}_\gamma - I\right)\right|}}, \tag{1.6}$$

where T_γ^0 is the primitive period of the orbit, and $\tilde{M}_\gamma$ is the $2(d-1)\times 2(d-1)$ symplectic stability matrix on any Poincaré section to which the orbit is transverse. The eigenvalues of $\tilde{M}_\gamma$ give the stability exponents of the orbit. Higher-order $\hbar$ corrections were first considered in Refs. [50] and recently studied in Ref. [51] (see also Refs. [52]). Equation (1.5) [with Eq. (1.6)] is referred to as the Gutzwiller trace formula. It is often stated in the literature that the Thomas-Fermi term gives the contribution from "zero-period" orbits only, whereas the Gutzwiller formula gives only the contribution from "positive period" ($T > 0$) orbits.

Since Eq. (1.5) is the density of states in the $S_\gamma(\varepsilon)/\hbar \gg 1$ limit of Feynman quantum mechanics, the Gutzwiller trace formula together with the leading terms of the smooth density of states is usually referred to as the semiclassical density of states.

The Berry-Tabor trace formula [5] (which has the same form as Eq. (1.5)) is the analogous trace formula for integrable systems that gives the semiclassical density of states as a sum over rational tori (which are covered by $(d-1)$-dimensional families of periodic orbits). There is an equivalence between quantization using the Berry-Tabor formula and the procedure known as EBK quantization in which the semiclassical energies are obtained from quantization of the action variables associated with invariant tori [7]. (For chaotic systems, invariant tori do not exist, and EBK quantization is no longer applicable.)

The trace formula for the generic case of mixed classical dynamics with both regular and chaotic regions in phase space is not yet well understood. A classical bifurcation occurs when the eigenvalues of the monodromy matrix pass through unity, and this is associated with a splitting or merging of two or more periodic orbits. For values of the classical parameters close to the bifurcation point, the periodic orbits are not well separated in phase space so that the stationary phase approximations used in the derivation of the Gutzwiller trace formula break down [36]. So, it is necessary to go beyond the stationary phase approximation and develop uniform approximations that give finite amplitudes near classical bifurcation points. Efforts along these lines can be found in Refs. [53].

POT has been widely applied to scaling systems where the classical phase space structure is the same for all values of energy. Some examples include billiard systems [54], the hydrogen atom in a strong magnetic field [13], and quartic oscillators [55]. In these studies, a common type of analysis called "inverse PO spectroscopy" is used to circumvent convergence problems. (It is also referred to as "inverse POT".) The procedure involves computing the Fourier transform of the quantum spectrum, which gives peaks at the periods or actions of the periodic orbits, and comparing this with the results of semiclassical calculations. The utility of this type of analysis is that information about classical phase space structures can be extracted directly from the quantum eigenvalues, and so the fundamental convergence problems associated with the forward procedure (i.e. using Eq. (1.5) to extract the quantum energies) do not arise. The reverse procedure has become an industry in atomic and molecular physics and is often referred to as "PO spectroscopy" or "scaled-energy spectroscopy" [56], and it is now well-established in investigations of atoms in external fields [57]. Application of POT to nonscaling systems is much harder. Low-

resolution analysis of the Nelson potential [58] and the Hénon-Heiles potential [59] are two important examples. (Note that POT can be readily applied to analyze coarse-grained spectra in which individual levels are not resolved.) The inverse procedure mentioned above for scaling systems does not apply to nonscaling systems. However, a technique based on the Gabor transform has been studied [60], which uses small energy windows instead of taking the Fourier transform of the entire quantum spectrum.

1.2.2 Perturbative analysis of symmetry breaking

As briefly discussed above, the semiclassical many-body problem is a special case of the more general class of problems for which there is continuous symmetry breaking caused by the variation of a continuous parameter in the full Hamiltonian. In this section, we review the idea of continuous symmetry breaking and its description using perturbation theory. Suppose there is a system described by a Hamiltonian H_0 that possesses a certain type of continuous symmetry. As a consequence of this symmetry, the periodic orbits of the classical system occur in degenerate families that exist on higher-dimensional tori in phase space. (The dimensionality of these orbit families will be the same as the number of degrees of freedom if H_0 is integrable.) The system is then perturbed by introducing a symmetry-breaking term:

$$H(\mathbf{z}) = H_0(\mathbf{z}) + \epsilon H_{\rm sb}(\mathbf{z}), \tag{1.7}$$

where ϵ is a (dimensionless) continuous parameter. Consequently, all periodic orbit families are broken up into isolated orbits[4]. The Hamiltonian system (1.7) will generally have mixed dynamics, and if $H_{\rm sb}$ breaks all the continuous symmetries of H_0, the system could become chaotic for large values of ϵ. In this regime, the standard Gutzwiller theory can be applied. For small values of ϵ, the Gutzwiller amplitudes become invalid and actually diverge in the limit $\epsilon \to 0$. Although the families are destroyed for $\epsilon \neq 0$, the periodic orbits are not sufficiently isolated since, for small values of ϵ, their perturbed actions differ by less than $\hbar$, and so the precondition that the orbits are isolated underlying the derivation of the Gutzwiller formula is not fulfilled.

The study of the effects of symmetry-breaking on trace formulas began with the

[4]More generally, higher-dimensional families are broken up into families of lower dimensionality that have a lesser degree of degeneracy than those of H_0. In Chapter 5, we shall consider problems for which the perturbed system is nonintegrable, and furthermore, there are no continuous symmetries present after perturbation.

work of Ozorio de Almeida [36] who considered the perturbation of generically integrable systems, and derived a "uniform approximation" that attempted to smoothly interpolate (divergence-free) between the Berry-Tabor and Gutzwiller limits. A more general approach was developed by Creagh [38] who introduced perturbative trace formulas valid for the breaking of arbitrary continuous symmetries. Classically, the symmetry-breaking transition is discontinuous (it happens as soon as the perturbation is turned on). Families are immediately destroyed, and replaced by isolated orbits. The quantum behavior is rather smooth and continuous, and the description using quantum perturbation theory varies smoothly as a function of the perturbation (symmetry-breaking) parameter. Creagh's approach is motivated by quantum mechanics, and uses a perturbative analysis of the classical dynamics around the periodic orbits (with ϵ as the small parameter). The result is a smooth semiclassical description of the symmetry-breaking transition.

In Chapter 5, the ideas of Ref. [38] will be applied although similar ideas can be found in Refs. [36, 37]. Creagh's approach [38] differs from that of Ozorio de Almeida [36] which uses action-angle variables. However, for integrable systems, the two approaches are equivalent. Creagh's approach concentrates on the symmetry group and regards the constants of motion (the action variables in integrable systems) as a secondary consequence of this symmetry. Creagh's theory is ultimately more useful for the analysis of interactions since it applies to the situation where the unperturbed system is nonintegrable, but possesses continuous symmetries. (This precisely describes noninteracting particles in a chaotic potential.) Such a situation lies outside the domains of both the Berry-Tabor and Gutzwiller formulas. Before summarizing the main results of Creagh's theory, it is useful to first review the case of exact symmetry for which there is no perturbation.

Perfect symmetry ($\epsilon = 0$)

The most straightforward way to derive the trace formula is to start with the semiclassical expansion for the energy Green function $G(\mathbf{q}, \mathbf{q}'; E) = \langle \mathbf{q}| \frac{1}{E-\hat{H}} |\mathbf{q}'\rangle$, and compute its trace $g(E) = \mathrm{Tr}\left(\frac{1}{E-\hat{H}}\right)$ in some convenient representation. (For example, we can compute the trace in the $\mathbf{q}$-representation through $g(E) = \int G(\mathbf{q}, \mathbf{q}; E) \mathrm{d}\mathbf{q}$.) The leading-order term of the semiclassical expansion for $G(\mathbf{q}, \mathbf{q}; E)$ is a sum over orbits with energy E beginning and ending at position $\mathbf{q}$ [2]. An integration over $\mathbf{q}$ using the stationary phase approximation is then performed, and it is found that the stationary phase contributions

arise from orbits that are periodic in phase space. If a continuous symmetry exists (as it does for H_0), the periodic orbits (at a given energy E) occur as continuous families (with a degeneracy f) rather than as isolated trajectories. The integrations transverse to a family can be performed using the stationary phase approximation, but the integrations parallel to the family remain. Thus, the sum over isolated periodic orbits [Eq. (1.5)], which is pertinent in the absence of symmetry, is replaced by a sum over discrete families of periodic orbits. The contribution of a single family Γ to the resolvant (which shall be denoted by $g_\Gamma(E)$) is a $(f+1)$-dimensional integral over the hypersurface formed in configuration space by the family.

At this point, it is necessary to make explicit assumptions about the symmetry. The main assumption relevant to the present discussion is that the generators of the Lie group G associated with the continuous symmetry and the Hamiltonian itself are all linearly independent. It then follows that the degeneracy f of the periodic orbit families is equal to the dimension of the Lie group. The members of each family can thus be transformed into each other by acting on any of them with the group elements $g \in G$, and the properties of the orbits remain invariant under the group operations. Starting with a reference orbit $\gamma_0(t)$, the other orbits in the family can be parametrized by the group elements g: $\gamma_g(t) = g \cdot \gamma_0(t)$. Individual points on the family manifold are parametrized by (t, g), which naturally suggests the $(f+1)$-dimensional measure $\mathrm{d}t\mathrm{d}\mu(g)$ as the integration variables for the integration over the orbit family[5]. The volume element $\mathrm{d}\mu(g)$ is the invariant measure ("Haar measure") of the Lie group. The contribution from a family of orbits Γ is then

$$\tilde{g}_\Gamma(E) = \frac{1}{i\hbar}\frac{1}{(2\pi i\hbar)^{f/2}} \int_\Gamma \left|\mathcal{K}_{\gamma_g(t)}\right|^{-1/2} \exp\left\{ i\left[\frac{S_{\gamma_g(t)}(E)}{\hbar} - \sigma_{\gamma_g(t)}\frac{\pi}{2}\right]\right\} \mathrm{d}t\mathrm{d}\mu(g). \tag{1.8}$$

In the above formula, the integration is over each phase space periodic orbit in the family, as parametrized by the coordinates (t, g). (Recall that the coordinates on the family manifold are (t, g).) The factor $\mathcal{K}$ is a classical invariant of the family (independent of $\hbar$), and determined by a linearization of the dynamics about a typical orbit of the family. More specifically,

$$\mathcal{K}_{\gamma_g(t)} = Q \det \mathcal{W}_{\gamma_g(t)} \det\left(\tilde{M}_{\gamma_g(t)} - I\right), \tag{1.9}$$

where $\tilde{M}$ is a linearization of the dynamics on a symmetry-reduced surface of section (the symbol $\tilde{}$ on M is to emphasize that all extra degrees of freedom due to symmetry have been

[5] In conservative Hamiltonian systems, the time t is the parameter associated with the generator H of time translation, and is present even in the absence of symmetry.

removed), Q is a Jacobian factor independent of dynamics ($Q = 1$ for Abelian symmetries), and the symmetric matrix $\mathcal{W}$ ("the anholonomy term") depends on the extent to which orbits that are periodic in the symmetry-reduced dynamics fail to be periodic in the full phase space. (See Refs. [33, 34] for a complete discussion. A more detailed description of $\mathcal{K}$ is given in Chapter 3 in the specific context of the few-body problem.) Finally, the phase terms $S(E)$ and σ are the action and phase index[6] of the orbits in the family. Note the invariant group measure $\mathrm{d}\mu(g)$ involves a f-dimensional set of group parameters $\boldsymbol{\Theta} = (\Theta_1, \ldots, \Theta_f)$ whose values define the elements of the symmetry group[7].

Broken symmetry ($\epsilon \neq 0$)

For small perturbations ($\epsilon \ll 1$), it is justified to use classical perturbation theory to obtain a trace formula with the correct amplitudes for $\epsilon \to 0$. All members of the continuous family of periodic orbits remain *approximately* periodic if the perturbation is weak enough. The basic procedure then is that for a family of unperturbed orbits, we determine the perturbed action after the perturbation is turned on. This is analogous to the treatment of isolated orbits under perturbation [36].

To study the effects of symmetry-breaking perturbations, the main step is to expand the action in the exponent to linear order in the perturbation parameter and assume that all other prefactors retain their unperturbed values. It is shown in Ref. [38] that, to first order in perturbation theory, the action changes by the amount

$$\Delta S_\Gamma(E; g, \epsilon) = -\epsilon \int_{\gamma_g(t)} H_{\mathrm{sb}}(\mathbf{z}(t; g))\mathrm{d}t, \tag{1.10}$$

where the integral is over an unperturbed orbit $\gamma_g(t)$ of the family Γ that is specified by the group element g. (The subscript Γ on the LHS of Eq. (1.10) denotes the fact that this is the action shift of the orbits that belong to Γ.) If the action shift vanishes at first-order, it is necessary to go to higher order in classical perturbation theory [39]. The integral over the group measure results in a multiplicative "modulation factor" in the amplitude of the

[6]The index in Eq. (1.8) is not the same as the index in Eq. (1.5), but unfortunately this notation is standard. The phase in Eq. (1.8) is discussed further in Chapter 3 and in more detail in Ref. [61].

[7]A Lie group is both a group and an analytic manifold. The group parameters are the coordinates for the group manifold.

unperturbed trace formula [38]:

$$\tilde{g}_\Gamma(E;\epsilon) = \frac{1}{i\hbar}\frac{1}{(2\pi i\hbar)^{f/2}}\mathcal{M}_\Gamma\left(\frac{\epsilon}{\hbar},E\right)\int_\Gamma \left|\mathcal{K}_{\gamma_g(t)}\right|^{-1/2}\exp\left\{i\left[\frac{S_{\gamma_g(t)}(E)}{\hbar}-\sigma_{\gamma_g(t)}\frac{\pi}{2}\right]\right\}\mathrm{d}t\mathrm{d}\mu(g), \tag{1.11}$$

where the modulation factor is an average of the action variation over the unperturbed family,

$$\mathcal{M}_\Gamma\left(\frac{\epsilon}{\hbar},E\right) = \frac{1}{\Omega}\int \exp\left[i\frac{\Delta S_\Gamma(E;g,\epsilon)}{\hbar}\right]\mathrm{d}\mu(g), \tag{1.12}$$

and the group volume $\Omega = \int \mathrm{d}\mu(g)$. The resulting expression for the resolvant interpolates between the continuous case and the situation of isolated periodic orbits.

Although this formalism correctly describes the transition from higher to lower symmetry for small to moderate perturbations, it fails for large perturbations, that is, the method does not recover the Gutzwiller amplitudes of the isolated orbits in the symmetry-broken system. (Therefore, it is necessary to replace the formula (1.11) by the Gutzwiller formula when $\epsilon \gg 1$.) However, there is an intermediate regime of perturbation strengths ($\epsilon \gtrsim 1$) for which the perturbed trace formula (1.11) and the Gutzwiller trace formula give essentially the same results. But, in general, it is difficult to predict precisely the range in which both methods agree. The asymptotic behavior of the modulation factor $\mathcal{M}_\Gamma(\epsilon/\hbar, E)$ for $\epsilon \gg 1$ gives information about the isolated orbits created by the symmetry-breaking perturbation. Each critical point of $\mathcal{M}_\Gamma(\epsilon/\hbar, E)$ corresponds to a periodic orbit of the Gutzwiller limit. These critical points are either stationary phase points or endpoints (boundary values) of the integration domain. Although this asymptotic analysis is helpful in finding isolated periodic orbits in nonintegrable systems whose dynamics may be unknown, the resulting amplitudes are quantitatively incorrect in the limit from which they are obtained ($\epsilon \gg 1$).

An approximation that exactly recovers the Gutzwiller trace formula (or its analog in systems where continuous symmetries persist) for large perturbations ($\epsilon \gg 1$), and also yields the correct trace formula for the unperturbed system H_0 as $\epsilon \to 0$ is called a uniform approximation. A uniform approximation for $U(1)$ symmetry breaking in a two-dimensional system is derived in Refs. [37]. This result applies to all systems where resonant tori break into pairs of stable and unstable isolated orbits. No analogous result is known for the breaking of arbitrary symmetries in any dimension. Uniform approximations for $SU(2)$ and $SO(3)$ symmetry breaking are studied in Ref. [40].

Chapter 2

Truncation of the Oscillating Density of States

2.1 Introduction

Trace formulas are Fourier-type expansions of the oscillating density of states expressed in terms of classical periodic orbits. The appeal of using such expansions is that the gross shell structure of many finite systems can be reproduced using only a few of the shortest orbits [7]. Periodic orbit quantization, on the other hand, is generally difficult and many orbits must be included before a good approximation to the exact result is obtained. For this purpose, the convergence of a trace formula is a central issue in semiclassics. In chaotic systems, the Gutzwiller trace formula actually diverges due to an exponential increase in the number of long-range periodic orbits with energy[1]. This problem inspired the development of various resummation methods (for example, see Ref. [62]) which attempt to utilize the fact that the periodic orbits are correlated (although they appear independently in the trace formula). As well, energy-smoothed versions of the trace formula (for example, Refs. [63]) have been devised to provide numerically efficient and convergent methods to evaluate various periodic orbit expansions. In integrable systems, the proliferation law is not exponential, but we are still confronted with infinite sums and the question of how these should be optimally truncated. A key point here is that different combinations of periodic orbits may "conspire" to produce stronger peaks or more cancellations.

In integrable systems, there is also the fundamental problem of near degeneracies

[1]The number of periodic orbits (at a specified energy E) with period less than T grows asymptotically as $\exp[\mathfrak{h}(E)T]/\mathfrak{h}(E)T$, where $\mathfrak{h}(E)$ is the topological entropy.

since the level spacing distribution has a Poisson character [64]. To achieve a sufficient resolution in energy space, we have to include contributions from orbits with very large actions. This problem also occurs in noninteracting few-body systems, where the combination of independent spectra leads to many near degeneracies even at low energies. In a recent paper [35], a coarse-grained EBK spectrum for a system of two noninteracting identical particles in a disk billiard was reproduced from periodic orbit quantization, but there were a few low-lying levels that could not be resolved despite using millions of periodic orbits. The convergence of the two-particle trace formula became an important consideration in the effort to resolve these levels. (This effort is justified since it is a precision test of the two-particle formula.) The problem is that the enormous increase in the number of periodic orbits with length[2] precludes standard length truncation of the two-particle trace formula, and alternative truncation schemes are necessary. An amplitude ordering of the periodic orbits reveals that orbits running close to the wall of the billiard ("grazing orbits") are largely unimportant for the quantization of the low-energy states of the two-body system. It is shown that an amplitude truncation of the trace formula better approximates the semiclassical density of states and in particular resolves near-degenerate levels that are otherwise unresolved using the standard approach.

To illustrate some common problems that arise when truncating an oscillating density, two other Fourier-type expansions will be studied numerically: Riemann's formula for the density of the primes [65, 66], and Berry's formula for the density of the Riemann zeros [67]. The density of integer powers of primes involves "fractional degeneracies", and it is crucial to explicitly verify that the spectral lines produced by the truncated Riemann series have the correct relative intensities. Berry's formula actually diverges, and an alternative to direct summation must be considered. The first problem can be solved by numerical convolution of the truncated series with a smooth response function. (This is a common technique in signal processing.) The convolution can be performed analytically by doing an asymptotic analysis of the convolution integral, which results in a so-called "sum rule", that is, a sum that absolutely converges to a coarse-grained version of the exact density. The sum rule for Riemann's formula is used to analyze the numerical convergence of the truncated series. The sum rule for Berry's formula is found to reproduce a coarse-grained spectrum of the Riemann zeros even though the original series is divergent.

[2] In L space (i.e. "action space" or the space of orbit lengths), $N_2(L) \ggg N_1(L)$, where $N_{1/2}(L)$ is the one- or two-particle cumulative density of orbits. This is analogous to E space, where $N_2(E) \ggg N_1(E)$.

2.2 Periodic Orbit Quantization of the Disk Billiard

The trace formula for the disk billiard is often used in applications. For example, a recent study used it to reproduce the quantum fluctuations in the cohesive force of metallic nanowires [68], and the formula has also been used to understand the shell structure of metal clusters [69, 70]. In these and other applications, few orbits are required, and the convergence of the trace formula is not an issue. As mentioned above, the issue arises when the goal is full quantization. Semiclassical quantization of the disk billiard has been achieved using Bogomolny's method [71] in Refs. [72], and from harmonic inversion of the trace formula in Ref. [73]. In the latter reference, the authors include $\hbar$ corrections and obtain results more accurate than EBK. If these corrections are not included, their results are consistent with EBK and periodic orbit theory.

The periodic orbit quantization of the one-particle disk billiard and its convergence have been studied in Ref. [74]. Although an exact (leading-order) trace formula is known for the one-particle disk billiard (and the proliferation law $N_1(L)$ is not exponential [75]), there remains the question of how to truncate the series most effectively [7]. The standard procedure is to specify a length cutoff $L_{\max}$ and use an ordered *subset* of the shorter orbits [74, 7]. To resolve near-degenerate levels using this scheme, a sufficiently large[3] $L_{\max}$ must be used. For the multibody situation, this is highly impractical. As mentioned above, the essential difficulty is that the number of periodic orbits with length $L < L_{\max}$ increases rapidly with additional degrees of freedom. If the interest is in reproducing a specific set of levels, it becomes crucial to have judicious selection criteria for choosing which orbits to include in the expansions.

In this section, the convergence of the trace formula for one- and two-body systems will be explored using an "amplitude ordering" technique similar to the stability ordering of cycle expansions [76, 10] used for nonintegrable systems in Refs. [77, 78]. The authors of Refs. [77] use the magnitude of the terms in an expansion for their ordering scheme. Similarly, only orbits whose amplitude exceeds some prescribed threshold will be included in the following numerical calculations. An immediate benefit is the possibility of more significant periodic orbit contributions at comparatively larger lengths. Since the goal is to resolve near degeneracies, this seems to be a more optimal strategy because it is the longer

[3] In Ref. [74], six levels having one-particle wave numbers $k < 15$ could not be resolved using orbits with length $L < L_{\max} = 30000R$, where R is the radius of the disk.

orbits that are responsible for short-range oscillations in the density of states.

2.2.1 One-body trace formula

Recall that the one-particle density of states is given by

$$\rho_1(k) = \bar{\rho}_1(k) + \tilde{\rho}_1(k). \tag{2.1}$$

The first term is an asymptotic series in powers of k arising from "zero-length" orbits. The second term is an asymptotic series in powers of $\sqrt{k}$, and to leading order, is a sum over topologically distinct families of periodic orbits. The periodic orbit families of the disk may be classified by two integers (v, w), where v is the number of specular reflections and w is the winding number around the center. The length of an orbit is then $L_{vw} = 2vR\sin(\pi w/v)$. Using this notation, the trace formula is [74, 7]

$$\tilde{\rho}_1(k) = 2\sqrt{\frac{kR^3}{\pi}} \sum_{w=1}^{\infty} \sum_{v=2w}^{\infty} d_{vw} A(v,w) \cos\left(kL_{vw} - 3v\frac{\pi}{2} + \frac{\pi}{4}\right), \tag{2.2}$$

where the amplitude

$$A(v,w) = \frac{\sin^{3/2}\left(\frac{\pi w}{v}\right)}{\sqrt{v}} = \frac{(L_{vw}/2R)^{3/2}}{v^2}. \tag{2.3}$$

The degeneracy factor d_{vw}, which accounts for negative windings ($w < 0$), is 1 for $v = 2w$ and 2 for $v > 2w$. Any numerical evaluation of Eq. (2.2) involves computing the contributions from a finite set of orbits. Since different sets will generate different results, the basic question is how to choose the best set. The problem is that knowledge of which set of orbits best reproduces the specific quantum states of interest is usually not available in advance, and so we start with the simplest truncation procedure.

In the following analysis, there will be three important parameters: the total number of positive winding orbits N_+ (which indicates the computational effort); the total number of periodic orbits used by the standard truncation (ST) procedure N_S; and the total number of periodic orbits used by the amplitude truncation (AT) procedure N_A. The latter two quantities include degeneracies due to negative-winding orbits.

Suppose that $N_+ = 10^4$. The most natural way [74, 7] to truncate the sum in Eq. (2.2) is to use *only* orbits that have $w \le w_{\max} = 100$ and $v \le v_{\max} = 2w_{\max} = 200$ [Fig. 2.1(a)]. In general, specifying $(v_{\max}, w_{\max})$ determines the length of the longest orbit used in the truncated sum, $L_{\max} = 2v_{\max}R$. It is important to note that we have not used

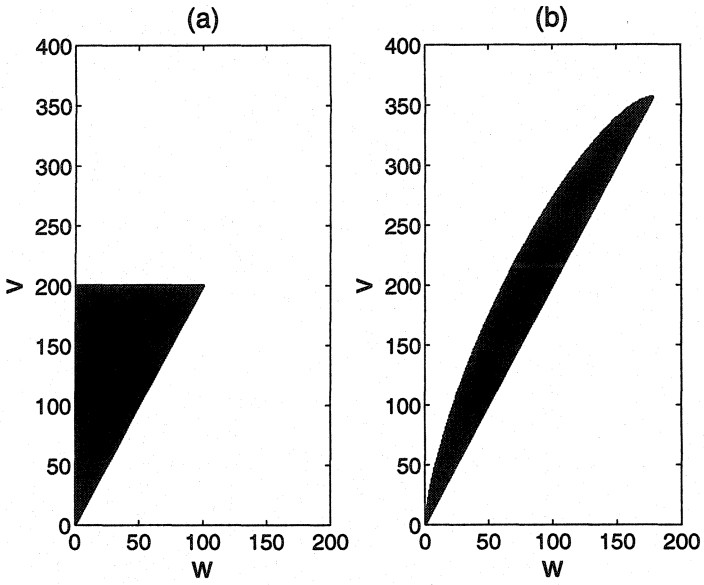

Figure 2.1: The positive-winding orbits (v, w) used by the two different truncation procedures. (a) The orbits used in a standard truncation of the sum in Eq. (2.2) with $w_{\max} = 100$, $v_{\max} = 200$. (b) The set of orbits for which the amplitude $A(v, w) > \epsilon = 0.052\ 987\ 251$. In each case, $N_+ = 10^4$.

all orbits that have a length $L \leq L_{\max}$. In fact, there is a countably infinite set of shorter periodic orbits. Nevertheless, *all* of the orbits that are used $[N_S = 1.99 \times 10^4]$ are shorter than $L_{\max} = 400R$, and in this sense, specifying $(v_{\max}, w_{\max})$ is equivalent to specifying a length cutoff $L_{\max}$.

Alternatively, an amplitude truncation uses only those orbits for which $A(v, w) > \epsilon$, where ϵ is some prescribed numerical constant. Specifying ϵ determines the maximum winding number: $w_{\max} = [1/2\epsilon^2]$. For each value of $w \leq w_{\max}$, we sweep through the values of $v \geq 2w$ until the amplitude falls below ϵ. If $\epsilon = 0.052\ 987\ 251$, then precisely $N_+ = 10^4$ orbits $[N_A = 1.9822 \times 10^4]$ satisfy $A(v, w) > \epsilon$. These orbits are plotted in Fig. 2.1(b). The significance of ϵ is that it can be varied to give the same number of orbits as the standard set. This allows us to directly compare the convergence of the two methods. It is reasonable to expect amplitude truncation to have better convergence since the most important terms in the sum are included. This conjecture is now tested by evaluating the trace formula (2.2) using these two different sets of orbits.

Before presenting the results, there is a very important observation to point out.

Inspection of Fig. 2.1 reveals a surprising result: amplitude truncation typically excludes many of the shorter orbits used in standard truncation. A common point of view, which is stressed in Ref. [7], is that for a low resolution of $\tilde{\rho}_1$, "only those orbits with the smallest actions (lengths) and *simultaneously* the largest amplitudes in the Fourier decomposition of $\tilde{\rho}_1$ are important." This statement does not seem to apply to the amplitudes of the disk. While it is true that the shortest few orbits have the largest amplitudes, it is not generally true that shorter orbits are more important than longer orbits.

The length spectrum of the one-body system shown in Fig. 6.9 of Ref. [7] appears to contradict this observation. However, the authors show the Fourier transform of the *Gaussian-averaged* trace formula. When the disk trace formula is Gaussian averaged over the variable k, the amplitudes in Eq. (2.3) are multiplied by the Gaussian factor $\exp(-\sigma^2 L_{vw}^2/2R^2)$. Without this factor, the importance of the longer orbits is clear. Of course, trace formulas averaged with various kinds of smoothing functions are now standard practice for reproducing coarse-grained level densities (see Appendix B of Ref. [79] for a general discussion). However, this is inappropriate here. The longer orbits are obviously important so there is no point in suppressing them. The usual argument is that if we are interested in the fine details of a quantum spectrum, then averaging using a small smoothing width is justified. But, reducing the size of the smoothing parameter raises the cutoff length (ordered length truncation). While this may not be a limitation for the one-body trace formula, the consequence is severe for the multibody trace formula. So if an amplitude truncation scheme is used, then damping the amplitudes makes no sense. The correct degeneracies can still be determined by numerical Gaussian convolution of the amplitude-truncated trace formula.

Comparing the two methods, the conclusion is that levels with small azimuthal quantum number [$m \leq 5$] are better resolved using amplitude truncation. For states with higher azimuthal quantum numbers [$m \geq 6$], the convergence depends on the radial quantum number n; ST is better for $n \leq 2$, but AT is better for $n > 2$. Some generic examples involving closely spaced levels are shown in Fig. 2.2. In the present context, "closely spaced" levels have a spacing $\Delta k \ll \overline{\Delta k}$, where $\overline{\Delta k} = 0.2190$ is the average level spacing for wave numbers $k < k_{\max} = 35$. For the levels shown in Fig. 2.2, it is obvious which method gives better resolution. In general, any level is "better resolved" if the peak is a better approximation to the exact result, which is a δ-function spike. In particular, the convergence of the two methods for isolated levels k_i (where $|k_{i\pm1} - k_i| > 2\,\overline{\Delta k}$) can be checked numerically by

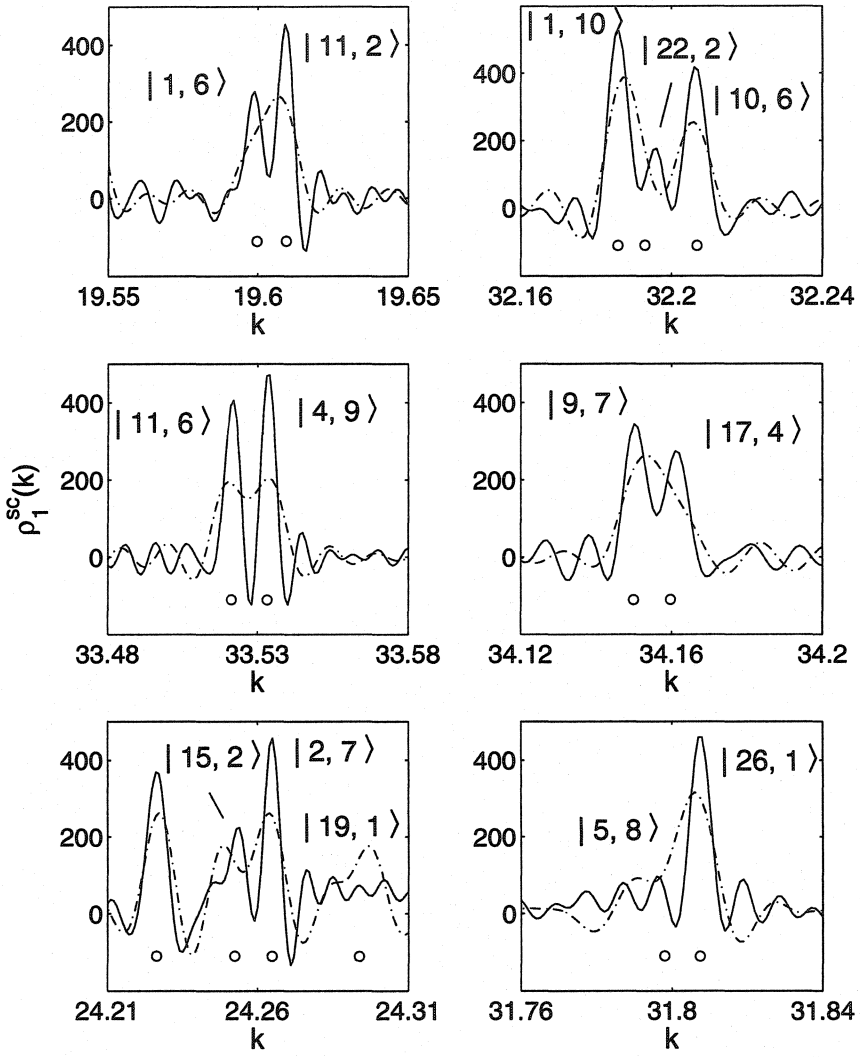

Figure 2.2: The semiclassical single-particle density of states computed using the two different sets of orbits in Fig. 2.1. The dashed-dotted line uses standard length truncation [Fig. 2.1(a)], and the solid line uses amplitude truncation [Fig. 2.1(b)]. Peaks correspond to the quantum states $|m, n\rangle$ indicated and circles denote the positions of single-particle levels obtained from EBK quantization (see Sec. 2.6.3 of Ref. [7]). Notice that away from peaks, the two methods are generally out of phase because different sets of orbits interfere.

computing moments for each peak and comparing with the exact result.

The semiclassical approximation $S_{vw} \gg \hbar \Leftrightarrow kL_{vw} \gg 1$ implies that both methods should improve with increasing energy. Since amplitude truncation also uses longer orbits, the approximation should be consistently more accurate, but this is not what is observed. The higher angular momentum states with the lowest energies are poorly reproduced by amplitude truncation. To understand these results, we first recognize that the states with large angular momentum and small energy are those for which the quantum particle is furthest from the center of the disk and therefore near to the wall of the billiard. To replicate these states, we need to use orbits that mimic this quantum behavior. In other words, we need classical orbits that graze the wall of the billiard. These are precisely the orbits that have many more reflections than windings. AT typically excludes such orbits, and therefore has trouble reproducing the higher m states with small n. ST includes more grazing orbits, and thus more accurately reproduces these states. As mentioned above, this deficiency of AT for the disk is not observed for fixed m as n increases (i.e. as the energy increases). This quantum-classical correspondence for the disk billiard can be summarized as follows: *The high angular momentum states with the smallest energies are reproduced semiclassically by the grazing orbits, which have the property* $v \gg w$. We now consider the two-particle system where knowledge of this correspondence is extremely useful.

2.2.2 Two-body trace formula

The two-particle density of states can be written as [35]

$$\rho_2(k) = (\bar{\rho}_1 * \bar{\rho}_1)(k) + 2(\bar{\rho}_1 * \tilde{\rho}_1)(k) + (\tilde{\rho}_1 * \tilde{\rho}_1)(k). \tag{2.4}$$

The second and third terms are an asymptotic series in powers of $\sqrt{k}$. For the disk, the last term in the decomposition is, to leading order,

$$\begin{aligned}(\tilde{\rho}_1 * \tilde{\rho}_1)(k) = 2\sqrt{\frac{k^3R^5}{\pi}} \sum_{(v_a,w_a)} \sum_{(v_b,w_b)} & A(v_a,w_a,v_b,w_b) \\ & \times d_{v_a w_a} d_{v_b w_b} \cos\left(kL_{ab} - 3(v_a+v_b)\frac{\pi}{2} + \frac{\pi}{4}\right),\end{aligned} \tag{2.5}$$

where

$$A(v_a,w_a,v_b,w_b) = \frac{\sin^2\left(\frac{\pi w_a}{v_a}\right)\sin^2\left(\frac{\pi w_b}{v_b}\right)}{\left[v_a^2\sin^2\left(\frac{\pi w_a}{v_a}\right) + v_b^2\sin^2\left(\frac{\pi w_b}{v_b}\right)\right]^{3/4}}. \tag{2.6}$$

As an illustration of the proliferation of periodic orbits that occurs as more particles are introduced into the billiard, choose a length cutoff $L_{\max} = 400R$. In this case, a standard length truncation implies that there are $N_+ = 10^4$ one-particle periodic orbits to include in Eq. (2.2) and $N_+ = 2.470\ 09 \times 10^7$ two-particle periodic orbits to include in Eq. (2.5). In Ref. [35], the semiclassical two-particle density of states was computed on the interval $0 \leq k \leq 10$ using a standard truncation of Eq. (2.5) [$N_+ = 6.25 \times 10^6$], and four multiplets could not be resolved. The preceding analysis clearly indicates that for the two-body system, an amplitude truncation is more suitable since most of the two-particle states at lower energies are states for which *each* particle is in a low angular momentum state. This is now demonstrated explicitly.

As before, specifying ϵ determines the maximum winding numbers. In this case, the combined winding numbers of each one-body periodic orbit to be used must satisfy the condition $w_a^2 + w_b^2 \leq [1/4\epsilon^{4/3}]$. Then, for given winding numbers (w_a, w_b) which satisfy this condition, we sweep through the allowed values of v_a and v_b until the two-particle amplitude (2.6) becomes less than ϵ.

To compare with a previous calculation in Ref. [35], the value $\epsilon = 0.000\ 398\ 374\ 925$ is prescribed so that precisely $N_+ = 6.25 \times 10^6$ two-particle periodic orbits satisfy the condition $A(v_a, w_a, v_b, w_b) > \epsilon$ [$N_S = 2.450\ 25 \times 10^7, N_A = 2.395\ 5589 \times 10^7$]. A plot of the two-particle orbits as in Fig. 2.1(b) reveals the same characteristics as before, the exclusion of grazing orbits and many longer orbits than those used in standard truncation. In fact, almost one-quarter of the total number of orbits used are longer than the longest orbit used in standard truncation [$L_{\max} = \sqrt{8} v_{\max} R = 100\sqrt{8}R$]. Computation of Eq. (2.4) using amplitude truncation of Eq. (2.5) yields more accurate results, but the unresolved multiplets [35] remain unresolved and still more orbits are required.

The result of one numerical calculation using $N_+ = 10^8$ two-particle orbits in Eq. (2.5) is given here. The calculation was done for $k \in (7.3380, 7.4380)$. In this interval, there should be two multiplets [35], a quartet $\{|0\ 1, \pm 1\ 2\rangle, |\pm 1\ 2, 0\ 1\rangle\}$ at $k = 7.3831$, and an octet $\{|\pm 1\ 1, \pm 3\ 1\rangle, |\pm 3\ 1, \pm 1\ 1\rangle\}$ at $k = 7.3932$. As shown in Fig. 2.3, ST [$w_{a_{\max}} = w_{b_{\max}} = 100, v_{a_{\max}} = v_{b_{\max}} = 200$] does not resolve these two multiplets, but AT [$\epsilon = 0.000\ 139\ 746\ 080$] does partially resolve them. It was further checked that the two peaks have the correct degeneracies consistent with a quartet and an octet by numerically computing the area under each peak. These areas are 3.91 and 8.6, which have relative errors of 2% and 7%, respectively. This error arises since the two peaks are not fully re-

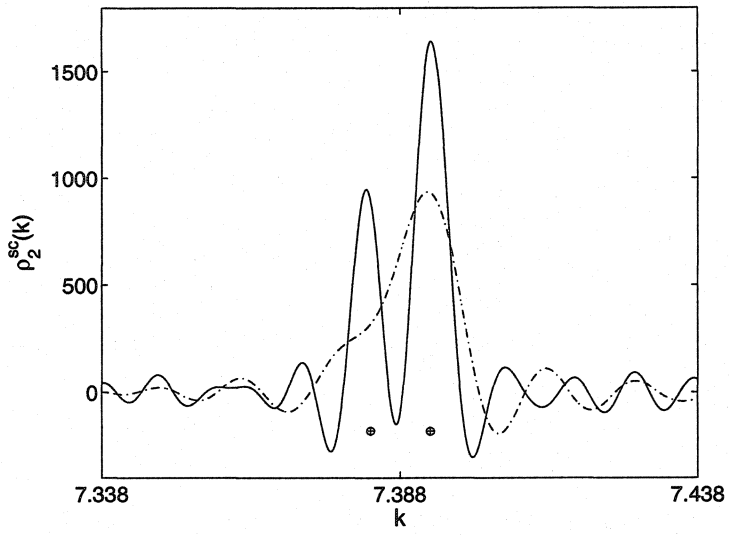

Figure 2.3: The semiclassical two-particle density of states [Eq. (2.4)] for $k \in (7.3380, 7.4380)$ using $N_+ = 10^8$ two-particle periodic orbits. The dashed-dotted line uses standard length truncation of Eq. (2.5) [$N_S = 3.9601 \times 10^8$], and the solid line uses amplitude truncation, that is, orbits for which $A(v_a, w_a, v_b, w_b) > \epsilon = 0.000\ 139\ 746\ 080$ [$N_A = 3.914\ 883\ 65 \times 10^8$]. $\oplus$ symbols indicate the positions of two-particle levels obtained from EBK quantization.

solved and decreases as more orbits are included. The area under the large unresolved peak is 12.25 which also has an error of about 2% relative to an unresolved 12-fold degenerate multiplet. A similar analysis for the other set of unresolved peaks gives comparable results.

The heterogeneous term $[\tilde{\rho}_2^{\rm h}(k) = (\bar{\rho} * \tilde{\rho})(k)]$ in Eq. (2.4) has not been mentioned. (Hereafter, this will be referred to as the mixed term and mathematical expressions which have the superscript "h" will denote quantities related to this term.) Amplitude truncation of the mixed term is not necessary since this contribution involves only a summation over periodic orbits of the one-body phase space, and hence the computational difficulties associated with the numerical evaluation of the dynamical term $[\tilde{\rho}_2^{\rm d}(k) = (\tilde{\rho} * \tilde{\rho})(k)]$ do not arise. The mixed term merely oscillates about zero with much smaller amplitude than any peak of the dynamical term [35]. Amplitude truncation of the mixed term results in a small increase in the number of short-range oscillations and a slight change in the amplitude of some of the discontinuities that occur at the positions of the single-particle spectrum, but this has no significant numerical effect on the two-particle density of states. Thus, standard length truncation of the mixed term suffices.

Nevertheless, the mixed term must be truncated carefully so that its length cutoff matches that of the dynamical term. For example, a standard truncation of the dynamical term such that $w_{a_{\max}} = w_{b_{\max}} = 50, v_{a_{\max}} = v_{b_{\max}} = 100$ requires the mixed term to be truncated at $(w_{\max} = 70, v_{\max} = 141)$ since

$$L^{\mathrm{h}}_{\max} = L^{\mathrm{d}}_{\max} \Rightarrow v^{\mathrm{h}}_{\max} = \sqrt{2} v^{\mathrm{d}}_{\max} = \sqrt{2}(100) \approx 141.$$

(This point was overlooked in the previous analysis of the disk in Ref. [35]. This has been corrected in the current analysis and does not significantly affect the previous numerical results. It is noted here to emphasize that the two oscillatory terms must be truncated consistently.) The corresponding amplitude truncation of the dynamical term requires the mixed term to be truncated at $(w_{\max} = 92, v_{\max} = 184)$ since the length of the longest two-particle orbit used by this method is $369R$.

If the two oscillatory terms are not truncated consistently in this manner, there will be further small numerical errors at the positions of the single-particle spectrum. In fact, this was observed in Ref. [35] where a slight inconsistency in the truncation procedure was overlooked. Clearly, there is a delicate cancellation between the mixed and dynamical terms in the vicinity of the levels of the one-particle spectrum that occurs only if the two terms are truncated as explained above. The residual peaks that remain (even after careful truncation) are presumably removed entirely if corrections to the one-body trace formula are included. These corrections were not included in Ref. [35].

In the present calculation $[N_+ = 10^8]$, for standard truncation, the mixed term should be truncated at $(w_{\max} = 141, v_{\max} = 282)$ $[v^{\mathrm{h}}_{\max} = \sqrt{2} v^{\mathrm{d}}_{\max} = \sqrt{2}(200) \doteq 283]$, and for amplitude truncation, the mixed term should be truncated at $(w_{\max} = 185, v_{\max} = 371)$. The latter is due to the fact that the longest orbit used in the AT method is $(w_a, v_a, w_b, v_b) = (97, 195, 158, 316)$ $[L^{\mathrm{d}}_{\max} \doteq 743]$ which implies $v^{\mathrm{h}}_{\max} \doteq 371$. The same principle applies to more particles. For example, for the three-particle density of states

$$\begin{aligned} \rho_3(k) = &\left(\bar{\rho}_1 * \bar{\rho}_1 * \bar{\rho}_1\right)(k) + 3\left(\bar{\rho}_1 * \bar{\rho}_1 * \tilde{\rho}_1\right)(k) \\ &+3\left(\bar{\rho}_1 * \tilde{\rho}_1 * \tilde{\rho}_1\right)(k) + \left(\tilde{\rho}_1 * \tilde{\rho}_1 * \tilde{\rho}_1\right)(k), \end{aligned} \tag{2.7}$$

we would use AT for the last two terms and ST for the second term, but all three oscillatory terms must be truncated consistently and the threshold constants for the last two terms must be chosen accordingly.

To summarize, it was shown that amplitude truncation of the trace formula for the disk billiard is more effective than standard length truncation for the quantization of low angular momentum states [$m \leq 5$]. It is inappropriate for the higher m states when the radial quantum number $n \leq 2$, but quickly improves with increasing energy. The reason for this is the direct correspondence between the classical and quantum angular momenta. This correspondence is useful for a multibody system where it will be more effective to resolve the low energy levels since they will arise from the situation where all the particles have small azimuthal quantum numbers. An important result of the analysis is that longer orbits generally possess larger amplitudes, unlike many systems where the shortest orbits play the dominant role [7].

We could also do an analogous study of the three-dimensional spherical billiard [80, 7] which has the same periodic orbits. While the amplitudes of the orbits are different for the spherical cavity, they do seem to have the same behavior as in the disk. In Fig. 4 of Ref. [69], we can clearly see that for a given winding w, the amplitude decays with v, the number of specular reflections. However, it is interesting to note that an orbit with an arbitrary large value of v becomes more important as the winding number is increased. The same nontrivial behavior is observed in the disk. The influence of the longer orbits on the shell structure of the magnetic susceptibility of N electrons in a spherical cavity has also been studied in Ref. [70] where the authors find no appreciable phase difference between the oscillations generated by the two shortest orbits and those due to longer orbits for small N. In contrast, it was shown above that there is such a difference for oscillations in the density of states.

2.3 Riemann Zeros and Integer Powers of Primes

There is a deep connection between the complex zeros of the Riemann zeta function and Random Matrix Theory [81]. The zeros possess the same statistical properties as the energy eigenvalues of a dynamical Hamiltonian that is nonintegrable and whose dynamics are not time-reversal invariant. Unfortunately, this Hamiltonian is not known in terms of its dynamical variables. The main source of insight into this unknown quantum chaotic system comes from the Gutzwiller trace formula. It is well known that the oscillatory part of the density of the Riemann zeros is given by a Gutzwiller-like sum, with one periodic term for every integer power of a prime number [67]. (A smoothed density of the Riemann zeros has

also been studied in Ref. [82].) From this perspective, it can be inferred that a spectrum consisting of the Riemann zeros is generated by a Hamiltonian (albeit unknown) whose classical orbits have actions that are logarithms of primes and integer powers of primes.

Conversely, we could ask whether it is also possible to calculate the prime number sequence from a sum of oscillatory terms, with one term for every zero of the zeta function. Although less widely known, such a series was actually given by Riemann himself [65]. Riemann derived an exact formula for the density of the primes (and their integer powers) that can be expressed as the sum of a smooth function and an infinite series of oscillatory terms involving the complex zeros of the zeta function. The smooth part has been thoroughly studied in the context of the prime number theorem, whereas the oscillatory part has been largely ignored. Interestingly, it is the latter that contains the essential information about the location of the primes, as shown below. There is a vast literature on the distribution of the prime numbers. It is recognized that their distribution exhibits global regularity and local irregularity [83]. The nearest-neighbor spacings (NNS) of the primes is known to be Poisson-like [84], corresponding to an almost uncorrelated random distribution. This is very different in character from the Gaussian Unitary Ensemble (GUE) distribution of the Riemann zeros. Nevertheless, it is possible to generate the almost uncorrelated sequence of the primes from the interference of the highly correlated Riemann zeros.

As mentioned above, from the perspective of semiclassical periodic orbit theory, the density of the Riemann zeros has the structure of a dynamical trace formula with periodic orbits. It is natural to ask whether Riemann's formula is a trace formula for the primes. Despite having the oscillatory terms, as discussed below, Riemann's formula is not a trace formula of dynamical origin. But, this does not preclude the existence of a trace formula for the primes, and if it does exist, then it would support the notion that there exists a Hamiltonian system whose quantum spectrum is the primes. In any case, the exclusion of Riemann's formula as a trace formula suggests that there would be no correspondence between the classical dynamics and the Riemann zeros for this system.

The purpose of this section is to study the density of the primes from the point of view of periodic orbit quantization, where a coarse-grained quantum spectrum is reproduced from a truncated periodic orbit sum[4]. It is first verified that Riemann's formula does produce spectral lines at the positions of the primes and their integer powers, even when

[4]See Sec. 5.5 of Ref. [7] for a general discussion, and Secs. 6.1.3 and 6.1.6 for examples.

the series is truncated. This is not completely unexpected since Riemann's series converges conditionally to the exact density which is a set of δ-function spikes. However, the δ functions arise from the *entire* series. The truncated series is an approximation to the exact density. It does not yield spikes, but rather lines of various widths, heights, and (unknown) shapes, and it is not at all obvious that the relative line intensities of the truncated series are correct. This problem is examined both numerically and analytically. A simple rule is also provided for estimating the value of the largest zero required to sufficiently resolve individual lines of a specific uniform shape in some interval of interest.

2.3.1 Riemann's formula for the density of primes

We start from the Euler product formula

$$\zeta(\beta) = \prod_p (1 - p^{-\beta})^{-1}, \qquad \text{Re } \beta > 1, \tag{2.8}$$

where the product is over all primes p. It follows that $\sum_p \sum_{n=1}^{\infty} \frac{1}{n} \exp(-n\beta \ln p) = \ln \zeta(\beta)$. Dividing both sides by β and then taking the inverse Laplace transform of both sides with respect to E, we immediately obtain

$$N(E) \equiv \sum_p \sum_n \frac{1}{n} \Theta\left(E - \ln p^n\right) = \frac{1}{2\pi i} \int_{a-i\infty}^{a+i\infty} \frac{\ln \zeta(\beta)}{\beta} e^{\beta E} \mathrm{d}\beta, \tag{2.9}$$

where $a > 1$. Riemann evaluated the RHS of Eq. (2.9) to obtain $N(E)$. Upon differentiation with respect to E and the subsequent substitution $x = e^E$, we obtain the density $\rho(x)$ of p^n/n along the real axis x as

$$\rho(x) \equiv \sum_p \sum_n \frac{1}{n} \delta\left(x - p^n\right) = \frac{1}{\ln x} - \frac{1}{x\left(x^2 - 1\right) \ln x} - 2 \sum_{\alpha > 0} \frac{\cos(\alpha \ln x)}{x^{1/2} \ln x}, \tag{2.10}$$

where $x > 1$. This formula assumes the Riemann hypothesis, which states that the infinite number of complex zeros of the zeta function all lie on the critical line $\beta = (1/2 \pm i\alpha)$, where α is real and positive. Note that explicit use of the symmetry of the complex zeros has been made to reduce the summation to cosine functions. A generalized version of the Riemann formula, where the zeros may lie anywhere in the critical strip, is given in Ref. [85]. We shall denote the sum over the oscillatory terms on the RHS of Eq. (2.10) as $\tilde{\rho}(x)$. Since Eq. (2.10) is exact, it is clear that the δ-function spikes of $\rho(x)$ must be generated from the interference of all terms in $\tilde{\rho}(x)$. In the following section, we focus on the spectral analysis of the truncated series.

Before presenting the results, however, we briefly review the pioneering numerical work of Riesel and Göhl [86]. The LHS of Eq. (2.9) is a set of step functions, with unit steps at every prime p, one-half steps at p^2, one-third steps at p^3, and so on, and may be obtained by taking the contour integral of $\ln\zeta(\beta)/\beta$ on the RHS of the equation. Riemann [65] denotes this function by $f(x)$ and Edwards by $J(x)$ [66]. (In Eq. (2.9), this function is rather denoted by $N(E)$, which is the conventional notation for the cumulative density of states.) The number of primes less than x, denoted by $\pi(x)$, may be expressed in terms of $f(x)$ as

$$\pi(x) = \sum_{n=1}^{\infty} \frac{\mu(n) f(x^{1/n})}{n} , \tag{2.11}$$

where $\mu(n)$ is the Möbius function [66]. The modulating effect of the oscillatory terms due to the first twenty nine pairs of the complex Riemann zeros was numerically examined by Riesel and Göhl [86] in 1970. This early work showed the approximate formation of the first few steps at the prime numbers, and modulations for some larger primes. Note that the series (2.11) requires a knowledge of the Möbius function, and is much more complicated than Eq. (2.10). Riesel and Göhl actually replaced the sum over the Möbius functions by the Gram series involving factorials which are difficult to compute accurately for large integers. We shall rather study formula (2.10) for $\rho(x)$ since it contains more information than the formula for the density of the primes (no powers) which can be obtained from the derivative of $\pi(x)$.

2.3.2 Spectral analysis of Riemann's formula

Numerically, we can only evaluate a finite number of terms from Riemann's infinite series. Although it would seem by inspection that all terms of the series are equally important and that there is no optimal ordering of the terms, Riemann states in his paper that the series is conditionally convergent and that it must be summed in the order of increasing size of α. (For any series whose convergence is conditional, the order of summation must be specified since different orderings produce different results.) Riemann also mentions that with this ordering, the truncated series should give an approximation to the density of primes (and their powers), but that using a different ordering, the resulting finite series could approach arbitrary real values. This has been verified numerically by using finite sets of zeros, chosen according to different rules. In the numerical work that follows, the "natural order" is used, since it gives the correct result.

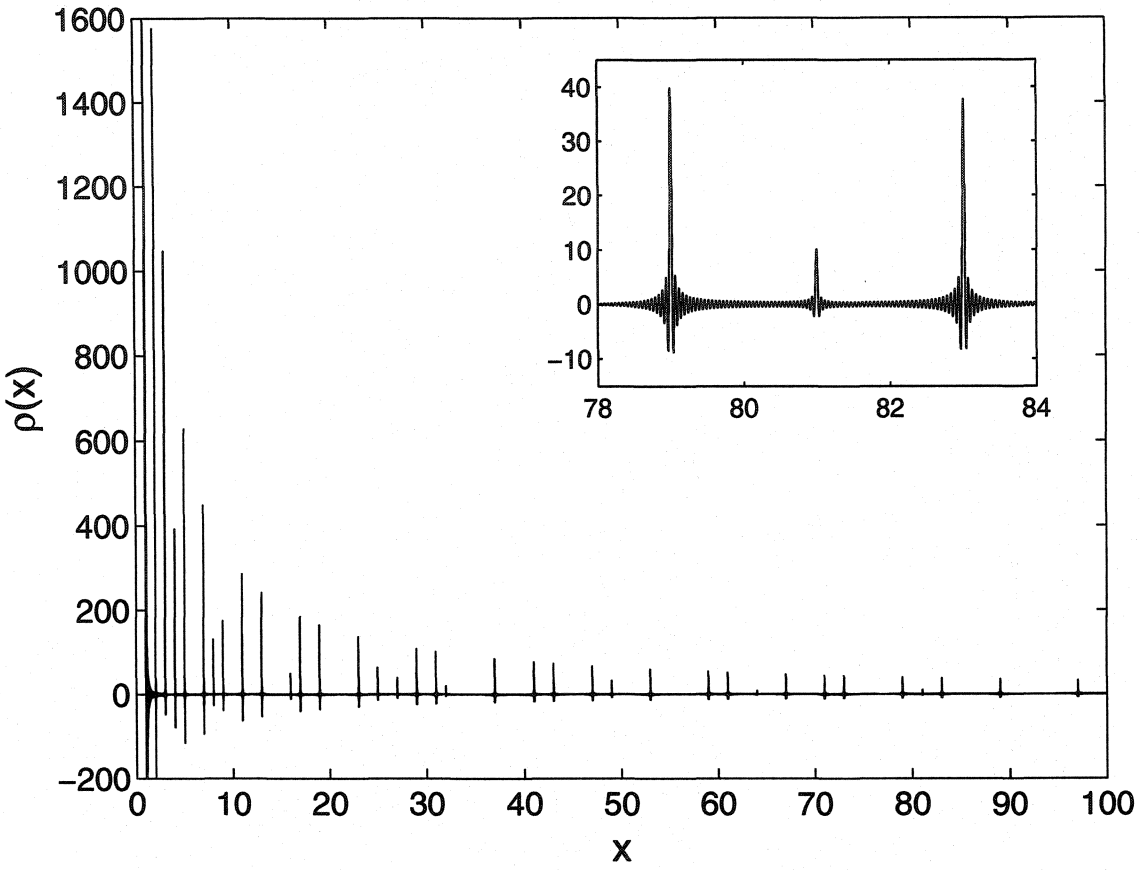

Figure 2.4: Riemann's formula [Eq. (2.10)], using the first 10^4 zeros for $x \in [1.5, 100]$. The inset shows a closer view of three lines that appear for $x \in [78, 84]$. The three lineshapes are similar, so that their relative heights approximately indicate their relative intensities. However, the lineshapes vary considerably throughout the entire range so that heights cannot be immediately interpreted as relative intensities.

Line intensities of the truncated series

Equation (2.10) was first computed using the lowest 10^4 zeros, and lines were observed at the positions of the primes and their integer powers for $x < 5000$. However, for $x > 2000$, many lines cannot be fully resolved and the signal eventually dies out. This is due to truncation, since only a small number of zeros have been included. (This will be discussed in more detail below.) Nevertheless, even this small number of zeros yields narrow lines at the lowest primes. In Fig. 2.4, the result is displayed for $x \in [1.5, 100]$. Although we can clearly observe lines at integer powers of primes, the relative intensities cannot be determined by inspection since the lineshapes are not uniform (see Fig. 2.5).

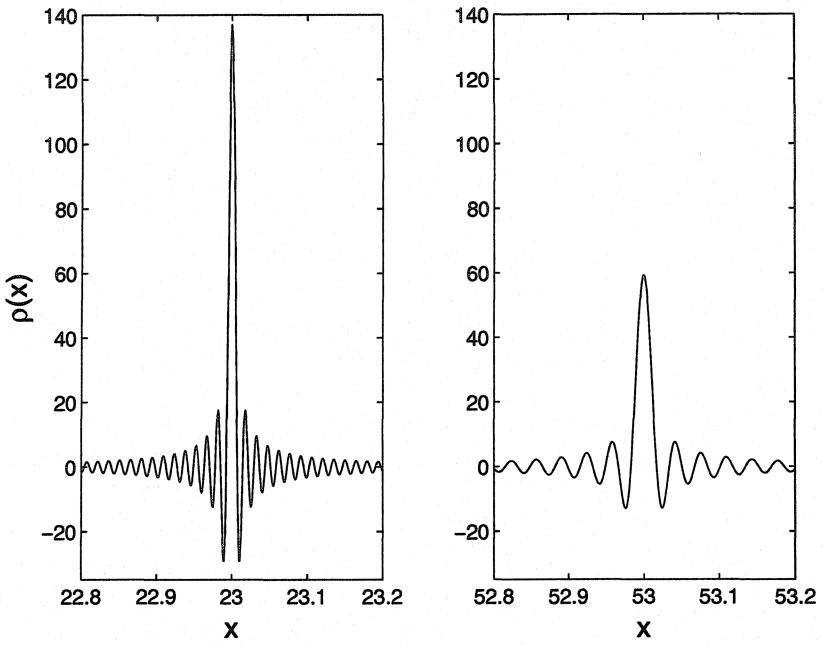

Figure 2.5: A closer view of two nonadjacent lines in Fig. 2.4. The lineshapes clearly differ, so that their relative heights are meaningless.

This is a common problem in spectral analysis, and is often resolved by imposing a more uniform lineshape through convolution of the signal with an appropriate smooth "response function" [87]. The response function is typically a peaked function that falls to zero in both directions from its maximum. Gaussian functions are positive-definite and decay rapidly. They are also convenient to use since their shape only depends on a single parameter (the variance) and therefore can be easily controlled.

Thus, the approximate density $\rho(x)$ (i.e. smooth term and truncated series) is next convolved with an *unnormalized* Gaussian of variance σ:

$$\rho(x) * G_\sigma(x) = \int_1^\infty \rho(x')G_\sigma(x - x')\mathrm{d}x', \tag{2.12}$$

where

$$G_\sigma(x) = \exp(-x^2/2\sigma^2). \tag{2.13}$$

The effect of the convolution is that rapidly oscillating features are washed out and smooth peaked features are smeared into the shape of the response function. If the lines were perfect δ functions of height D_n, then from Eq. (2.12), these would be replaced by $D_n G_\sigma(x - x_n)$,

i.e. Gaussians of variance σ with height D_n at $x = x_n$. Of course, the lines are not δ-function spikes, so that the resultant lineshapes are not exactly Gaussian, but as long as the intrinsic linewidth is sufficiently small compared to the variance, the deviation from a perfect Gaussian is quite negligible. Therefore, the convolution produces a series of Gaussian lines, each of the same width. The key point is that the lineshapes are now essentially uniform, so that the actual heights can be meaningfully compared and immediately interpreted as the relative intensities. It is important to keep in mind that since the response function has a maximum height of unity, the height of a line *after* convolution should be the area under that line *before* convolution. The reason for this is that although the lines of the original signal act like δ functions with respect to the response function, they do have nonzero widths and so their effective δ-function "heights" D_n are equal to the areas. In this sense, the convolution procedure is equivalent to directly integrating the area under each line of the signal. However, the convolution technique is much simpler and avoids errors that can arise from the long oscillatory tails of individual lines. Note that this procedure cannot resolve two adjacent lines when the spacing between them is smaller than σ and thus $\sigma_{\max} = 1/4$.

Equation (2.12) was computed for the range of interest in Fig. 2.4. This is shown in Fig. 2.6 using $\sigma = 0.05$. Note that the heights do not depend on the specific value of σ due to the fact the Gaussian is not normalized. As more terms are included in the sum, the natural linewidths decrease and the convolution becomes more accurate. It is then possible to produce high-resolution lines by using smaller variances. For example, using 10^5 zeros, lines with a variance $\sigma = 0.01$ were produced. As a final example, Eq. (2.12) was computed using 10^6 zeros on the interval $[5000, 5100]$. This is shown in Fig. 2.7.

It would be useful to know how many primes can be resolved using a prescribed number of zeros. In the present scheme, we simply observe where the lines of the original signal develop a sufficiently large width. The important criterion here is that all linewidths should be at least smaller than the mean spacing between all integer powers of primes in the interval of interest. Of course, the width of any line is related to the number of terms used in truncating the series. Although this relationship can be determined, there is still the problem that all the lines have different shapes. Thus, it is more useful to determine, for what values of x the truncated formula can no longer produce lines of a specific uniform shape.

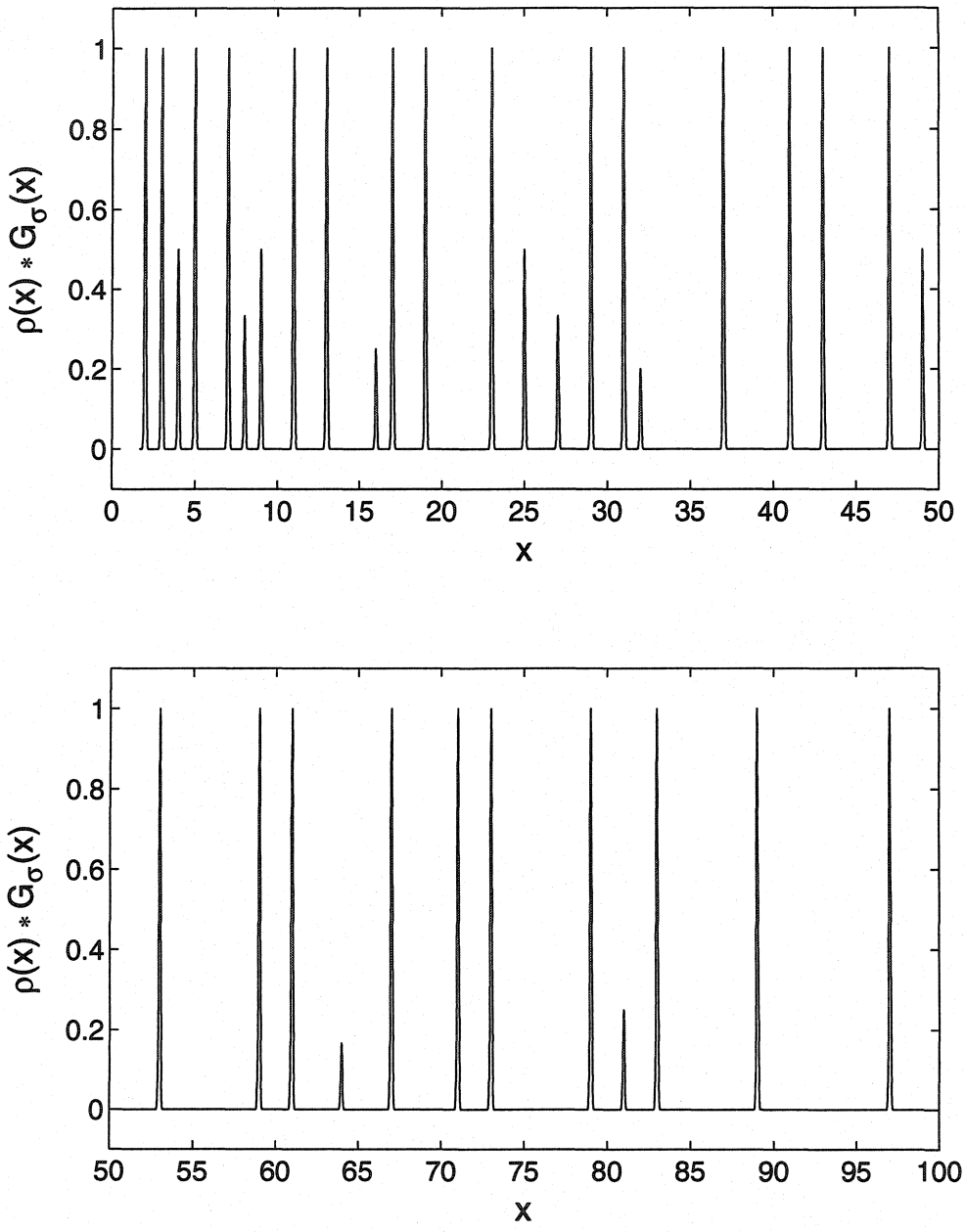

Figure 2.6: Gaussian-convolved signal [Eq. (2.12)], using the first 10^4 zeros and $\sigma = 0.05$. The range is the same as in Fig. 2.4. Note that lines with height less than unity occur at integer powers of primes p^n and have height $1/n$ (for example, the line at $2^6 = 64$ has height $1/6 = 0.1\dot{6}$).

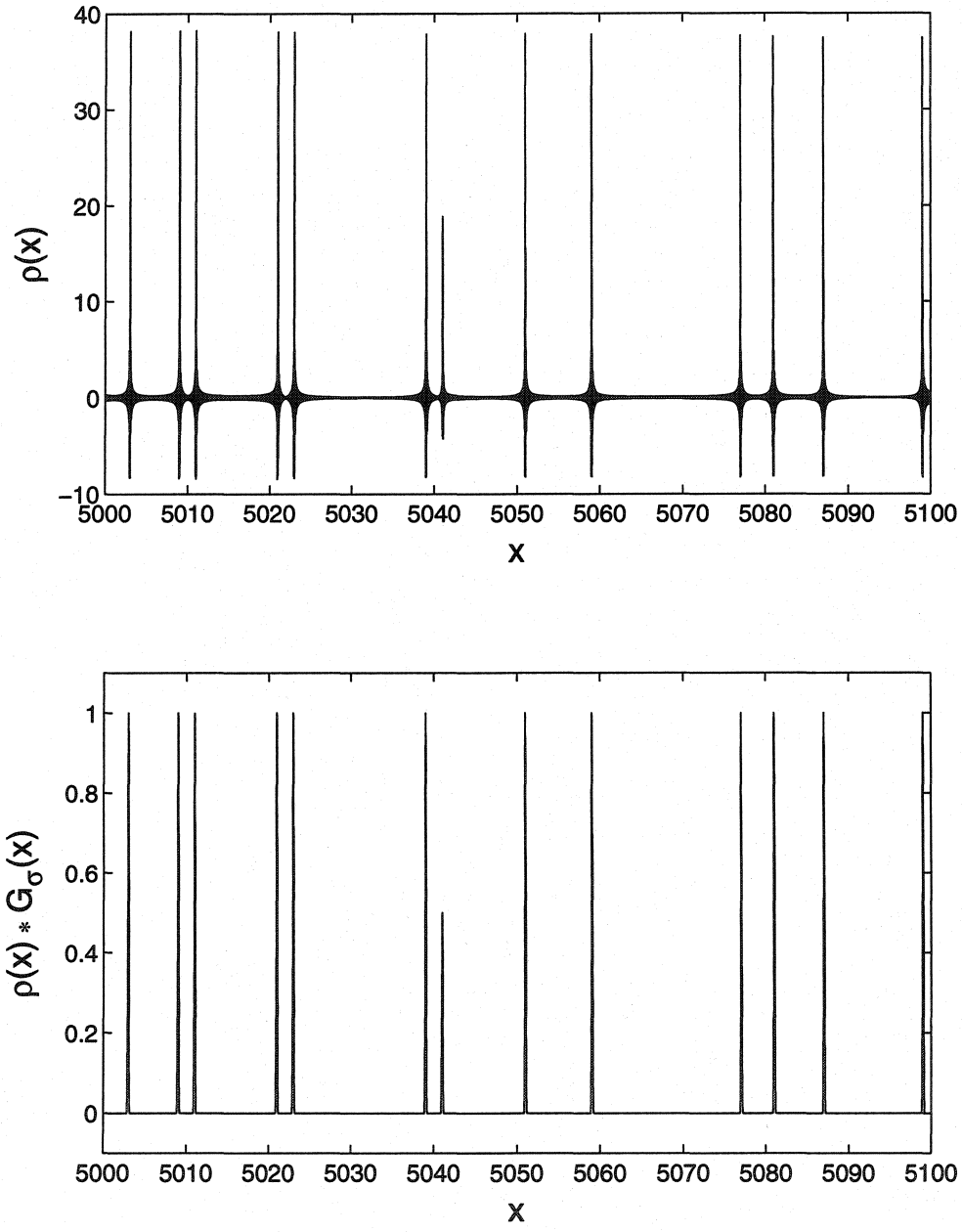

Figure 2.7: Riemann's formula for $x \in [5000, 5100]$ using the first 10^6 zeros. The upper panel shows the original signal [Eq. (2.10)], and the bottom shows the Gaussian-convolved signal [Eq. (2.12)] with $\sigma = 0.05$. The line with height $1/2$ occurs at $5041 = 71^2$.

Sum rule and numerical convergence

The convergence of the series can be analyzed using a more controlled application of the convolution procedure described above. The general idea is to construct a series ("sum rule") that absolutely converges to a "coarse-grained" version of the exact density. This density is obtained by replacing all spikes of the exact density by smooth peaked functions. An immediate advantage is improved convergence, since it is easier to reproduce the well defined *smooth* peaked functions of a coarse-grained density using a truncated sum rule than it is to reproduce spikes using the original truncated series. However, the more important reason for using a sum rule here is to *control* the convergence of the series. This will become evident after the sum rule is given. The sum rule itself is obtained from a direct convolution of the original series with a "smoothing function", that is, some smooth function whose Fourier coefficients rapidly decrease. (Since the original series consists of cosines, the resulting integral is essentially a cosine transform of the smoothing function.)

The above discussion is quite general. This idea is now connected with the numerical calculations described above. Assume the coarse-grained density consists of a set of Gaussian functions of variance σ centered at each prime (and its integer powers) with heights equal to unity (or the reciprocal of the integer power). We want to construct a series as described above, which converges to this density, that is, we want to find a Gaussian sum rule for Riemann's series. To do this, we convolve Riemann's series term-by-term with a Gaussian smoothing function. For the following calculation, we will define $S_\alpha(x) = \alpha \ln x$, and $A(x) = -2/\sqrt{x} \ln x$. Then, we can write Riemann's formula as $\tilde{\rho}(x) = A(x) \sum_\alpha \mathrm{Re}\{\exp[iS_\alpha(x)]\}$. The Gaussian sum rule is

$$\begin{aligned} \tilde{\rho}_\sigma(x) &= \tilde{\rho}(x) * G_\sigma(x) = \int_{-\infty}^{\infty} \tilde{\rho}(x') e^{-(x-x')^2/2\sigma^2} \mathrm{d}x' \\ &= \sum_\alpha \mathrm{Re}\left\{ \int_{-\infty}^{\infty} A(x') e^{iS_\alpha(x')} e^{-(x-x')^2/2\sigma^2} \mathrm{d}x' \right\}, \qquad x > 1. \end{aligned} \tag{2.14}$$

For $\sigma \leq \sigma_{\max}$, the Gaussian rapidly decays to zero. This implies that the main contribution to the integral comes from a small interval centered about $x' = x$. Elsewhere, the integrand is practically zero. Thus, we make two approximations to proceed further. First, the amplitude function $A(x')$ changes very slowly and on the small interval of interest $A(x') \approx A(x)$. Second, the phase function $S_\alpha(x')$ can be replaced by its Taylor series expansion about $x' = x$: $S_\alpha(x') = S_\alpha(x) + S'_\alpha(x)(x' - x) + \cdots$. If we retain the leading-order term

only,

$$\begin{aligned}\tilde{\rho}_\sigma(x) &\approx A(x)\sum_\alpha \mathrm{Re}\left\{\int_{-\infty}^{\infty} e^{i[S_\alpha(x)+S'_\alpha(x)(x'-x)]}e^{-(x-x')^2/2\sigma^2}\mathrm{d}x'\right\} \\ &= A(x)\sum_\alpha \mathrm{Re}\left\{e^{i[S_\alpha(x)-xS'_\alpha(x)]}e^{-x^2/2\sigma^2}\int_{-\infty}^{\infty} e^{-[x'^2-(2x+2i\sigma^2 S'_\alpha(x))x']/2\sigma^2}\mathrm{d}x'\right\} \\ &= \sqrt{2\pi}\sigma A(x)\sum_\alpha e^{-\sigma^2 S'^2_\alpha(x)/2}\mathrm{Re}\left\{e^{iS_\alpha(x)}\right\}, \end{aligned} \tag{2.15}$$

where we have used the standard result for the Gaussian integral[5]. Finally, the Gaussian sum rule for Riemann's series is

$$\tilde{\rho}_\sigma(x) = -\frac{2\sqrt{2\pi}\sigma}{\sqrt{x}\ln x}\sum_\alpha e^{-\sigma^2\alpha^2/2x^2}\cos(\alpha\ln x). \tag{2.16}$$

This sum rule explicitly shows the effect of convolution on the series; each term is modulated by an exponential factor. This factor essentially controls the convergence of the series for all values of x. Although the original series is conditionally convergent, as long as the correct ordering is used, this sum rule is *absolutely* convergent. As stated above, we seek a relation between the maximum zero included in the sum and the maximum prime that can be resolved. One way to determine this is as follows. First, specify the value of the largest zero $\alpha_{\max}$, and include all zeros $\alpha \le \alpha_{\max}$. Then, there exists a set of values $x < x_{\max}$ for which the exponential factor falls below some threshold parameter ϵ. This condition immediately gives the simple relation

$$x_{\max} = \left[\frac{\sigma}{\sqrt{-2\ln(\epsilon)}}\right]\alpha_{\max}, \tag{2.17}$$

where $0 < \epsilon < M$. For $\alpha > \alpha_{\max}$ and $x \le x_{\max}$, all terms are exponentially smaller than ϵ and are thus numerically insignificant. The choice of the parameter ϵ depends on the desired precision of a resolved line. An upper bound M for the parameter is the value of the exponential factor $(e^{-3/2})$ at its inflection point[6] $x_I = (1/\sqrt{3})\sigma\alpha$. This implies $x_{\max} < x_I$. The lower bound can be as small as machine zero (for example, 10^{-16}). However, there is

[5] $\int_{-\infty}^{\infty} e^{-ax'^2+bx'}\mathrm{d}x' = \sqrt{\frac{\pi}{a}}e^{b^2/4a}$ $(a > 0)$. It is not necessary to evaluate the convolution integral over the interval $(1,\infty)$. If we insisted on doing so, the integral at the end is rather $\int_1^{\infty} e^{-ax'^2+bx'}\mathrm{d}x' = \sqrt{\frac{\pi}{4a}}e^{b^2/4a}\mathrm{erfc}\left(-\frac{b}{2\sqrt{a}}+\sqrt{a}\right)$. The resulting sum rule is slightly more complicated, but the difference is insignificant when σ is small.

[6] For smaller values of x, a more accurate upper bound is given by the inflection point of $x^{-1/2}e^{-\sigma^2\alpha^2/2x^2}$ which is $\frac{\sqrt{2(12-3\sqrt{13})}}{3}\sigma\alpha$. If the logarithmic term is also included, the inflection points are roots of a transcendental equation.

no reason for such an extreme choice since the primary interest here is in determining where numerical errors become significant (i.e. where lines are no longer *visibly* resolved and the intensities are erroneous by more than 1%). Of course, higher precision can be imposed at the cost of resolving fewer primes. But, since the improved precision will not be apparent in the graph of $\rho_\sigma(x)$, there is no compelling reason to choose exceedingly small values. A convenient choice is $\epsilon = e^{-7/2}$.

A few examples are now provided to illustrate the utility of relation (2.17). As the first example, take $\alpha_{\max} \doteq 9878$, which is the 10^4th zero. Using the above formula ($\sigma = 0.1$) yields $x_{\max} \doteq 373$. In Fig. 2.8, Eq. (2.16) was evaluated using the first 10^4 zeros (and the smooth term included). We can clearly see significant errors for $x > 400$. As the second example, take $\alpha_{\max} \doteq 74921$ (the 10^5th zero). The formula then gives $x_{\max} \doteq 2832$. In Fig. 2.9, Eq. (2.16) was truncated at this value of $\alpha_{\max}$, and we can observe significant errors for $x > 2900$.

An additional benefit of the sum rule is that it gives an immediate measure of the error incurred from truncation. The largest error occurs in the vicinity of $x_{\max}$, where there are contributions $O(\epsilon)$ that have been excluded. For all other values of $x < x_{\max}$, the excluded terms are exponentially smaller. Of course, we have complete control of this error through the freedom in specifying ϵ. The error in the original truncated series is not immediately obvious, but it could be estimated using more rigorous analysis.

2.3.3 Berry's formula for the density of Riemann zeros

It is worth the effort to also check that the line intensities of the density of the Riemann zeros are correct. The oscillating part of the density of Riemann zeros is given by the divergent series [67]

$$\tilde{\rho}(E) = -\frac{1}{\pi} \sum_p \sum_{n=1}^{\infty} \frac{\ln p}{p^{n/2}} \cos(E \ln p^n). \tag{2.18}$$

If this is a genuine trace formula for the Riemann zeros, then the most natural way to truncate the series is by "orbit length". (It is incorrect to arbitrarily specify an upper truncation limit for each sum. Such a truncation is inconsistent since it includes higher harmonics while excluding some lower harmonics.) Unfortunately, length truncation of Eq. (2.18) has not had much numerical success. It has already been pointed out that, as more "periodic orbits" (prime numbers) are included in the sum, the peaks of the level

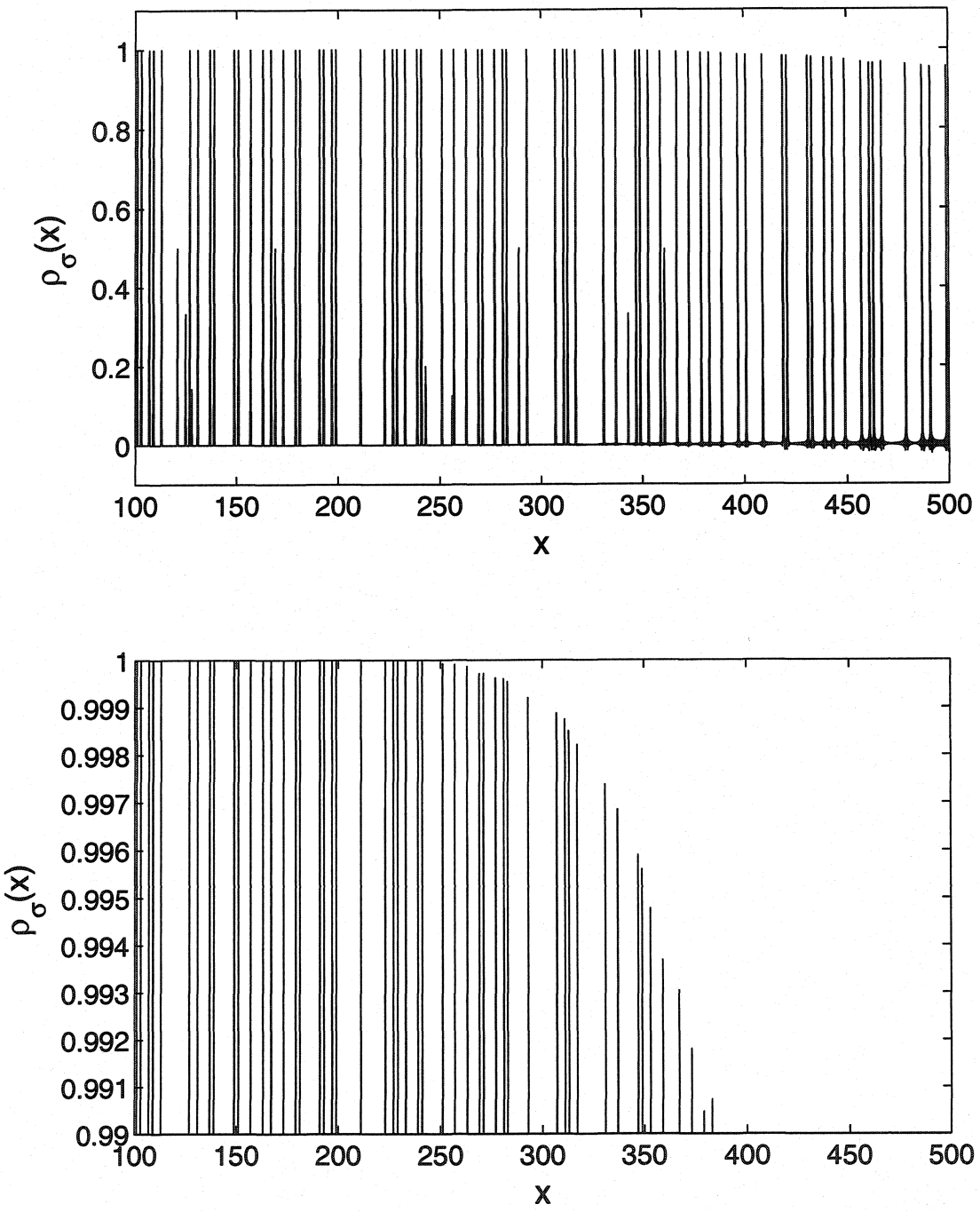

Figure 2.8: The sum rule (2.16), using the first 10^4 zeros and $\sigma = 0.1$. The lower window shows a closer view of the lines in the interval $0.99 < \rho_\sigma(x) < 1$. Formula (2.17) indicates that for $x \leq x_{\max} \doteq 373$, all lines should be resolved and intensities should have errors less than $O(\epsilon) \sim \sigma^2 = 0.01$.

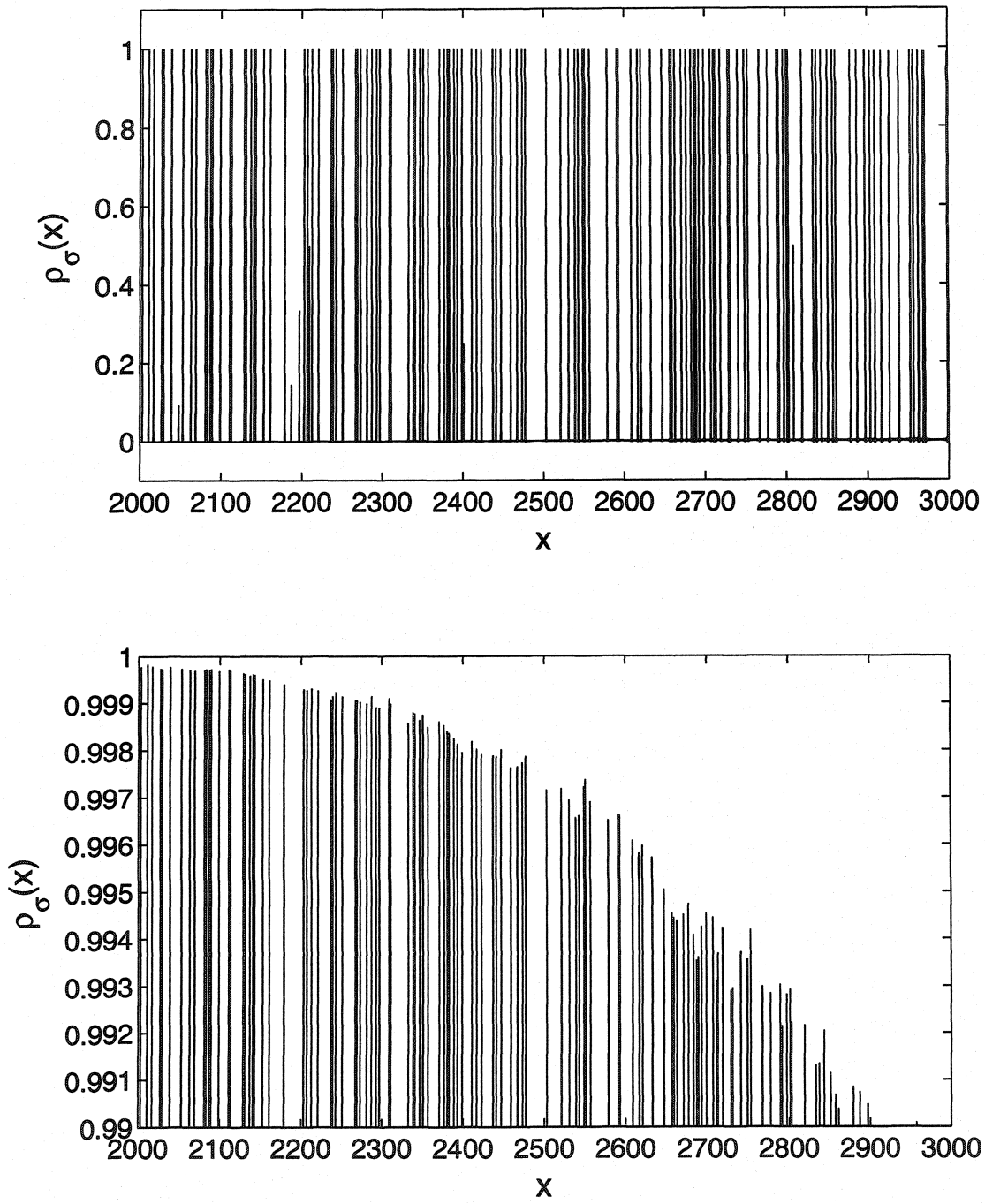

Figure 2.9: The sum rule (2.16), using the first 10^5 zeros and $\sigma = 0.1$. The lower window shows a closer view of the lines in the interval $0.99 < \rho_\sigma(x) < 1$. Formula (2.17) indicates that for $x \leq x_{\max} \doteq 2832$, all lines should be resolved and intensities should have errors less than $O(\epsilon) \sim \sigma^2 = 0.01$.

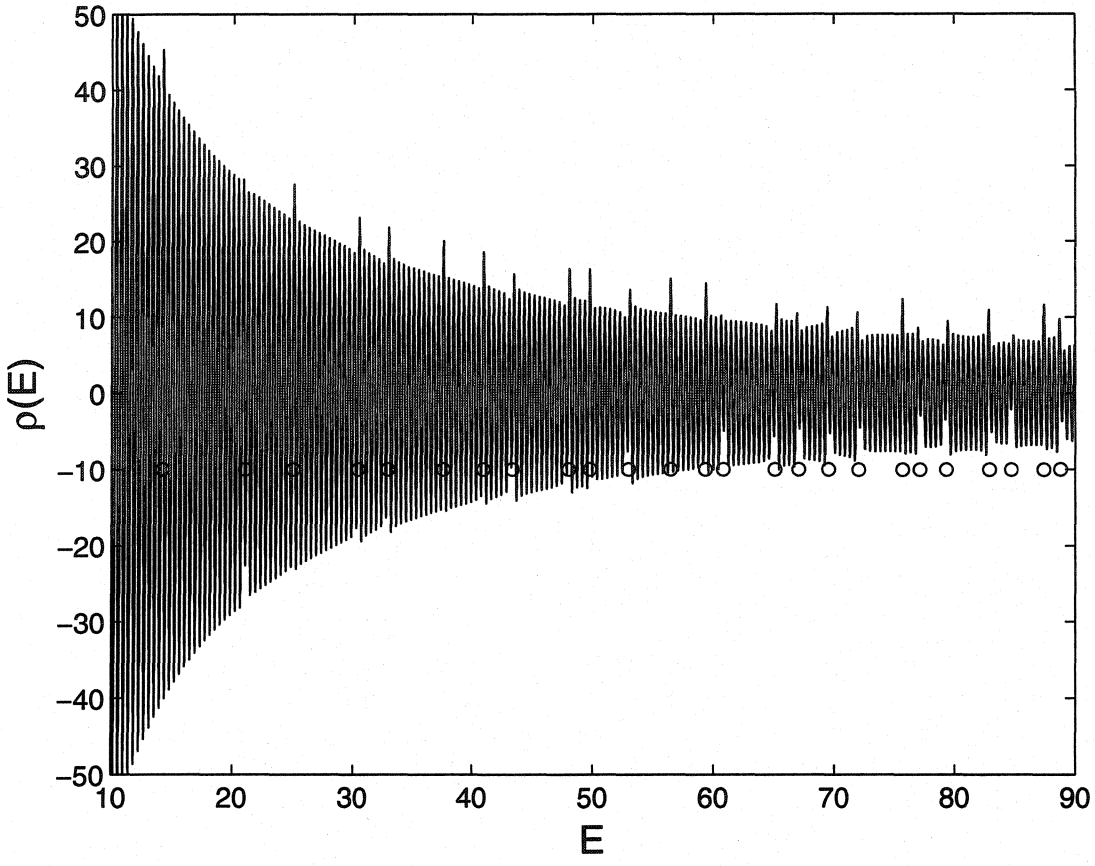

Figure 2.10: The density of Riemann zeros using 235,220 terms of Eq. (2.18). The series is truncated by "orbit length", that is, all orbits $\gamma = (p, n)$ with length $L_\gamma = n \ln p < 15$ are included in the sum. Circles indicate the positions of Riemann zeros. The leading-order smooth term is added to the truncated series.

density become submerged in oscillations [92]. An example is shown in Fig. 2.10. A length cutoff $L_{\max} = 15$ is prescribed, and all terms with $p \leq p_{\max} = 3\ 269\ 011$ and $n \leq n_{\max} = 22$ are included. (In this case, there are a total of 235,220 terms included in the sum.) The truncation limits are determined from the conditions $\ln p_{\max} = L_{\max}$ and $n_{\max} = L_{\max}/\ln 2$. Note that the leading-order term of the smooth component $\bar{\rho}(E) = \ln(E/2\pi)/2\pi$ is also included.

Clearly, the formula is not generating narrow peaks at the positions of the zeros. Thus, it seems pointless to proceed with numerical convolution for the purpose of checking the intensities. Nevertheless, it is still worthwhile to try the Gaussian sum rule (2.15) with

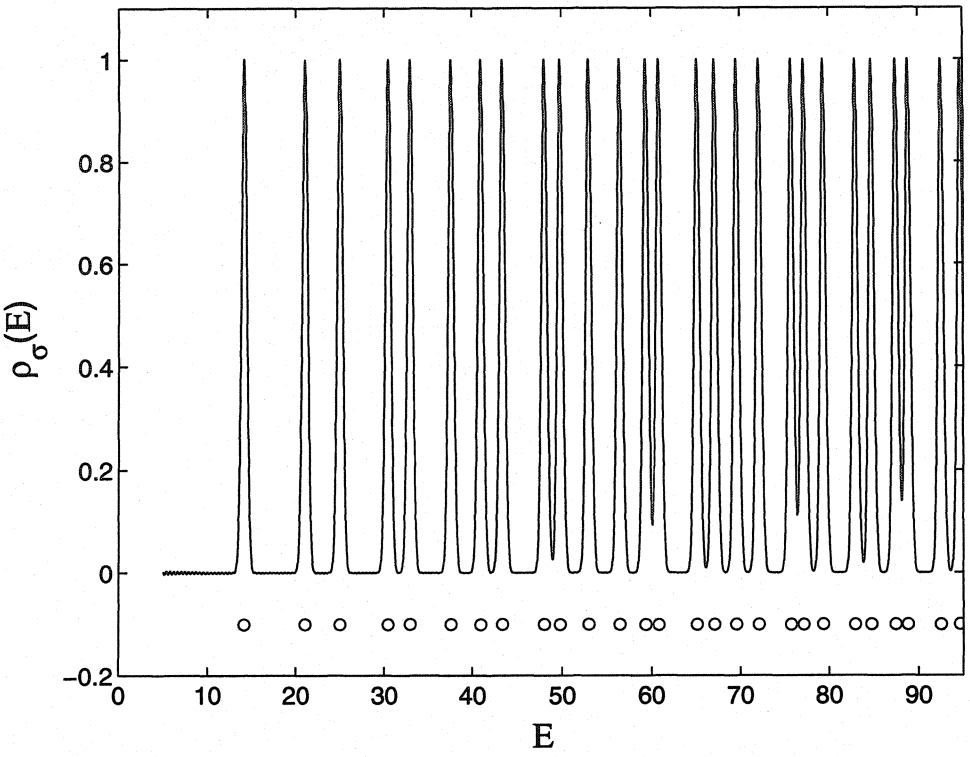

Figure 2.11: The density of Riemann zeros using 235,220 terms of the sum rule (2.19). The series is truncated at $L_{\max} = 15$ and $\sigma = 0.3$.

$\gamma = (p, n)$, $A_\gamma(E) = -(\ln p/\pi p^{n/2}) \equiv A_\gamma$, $S_\gamma(E) = E \ln p^n$, and $S'_\gamma(E) = \ln p^n \equiv S'_\gamma$. The Gaussian sum rule for the trace formula of the Riemann zeros is then

$$\tilde{\rho}_\sigma(E) = -\sqrt{\frac{2}{\pi}}\sigma \sum_p \sum_{n=1}^{\infty} \frac{\ln p}{p^{n/2}} \exp\left[-\frac{(\sigma \ln p^n)^2}{2}\right] \cos(E \ln p^n). \tag{2.19}$$

If this series is truncated at $L_{\max} = 15$ and $\sigma = 0.3$, then the density of Riemann zeros is as shown in Fig. 2.11. For orbits γ with length $L_\gamma > 15$, the Gaussian factor becomes less than 10^{-4}. Clearly, there are Gaussian lines of variance σ and the correct unit heights. It is also interesting that the sum rule continues to correctly generate lines with unit degeneracy at higher zeros. Of course, many lines are not fully resolved since σ is much larger than the mean spacing of the zeros. Whenever the spacing between zeros is sufficiently less than σ, the degeneracies will be greater than unity, but still consistent with the cumulative density of states $N(E)$.

2.3.4 Number theory, quantum chaos, and semiclassics

By writing $\zeta(\beta) = \zeta(s+it) = |\zeta(s+it)| \exp[-i\theta_s(t)]$, we see that all the information about the zeros along the $t-$axis is contained in the phase $\theta_s(t)$. This phase has to jump by π to accommodate the sign change in ζ at every zero, and it can be shown that the oscillating part of the density of the zeros on the critical line is proportional to the derivative of the imaginary part of $\ln\zeta(\beta)$ with respect to t [7]. On the other hand, we see from Eq. (2.9) that the appropriate contour integral over $\ln\zeta(\beta)$ also yields $\rho(x)$. Thus, the phase of the zeta function, as defined above, connects the Riemann zeros to the primes.

As mentioned above, if the series is truncated, the signal gradually dies out as x increases. This can be understood by noting that due to the logarithmic dependence, each term produces an oscillation whose period continually increases while its amplitude decays. Clearly, more high frequency (large α) terms are required for sufficient constructive interference. This explains the fact that lines at small values of x are resolved more quickly than at larger values. Although the higher frequency terms are responsible for short-range oscillations and one could imagine exclusive use of those terms rather than lower frequency terms, the difficulty is the conditional convergence of the series and the fact that all the terms are equally important. Unfortunately, this implies that Riemann's formula is impractical for resolving lines at large primes. This is also consistent with Eq. (2.17). If one is interested in using Riemann's series to find large primes in some window of interest $\mathfrak{X} = [x_{\min}, x_{\max}]$, then one requires an accurate knowledge of all zeros $\alpha \lesssim x_{\max}$, even for a low resolution spectrum. So, for example, suppose one seeks primes of the order of $10^{250\ 000}$, then all zeros $\alpha \lesssim 10^{250\ 000}$ must be available, which is itself a formidable computational problem.

Remember that Riemann's formula is correct only if the Riemann hypothesis is true. Otherwise, if a pair of zeros occur at $\beta_\pm = \eta \pm i\alpha$, the factor $x^{1/2}$ in the denominator of the oscillating term of Eq. (2.10) should be replaced by $x^{(1-\eta)}$ [85]. An interesting numerical experiment is to move the zeros off the critical line, that is, to arbitrarily change their real parts. This procedure still produces lines at integer powers of primes, but the relative intensities are incorrect. This is interesting since it demonstrates that the location of the primes depends only on the imaginary part of the zero. The real part only affects the intensities, which cannot be immediately identified from a direct evaluation of the series.

It is natural to compare the oscillating part of the density $\tilde{\rho}(x)$ with the semiclassical trace formula [2, 9] of a dynamical system. We could identify α as an orbit label, one

for each zero of the zeta function, and x as the single-particle energy variable. Then, $\rho(x)$ in Eq. (2.10) may be interpreted as the density of states, as a function of energy with the first term on the RHS corresponding to the smooth Thomas-Fermi (TF) contribution[7]. In the oscillating part, the argument $\alpha \ln x$ of the cosine term should then correspond to the action $S_\alpha(x)$ of orbit α. Note, however, that there are no implicit repetition indices in Eq. (2.10), thereby implying that even if we give a dynamical interpretation to $\tilde{\rho}(x)$, the orbits are not periodic. This is in direct contrast to the trace formula for the Riemann zeros, in which the orbits are periodic with primitive period $\ln p$ for each prime [67]. The most striking feature is that the amplitude has no α dependence. Even oscillatory contributions to the density of states from nonperiodic trajectories usually have amplitudes that depend on the orbit [88]. In the event that there is a fortuitous cancellation of the index α, it is unlikely that the energy dependence in the denominator of the oscillating term as well as the TF term can then be generated consistently by the same Hamiltonian. Consequently, Riemann's formula is not a trace formula of dynamical origin.

With regard to spectral statistics, it is well known that nearest-neighbor spacings (NNS) [89] of the Riemann zeros obey the GUE distribution of Random Matrix Theory, characteristic of a chaotic quantum system without time-reversal symmetry [90, 91]. The same zeros also generate the primes through Riemann's formula (2.10). As mentioned earlier, the NNS distribution of the primes is Poisson-like [84], with some level repulsion, which, if at all of dynamical origin, suggests near-integrability [9]. Thus, it is quite remarkable that the highly correlated sequence of the zeros can interfere to produce the almost uncorrelated sequence of the primes.

In conclusion, it was demonstrated that the spectrum of the primes and their integer powers can be accurately generated from a sum of periodic terms, each term involving a complex zero of the zeta function. This is in the spirit of periodic orbit quantization, where the individual levels of a quantum spectrum may be resolved from a sum of oscillatory terms, each arising from periodic orbits. Nevertheless, Riemann's formula is not a trace formula. However, this does not imply that there is no such formula, and it would still be interesting to understand the spectrum of the primes in terms of periodic orbits. This could provide insight into the structure of a possible trace formula for the primes. If this formula could be found, the remaining challenge would be to obtain the corresponding Hamiltonian.

[7]The second smooth term on the RHS of Eq. (2.10) arises from the trivial zeros, and may not be included as part of a TF term.

Chapter 3

Noninteracting Systems

The semiclassical analysis of noninteracting many-body systems is quite subtle. The standard Gutzwiller trace formula for isolated orbits does not apply since the energy of each particle is separately conserved causing the periodic orbits to occur in continuous families. The case of two noninteracting identical particles has been previously studied using a convolution method [35], which involves the asymptotic analysis of convolution integrals that arise in a formal decomposition of the semiclassical approximation to the two-particle density of states. In principle, albeit tedious, this technique can be generalized to more than two identical particles (see, for example, Appendix C). However, in this chapter, a more fundamental semiclassical theory for noninteracting many-body systems is developed using the formalism of Creagh and Littlejohn [33], who have studied semiclassical dynamics in the presence of continuous symmetries. This approach recovers the results of the convolution method, but also has several conceptual advantages. For example, the issue of spurious endpoint contributions from convolution integrals does not arise and therefore need not be explained away. (The other advantages will become clear as we proceed.) However, the ultimate motivation is that the convolution method cannot be used when there are interactions between the particles, whereas the analysis of this chapter can be extended to include interactions (see Chapter 5). Numerical studies of the two- and three-particle cardioid billiard are used to explicitly illustrate and test the results of the theory.

3.1 Two Noninteracting Identical Particles

3.1.1 Quantum density of states

The quantum Hamiltonian for two identical noninteracting particles, a and b, is

$$\hat{H} = \hat{h}(\hat{z}_a) + \hat{h}(\hat{z}_b), \tag{3.1}$$

where $\hat{z}_{a/b}$ denote the set of operators $(\hat{x}_{a/b}, \hat{p}_{a/b})$ and $\hat{h}$ is a one-particle Hamiltonian. The full Hamiltonian (3.1) is invariant under the unitary transformation $\hat{U}$ that exchanges a and b. The single-particle energies and eigenstates are defined by

$$\hat{h}|j\rangle = \varepsilon_j|j\rangle. \tag{3.2}$$

Then, the two-particle energies and eigenstates are $E_{ij} = \varepsilon_i + \varepsilon_j$ and $|ij\rangle$ so that

$$\hat{H}|ij\rangle = E_{ij}|ij\rangle. \tag{3.3}$$

The one- and two-particle densities of states are

$$\rho_1(\varepsilon) = \sum_j \delta(\varepsilon - \varepsilon_j), \tag{3.4a}$$

$$\rho_2(E) = \sum_{i,j} \delta(E - E_{ij}), \tag{3.4b}$$

and these are related by the convolution identity (see Ref. [93])

$$\rho_2(E) = (\rho_1 * \rho_1)(E). \tag{3.5}$$

A useful result is the relation between the density of states and the trace of the energy Green function or resolvant $g(E) = \mathrm{Tr}(\hat{G}(E))$, where $\hat{G}(E) = 1/(E - \hat{H})$ is the one-sided Fourier transform of the quantum propagator. In terms of the resolvant,

$$\rho(E) = -\frac{1}{\pi}\mathrm{Im}\left\{g(E + i\epsilon)\right\}, \tag{3.6}$$

and this applies to either the one- or two-particle density of states as long as the appropriate resolvant is used on the right-hand side of Eq. (3.6). In the limit $\epsilon \to 0^+$, the exact density of states is recovered [7]. Henceforth, the $i\epsilon$ will be implicit.

3.1.2 Semiclassical formulation

As stated above, the density of states for two noninteracting particles is the autoconvolution of the one-particle density of states (3.5). Using Eq. (1.1)

$$\rho_2(E) = (\rho_1 * \rho_1)(E) = \bar{\rho}_2(E) + \tilde{\rho}_2(E), \tag{3.7}$$

where

$$\bar{\rho}_2(E) = (\bar{\rho}_1 * \bar{\rho}_1)(E), \tag{3.8a}$$

$$\tilde{\rho}_2(E) = 2(\bar{\rho}_1 * \tilde{\rho}_1)(E) + (\tilde{\rho}_1 * \tilde{\rho}_1)(E). \tag{3.8b}$$

The mixed term $2(\bar{\rho}_1 * \tilde{\rho}_1)(E)$ also belongs to the oscillating component of $\rho_2(E)$. This is because an asymptotic endpoint analysis of the convolution integral results in an oscillatory function as shown in Ref. [35], where all components have been evaluated and given explicit semiclassical interpretations in terms of one- and two-particle dynamics that support this decomposition[1].

The (leading-order) trace formulas for $(\bar{\rho}_1 * \tilde{\rho}_1)(E)$ and $(\tilde{\rho}_1 * \tilde{\rho}_1)(E)$ (see Ref. [35]) can also be understood from a semiclassical analysis in the full phase space. This analysis is not only more fundamental, but it is also necessary if we want to include interparticle interactions since the particle dynamics then become coupled and we can no longer make use of calculations that involve the individual one-particle phase spaces. In the following subsections, trace formulas for the total density of states are derived from semiclassical calculations in the full two-particle phase space. (The symmetrized densities are considered in the next chapter.) Since the main objective is the extension of the Gutzwiller theory, the focus is on the fluctuating part of the density of states. However, since the smooth part is important for numerical purposes, a discussion of the two-particle Thomas-Fermi term is given in Appendix A.1. To calculate the fluctuating part of the total density of states, we need to find all periodic orbits in the full phase space at a specified energy E.

3.1.3 Two-particle dynamics

The two identical particles, a and b, evolve independently in their own one-particle configuration space, which has dimension d so that the one-particle phase spaces have di-

[1]There is an analogous decomposition for nonidentical particles. However, the interpretation of the various terms does not apply to nonidentical particles in a harmonic oscillator. See Appendix C.1.

mension $2d$. The full two-particle configuration space has dimension $2d$, and the corresponding phase space has dimension $4d$. The symbol $\mathbf{z}$ collectively denotes these $4d$ phase space coordinates, and $\mathbf{z} = (\mathbf{z}_a, \mathbf{z}_b)$, where $\mathbf{z}_{a/b}$ denote the $2d$-dimensional one-particle phase space coordinates of each particle. Recall that dynamics in the full phase space consist of each particle evolving separately in its own phase space. The dynamics of $\mathbf{z}$ are defined through one-particle dynamics by $\Phi_t\mathbf{z} = (\phi_t\mathbf{z}_a, \phi_t\mathbf{z}_b)$, where ϕ_t is the flow for one particle. The (noninteracting) two-particle Hamiltonian is $H(\mathbf{z}) = h(\mathbf{z}_a) + h(\mathbf{z}_b)$, where $h(\mathbf{z}_{a/b})$ is a one-particle Hamiltonian.

We seek periodic orbits with phase space coordinates $\mathbf{z}'$ such that $\Phi_T\mathbf{z}' = \mathbf{z}'$ for some period T. This is possible if the two particles are on (generally distinct) periodic orbits with the same period. In general, two arbitrary periodic orbits will have different periods. However, there is a parameter which we can vary, namely, the way in which the total energy is partitioned between the two particles. Generally, we can find an energy E_a (and $E_b = E - E_a$) such that the two periods are the same. We will assume henceforth that there is only one energy E_a for which there is a solution. (This assumption can be relaxed at the cost of heavier notation.) There is another way to have a periodic orbit in the full phase space; one particle can evolve dynamically on a periodic orbit with all of the energy while the other is stationary at a fixed point of the potential. This is discussed later.

Dynamical periodic orbits

If *both* particles are on periodic orbits, the full phase space periodic orbit will be called a *dynamical* periodic orbit. Note that these orbits occur in continuous families. To see this, imagine that a full phase space periodic orbit consists of one particle on a periodic orbit γ_a and the other particle on a distinct periodic orbit γ_b (see Fig. 3.1) and that the energy partition is such that both orbits have the same period T. We have complete freedom in specifying which points on the respective orbits we choose as initial conditions. Given that we define $t = 0$ to be when particle b is at some specified point on γ_b, we can then vary the position of particle a on γ_a. By changing the initial position of particle a along the orbit, we map out a continuous family of congruent periodic orbits.

This can be formalized as follows. In addition to the total Hamiltonian H, there is a second constant of motion $J = h(\mathbf{z}_a)$ in involution with H. It generates time translations of particle a while leaving particle b fixed. (In fact, J can be chosen as any linear combination

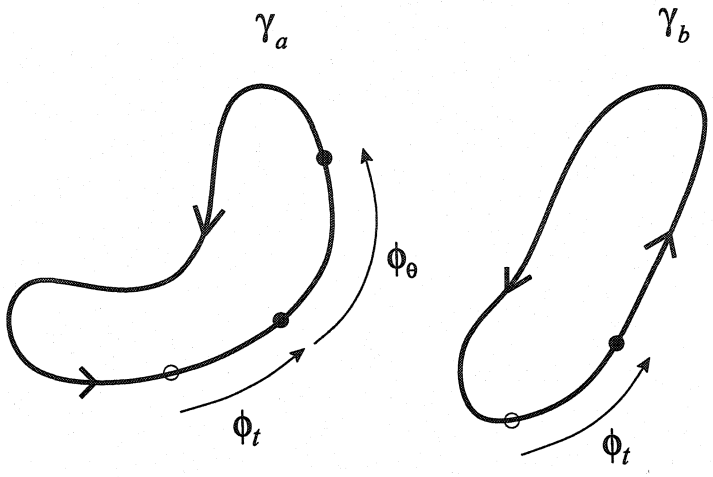

Figure 3.1: Two periodic orbits γ_a and γ_b, which constitute a periodic orbit Γ of the full phase space. The full Hamiltonian $H(\mathbf{z}_a, \mathbf{z}_b)$ generates time translations for both particles (as denoted by the single-particle flow ϕ_t acting on both particles) while the single-particle Hamiltonian $J = h(\mathbf{z}_a)$ generates time translations for particle a while leaving particle b fixed (as denoted by the single-particle flow ϕ_θ acting on particle a only). The flows generated by H and J are Φ_t and Ψ_θ, respectively. A combination of these two flows [see Eq. (3.9)] is shown here.

of $h(\mathbf{z}_a)$ and $h(\mathbf{z}_b)$ as long as it is independent of H.) Flows generated by J are denoted by Ψ_θ and are mapped in the full phase space as follows: $\Psi_\theta \mathbf{z} = (\phi_\theta \mathbf{z}_a, \mathbf{z}_b)$. The symmetry parameter θ is conjugate to J and has the dimension and interpretation of time. However, since it only measures the evolution of particle a, it is not time in the usual sense. A combination of flows in H and J is

$$\Phi_t \Psi_\theta \mathbf{z} = (\phi_t \phi_\theta \mathbf{z}_a, \phi_t \mathbf{z}_b) = (\phi_{t+\theta} \mathbf{z}_a, \phi_t \mathbf{z}_b). \tag{3.9}$$

Since Ψ_θ and Φ_t commute and separately conserve both H and J, the surface mapped out by these flows has constant H and J (i.e. $H = E$ and $J = E_a$) . Starting at some point on the full phase space periodic orbit, flows in H and J map out a two-dimensional torus. This means there is a 1-parameter degenerate family of periodic orbits (the other dimension is parametrized by time and is present even in the case of isolated orbits). Therefore, we cannot use the Gutzwiller trace formula for isolated orbits since it will give a spurious infinity. Due to the continuous family, there is one fewer stationary phase integrals to do when evaluating the trace so that this family of orbits contributes $O(1/\sqrt{\hbar})$ more strongly than an isolated orbit, and the calculation of its amplitude must be performed carefully.

Hereafter, it is assumed that there are no symmetries other than J so that all periodic orbits of the one-particle phase space are isolated. The flow directions generated by H and J are stable as are the two directions transverse to the constant H and J surfaces. Thus, there are four directions of neutral stability in phase space. The remaining $(4d-4)$ directions decompose into separate subspaces of dimension $(2d-2)$ within each of which there are the standard symplectic possibilities for stability.

In general, the leading-order contribution of one f-parameter family of orbits (generated by Abelian symmetry) to the resolvant is [33]

$$\tilde{g}_\Gamma(E) = \frac{1}{i\hbar}\frac{1}{(2\pi\hbar)^{f/2}}\frac{T_\Gamma^0 V_\Gamma^0}{\sqrt{\left|\det\left(\frac{\partial\Theta}{\partial J}\right)_\Gamma\right|\left|\det\left(\tilde{M}_\Gamma - I\right)\right|}}\exp\left[i\left(\frac{S_\Gamma(E)}{\hbar} - (\mu-\delta)_\Gamma\frac{\pi}{2} - f\frac{\pi}{4}\right)\right]. \tag{3.10}$$

This contribution is $O(1/\hbar^{f/2})$ stronger than an isolated periodic orbit. As mentioned above, every constant of motion implies one fewer stationary phase integral and therefore f fewer powers of $\sqrt{\hbar}$ in the prefactor. For a similar reason, there is an additional phase factor of $-f\pi/4$. The total contribution to the resolvant is a sum over all families of periodic orbits, the capital Γ indicating that these are indeed families and not isolated orbits as in the more familiar Gutzwiller trace formula. For the case of two noninteracting particles, the sum over Γ can be expressed as a double sum over γ_a and γ_b indicating the periodic orbits on which the particles are evolving. The various factors in Eq. (3.10) are now described in detail for the present situation ($f=1$).

The volume term $T_\Gamma^0 V_\Gamma^0$ is the integral over the flows generated by H and J [i.e. $\oint_\Gamma dt d\theta$], integrated over the periodic orbit family. The time integral gives the period of the family $T_\Gamma = T_{\gamma_a}(E_a) = T_{\gamma_b}(E_b = E - E_a) \equiv T$ while the θ integral gives $V_\Gamma = T_{\gamma_a}(E_a)$ since a flow in J by that amount returns particle a to where it began. (Hence, the initial phase space coordinate is mapped back to itself under the dynamics.) However, there can be discrete symmetries such that a combination of flows in H and J for less than T restores the initial conditions. This situation occurs when one or both particles are on a repetition of some primitive periodic orbit. To see this, suppose that particle a is on the n_ath repetition of its orbit while particle b is on the n_bth repetition of its orbit. Then, the torus is partitioned into $n_a n_b$ equivalent segments and the *primitive* volume term is $T_\Gamma^0 V_\Gamma^0 = T_\Gamma V_\Gamma / n_a n_b$. The full periods are defined through the primitive periods by $T_{\gamma_a}(E_a) = n_a T^0_{\gamma_a}(E_a)$, and similarly for particle b. Thus, $T_\Gamma^0 V_\Gamma^0 = T^0_{\gamma_a}(E_a) T^0_{\gamma_b}(E_b = E - E_a)$, which is the product of

the primitive periods.

The matrix $\tilde{M}_\Gamma$ is a $(4d-4)\times(4d-4)$ matrix linearizing motion on a reduced surface of section. Specifically, it is the section at constant $(H, J, \mathbf{x}_{\|a}, \mathbf{x}_{\|b})$ where $\mathbf{x}_{\|a/b}$ are chosen so that the dynamics are transverse to the surface on which these both are constant. This section is simply the direct product of the normal Poincaré surfaces of section for each of the two motions (where we would specify the one-particle energy and some fixed coordinate in each case). As a result, $\tilde{M}_\Gamma$ has a block diagonal structure since there is no coupling between the two particle spaces. We conclude that $\det(\tilde{M}_\Gamma - I) = \det(\tilde{M}_{\gamma_a} - I)\det(\tilde{M}_{\gamma_b} - I)$, where $\tilde{M}_{\gamma_a/\gamma_b}$ are the stability matrices of each periodic orbit and I is the appropriately dimensioned unit matrix on both sides of the equality.

The anholonomy term $(\partial\Theta/\partial J)_\Gamma$ measures the amount by which orbits that are periodic in the symmetry-reduced dynamics fail to be periodic in the full phase space. Suppose we vary the value of J infinitesimally while keeping the total energy fixed; this amounts to a slight change of the energy partition between the two particles. The periodic orbit is launched as before with the same initial conditions except for $\mathbf{p}_{\|}$ (the momentum conjugate to $\mathbf{x}_{\|}$), which must be changed appropriately to effect the change in J. After the original period T, an initial phase space coordinate will not be mapped back to where it began, but rather infinitesimally close to this initial condition. A flow in H for some extra amount of time Δt and a flow in J by an extra amount $\Delta\theta$ (or vice-versa since the flows commute) closes the orbit in the full phase space. The factor $\partial\Theta/\partial J$ is simply the ratio $\Delta\theta/\Delta J$ (in the limit $\Delta J \to 0$). (Θ is capitalized to stress that J and θ can also be used as labels for families of surfaces, in which case this factor can be interpreted as a Jacobian for a change of label from J to θ.) Recall that the value of $J = h(\mathbf{z}_a)$ is just the energy of particle a. If $J_a \to J_a + \Delta J_a$, then $E_b \to E_b - \Delta J_a$, since the total energy is fixed. γ_a now has a perturbed period $T + \Delta T_{\gamma_a} = T + T'_{\gamma_a}\Delta J_a$ while γ_b now has a perturbed period $T + \Delta T_{\gamma_b} = T - T'_{\gamma_b}\Delta J_a$, where the primes denote differentiation with respect to energy:

$$T'_{\gamma_a} = \left.\frac{\mathrm{d}T_{\gamma_a}(\xi)}{\mathrm{d}\xi}\right|_{\xi=E_a}, \quad T'_{\gamma_b} = -\left.\frac{\mathrm{d}T_{\gamma_b}(E-\xi)}{\mathrm{d}\xi}\right|_{\xi=E_a}. \tag{3.11}$$

Let $\mathbf{z}' = (\mathbf{z}'_a, \mathbf{z}'_b)$ and $\mathbf{z}$ denote the initial and final phase space coordinates, respectively. Then, after the original period T,

$$\Phi_T\mathbf{z}' = \mathbf{z} = (\phi_{-\Delta T_{\gamma_a}}\mathbf{z}'_a, \phi_{-\Delta T_{\gamma_b}}\mathbf{z}'_b). \tag{3.12}$$

We need to find $(\Delta t, \Delta\theta)$ that map $\mathbf{z}$ back to $\mathbf{z}'$. Using Eq. (3.9), the condition for a periodic

orbit $\Phi_{\Delta t}\Psi_{\Delta\theta}\mathbf{z} = \mathbf{z}'$ implies $\Delta t = \Delta T_{\gamma_b}$ and $\Delta\theta = \Delta T_{\gamma_a} - \Delta T_{\gamma_b}$ so that

$$\left(\frac{\partial\Theta}{\partial J}\right)_\Gamma = T'_{\gamma_a} + T'_{\gamma_b}. \tag{3.13}$$

The action $S_\Gamma(E) = S_{\gamma_a}(E_a) + S_{\gamma_b}(E_b = E - E_a)$ is the action of the periodic orbits in the family (all orbits in Γ have the same action because of symmetry). The phase factor μ_Γ is determined from the dynamics in the symmetry-reduced surface of section in the same way as for isolated orbits in the usual Gutzwiller trace formula and using the same logic as described above for $\tilde{M}_\Gamma$, it follows that $\mu_\Gamma = \sigma_{\gamma_a} + \sigma_{\gamma_b}$. The phase factor δ_Γ is defined as the number of positive eigenvalues of $(\partial\Theta/\partial J)_\Gamma$ [61]. In this case, the anholonomy term is simply a scalar, and therefore $\delta_\Gamma = 1$ if the Jacobian is positive or $\delta_\Gamma = 0$ if the Jacobian is negative. We conclude that the contribution to the resolvant from one family of dynamical orbits is

$$\tilde{g}^{\mathrm{d}}_\Gamma(E) = \frac{i\hbar}{\sqrt{2\pi\hbar}} \prod_{p=a,b} \left(\frac{T^0_{\gamma_p}(E_p)}{i\hbar} \frac{\exp\left[i\left(\frac{S_{\gamma_p}(E_p)}{\hbar} - \sigma_{\gamma_p}\frac{\pi}{2}\right)\right]}{\sqrt{\left|\det\left(\tilde{M}_{\gamma_p} - I\right)\right|}} \right) \frac{\exp\left[i\left(\delta_\Gamma\frac{\pi}{2} - \frac{\pi}{4}\right)\right]}{\sqrt{\left|T'_{\gamma_a}(E_a) + T'_{\gamma_b}(E_b)\right|}}. \tag{3.14}$$

As mentioned above, it was assumed that there is only one energy partition such that both particles have the same period. This will be the case when the period is a monotonic function of energy, which is a typical situation. If the period is a more complicated function of energy, there may be further solutions and if so then there is a sum over (γ_a, γ_b) for each possible solution of this condition, but this possibility is suppressed for notational simplicity. Furthermore, there are no explicit repetition indices since this dependence is implicit in the definition of the various orbit properties.

Equation (3.14) was obtained in Ref. [35] by doing a stationary phase analysis of the autoconvolution of Eq. (1.5). (The phase index ν in Eq. (18) of Ref. [35] has a different definition than δ_Γ in Eq. (3.14), but the overall phase is consistent in the two formulas.) The condition of stationary phase immediately implied that the energy must be partitioned so that the periods of the two orbits are the same. The stationary phase integral then introduces a factor of $\sqrt{\hbar}$ as well as the sum of the second derivatives of the actions with respect to energy evaluated at the stationary phase energy. This is precisely the first derivatives of the periods with energy. Thus, these two different approaches yield consistent results.

We observe that the amplitude of Eq. (3.14) is proportional to the product of the amplitudes for the single-particle dynamics. The trace formula for two noninteracting

particles contains an additional prefactor of $i\hbar/\sqrt{2\pi\hbar}$, a factor involving the derivatives of the periods with respect to energy (and the associated phase index δ) and an additional phase factor of $\pi/4$. This result generalizes to cases where the amplitudes are not given by Eq. (1.6). We simply replace the single-particle amplitudes in large brackets by the amplitudes for the system under consideration. This can be understood by noting that the only coupling between the particles is as described above, and any further symmetry can be handled within the single-particle phase spaces. This conclusion can also be understood in the convolution picture by simply using the appropriate single-particle amplitudes when doing the stationary phase analysis [35].

3.1.4 One-particle dynamics

There are also contributions to the resolvant from periodic orbits in the full phase space where one particle executes dynamics while the other particle remains stationary. In particular, suppose that particle a is stationary at some point in phase space while particle b evolves dynamically on a periodic orbit. This will be called a *heterogeneous* periodic orbit. The structure of such orbits is qualitatively different for potential systems and billiards.

For analytic potentials, the stationary particle must be at some extremum of the potential with zero momentum. In this case, the full heterogeneous orbit is isolated in phase space since a flow in $J = h(\mathbf{z}_a)$ does not map an initial condition $\mathbf{z}'$ to any new phase space point $\mathbf{z}$. Therefore, we can use the Gutzwiller trace formula for isolated orbits. In billiards, the stationary particle has zero momentum, but it can be anywhere in the billiard. So rather than being isolated, the heterogeneous orbits occur in d-dimensional families. This means that we can use the formalism of Ref. [33] to calculate the amplitudes of these orbits.

Analytic potentials

Suppose particle b traverses a periodic orbit γ with action S_γ, primitive period T_γ^0, stability matrix $\tilde{M}_\gamma$, and topological index σ_γ. Particle a is assumed to be stationary at a potential minimum with energy $E_a = 0$. At the minimum, the potential is locally harmonic with d frequencies ω_j. As explained above, the full heterogeneous orbit is isolated and so we can use the Gutzwiller trace formula for isolated orbits. The only required information is the monodromy matrix in the phase space of particle a since $\det(\tilde{M}_\Gamma - I) = \det(M_a - I)\det(\tilde{M}_\gamma - I)$, where $\tilde{M}_\Gamma$ is the $(4d-2)\times(4d-2)$ stability matrix of the full

heterogeneous orbit, M_a is the $2d \times 2d$ monodromy matrix of particle a, and $\tilde{M}_\gamma$ is the $(2d-2) \times (2d-2)$ stability matrix of particle b on γ. Since the perturbed dynamics of particle a are locally harmonic, we can use the result for a d-dimensional harmonic oscillator (see Appendix B.1 and B.2), $\sqrt{|\det(M_a - I)|} = \prod_{j=1}^{d} 2\sin(\omega_j T_\gamma(E)/2)$. The phase index of this motion is simply d, one for each transverse harmonic degree of freedom (see Appendix B.3). Thus, the contribution of one heterogeneous orbit to the resolvant is

$$\tilde{g}_\Gamma^{\rm h}(E) = \frac{1}{i\hbar} \frac{T_\gamma^0(E)}{\sqrt{\left|\det\left(\tilde{M}_\gamma - I\right)\right| \prod_{j=1}^{d} 2\sin\left(\frac{\omega_j T_\gamma(E)}{2}\right)}} \exp\left[i\left(\frac{S_\gamma(E)}{\hbar} - \sigma_\gamma \frac{\pi}{2} - d\frac{\pi}{2}\right)\right], \quad (3.15)$$

where the symbol Γ is retained to denote the full heterogeneous orbit and γ to emphasize that this is the contribution from the situation where only one particle is evolving dynamically. There is also an identical contribution from the situation where particle b is fixed while particle a evolves dynamically. As before, repetitions can be understood to be implicit in the definitions of the action, period, phase index, and stability matrix. Equation (3.15) can also be understood from the convolution formalism (the case $d = 1$ is analyzed in Appendix C.2).

We can also consider extrema other than potential minima, such as saddles or potential maxima. The Taylor expansion for a d-dimensional potential around an extremum x_0 (to second order) is

$$V(x - x_0) = \frac{1}{2}\left(\sum_{j=1}^{d_+} \omega_j^2 \xi_j^2 - \sum_{j=d_+ +1}^{d} \omega_j^2 \xi_j^2\right), \quad (3.16)$$

where the ξ_j measure the deviations of x from x_0. In general, there are d_+ stable directions and $d_- = (d - d_+)$ unstable directions. Then, the expression (3.15) is still valid, except the energy of the dynamically evolving particle is replaced by $E - V(x_0)$, the phase factor $d\pi/2$ is replaced by $d_+\pi/2$, and the $\sin(\omega_j T_\gamma/2)$ is replaced by $\sinh(\omega_j T_\gamma/2)$ for the unstable directions. Finally, note that for smooth potentials, dynamical orbits give the leading-order contribution to $\tilde{\rho}_2(E)$. The heterogeneous orbits give corrections of higher order in $\hbar$.

Billiard systems

As mentioned above, heterogeneous orbits in a d-dimensional billiard occur in d-dimensional families and we may therefore use Eq. (3.10) with $f = d$ to determine the appropriate trace formula. The orbit manifold has the topology of $\mathcal{B} \times \mathcal{S}^1$, where $\mathcal{B}$ denotes

the billiard domain and $\mathcal{S}^1$ is the 1-torus associated with the dynamics of the evolving particle b on the periodic orbit γ. We first consider a two-dimensional billiard ($d = 2$), although the result is easily generalized. For this case, there are two constants of the motion: $J_1 = p_{x_a}$ and $J_2 = p_{y_a}$ [$\mathbf{J} = (J_1, J_2)$], and the (conjugate) group variables $\Theta = (x_a, y_a)$. Clearly,

$$\det\left(\frac{\partial\Theta}{\partial\mathbf{J}}\right)_\Gamma = \det\begin{pmatrix} \frac{\partial x_a}{\partial p_{x_a}} & \frac{\partial x_a}{\partial p_{y_a}} \\ \frac{\partial y_a}{\partial p_{x_a}} & \frac{\partial y_a}{\partial p_{y_a}} \end{pmatrix} = \frac{\partial x_a}{\partial p_{x_a}}\frac{\partial y_a}{\partial p_{y_a}}, \tag{3.17}$$

since the off-diagonal elements vanish due to the fact that the x and y motions are uncoupled. After particle b has traversed the primitive orbit n_γ times, $\partial x_a/\partial p_{x_a} = \partial y_a/\partial p_{y_a} = -n_\gamma T^0_\gamma(E)/m$, where $T^0_\gamma(E)$ is the primitive period of the orbit and m is the mass of the particle. (The minus sign indicates that a backwards flow is required to close the orbits in the full phase space.) This immediately implies that the phase index $\delta \equiv 0$. The stability matrix defined in Eq. (3.10) in this case is simply the stability matrix of the motion of particle b. The volume for a family of such orbits is the area of the billiard and combining all of the factors, the leading-order contribution of a family of heterogeneous orbits Γ to the two-particle density of states is

$$\tilde{\rho}^{\rm h}_\Gamma(E) = \frac{\alpha\mathcal{A}}{4\pi^2}\frac{1}{n_\gamma\sqrt{\left|\det(\tilde{M}_\gamma - I)\right|}}\cos\left(\frac{S_\gamma(E)}{\hbar} - \sigma_\gamma\frac{\pi}{2} - \frac{\pi}{2}\right). \tag{3.18}$$

Equation (3.18) was obtained in Ref. [35] by doing an energy convolution integral of the first term of Eq. (1.3) with Eq. (1.5). This once again underlines the equivalence of the two methods. The corrections that involve the higher-order terms of Eq. (1.3) can be obtained through a more careful analysis of boundary or surface terms, but this analysis is not pursued here. Also, the generalization of Eq. (3.18) to d dimensions is

$$\tilde{\rho}^{\rm h}_\Gamma(E) = \frac{1}{\pi\hbar}\left(\frac{\hbar\alpha}{4\pi}\right)^{d/2}\frac{T^0_\gamma(E)\Omega_d}{\left(n_\gamma T^0_\gamma(E)\right)^{d/2}\sqrt{\left|\det(\tilde{M}_\gamma - I)\right|}}\cos\left(\frac{S_\gamma(E)}{\hbar} - \sigma_\gamma\frac{\pi}{2} - d\frac{\pi}{4}\right), \tag{3.19}$$

where Ω_d is the d-dimensional volume of the billiard. This is $O(1/\hbar^{d/2})$ stronger than an isolated orbit, the factor arising from the fact that this class of orbits occur in d-dimensional families. The contribution from heterogeneous orbits is also $O(1/\hbar^{(d-1)/2})$ stronger than the contribution from dynamical orbits. Thus, for billiards, heterogeneous orbits give the leading-order contribution to $\tilde{\rho}_2(E)$ while dynamical orbits give corrections of higher order in $\hbar$.

3.2 Several Noninteracting Identical Particles

We now consider the extension to N identical particles. The smooth term can be written as an $(N-1)$-fold convolution integral of the single-particle smooth terms and also as a single integral in the N-particle phase space. (The reader is referred to appendix A for further discussions on the smooth term.) For the oscillating term, there are again two possibilities. Either all of the particles are evolving dynamically or a subset of them is stationary at various potential extrema (or anywhere in a billiard). The analysis of the first situation closely parallels the two-particle case. The only nontrivial quantity to determine is the anholonomy matrix $(\partial\boldsymbol{\Theta}/\partial\mathbf{J})_\Gamma$. This is evaluated below for $N = 3$ particles, but the result readily generalizes.

3.2.1 Dynamical orbits

For three particles a, b, and c, there are three one-particle phase spaces (with coordinates $\mathbf{z}_a$, $\mathbf{z}_b$, and $\mathbf{z}_c$) so that the full three-particle phase space has coordinates $\mathbf{z} = (\mathbf{z}_a, \mathbf{z}_b, \mathbf{z}_c)$, and the total Hamiltonian $H(\mathbf{z}) = h(\mathbf{z}_a) + h(\mathbf{z}_b) + h(\mathbf{z}_c)$. Two other constants of motion which are in involution with H are $J_a = h(\mathbf{z}_a)$ and $J_b = h(\mathbf{z}_b)$, and these generate time translations of particles a and b, respectively, while having no effect on the other particles. Flows generated by H, J_a, and J_b are denoted by Φ_t, Λ_{θ_a}, and Ψ_{θ_b}, respectively. If ϕ is a single-particle flow, then flows in the full phase space are mapped as follows:

$$\Phi_t(\mathbf{z}_a, \mathbf{z}_b, \mathbf{z}_c) = (\phi_t\mathbf{z}_a, \phi_t\mathbf{z}_b, \phi_t\mathbf{z}_c), \tag{3.20a}$$

$$\Lambda_{\theta_a}(\mathbf{z}_a, \mathbf{z}_b, \mathbf{z}_c) = (\phi_{\theta_a}\mathbf{z}_a, \mathbf{z}_b, \mathbf{z}_c), \tag{3.20b}$$

$$\Psi_{\theta_b}(\mathbf{z}_a, \mathbf{z}_b, \mathbf{z}_c) = (\mathbf{z}_a, \phi_{\theta_b}\mathbf{z}_b, \mathbf{z}_c). \tag{3.20c}$$

The periodic orbits of the full phase space (at a given total energy E) can be found from the one-particle periodic orbits by balancing the energy partition among the three particles (i.e. varying J_a and J_b while holding H fixed) so that all the one-particle periodic orbits have the same period. (The result is a three-particle periodic orbit in the full phase space.) Imagine a slight departure from this equilibrium situation so that $J_a \to J_a + \Delta J_a$, while holding J_b and H fixed. Then,

$$\begin{aligned} E_a &\to E_a + \Delta J_a, & T_a &\to T_a + \Delta T_a, \\ E_b &\to E_b, & T_b &\to T_b, \\ E_c &\to E_c - \Delta J_a, & T_c &\to T_c + \Delta T_c, \end{aligned}$$

where $\Delta T_a = T_a' \Delta J_a$ and $\Delta T_c = -T_c' \Delta J_a$, the primes denoting differentiation with respect to energy. The initial condition $\mathbf{z}' = (\mathbf{z}_a', \mathbf{z}_b', \mathbf{z}_c')$ with these modified energies (but each particle still on its periodic orbit at that modified energy) is not on a periodic orbit of the full phase space. However, it is on a generalized periodic orbit; that is, the trajectory can be made to close by allowing additional flows in (H, J_a, J_b). Suppose there is a flow in H for the original period T. The orbits of particles a and c will fail to close by the amount by which their period is longer (or shorter) due to the changed energy: $\Phi_T \mathbf{z}' = (\phi_{-\Delta T_a} \mathbf{z}_a', \mathbf{z}_b', \phi_{-\Delta T_c} \mathbf{z}_c')$. Additional flows in (H, J_a, J_b) close the trajectory. First, a flow in H by the amount ΔT_c returns particle c to $\mathbf{z}_c'$: $\Phi_{\Delta T_c} \Phi_T \mathbf{z}' = (\phi_{-\Delta T_a + \Delta T_c} \mathbf{z}_a', \phi_{\Delta T_c} \mathbf{z}_b', \mathbf{z}_c')$. The condition for a periodic orbit $\Lambda_{\Delta\theta_a} \Psi_{\Delta\theta_b} \Phi_{\Delta T_c} \Phi_T \mathbf{z}' = \mathbf{z}'$ immediately implies

$$\Delta\theta_a = (T_a' + T_c') \Delta J_a, \tag{3.22a}$$

$$\Delta\theta_b = T_c' \Delta J_a. \tag{3.22b}$$

We get a similar result from a deviation in J_b (holding J_a and H fixed) and conclude that

$$\left(\frac{\partial \boldsymbol{\Theta}}{\partial \mathbf{J}} \right)_\Gamma = \begin{pmatrix} T_a' + T_c' & T_c' \\ T_c' & T_b' + T_c' \end{pmatrix}. \tag{3.23}$$

The determinant is $T_a' T_b' + T_b' T_c' + T_c' T_a'$ and is invariant under a permutation of the indices. Note that we could have chosen the two generators J_a and J_c, and followed through the analogous calculation. In that case, the anholonomy matrix would be modified by permuting b and c in Eq. (3.23). Therefore, the eigenvalues of $(\partial \boldsymbol{\Theta} / \partial \mathbf{J})_\Gamma$ are not invariant. But, since the determinant is invariant, the number of positive eigenvalues (which determines the phase index δ) is also invariant. Therefore, the final result is invariant. For $N > 3$ particles, this generalizes to

$$\det \left(\frac{\partial \boldsymbol{\Theta}}{\partial \mathbf{J}} \right)_\Gamma = \left(\prod_{p=1}^{N} T_p' \right) \left(\sum_{p=1}^{N} \frac{1}{T_p'} \right), \tag{3.24}$$

where T_p is the period of the orbit on which particle p is residing. This can be shown by induction.

The other parts of Eq. (3.10) are straightforward to determine (the discussion is similar to the two-particle case and some details are left out). For N particles, flows in H and $\mathbf{J} = (J_1, ..., J_{N-1})$ map out an N-dimensional torus. This means there are $(N-1)$-parameter families of periodic orbits in the full phase space. The total action is the sum of all the single-particle actions, and similarly for the total phase index μ. The monodromy

matrix is defined holding all of the single-particle energies constant in such a way that it is block diagonal among the various single-particle motions. The volume of the periodic orbit family is the product of the primitive periods. (To see this, recall that the volume term $T_\Gamma V_\Gamma = \oint_\Gamma \mathrm{d}t\mathrm{d}\theta_1\mathrm{d}\theta_2\cdots\mathrm{d}\theta_{N-1}$ and that the primitive volume should only count distinct configurations.) Using Eq. (3.10) with $f = (N-1)$, we conclude that the contribution to the resolvant from one family of dynamical periodic orbits is

$$\tilde{g}^{\mathrm{d}}_\Gamma(N,E) = \frac{1}{i\hbar}\frac{1}{(2\pi i\hbar)^{(N-1)/2}}\left\{\prod_{p=1}^{N}\frac{T_p^0(E_p)\exp\left[i\left(\frac{S_p(E_p)}{\hbar}-\sigma_p\frac{\pi}{2}\right)\right]}{\sqrt{\left|\det(\tilde{M}_p-I)\right|}\sqrt{\left|T_p'(E_p)\right|}}\right\}\frac{\exp\left(i\delta_\Gamma\frac{\pi}{2}\right)}{\sqrt{\left|\sum_{p=1}^{N}\frac{1}{T_p'(E_p)}\right|}}. \tag{3.25}$$

In Eq. (3.25), the label p is used rather than the more cumbersome γ_p to refer to the periodic orbit on which particle p resides. The phase factor δ_Γ is the number of positive eigenvalues of the $(N-1)\times(N-1)$ matrix $(\partial\boldsymbol{\Theta}/\partial\mathbf{J})_\Gamma$. If all of the particles are on distinct orbits, then there are $N!$ congruent but distinct full phase space orbits, corresponding to the choice of which particle to assign to which orbit. If there is more than one particle on the same orbit, then the number of combinatoric possibilities is accordingly modified. This combinatoric factor is taken to be implicit in the sum over orbits and is not explicitly accounted for here.

3.2.2 Heterogeneous orbits

The other possibility is that some of the particles are not evolving dynamically, but rather are stationary in a billiard or at potential extrema. Suppose that D particles are evolving dynamically and $(N-D)$ particles are fixed at extrema. Then, these heterogeneous orbits come in $(D-1)$-fold families. In the special case where the nonevolving particles are stationary at potential minima,

$$\tilde{g}^{\mathrm{h}}_\Gamma(D,N,E) = \tilde{g}^{\mathrm{d}}_\Gamma(D,E_D)\left\{\prod_{p=(D+1)}^{N}\frac{\exp\left(-i\frac{\pi d}{2}\right)}{\prod_{j=1}^{d}2\sin\left(\frac{\omega_{jp}T}{2}\right)}\right\}. \tag{3.26}$$

The evolving particles share the energy $E_D = E - \sum_{p=(D+1)}^{N} V(x_p)$, where x_p denote the positions of the stationary particles. Recall that d is the dimension of the one-particle dynamics and the ω_{jp} denote the d local harmonic frequencies around the minimum at which particle p resides. As in the two-particle case, if a particle is at a saddle or maximum, we replace the phase $d\pi/2$ by $d_+\pi/2$, where d_+ denotes the number of stable directions, and also

replace the $\sin(\cdots)$ in the amplitude by $\sinh(\cdots)$ for the unstable directions. Again, there are distinct but congruent heterogeneous orbits in which different particles are chosen to be on different orbits or extrema, but an explicit discussion on the combinatoric possibilities will not be given here.

Next suppose that $(N-D)$ particles are stationary in a d-dimensional billiard. In addition to the $(D-1)$ independent generators that exist for the potential system, there are $(N-D)d$ generators $\mathbf{J_q} = (\mathbf{p}_1, \ldots, \mathbf{p}_{(N-D)})$. The conjugate group variables are $\mathbf{\Theta_q} = (\mathbf{q}_1, \ldots, \mathbf{q}_{(N-D)})$. (Both $\mathbf{p}$ and $\mathbf{q}$ are d-dimensional.) Since the generators associated with the stationary particles also generate new orbits, the dimensionality of the orbit families is $f = (D-1) + (N-D)d$. The volume term $T_\Gamma^0 V_\Gamma^0 = \oint_\Gamma \mathrm{d}t\mathrm{d}\theta_1 \cdots \mathrm{d}\theta_{(D-1)}\mathrm{d}\mathbf{q}_1 \cdots \mathrm{d}\mathbf{q}_{(N-D)} = T_1^0(E_1)\cdots T_D^0(E_D)\Omega_d^{(N-D)}$. The phase index δ_Γ is the number of positive eigenvalues of the $f \times f$ matrix $(\partial\mathbf{\Theta}/\partial\mathbf{J})_\Gamma$ which has a block-diagonal structure; one block is the anholonomy associated with the evolving particles analogous to Eq. (3.23), and the other block is the anholonomy associated with the stationary particles analogous to Eq. (3.17). Thus, the contribution to the resolvant from a family of billiard heterogeneous orbits is

$$\tilde{g}_\Gamma^{\mathrm{h}}(D,N,E) = \tilde{g}_\Gamma^{\mathrm{d}}(D,E)\left\{\prod_{p=(D+1)}^{N} \frac{\Omega_d \exp\left(-i\frac{\pi d}{4}\right)}{\left(\frac{2\pi\hbar T}{m}\right)^{d/2}}\right\}. \tag{3.27}$$

In Eqs. (3.26) and (3.27), T is the global period[2], and $\delta_\Gamma \equiv 0$ if $D = 1$. As in the two-particle case, heterogeneous orbits are more important in billiards than in smooth potentials. Their leading-order contribution to $\tilde{\rho}_N(E)$ is $O(1/\hbar^{(N-D)(d-1)/2})$ stronger for billiards and $O(\hbar^{(N-D)/2})$ weaker for potentials than the corresponding contribution from dynamical orbits.

Some final comments. The above expressions apply for any of the particles executing multiple repetitions of its primitive orbit provided the energy is partitioned among the dynamically evolving particles so that all single-particle periodic orbits have a common period. Then, the various orbit properties, which appear in the formulas are understood to be those for the repeated orbit. The formulas written above only account for the contribution of a single family of orbits. The oscillatory part of the resolvant is a sum over all families: $\tilde{g}(E) = \sum_\Gamma \tilde{g}_\Gamma(E)$. Equations (3.25)-(3.27) can also be obtained from convolution integrals by doing a stationary phase analysis of the N-particle dynamical term and taking

[2]Recall that the energies of all the dynamically evolving particles have been partitioned so that all of the periodic orbits have a common period

appropriate combinations of stationary phase and endpoint contributions from the various convolution integrals. However, the approach outlined above is more illuminating since it reveals the underlying structure of the periodic orbit families. The many-particle trace formulas involve only the periodic orbits of the one-particle phase space. Thus, after studying a one-particle system, we can immediately work out the details of the many-particle system. This parallels the situation in quantum mechanics where the problem of N noninteracting particles in a potential is a simple extension of the one-particle problem.

3.3 Three Identical Particles in a Cardioid Billiard

To illustrate the use of the trace formulas derived above, we now study a system of three noninteracting identical particles in a two-dimensional cardioid billiard. In a billiard, classical orbits possess simple scaling properties. For instance, the action and period of an orbit γ are

$$S_\gamma(\varepsilon) = \sqrt{2m\varepsilon}L_\gamma = \hbar\sqrt{\alpha\varepsilon}L_\gamma, \tag{3.28a}$$

$$T_\gamma(\varepsilon) = S'_\gamma(\varepsilon) = \frac{\sqrt{2m}L_\gamma}{2\sqrt{\varepsilon}} = \frac{\hbar\sqrt{\alpha}}{2\sqrt{\varepsilon}}L_\gamma. \tag{3.28b}$$

For this reason, it is natural and convenient to analyze the length (action) spectrum of the various trace formulas. This involves comparing Fourier transforms of quantum spectra with their semiclassical approximations in the reciprocal space of orbit lengths L. In reciprocal L space, we expect peaks at the lengths of the periodic orbits of the three-particle system. In the subsequent analysis, peaks in the various length spectra are identified with particular periodic orbit families of the full classical phase space. We first consider the total density of states for the three-particle system. In the following chapter, we study its decomposition among the irreps of S_3.

3.3.1 Quantum mechanics

The analog of Eqs. (3.4) and (3.5) for the quantum three-particle density of states is

$$\rho_3(E) = \sum_{i,j,k} \delta(E - (\varepsilon_i + \varepsilon_j + \varepsilon_k)) = (\rho_1 * \rho_1 * \rho_1)(E). \tag{3.29}$$

This relation applies even if the particles are not identical, but the total density is the convolution of three distinct single-particle densities. The three-particle spectrum is constructed

by adding the energies of the one-particle spectrum. (The billiard has a reflection symmetry, which implies that all the single-particle states are either even or odd; this symmetry should not be confused with the symmetry due to particle exchange.) In the subsequent analysis, the odd-parity one-particle spectrum is used exclusively. The first 500 single-particle energies were used to construct the first 19 317 062 energy levels representing all three-particle energies less than 2.8148×10^3. (The spectrum was truncated at $E_{\max} = 2\varepsilon_1 + \varepsilon_{500}$ to ensure that there were no missing levels.) It is possible to improve the resolution in L space by truncating the spectrum at a higher energy. But, this would require a precise spectrum since there is a rapid increase in the number of three-particle levels with increasing energy and errors accumulate.

3.3.2 Weyl expansion

The smooth three-particle density of states is just the two-fold convolution integral of the smooth single-particle density of states:

$$\bar{\rho}_3(E) = (\bar{\rho}_1 * \bar{\rho}_1 * \bar{\rho}_1)(E). \tag{3.30}$$

For a two-dimensional billiard, we use Eq. (1.3) for $\bar{\rho}_1(E)$. After performing the necessary integrations [ignoring terms $O(1/\hbar^3)$], the three-particle smooth term is found to be

$$\bar{\rho}_3(E) = \frac{\alpha^3 \mathcal{A}^3}{128\pi^3} E^2 - \frac{\alpha^{5/2} \mathcal{A}^2 \mathcal{L}}{32\pi^3} E^{3/2} + \frac{3}{2}\alpha^2 \left(\frac{\mathcal{A}\mathcal{L}^2}{128\pi^2} + \frac{\mathcal{A}^2 \mathcal{K}}{16\pi^2} \right) E. \tag{3.31}$$

For the odd-parity single-particle spectrum of the cardioid, $\mathcal{A} = 3\pi/4$, $\mathcal{L} = 6$, and $\mathcal{K} = 3/16$. Some of the contributions of the higher-order terms of $\bar{\rho}_3(E)$ can be calculated, but it is formally meaningless to include them since there are corrections of the same relative order in $\hbar$, which are not known. The terms that are $O(\sqrt{\alpha^3 E})$ and $O(\alpha E^0)$ can be computed numerically.

3.3.3 Heterogeneous orbits

For three particles in a two-dimensional billiard, there are two types of heterogeneous orbits. The first type occurs when one particle is on a periodic orbit while the other two particles are stationary. These orbits come in 4-parameter families. The trace formula is obtained by using Eq. (3.27) with $D = 1, N = 3$. For the situation where particles a

and b are stationary and particle c evolves on the orbit γ, the leading-order contribution to $\tilde{\rho}_3(E)$ is

$$\tilde{\rho}_3^{\mathrm{h1}}(E) = \frac{\alpha^{3/2}\mathcal{A}^2 E^{1/2}}{8\pi^3} \sum_{\gamma} \frac{(L_\gamma^0/L_\gamma^2)}{\sqrt{\left|\det(\tilde{M}_\gamma - I)\right|}} \cos\left(\sqrt{\alpha E} L_\gamma - \sigma_\gamma \frac{\pi}{2} - \pi\right). \tag{3.32}$$

The second type of heterogeneous orbit arises from the situation where only one particle is stationary while the other two evolve on periodic orbits. For instance, particle c is stationary while particle a evolves on γ_a and particle b evolves on γ_b. Using formula (3.27) with $D = 2, N = 3$, we conclude the leading-order contribution to $\tilde{\rho}_3(E)$ from these heterogeneous orbits is

$$\tilde{\rho}_3^{\mathrm{h2}}(E) = \frac{\alpha^{5/4}\mathcal{A} E^{1/4}}{(2\pi)^{5/2}} \sum_{\Gamma=(\gamma_a,\gamma_b)} \frac{1}{L_\Gamma^{3/2}} \left(\prod_{p=a,b} \frac{L_{\gamma_p}^0}{\sqrt{\left|\det(\tilde{M}_{\gamma_p} - I)\right|}} \right) \cos\left(\sqrt{\alpha E} L_\Gamma - \sigma_\Gamma \frac{\pi}{2} - \frac{3\pi}{4}\right), \tag{3.33}$$

where $L_\Gamma = \sqrt{L_{\gamma_a}^2 + L_{\gamma_b}^2}$ and $\sigma_\Gamma = (\sigma_{\gamma_a} + \sigma_{\gamma_b})$.

For the total density of states, both formulas are multiplied by a factor of 3 since there are three identical contributions depending on the choice of which particle is evolving and which is stationary. Higher-order contributions can be obtained using the convolution formalism and the results are given in Appendix C.3.

3.3.4 Dynamical orbits

To use formula (3.25), we must first determine energies E_a, E_b, and E_c such that

$$T_{\gamma_a}(E_a) = T_{\gamma_b}(E_b) = T_{\gamma_c}(E_c), \tag{3.34a}$$

$$E_a + E_b + E_c = E. \tag{3.34b}$$

This leads to a simple linear system, which can be solved to give

$$E_i = \left(\frac{L_{\gamma_i}^2}{L_{\gamma_a}^2 + L_{\gamma_b}^2 + L_{\gamma_c}^2} \right) E \tag{3.35}$$

for $i = a, b, c$. We can now proceed to compute each of the quantities involved in formula (3.25). The anholonomy term [see Eq. (3.23)] is

$$\det\left(\frac{\partial\Theta}{\partial \mathbf{J}}\right)_\Gamma = T'_{\gamma_a}T'_{\gamma_b} + T'_{\gamma_b}T'_{\gamma_c} + T'_{\gamma_c}T'_{\gamma_a} = \frac{\hbar^2\alpha}{16} \frac{L_\Gamma^8}{L_{\gamma_a}^2 L_{\gamma_b}^2 L_{\gamma_c}^2 E^3}. \tag{3.36}$$

In addition, $\mathrm{Tr}\left(\frac{\partial\Theta}{\partial\mathbf{J}}\right)_\Gamma < 0$ and this implies the phase factor $\delta_\Gamma \equiv 0$. Then, the three-particle dynamical term can be written as

$$\tilde{\rho}_3^{\mathrm{d}}(E) = \frac{\alpha}{(2\pi)^2} \sum_{\Gamma=(\gamma_a,\gamma_b,\gamma_c)} \frac{1}{L_\Gamma} \left(\prod_{p=a,b,c} \frac{L^0_{\gamma_p}}{\sqrt{\left|\det(\tilde{M}_{\gamma_p} - I)\right|}} \right) \cos\left(\sqrt{\alpha E} L_\Gamma - \sigma_\Gamma \frac{\pi}{2} - \frac{\pi}{2}\right), \tag{3.37}$$

where $L_\Gamma = \sqrt{L^2_{\gamma_a} + L^2_{\gamma_b} + L^2_{\gamma_c}}$ and $\sigma_\Gamma = (\sigma_{\gamma_a} + \sigma_{\gamma_b} + \sigma_{\gamma_c})$.

3.3.5 Numerics

For billiards, it is common to express the density of states in terms of the wave number k, where $\varepsilon = k^2/\alpha$ so that $\rho(k) = 2k\rho(\varepsilon)/\alpha$. This is convenient here since k is conjugate to the periodic orbit length L. Therefore, the numerical results will be quoted as functions of k with the understanding that these functions have been converted to the k domain from the energy domain using the Jacobian relation above. This will always be the case when the argument is k.

We now compare the Fourier transform of the oscillatory part of the density of states

$$\tilde{F}_3^{\mathrm{sc}}(L) = \mathcal{F}\{\tilde{\rho}_3(k)\} = \mathcal{F}\{3\tilde{\rho}_3^{\mathrm{h1}}(k) + 3\tilde{\rho}_3^{\mathrm{h2}}(k) + \tilde{\rho}_3^{\mathrm{d}}(k)\}, \tag{3.38}$$

and its quantum mechanical analog, which is defined to be

$$\tilde{F}_3^{\mathrm{qm}}(L) = \mathcal{F}\{\rho_3(k) - \bar{\rho}_3(k)\}. \tag{3.39}$$

In Eq. (3.39), the first term is the quantum three-particle density of states, $\rho_3(k) = \sum_I \delta(k - k_I)$, where the superindex I denotes a triplet of integers (i, j, k). The subtracted term is the smooth density of states as determined from Eq. (3.31). The oscillatory part has contributions from heterogeneous orbits [Eqs. (3.32) and (3.33)] and dynamical orbits [Eq. (3.37)]. In all formulas, γ_p are periodic orbits in the fundamental domain (i.e. the half-cardioid) and $L^0_{\gamma_p}$ are their primitive lengths. Orbit properties (such as Maslov indices) are discussed in Refs. [94, 95], and some of the shorter geometrical orbits are shown in Fig. 3.2. The stability matrices of the Gutzwiller amplitudes were computed using the standard procedure for the stability of free-flight billiards (see, for example, Ref. [10]). The Fourier transform

$$\mathcal{F}\{\rho(k)\} = \int_{-\infty}^{\infty} \mathrm{w}(k) \exp(ikL)\rho(k)\mathrm{d}k \tag{3.40}$$

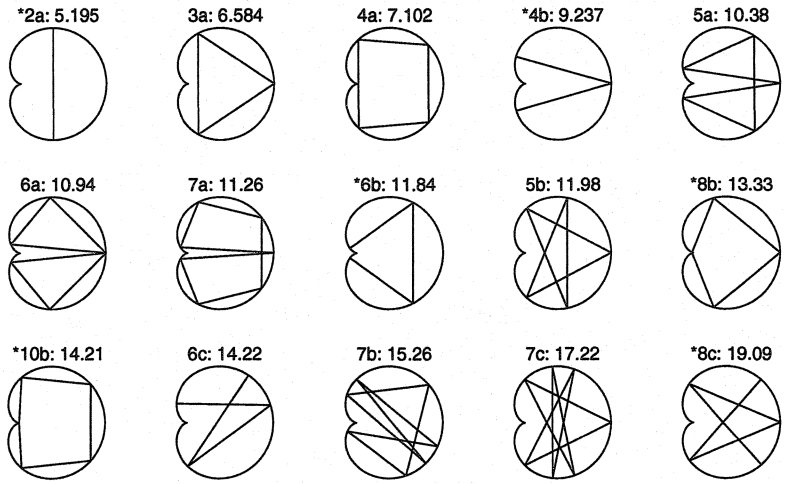

Figure 3.2: Some of the shorter periodic orbits of the cardioid in the full domain. The label of each orbit includes the number of reflections and also a letter index to further distinguish it. The asterisk designates a self-dual orbit. The two orbits *8b and *10b reflect specularly near the cusp, contrary to appearances, while the orbit 4a misses the cusp. From Ref. [94]. (Courtesy of N.D. Whelan)

is defined here as a function of the conjugate variable L. The function $\mathrm{w}(k)$ is the three-term Blackman-Harris window function [96]

$$\mathrm{w}(k) = \begin{cases} \sum_{j=0}^{2} a_j \cos\left(2\pi j \frac{k-k_0}{k_f-k_0}\right), & k_0 < k < k_f \\ 0, & \text{otherwise} \end{cases} \tag{3.41}$$

with $(a_0, a_1, a_2) = (0.42323, -0.49755, 0.07922)$. The parameters k_0 and k_f were chosen so that the window function goes smoothly to zero at the first and last eigenvalues of the three-particle spectrum. Numerical integration of Eqs. (3.38) and (3.39) using this integral operator is displayed in Fig. 3.3. In the semiclassical transform, a total of 212 periodic orbits (including multiple repetitions) were used.

There is good agreement between quantum and semiclassical results for $L < 7$. In fact, it is difficult to distinguish between the two curves. For this reason, the difference between them is plotted in Fig. 3.4. Clearly, the errors are small with respect to individual peak heights. Furthermore, the errors are largely due to the heterogeneous orbit contributions. This can be understood by considering the first three structures in L space. The first structure ($L \approx 2.60$) is due to the family of type-1 heterogeneous orbits where two particles are stationary and one particle evolves on $\gamma = \frac{1}{2}(*2a)$ with energy E. The second

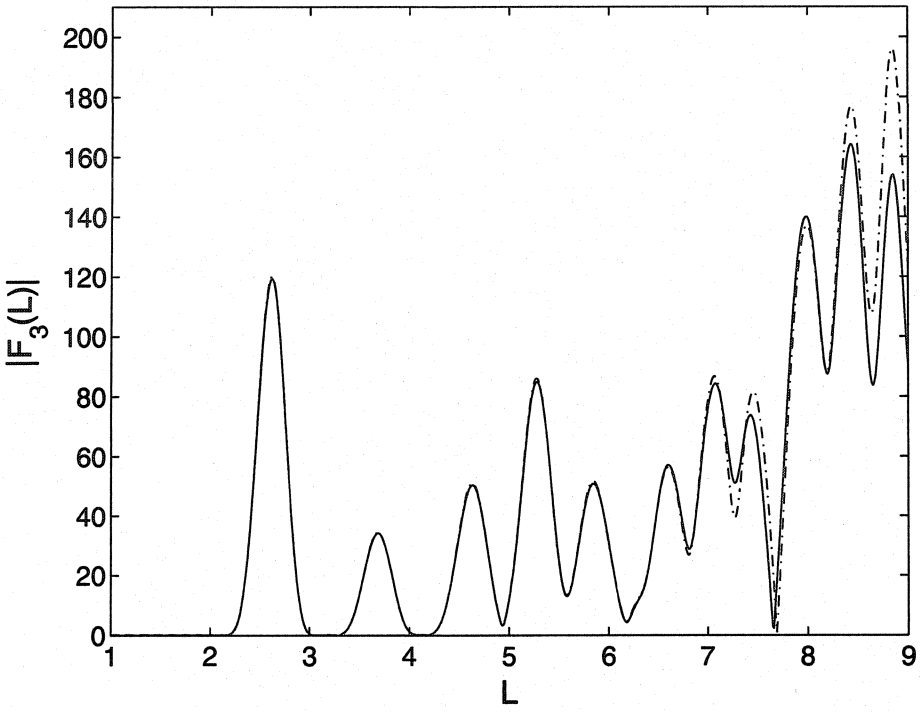

Figure 3.3: Fourier transform of the oscillatory part of the three-particle density of states for $L < 9$. The solid line is the transform of the quantum three-particle spectrum (3.39) and the dashed-dotted line is the transform of the combined semiclassical three-particle trace formulas (3.38). Each structure is due to one or several periodic orbit families of the full phase space.

structure ($L \approx 3.67$) is associated with the family of type-2 heterogeneous orbits where one particle is stationary and two particles evolve independently on the same orbit $\gamma = \frac{1}{2}(*2a)$ with the same energy $E/2$. The third structure arises from the interference between the family of type-1 heterogeneous orbits ($L \approx 4.62$) where one of the three particles is on $\gamma = \frac{1}{2}(*4b)$ and the family of dynamical orbits ($L \approx 4.50$) where all three particles evolve independently on $\gamma = \frac{1}{2}(*2a)$ with energy $E/3$. We see that the first and third structures have similar errors, and thus conclude that the error introduced from the dynamical term is much smaller than that from the heterogeneous terms. All other L-space structures arise from the interference of many orbit families and can be accounted for in a similar manner. For $L > 7$, the discrepancies are more significant and mostly due to the problematic orbits $\gamma = 4a$ and $\gamma = \frac{1}{2}(*10b)$, which are not well isolated in phase space and pass close to the cusp of the cardioid (see Table 3.1). These orbits have inaccurate Gutzwiller amplitudes for reasons explained in Refs. [94, 35].

L_Γ	γ_1	γ_2	γ_3
7.5637	$\frac{1}{2}$(*2a)	4a	
7.5650	$\frac{1}{2}$(*2a)	$\frac{1}{2}$(*10b)	
7.9975	$\frac{1}{2}$(*2a)	4a	$\frac{1}{2}$(*2a)
7.9987	$\frac{1}{2}$(*2a)	$\frac{1}{2}$(*2a)	$\frac{1}{2}$(*10b)
8.4731	$\frac{1}{2}$(*4b)	4a	
8.4742	$\frac{1}{2}$(*4b)	$\frac{1}{2}$(*10b)	
8.8011	2a	4a	
8.8022	2a	$\frac{1}{2}$(*10b)	
8.8624	$\frac{1}{2}$(*2a)	4a	$\frac{1}{2}$(*4b)
8.8636	$\frac{1}{2}$(*2a)	$\frac{1}{2}$(*4b)	$\frac{1}{2}$(*10b)

Table 3.1: Some of the orbits responsible for numerical discrepancies. The first column gives the length of the periodic orbit family Γ in the full three-particle phase space while the other columns specify the constituent periodic orbits γ_i of the one-particle phase space. (Type-2 heterogeneous orbits involve only two orbits since one of the particles is stationary.)

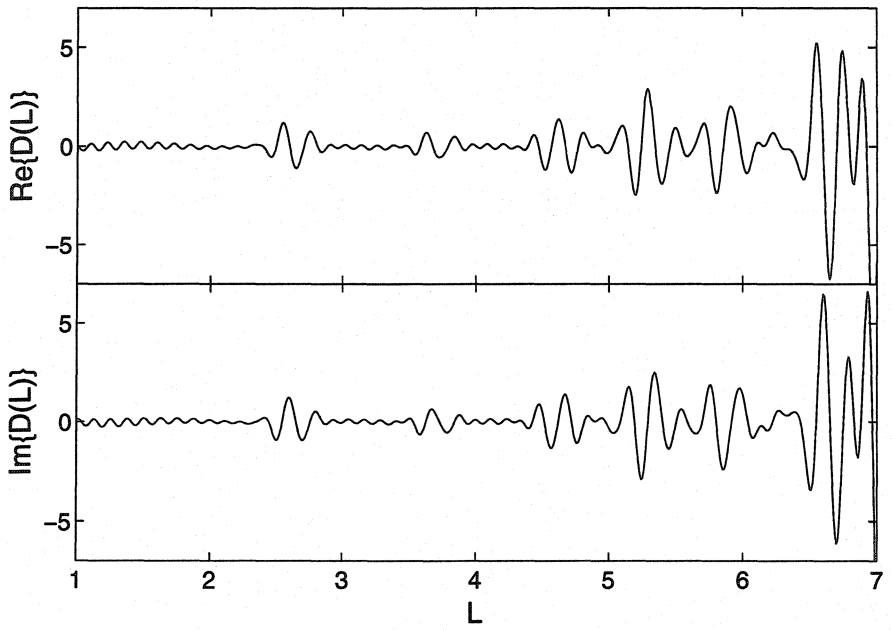

Figure 3.4: Fourier transform of the difference between the quantum and semiclassical densities of states for $L < 7$. The upper and lower windows show the real and imaginary parts, respectively.

3.4 Nonidentical Particles

The trace formula for dynamical orbits [Eq. (3.25) of Sec. 3.2] still applies to nonidentical particles[3]. For identical particles, the actions and periods [Eq. (3.28)] of all one-particle orbits involve the same mass m. For nonidentical particles, there is a different mass for each particle. The calculation outlined in Sec. 3.3.4 can be repeated to obtain the dynamical term for three nonidentical particles. It is only a matter of inserting the correct masses in the different actions and periods of the three nonidentical particles when using Eq. (3.25). The final trace formula is the same as before, except that the single scaling parameter $\alpha = 2m/\hbar^2$ appearing in Eq. (3.37) is replaced by $\sqrt{\alpha_a \alpha_b \alpha_c}$, where $\alpha_p = 2m_p/\hbar^2$ $(p = a, b, c)$, and $L_\Gamma = \sqrt{\alpha_a L_{\gamma_a}^2 + \alpha_b L_{\gamma_b}^2 + \alpha_c L_{\gamma_c}^2}$ for nonidentical particles. The trace formula for heterogeneous orbits [Eq. (3.27) of Sec. 3.2] does not apply to nonidentical particles. The modifications for three-particle heterogeneous orbits are discussed below.

[3]In the present context, particles are nonidentical if their masses differ. Of course, in general, nonidentical particles can have the same mass. For example, electrons and positrons, which are nonidentical particles, have equal masses, but differ in their charge. However, the effect of such properties is currently beyond the scope of semiclassics.

3.4.1 Three-particle heterogeneous orbits

As before, there are three contributions from type-1 heterogeneous orbits. Obviously, these are no longer equal to each other, but each separately has the same structure. For example, if particles a and b are fixed in the billiard while particle c evolves on a periodic orbit, then Eq. (3.32) is replaced by

$$\tilde{\rho}_3^{\mathrm{h1}}(E) = \frac{\alpha_a \alpha_b \mathcal{A}^2 E^{1/2}}{8\pi^3 \sqrt{\alpha_c}} \sum_{\gamma_c} \frac{(L^0_{\gamma_c}/L^2_{\gamma_c})}{\sqrt{\left|\det(\tilde{M}_{\gamma_c} - I)\right|}} \cos\left(\sqrt{\alpha_c E} L_{\gamma_c} - \sigma_{\gamma_c}\frac{\pi}{2} - \pi\right). \tag{3.42}$$

If particles a and c are fixed while particle b is on a periodic orbit, then $b \leftrightarrow c$ in Eq. (3.42).

There are also three distinct contributions from type-2 heterogeneous orbits. The major difference for nonidentical particles is that it is not possible to have contributions from orbits in the full phase space where each particle is on the same periodic orbit of the one-particle phase space. The is due to the fact that the particle energies can never be equal. For example, suppose that particles a and b evolve on periodic orbits while particle c is fixed. To have a periodic orbit in the full phase space, the evolving nonidentical particles must have the same period, and for billiard orbits, this implies the particle energies are

$$E_{a/b} = \left(\frac{m_{a/b} L^2_{\gamma_a/\gamma_b}}{m_a L^2_{\gamma_a} + m_b L^2_{\gamma_b}}\right) E. \tag{3.43}$$

Therefore, the formula for $\tilde{\rho}_3^{\mathrm{h2}}(E)$ still has the same basic structure as before, but obviously the double sum over periodic orbits involves only distinct[4] periodic orbits for particles a and b. The generalization of Eq. (3.33) is then

$$\tilde{\rho}_3^{\mathrm{h2}}(E) = \frac{\sqrt{\alpha_a}\sqrt{\alpha_b}\alpha_c \mathcal{A}}{(2\pi)^{5/2} E^{-1/4}} \sum_{\Gamma=(\gamma_a,\gamma_b)} \frac{1}{L_\Gamma^{3/2}} \left(\prod_{p=a,b} \frac{L^0_{\gamma_p}}{\sqrt{\left|\det(\tilde{M}_{\gamma_p} - I)\right|}}\right) \cos\left(\sqrt{E} L_\Gamma - \sigma_\Gamma \frac{\pi}{2} - \frac{3\pi}{4}\right), \tag{3.44}$$

where $\sigma_\Gamma = (\sigma_{\gamma_a} + \sigma_{\gamma_b})$, and $L_\Gamma = \sqrt{\alpha_a L^2_{\gamma_a} + \alpha_b L^2_{\gamma_b}}$ for nonidentical particles. It is straightforward to check that these more general formulas reduce to the formulas given before for the special case of identical particles.

[4]Nonidentical particles can still evolve on the same periodic orbit in configuration space, but since their energies differ, the particles are not evolving on the same periodic orbit in phase space.

Brief derivations for $\tilde{\rho}_3^{\mathbf{h1}}(E)$ and $\tilde{\rho}_3^{\mathbf{h2}}(E)$

The trace formula (3.27) applies only to identical particles since it assumes equal masses. The more general formula for nonidentical particles is obtained from replacing m in Eq. (3.27) with m_p, where p is one of the $(N-D)$ fixed particles. The results for heterogeneous orbits [Eqs. (3.42) and (3.44)] are briefly derived here from Eq. (3.10). In this subsection, it is useful to include some algebraic details (usually excluded) since it is important to observe how the final mass dependence emerges.

For type-1 heterogeneous orbits, one particle is on a periodic orbit while two other particles are fixed. The contribution of orbits where particles a and b are fixed and particle c is evolving on a periodic orbit [Eq. (3.42)] is derived here. The generators $\mathbf{J} = (p_{x_a}, p_{y_a}, p_{x_b}, p_{y_b})$ and conjugate group parameters $\mathbf{\Theta} = (x_a, y_a, x_b, y_b)$. The primitive volume

$$T_\Gamma^0 V_\Gamma^0 = \oint_\Gamma \mathrm{d}t \mathrm{d}x_a \mathrm{d}x_b \mathrm{d}y_a \mathrm{d}y_b = T_{\gamma_c}^0(E)\mathcal{A}^2 = \frac{\sqrt{2m_c}L_{\gamma_c}^0}{2\sqrt{E}}\mathcal{A}^2.$$

The anholonomy matrix can be obtained using results from Sec. 3.1.4:

$$\det\left(\frac{\partial\mathbf{\Theta}}{\partial\mathbf{J}}\right)_\Gamma = \det\begin{pmatrix} \frac{-T_{\gamma_c}(E)}{m_a} & 0 & 0 & 0 \\ 0 & \frac{-T_{\gamma_c}(E)}{m_a} & 0 & 0 \\ 0 & 0 & \frac{-T_{\gamma_c}(E)}{m_b} & 0 \\ 0 & 0 & 0 & \frac{-T_{\gamma_c}(E)}{m_b} \end{pmatrix} = \left(\frac{T_{\gamma_c}^2(E)}{m_a^2}\right)\left(\frac{T_{\gamma_c}^2(E)}{m_b^2}\right),$$

$$\Longrightarrow \mathcal{D}_\Gamma = \sqrt{\left|\det\left(\frac{\partial\mathbf{\Theta}}{\partial\mathbf{J}}\right)_\Gamma\right|} = \frac{T_{\gamma_c}^2(E)}{m_a m_b} = \frac{m_c L_{\gamma_c}^2}{2E m_a m_b}.$$

The amplitude (apart from the stability factor) is then given by

$$\frac{2}{(2\pi\hbar)^3}\frac{T_\Gamma^0 V_\Gamma^0}{\mathcal{D}_\Gamma} = \frac{L_{\gamma_c}^0 \alpha_a \alpha_b \sqrt{E}\mathcal{A}^2}{(2\pi)^3\sqrt{\alpha_c}L_{\gamma_c}^2}.$$

The phase index $\delta \equiv 0$ since the anholonomy matrix has four negative eigenvalues, and $f = 4$ since type-1 heterogeneous orbits occur in 4-parameter families.

For type-2 heterogeneous orbits, one particle is fixed while the other two particles are on periodic orbits. The contribution from orbits where particles a and b evolve on periodic orbits while particle c is fixed [Eq. (3.44)] is derived below. The generators and group parameters are $\mathbf{J} = (h_a, p_{x_c}, p_{y_c})$ and $\mathbf{\Theta} = (\theta_a, x_c, y_c)$, respectively. The determinant of the anholonomy matrix

$$\det\left(\frac{\partial\mathbf{\Theta}}{\partial\mathbf{J}}\right)_\Gamma = \left(\frac{\partial\theta_a}{\partial h_a}\right)\left(\frac{\partial x_c}{\partial p_{x_c}}\right)\left(\frac{\partial y_c}{\partial p_{y_c}}\right) = \left(T'_{\gamma_a}(E_a) + T'_{\gamma_b}(E_b)\right)\left(-\frac{T_{\gamma_a}(E_a)}{m_c}\right)\left(-\frac{T_{\gamma_b}(E_b)}{m_c}\right),$$

since the off-diagonal elements are zero. Using the energies given in Eq. (3.43) and the usual relations for the periods (3.28b),

$$T'_{\gamma_a}(E_a) + T'_{\gamma_b}(E_b) = -\frac{\sqrt{2}\mathscr{L}_\Gamma^5}{4m_a m_b E^{3/2} L_{\gamma_a}^2 L_{\gamma_b}^2},$$
$$T_{\gamma_a}(E_a) T_{\gamma_b}(E_b) = \frac{\mathscr{L}_\Gamma^2}{2E},$$
$$\mathcal{D}_\Gamma = \frac{\mathscr{L}_\Gamma^{7/2}}{2^{1/4} m_c \sqrt{(2m_a)(2m_b)} E^{5/4} L_{\gamma_a} L_{\gamma_b}},$$

where $\mathscr{L}_\Gamma = \sqrt{m_a L_{\gamma_a}^2 + m_b L_{\gamma_b}^2}$. The primitive volume is given by

$$T_\Gamma^0 V_\Gamma^0 = \oint_\Gamma \mathrm{d}t \mathrm{d}\theta_a \mathrm{d}x_c \mathrm{d}y_c = T_{\gamma_a}^0(E_a) T_{\gamma_b}^0(E_b) \mathcal{A} = \frac{L_{\gamma_a}^0 L_{\gamma_b}^0 \mathscr{L}_\Gamma^2 \mathcal{A}}{2E L_{\gamma_a} L_{\gamma_b}},$$

and therefore the amplitude (excluding the stability factor) is

$$\frac{2}{(2\pi\hbar)^{5/2}} \frac{T_\Gamma^0 V_\Gamma^0}{\mathcal{D}_\Gamma} = \frac{L_{\gamma_a}^0 L_{\gamma_b}^0 E^{1/4} \sqrt{\alpha_a} \sqrt{\alpha_b} \alpha_c \mathcal{A}}{(2\pi)^{5/2} (\alpha_a L_{\gamma_a}^2 + \alpha_b L_{\gamma_b}^2)^{3/4}}.$$

The anholonomy matrix has three negative eigenvalues, which implies the phase index $\delta \equiv 0$, and $f = 3$ since the orbits occur in 3-parameter families.

The results of Secs. 3.3.3 and 3.3.4 have been generalized above to nonidentical particles. Note that Eqs. (3.32), (3.33), (3.42), and (3.44) apply to *any* two-dimensional billiard whose one-particle dynamics is free of continuous symmetry, although Eqs. (3.32) and (3.33) were originally obtained for specific application to the cardioid billiard. (Equation (3.37) and its generalization are valid for a billiard of any dimension.) The numerical analysis of Sec. 3.3.5 could now be repeated for a system of three nonidentical particles, but it is much simpler and equally informative to study a system of two nonidentical particles. The objective is to examine how removing the particle symmetry affects the periodic orbit structure.

3.4.2 Two nonidentical particles in a cardioid billiard

Particle symmetry is responsible for the degeneracies in the multiparticle energy spectrum[5]. These degeneracies are destroyed as soon as the scaling parameters α_p become unequal. Thus, regardless of the relative sizes of these parameters, the energy spectrum is

[5] Assuming, of course, the one-particle spectrum is nondegenerate.

drastically altered as a result of broken symmetry. (Similar comments apply to the wave number spectrum, which is discussed in more detail below.) There is an analogous effect on the length spectrum (the Fourier transform of the wave number spectrum) since degenerate periodic orbit structures must also be destroyed after particle symmetry is removed.

For the quantum calculation, it is important to first understand the scaling properties of the wave number spectrum. The two-particle spectrum is

$$E_{ij} = \frac{\hbar^2}{2m_a}k_i^2 + \frac{\hbar^2}{2m_b}k_j^2 = \frac{\hbar^2}{2\mathcal{M}}\left(\frac{k_i^2}{\left(\frac{m_a}{\mathcal{M}}\right)} + \frac{k_j^2}{\left(\frac{m_b}{\mathcal{M}}\right)}\right) = \frac{\hbar^2}{2\mathcal{M}}\left(\frac{k_i^2}{m_a} + \frac{k_j^2}{m_b}\right) = \frac{\hbar^2}{2\mathcal{M}}k_{ij}^2. \qquad (3.50)$$

The above definition of the two-particle wave number spectrum $\{k_{ij}\}$ involves two dimensionless scaling parameters $m_{a/b} = m_{a/b}/\mathcal{M}$, where $\mathcal{M}$ is an arbitrary mass. (The two-particle energy spectrum involves the two scaling parameters $\alpha_{a/b}$.) The relation between the energy and wave number density of states then involves the parameter $\alpha_{\mathcal{M}} = 2\mathcal{M}/\hbar^2$: $\rho(k) = 2k\rho(E)/\alpha_{\mathcal{M}}$ and $E = k^2/\alpha_{\mathcal{M}}$. The indirect mass dependence in the multiparticle wave number spectrum might seem unusual since in a one-body system, the wave number spectrum does not depend on the mass of a particle. Recall that the energy of a particle in a box depends on the mass, but the wave number depends only on the geometry of the box and is independent of the mass[6]. This convenient property of single-particle wave number spectra remains intact for a system of identical particles. This means the length spectrum is then also independent of the particle masses. For example, a box of protons has the same wave number spectrum (and therefore the same length spectrum) as a box of neutrons, regardless of the differing masses[7]. If the particles in the box are not identical (i.e. the masses differ), the spectrum is not the same as the spectrum for identical particles, and is different for different systems of nonidentical particles. Therefore, unlike the case of identical particles, the multiparticle wave number spectrum of nonidentical particles does depend on the masses if the masses are different.

The above facts about the length spectrum can also be understood from semiclassics. The k-space trace formulas have no functional dependence on mass if the particles are identical. (The trace formulas depend on mass only in E space.) Since the actions of the periodic orbits are independent of mass, the length (action) spectrum is invariant under

[6]It is also independent of the value of $\hbar$. This is the reason why it is most common to use the k-space density of states for billiards.

[7]This invariant character of the k-space and L-space spectra of identical particles in a box implies that the numerical results of the previous section are general, i.e. *any* system of three identical particles in a cardioid has the same length spectrum. For this reason, it was not necessary to specify the mass.

any changes in mass. If the particles are nonidentical, then there is mass dependence in the actions, and so variations in mass will lead to different length (action) spectra.

Trace formulas

Consider now a system of two noninteracting nonidentical particles evolving in the cardioid billiard. The two-particle density of states in E space is

$$\rho_2(E) = \bar{\rho}_2(E) + \tilde{\rho}_2^{\rm h}(E) + \tilde{\rho}_2^{\rm d}(E). \tag{3.51}$$

The formulas for each term in the decomposition (3.51) are given below (the derivation of these results is left out as usual). It can be shown that the smooth term [to $O(1/\hbar^2)$] is

$$\bar{\rho}_2(E) = \frac{\alpha_a\alpha_b\mathcal{A}^2}{16\pi^2}E - (\sqrt{\alpha_a}+\sqrt{\alpha_b})\frac{\sqrt{\alpha_a\alpha_b}}{16\pi^2}\mathcal{A}\mathcal{L}\sqrt{E} + \frac{\sqrt{\alpha_a}\sqrt{\alpha_b}\mathcal{L}^2}{64\pi} + \frac{(\alpha_a+\alpha_b)\mathcal{A}\mathcal{K}}{4\pi}. \tag{3.52}$$

The asymptotic expansion for the contribution from the heterogeneous orbits [to $O(1/\hbar)$] is

$$\begin{aligned}\tilde{\rho}_2^{\rm h}(E) \;=\; \sum_{\gamma_b} C^0_{\gamma_b}\Bigg[&\frac{\alpha_a\mathcal{A}}{4\pi^2 L_{\gamma_b}}\cos\left(\Phi_{\gamma_b}-\frac{\pi}{2}\right) - \frac{\alpha_a^{1/2}\alpha_b^{1/4}\mathcal{L}}{8\sqrt{2}\pi^{3/2}E^{1/4}\sqrt{L_{\gamma_b}}}\cos\left(\Phi_{\gamma_b}-\frac{\pi}{4}\right)\\ &+\frac{\mathcal{K}\sqrt{\alpha_b}}{2\pi\sqrt{E}}\cos\left(\Phi_{\gamma_b}\right)\Bigg] + \{a\leftrightarrow b\},\end{aligned} \tag{3.53}$$

where $\Phi_{\gamma_a/\gamma_b} = \sqrt{\alpha_{a/b}E}L_{\gamma_a/\gamma_b} - \sigma_{\gamma_a/\gamma_b}\pi/2$, and $C^0_{\gamma_a/\gamma_b} = L^0_{\gamma_a/\gamma_b}/\sqrt{|\det(\tilde{M}_{\gamma_a/\gamma_b}-I)|}$. The sum over γ_b is from heterogeneous orbits where particle a is fixed while particle b evolves on a periodic orbit γ_b, and the second sum in curly brackets is the contribution from heterogeneous orbits where particle b is fixed while particle a evolves on a periodic orbit γ_a. The leading-order contribution from dynamical orbits [using Eq. (3.14)] is

$$\tilde{\rho}_2^{\rm d}(E) = \frac{\sqrt{\alpha_a}\sqrt{\alpha_b}}{(2\pi)^{3/2}E^{1/4}}\sum_{\Gamma=(\gamma_a,\gamma_b)} C^0_{\gamma_a}C^0_{\gamma_b}L_\Gamma^{-1/2}\cos\left(\sqrt{E}L_\Gamma - \sigma_\Gamma\frac{\pi}{2}-\frac{\pi}{4}\right), \tag{3.54}$$

where $L_\Gamma = \sqrt{\alpha_a L_{\gamma_a}^2 + \alpha_b L_{\gamma_b}^2}$, and $\sigma_\Gamma = (\sigma_{\gamma_a}+\sigma_{\gamma_b})$.

Numerics

It is assumed here that $m_b = \lambda m_a$ so that $\alpha_b = \lambda\alpha_a$. In the following numerical calculation, $\alpha_a = 1$ (i.e. $\hbar = 1, m_a = 1/2$) and $\lambda = 2$ (i.e. $m_b = 2m_a = 1$). We first compare the length spectrum of the heterogeneous orbits

$$\tilde{F}_{\rm 2h}^{\rm sc}(L) = \mathcal{F}\{\tilde{\rho}_2^{\rm h}(k)\} \tag{3.55}$$

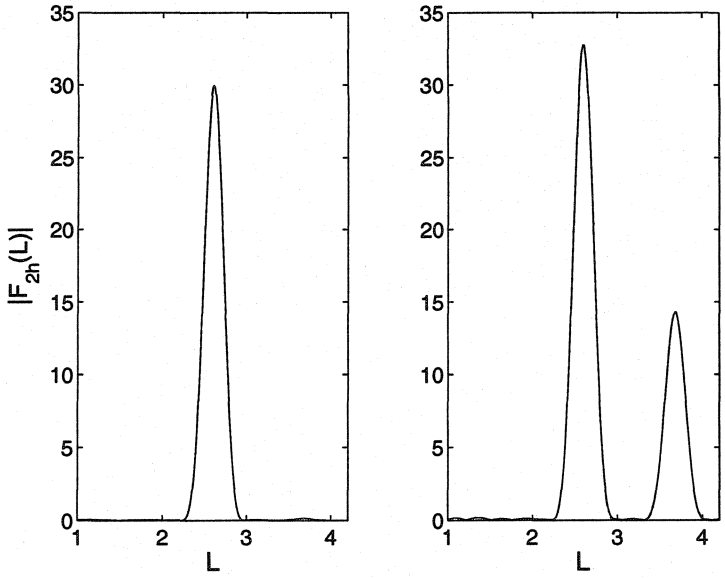

Figure 3.5: Peak splitting in the length spectrum due to broken symmetry. The left window shows the spectrum for identical particles ($m_a = m_b$), and the right window shows the spectrum for nonidentical particles ($m_b = 2m_a$). The solid line is the transform of the quantum two-particle spectrum (3.56), and the dashed-dotted line is the transform of the semiclassical formula for the heterogeneous orbits (3.55).

with its quantum counterpart

$$\tilde{F}_{2h}^{qm}(L) = \mathcal{F}\{\rho_2(k) - \bar{\rho}_2(k) - \tilde{\rho}_2^{d}(k)\}. \tag{3.56}$$

As before, all quantities are expressed in terms of the wave number k (see the comments at the beginning of Sec. 3.3.5). In Eq. (3.56), $\rho_2(k)$ is the quantum two-particle density of states $\rho_2(k) = \sum_I \delta(k - k_I)$, where the superindex I denotes the pair of integers (i, j) and $k_I = \sqrt{k_i^2 + (1/\lambda)k_j^2}$. (Recall that $E_I = k_I^2/\alpha_a$.) The first 377 757 energies of the two-particle spectrum were obtained by adding the first 1250 energies of the one-particle spectrum. The window function parameters are $k_0 = \sqrt{[1 + (1/\lambda)]}k_1$ and $k_f = \sqrt{k_1^2 + (1/\lambda)k_{1250}^2}$. In the quantum transform (3.56), both smooth and dynamical terms are subtracted for a precise comparison. The result is shown in Fig. 3.5. There is excellent agreement between quantum and semiclassical results as expected, but the more interesting aspect is the semiclassical interpretation of the spectrum. It is evident that if particle symmetry is destroyed, then peak splittings occur in the length spectrum. The peaks in Fig. 3.5 are from families of heterogeneous orbits where one of the particles is fixed in the cardioid and the other particle evolves on the diameter orbit $\gamma = \frac{1}{2}(^*2a)$. (The diameter orbit will be denoted by ⌀ in

the following discussion.) There are two such families of orbits. For identical particles, the contribution from each family is the same, and this results in a single peak as shown in the left window of Fig. 3.5. For nonidentical particles, the two contributions are not equal. The first sum in Eq. (3.53) accounts for the situation where particle b evolves on an orbit and produces peaks at $\sqrt{\alpha_b}L_{\gamma_b} = \sqrt{\lambda}L_{\gamma_b}$. The second sum in Eq. (3.53) accounts for the situation where particle a evolves on an orbit and produces peaks at $\sqrt{\alpha_a}L_{\gamma_a} = L_{\gamma_a}$. Therefore, the shorter peak (at $\sqrt{2}L_{\textcircled{D}} \approx 3.67$) is due to the family of heterogeneous orbits where particle a is fixed anywhere in the cardioid while particle b evolves on the diameter orbit with all of the energy. The taller peak (at $L_{\textcircled{D}} \approx 2.6$) is then due to the family of heterogeneous orbits where particle b is fixed anywhere in the cardioid while particle a evolves on the diameter orbit with all of the energy. All peaks in the length spectrum of the heterogeneous orbits split and these splittings can be accounted for in a similar manner.

The spectrum of the dynamical orbits will experience similar splittings. However, not all peaks split; some peaks shift. An example of a shift in the spectrum of the dynamical orbits can be observed in Fig. 3.6. This is obtained by comparing the transform of the dynamical term

$$\tilde{F}_{2\mathrm{d}}^{\mathrm{sc}}(L) = \mathcal{F}\{\tilde{\rho}_2^{\mathrm{d}}(k)\} \tag{3.57}$$

with its quantum counterpart

$$\tilde{F}_{2\mathrm{d}}^{\mathrm{qm}}(L) = \mathcal{F}\{\rho_2(k) - \bar{\rho}_2(k) - \tilde{\rho}_2^{\mathrm{h}}(k)\}. \tag{3.58}$$

The peak in Fig. 3.6 is due to the family of dynamical orbits where both particles evolve on the diameter orbit. The left window shows the spectrum for identical particles where each particle has the same energy $E/2$. The right window shows the spectrum for nonidentical particles where the particle energies are $E_a = E/3$ and $E_b = 2E/3$ [see Eq. (3.43)]. Generally speaking, the peaks that just shift in L space as the symmetry is broken are those produced by dynamical orbits where each of the particles evolve on the same configuration space periodic orbit. These orbits can only occur in one way, unlike the situation where the particles evolve on different configuration space periodic orbits which can occur in two distinct ways. This is analogous to E space where the nondegenerate levels do not experience splitting, but are rather shifted. The location of the peak positions can be understood by noting the dynamical term (3.54) produces peaks at $\sqrt{\alpha_a(L_{\gamma_a}^2 + \lambda L_{\gamma_b}^2)} = \sqrt{L_{\gamma_a}^2 + \lambda L_{\gamma_b}^2}$. If the particles are identical ($\lambda = 1$), then a peak is expected at $\sqrt{2}L_{\textcircled{D}} \approx 3.67$, whereas for

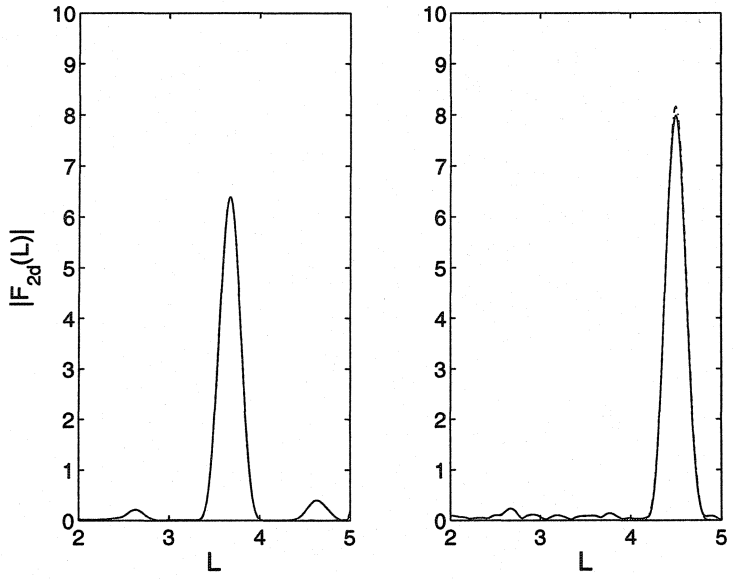

Figure 3.6: Peak shift in the length spectrum of the dynamical orbits due to broken symmetry. The left window shows the spectrum for identical particles ($m_a = m_b$), and the right window shows the spectrum for nonidentical particles ($m_b = 2m_a$). The solid line is the transform of the quantum two-particle spectrum (3.58), and the dashed-dotted line is the transform of the trace formula for the dynamical orbits (3.57).

nonidentical particles ($\lambda = 2$), the peak is expected at $\sqrt{3}L_{\textcircled{D}} \approx 4.5$. The amplitude of the peak also changes. (This is a generic feature of all shifting peaks.) Although the amplitude of a peak is related to the stability of the orbit, there is no change in stability here. The change is due to the mass dependence, which exists only if the symmetry is broken. The change in peak height can be determined semiclassically by comparing the amplitudes of the trace formulas for identical and nonidentical cases. To leading order, the peak height changes by a factor of $\lambda^{1/2}[2/(1+\lambda)]^{1/4}$ after symmetry breaking. For $\lambda = 2$, this factor is 1.28, which can be easily compared with the numerics by inspection of the peak heights in Fig. 3.6. Note the residual structures at $L \approx 2.6$ and $L \approx 4.6$. These arise from errors in the asymptotic expansion for $\tilde{\rho}_2^{\mathrm{h}}(E)$, which is incomplete since there are small corrections from the one-particle Gutzwiller trace formula that are not included. (The corrections to the leading-order term of $\tilde{\rho}_2^{\mathrm{d}}(E)$ are less significant numerically.) Both structures remain after symmetry breaking, and in fact, the structure at $L \approx 4.6$ is the cause of a visible discrepancy between the quantum and semiclassical results for the case of broken symmetry.

Chapter 4

Identical Particles and Symmetry Decomposition

It is important to include the restrictions imposed by particle symmetry into the semiclassical framework and to thereby establish the connection between the classical and quantum mechanics of identical particles. Weidenmüller [42] considered the necessary revisions to the Gutzwiller theory for the special case of interacting fermions in one dimension, but the derivation assumed the periodic orbits to be isolated, which is only true if the particles are *strongly* interacting[1]. There is also a brief discussion in Ref. [42] on noninteracting fermions involving convolutions of one-body level densities[2]. If the particles are *weakly* interacting, the Weidenmüller formalism fails; neither the convolution formalism nor that of the main discussion in Ref. [42] is applicable to the regime of weak to moderate interactions. To develop a uniform theory for the symmetrized many-body problem, it is necessary to first understand the noninteracting system from a semiclassical analysis in the full phase space. Therefore, the main objective in this chapter is to understand how the exchange terms of the symmetrized densities of states arise from purely classical structures.

4.1 Two Noninteracting Identical Particles

The most interesting aspect of the existence of identical particles is the fact that only certain states are occupied, the fully symmetric states if the particles are bosons or the

[1] As discussed in the preceding chapter, noninteracting systems possess continuous time-translational symmetries. The identical nature of the particles also introduces discrete permutational symmetries. Thus, for noninteracting systems of identical particles, discrete and continuous symmetries coexist.

[2] It is surprising that no explicit trace formulas are given and the subtle issue of continuous symmetries is completely overlooked.

fully antisymmetric states if the particles are fermions. It is therefore important to understand how the total density of states decomposes into the separate densities of symmetric and antisymmetric states. Although not absolutely necessary for the present discussion, it will be useful for later to introduce projection operators. The Hamiltonian (3.1) is invariant under exchange of the particles a and b, an operation denoted by ς (leaving the particles unchanged is denoted by ι). There is a two-element discrete group that consists of these operations, and the representation of the two group elements in the Hilbert space (i.e. the quantum operators that exchange the particles) are $\hat{U}$ and $\hat{I}$. Both operators commute with $\hat{H}$. This is a simple group with two irreducible representations (irreps), which are identified as the bosonic (symmetric) representation and the fermionic (antisymmetric) representation. Given an arbitrary state with components belonging to both irreps, the separate components belonging to each irrep can be obtained through the use of the projection operators [97]

$$\hat{P}_{\pm} = \frac{1}{2}\left(\hat{I} \pm \hat{U}\right), \tag{4.1}$$

where the $\pm$ refer to the bosonic and fermionic irreps, respectively.

In terms of these projection operators, the bosonic and fermionic densities of states are defined as

$$\rho_{\pm}(E) = \mathrm{Tr}\left(\hat{P}_{\pm}\delta(E-\hat{H})\right). \tag{4.2}$$

The sum of the bosonic and fermionic densities is the total two-particle density of states $\rho_2(E)$. The difference is given by $\mathrm{Tr}(\hat{U}\delta(E-\hat{H}))$, and expressing the trace in the energy eigenbasis,

$$\begin{aligned}\rho_+(E) - \rho_-(E) &= \sum_{i,j}\langle ij|\hat{U}\delta(E-\hat{H})|ij\rangle \\ &= \sum_{i,j}\langle ji|ij\rangle\delta(E-E_{ij}) \\ &= \sum_{j}\delta(E-2\varepsilon_j),\end{aligned} \tag{4.3}$$

where we have used the fact that $\hat{U}$ exchanges the state labels in the second line and the fact that $E_{jj} = 2\varepsilon_j$ in the third. The final line we recognize as $\rho_1(E/2)/2$ and thereby conclude

$$\rho_{\pm}(E) = \frac{1}{2}\left[\rho_2(E) \pm \frac{1}{2}\rho_1\left(\frac{E}{2}\right)\right]. \tag{4.4}$$

The symmetrized semiclassical densities are obtained by formally replacing the exact quantum densities with their semiclassical approximations. It is of fundamental importance to understand how the *exchange term* [i.e. the second term of Eq. (4.4)] arises from purely classical structures in the full phase space. In the following section, the exchange term is deduced from a semiclassical analysis in the full two-particle phase space (the symmetry decomposition of the smooth part can be analyzed using the theory of Ref. [98] and is discussed in Appendix A.2). To calculate the fluctuating part of the symmetric or antisymmetric density of states, we need to find all orbits in the full phase space (at a specified energy E) that are periodic under time evolution *and* particle exchange.

4.1.1 Dynamical pseudoperiodic orbits (DPPOs)

As discussed initially by Gutzwiller [29] and later in more generality by Robbins [30], in the presence of a discrete symmetry, the fluctuating density of states can be decomposed among the various irreducible representations (irreps). (This was also discussed by Lauritzen [31] who further examined the contribution of boundary orbits.) For the case of two identical particles, these are the symmetric (bosonic) and antisymmetric (fermionic) irreps. To evaluate the separate densities of states, we must calculate $g_{\pm}(E) = \mathrm{Tr}(\hat{P}_{\pm}\hat{G}(E))$ using the projection operators in Eq. (4.1). The first term of the projection operator results in the standard sum over dynamical periodic orbits (3.14). There is a factor of $1/2$, which indicates that this contribution is simply divided evenly between the symmetric and the antisymmetric spectra. It is the second term of the projection operator, which requires careful analysis.

The oscillating part of $\mathrm{Tr}(\hat{U}\hat{G}(E))$ can be expressed in terms of orbits γ' on which particles begin at a point in phase space, evolve for some time T, are then exchanged using the classical analog of $\hat{U}$ with the net result that the particles are returned to their initial conditions. These orbits will be referred to as *pseudoperiodic* to distinguish them from the (standard) dynamical periodic orbits discussed earlier. The symplectic mapping u corresponding to classical particle exchange will be defined as $u(\mathbf{z}_a, \mathbf{z}_b) = (\mathbf{z}_b, \mathbf{z}_a)$. It has the property that u^2 is the identity mapping. The combination of time evolution for time t and particle exchange maps a phase space coordinate $\mathbf{z}' = (\mathbf{z}'_a, \mathbf{z}'_b)$ to $\mathbf{z} = u\Phi_t\mathbf{z}' = (\phi_t\mathbf{z}'_b, \phi_t\mathbf{z}'_a)$. To find orbits which are periodic under these combined operations, periods T are required such that $\mathbf{z}' = u\Phi_T\mathbf{z}'$. Applying this combined operation twice, we find that $\mathbf{z}' = \Phi_{2T}\mathbf{z}'$.

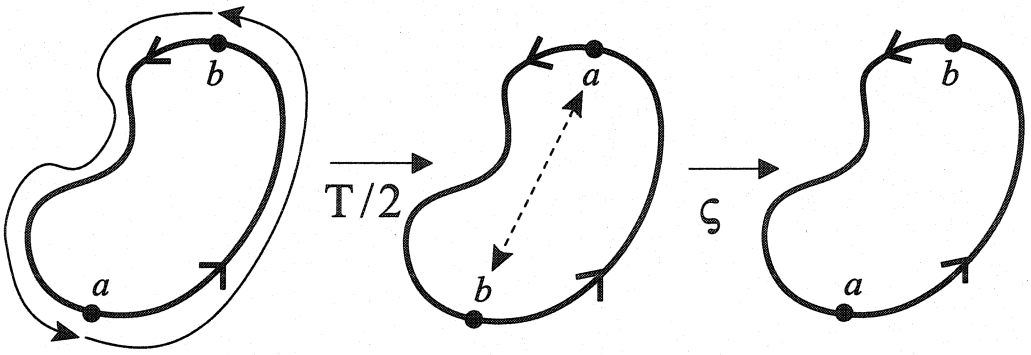

Figure 4.1: A dynamical pseudoperiodic orbit (DPPO) of the full (two-particle) phase space is constructed by placing two particles on a periodic orbit of the one-particle phase space. If $E_a = E_b$ and the particles are half a period out of phase, then after the combined operations of time evolution and particle exchange, the initial conditions are restored.

This is just the condition for a periodic orbit of period $2T$ in the full phase space without particle exchange. So we conclude that the initial coordinate $\mathbf{z}'$ must be on a periodic orbit of the full phase space. However, this condition is still more restrictive since the above considerations also imply that after time T, particle a must be where particle b began and vice-versa. This is only possible if the two particles are traversing the *same* periodic orbit, with the same energy and furthermore are exactly half a period out of phase. This shall be referred to as a type-1 dynamical pseudoperiodic orbit (DPPO). There is also the degenerate case where both particles begin and evolve together. This shall be called a type-0 DPPO and is discussed below.

Therefore, the set of possible pseudoperiodic orbits is much more restricted than the set of standard periodic orbits since pseudo-orbits occur only when both particles are executing the same dynamics. Furthermore, these orbits are isolated and do not come in a 1-parameter family. The existence of families for the standard periodic orbits is due to the freedom in specifying the relative phases of the two motions. This freedom no longer exists and immediately implies that contributions from pseudoperiodic orbits will be weaker by $\sqrt{\hbar}$ because there is one more stationary phase integral to do than for the standard periodic orbits. (This can also be understood from the fact that particle exchange does not conserve the separate energies and so does not commute with J.) Therefore, the usual Gutzwiller trace formula can be used to determine the actions, periods, and stabilities of these isolated pseudoperiodic orbits.

Consider an arbitrary periodic orbit γ of the one-particle phase space with period T_γ and choose some arbitrary initial condition on it $\mathbf{z}'_a$. To have a pseudoperiodic orbit in the full phase space, suppose the initial condition $\mathbf{z}' = (\mathbf{z}'_a, \mathbf{z}'_b = \phi_{T_\gamma/2}\mathbf{z}'_a)$. A flow for a time $T_\gamma/2$ and then particle exchange maps $\mathbf{z}'$ onto itself (see Fig. 4.1). Therefore, the set of pseudoperiodic orbits in the full two-particle phase space is one-to-one with the set of standard periodic orbits in the one-particle phase space. The periods of the pseudoperiodic orbits in the full phase space are one-half of the periods of the corresponding standard periodic orbits in the one-particle phase space. Nevertheless, when evaluating the trace integral we must integrate over all initial conditions on the orbit, and this gives a full factor of T_γ^0 in the amplitude. The actions and phase indices for the pseudo-orbit are the same as for the standard orbit; although the flow is for only time $T_\gamma/2$, both particles are in motion, and so together, the two particles execute one full motion of the periodic orbit. The stability matrix in the full phase space requires careful analysis. Let $\tilde{M}_\gamma$ be the stability matrix of the full periodic orbit γ of the one-particle phase space, and $\tilde{M}_{\gamma'}$ be the stability matrix of the pseudoperiodic orbit γ' in the full phase space. It is shown in Appendix B.4 that $\det(\tilde{M}_{\gamma'} - I) = 4\det(\tilde{M}_\gamma - I)$, where on each side of the equation I is understood to be an appropriately dimensioned unit matrix. We conclude that the contribution of this pseudo-orbit to the oscillating part of $\mathrm{Tr}(\hat{U}\hat{G}(E))$ is

$$\tilde{g}^{\mathrm{d}}_{\varsigma}(E) = \frac{1}{2i\hbar}\frac{T_\gamma^0}{\sqrt{\left|\det(\tilde{M}_\gamma - I)\right|}}\exp\left[i\left(\frac{S_\gamma}{\hbar} - \sigma_\gamma\frac{\pi}{2}\right)\right], \tag{4.5}$$

where all classical quantities are evaluated at the single-particle energy $E/2$. (Recall the symbol ς denotes the group element that exchanges the particles.) Apart from the energy dependence and the factor of 2 in the denominator, this contribution is the same as the corresponding primitive orbit for the single-particle density of states [Eqs. (1.5) and (1.6)].

As mentioned above, there is also the situation where both particles start at the same point on the orbit and evolve together. Interchanging them at the end trivially returns them to the same coordinates. This pseudo-orbit has action $2S_\gamma$, but should not be confused with the standard dynamical periodic orbit where the two particles start at independent points on the orbit and therefore occur in a 1-parameter family. The particle exchange at the end ensures that the pseudo-orbit is isolated and does not occur in a family. The standard orbit and the pseudo-orbit share the same action, but the standard orbit has a larger amplitude due to the different $\hbar$ prefactor and will tend to dominate. This situation

of coexisting contributions with the same action is analogous to a potential system with a reflection symmetry where there is a boundary orbit, which contributes to both the identity term in the symmetrized density of states and also to the reflection term. The difference here is that the two types of dynamical orbits contribute with different powers of $\hbar$.

The analysis of the contribution of the type-0 DPPO is similar to above. Its amplitude is simply the same as the double repetition of the orbit γ, again divided by two. (The proof of this fact will not be given here.) This pattern continues for higher repetitions, where for odd multiples of the action the particles start $T_\gamma/2$ out of phase while for even multiples the particles start in phase and interfere with stronger (in an $\hbar$ sense) contributions from the standard dynamical orbits. Apart from the energy dependence and the factor of 2 in the denominator, the sum over repetitions is the same as for the single-particle density of states.

Thus, the contribution of the pseudoperiodic orbits to the bosonic and fermionic densities of states is precisely the same as the fluctuating density of states of the one-particle spectrum except that it is to be evaluated at half the total energy (since the total energy is partitioned equally between the two particles) and should also be divided by an overall factor of 2. In conclusion,

$$\tilde{\rho}_\pm(E) = \frac{1}{2}\left[\tilde{\rho}_2(E) \pm \frac{1}{2}\tilde{\rho}_1\left(\frac{E}{2}\right)\right], \tag{4.6}$$

which is consistent with Eq. (4.4).

The symmetry decomposition for heterogeneous orbits is trivial. Since the two particles are executing completely different dynamics, the combination of time evolution and particle exchange, as above, can never return the particles to their initial conditions. This requires an equivalence of the two motions. Thus, the contribution from heterogeneous orbits is simply divided evenly between the symmetric and antisymmetric representations, and belongs to the $\tilde{\rho}_2(E)$ term of Eq. (4.6).

4.2 Two Identical Particles in a Cardioid Billiard

The formal symmetrization of two noninteracting identical particles in a cardioid billiard was examined in Ref. [35]. The symmetry reduction is further examined here in the context of the preceding section. A detailed discussion of the numerics can be found in Ref. [35] (see Fig. 3.2 for a list of the short periodic orbits).

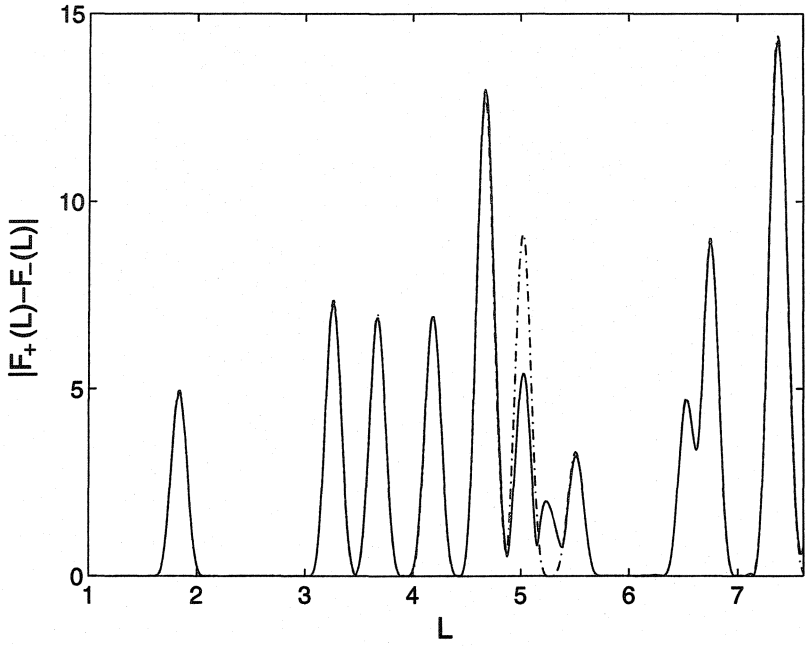

Figure 4.2: Fourier transform of the two-particle exchange term. Quantum (solid line) and semiclassical (dashed-dotted line) results for $L < 7.6$. Each peak is due to a dynamical pseudoperiodic orbit (DPPO) of the full phase space.

The smooth and oscillating parts of the symmetrized densities of states are given by Eqs. (A.8) and (4.6), respectively (expressed in terms of the wave number k). Numerically, the procedure here is to compare the quantum mechanical exchange term and its semiclassical analog in reciprocal L space, that is, to compare

$$\mathcal{F}\{[\rho_+(k) - \rho_-(k)] - [\bar{\rho}_+(k) - \bar{\rho}_-(k)]\} \tag{4.7}$$

and

$$\mathcal{F}\{\tilde{\rho}_+(k) - \tilde{\rho}_-(k)\}, \tag{4.8}$$

where the integral operator $\mathcal{F}$ denotes the Fourier transform as defined in Eq. (3.40). In L space, peaks are expected at the lengths of the dynamical pseudo-orbits (DPPOs).

As discussed in Sec. 4.1.1, there are two types of DPPOs. In each case, both particles are on the same periodic orbit γ of the one-particle phase space. If this orbit has length $L_\gamma = n_\pm L^0_\gamma$ (where $n_\pm$ is an even or odd integer repetition index and L^0_γ is the primitive length of the orbit), then type-0 and type-1 DPPOs have lengths $n_+L^0_\gamma$ and $n_-L^0_\gamma$, respectively. However, we should not expect peaks at these positions, but rather

at $n_{\pm}L_{\gamma}^{0}/\sqrt{2}$ since each particle has energy $E/2$. (Recall that a billiard orbit with length L_{γ} has action $S_{\gamma}(\varepsilon) = \hbar\sqrt{\alpha\varepsilon}L_{\gamma}$; each particle on a (primitive) type-0 orbit traverses the full orbit γ while each particle on a (primitive) type-1 orbit completes only one half of the motion.) Fig. 4.2 shows the length spectrum of the DPPOs. In Table 4.1, some of the peaks are identified with one or several of the orbits shown in Fig. 3.2. As stated above, this can be done systematically for each structure, but only a partial listing is given here. (The peak at $L \approx 5.25$ is completely undetected by the trace formulas since it arises from a *diffractive* orbit. Such orbits require a separate analysis since they are not included in the standard Gutzwiller theory [94]). The discrepancy that occurs at $L \approx 5$ arises from two orbits $\gamma^0 = 4\text{a}$ and $\gamma^0 = \frac{1}{2}(*10\text{b})$ that are not well isolated in phase space and pass close to the cusp of the cardioid.

Consider the first and third peaks in L space. The first peak can be identified with the type-1 DPPO consisting of both particles evolving on the primitive orbit $\gamma^0 = \frac{1}{2}(*2\text{a})$ with the same energy and exactly half a period out of phase. Each particle traverses one half of the orbit and is then exchanged. Note that this is distinct from the situation where the two particles start and evolve in phase and each complete one full motion on the orbit before being exchanged. This type-0 DPPO accounts for the third peak . The first repetition of the type-1 DPPO is the same as before except each particle traverses *one and one half* of the orbit before particle exchange. This accounts for the peak at $L \approx 5.51$. For the first repetition of the type-0 DPPO, each particle completes two full motions on the orbit before particle exchange. This gives a contribution at $L \approx 7.35$. All other L-space structures can be accounted for in a similar manner.

4.3 Several Noninteracting Identical Particles

If the system consists of N identical particles, it is invariant under S_N, the permutation group of N identical particles. This group has many different irreps for $N > 2$, but only the one-dimensional bosonic and fermionic irreps, which are fully symmetric or antisymmetric under particle exchange are considered here. For the following discussion, it is first necessary to introduce the projection operators [97]

$$\hat{P}_{\pm} = \frac{1}{N!}\sum_{\tau}(\pm 1)^{s_\tau}\hat{U}_{\tau}, \tag{4.9}$$

L	Type	γ^0
1.84	1	$\frac{1}{2}$(*2a)
3.27	1	$\frac{1}{2}$(*4b)
3.67	0	$\frac{1}{2}$(*2a)
4.18	1	$\frac{1}{2}$(*6b)
4.66	1	3a
4.72	1	$\frac{1}{2}$(*8b)
5.51	2(1)	$\frac{1}{2}$(*2a)
6.53	0	$\frac{1}{2}$(*4b)
6.75	1	$\frac{1}{2}$(*8c)
7.34	1	5a
7.35	2(0)	$\frac{1}{2}$(*2a)
7.41	1	$\frac{1}{2}$(*10h)

Table 4.1: Some DPPOs of a two-particle system in a cardioid billiard. The first column gives the position of the peak in L space arising from the DPPO, and the third column specifies the primitive orbits of the one-particle phase space on which the particles evolve. The second column indicates the type of DPPO using the classification scheme introduced in Sec. 4.1.1. The DPPOs that produce peaks at $L \approx 5.51$ and $L \approx 7.35$ have prefactors of 2 indicating that these are first repetitions of type-1 or type-0 DPPOs. These two situations are described further in the text.

where $\pm$ refer to the bosonic and fermionic irreps, respectively. The sum is over the group elements τ of S_N, which denote particular permutations of the particles, $\hat{U}_\tau$ is the representation of the group element in the Hilbert space (i.e. the quantum operator that exchanges the particles), s_τ is the number of two-particle exchanges required to obtain τ, and the factor $(\pm 1)^{s_\tau}$ is a group character. For fermions, the sign of the character depends on the number of times two particles must be interchanged. As before, we need to evaluate $g_\pm(E) = \mathrm{Tr}(\hat{P}_\pm \hat{G}(E))$ and therefore $\mathrm{Tr}(\hat{U}_\tau \hat{G}(E))$ for each τ. This is a class function depending only on the cyclic structure of τ.

Each permutation τ can be decomposed uniquely into mutually commuting cycles [97]; in each of these cycles, a subset of the particles is being permuted. An n-cycle is a permutation in which only n of the particles are being permuted. In particular, a 1-cycle corresponds to an individual particle being exchanged with itself (i.e. unchanged), a 2-cycle corresponds to two particles being exchanged with each other, and so on. A general permutation τ may consist of cycles of various sizes and may also have several cycles of the same size. In general, for a given τ, there are ν_1 1-cycles, ν_2 2-cycles, and so on. Then, the cycle structure of a class of permutations can be given as a set of integers $(\nu_1, \nu_2, \ldots, \nu_N)$. This set $\boldsymbol{\nu}$ labels the conjugacy classes. Two permutations with the same $\boldsymbol{\nu}$ belong to the same class and thus have the same value of $\mathrm{Tr}(\hat{U}_\tau \hat{G})$. The analysis of the preceding chapter can be understood as being the special case of the identity element. To decompose the complete density of states, we need to determine both the smooth and the oscillatory components of $\mathrm{Tr}(\hat{U}_\tau \hat{G})$. The smooth component is discussed in Appendix A.3. In this section, we examine the oscillatory component.

4.3.1 Dynamical cycles ($n_\mathbb{k}$-cycle DPPOs)

Consider first the case for which all particles are evolving dynamically. A group element τ consists of n_τ cycles, a given cycle $\mathbb{k}$ consisting of interchanging $n_\mathbb{k}$ particles. As in the two-particle case, particle exchange does not commute with all of the single-particle energies and so we do not expect periodic orbit families of dimension $(N-1)$. However, for each cycle, there is a generator $J_\mathbb{k}$, which is the sum of the single-particle Hamiltonians of the particles involved in this cycle and is preserved under the action of the group element τ. These generators commute with each other and with the total Hamiltonian H. However, this is not an independent set since $\sum_\mathbb{k} J_\mathbb{k} = H$. There are $(n_\tau - 1)$ independent commuting

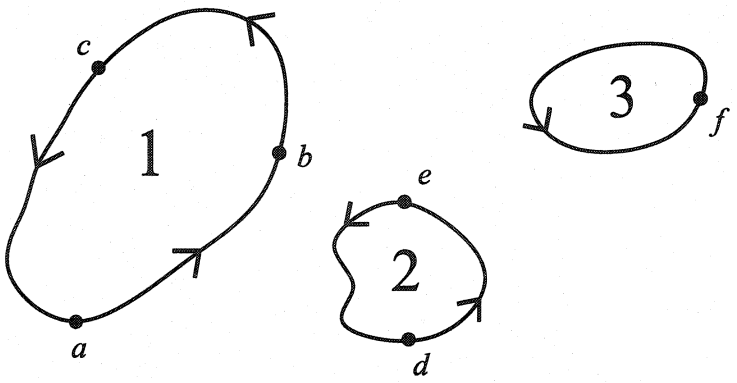

Figure 4.3: A specific permutation of six particles is decomposed into three dynamical cycles. Each of the particles belonging to a particular cycle is on a periodic orbit of the one-particle phase space with $T_1(E_a = E_b = E_c \equiv E_1)/3 = T_2(E_d = E_e \equiv E_2)/2 = T_3(E_f \equiv E_3) \equiv T(E)$.

generators other than the full Hamiltonian and so we expect periodic orbit families of this dimensionality to contribute to $\mathrm{Tr}(\hat{U}_\tau \hat{G})$.

We seek structures in the full phase space which are invariant under the combined operations of time evolution (for time T) generated by H and particle exchange as specified by τ. Clearly, this is only possible if all particles of a given cycle $\mathbb{k}$ are on the *same* periodic orbit $\gamma_\mathbb{k}$. These all must have the same energy $E_\mathbb{k}$ and then $J_\mathbb{k} = n_\mathbb{k} E_\mathbb{k}$. For example, suppose that particles a, b, and c constitute a 3-cycle. Starting with particle a at some arbitrary point on a periodic orbit γ of the one-particle phase space, particle b an amount $T_\gamma/3$ ahead of it, and particle c an amount $T_\gamma/3$ behind. Then, after a time $T = T_\gamma/3$, $a \to b$, $b \to c$, and $c \to a$. However, the group element $\tau = (acb)$ maps $a \to c$, $c \to b$ and $b \to a$ simply undoes this change and the original configuration is restored. Such a cycle is shown at the left of Fig. 4.3. For each cycle of τ, there is a set of particles with identical energies traversing a periodic orbit of the one-particle phase space. Each particle completes $(1/n_\mathbb{k})$ of the full motion on the periodic orbit.

Now assign each cycle a periodic orbit $\gamma_\mathbb{k}$. (Henceforth, the subscript $\mathbb{k}$ will be used for the orbit label rather than the more cumbersome $\gamma_\mathbb{k}$.) Then, partition the energy (i.e. the values of $J_\mathbb{k}$) so that the periods $T_\mathbb{k}/n_\mathbb{k}$ are all the same (call this quantity T). After time T and permutation τ, the resulting structure is guaranteed to be globally periodic in the full phase space. Such an orbit comes in an $(n_\tau - 1)$ degenerate family, which can be understood as follows. For each cycle, it is enough to specify the initial condition of

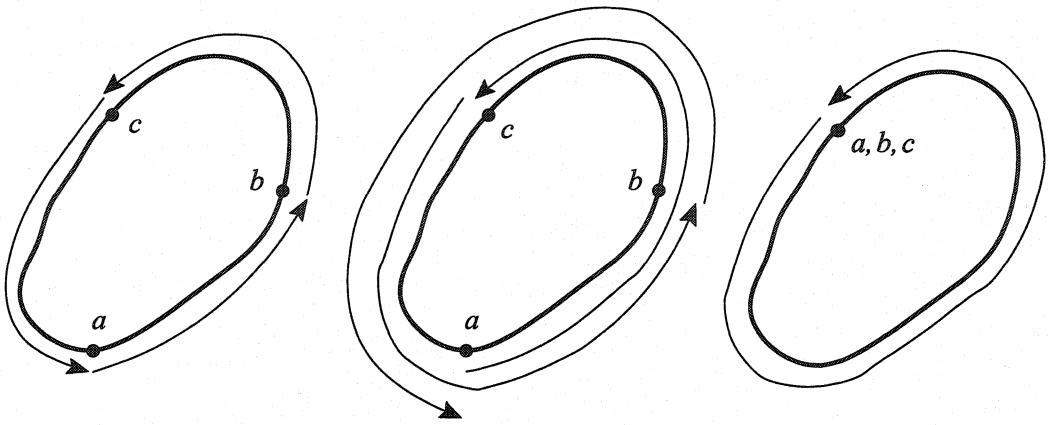

Figure 4.4: (Left) The same type-1 dynamical 3-cycle (type-1 3-cycle DPPO) of Fig. 4.3. The total action is S_1. (Middle) A type-2 dynamical 3-cycle (type-2 3-cycle DPPO). The same periodic orbit, but each particle executes two-thirds of the complete motion and the net action is $2S_1$. (Right) A type-0 dynamical 3-cycle (type-0 3-cycle DPPO). Each particle executes one complete motion and the net action is $3S_1$.

one particle after which the initial conditions of all the other particles are known. The initial condition of the first particle can be chosen arbitrarily for the first cycle. The first particle of the other $(n_\tau - 1)$ cycles can then begin anywhere on their respective orbits (this constituting the dimensionality of the family). This can also be understood from the fact that starting at the arbitrary initial condition, flows generated by any of the $(n_\tau - 1)$ generators $J_{\mathbb{k}}$ map out an $(n_\tau - 1)$-dimensional surface. Together with a flow in H, the periodic orbit manifold is a torus of dimension n_τ.

For the symmetry decomposition (involving the DPPOs) of a two-particle system, there were contributions from higher multiples. For instance, we could start both particles at the same point on a periodic orbit, let them evolve for a full period and then interchange them. There is an analogous structure in the N-particle case; the particles are allowed to execute a fraction $l_{\mathbb{k}}/n_{\mathbb{k}}$ of an orbit as depicted in Fig. 4.4. As before, the additional factor $l_{\mathbb{k}}$ can be absorbed into the definitions of the various classical parameters.

The contribution of an n_τ-torus of orbits can now be inferred from the results of the last chapter. The only detail is in the determination of $(\partial\Theta/\partial\mathbf{J})$. It is as in Eq. (3.24), but with the understanding that the sum (product) over orbits should be replaced by a sum (product) over cycles. These become equivalent in the identity contribution, which was considered there. Also, since the anholonomy term measures deviations away from global periodicity arising from a change in the energy partition (now among the cycles), T_p' should

be replaced by $T'_{\mathbb{k}}/n_{\mathbb{k}}^2$. A factor of $1/n_{\mathbb{k}}$ comes from the fact that the energy of the cycle must be divided evenly among the $n_{\mathbb{k}}$ particles belonging to this cycle. A second factor of $1/n_{\mathbb{k}}$ comes from the fact that the orbit has time $T_{\mathbb{k}}/n_{\mathbb{k}}$ for the anholonomy to evolve. (Note that if this orbit is a multiple repeat, then it is understood that $T'_{\mathbb{k}} = l_{\mathbb{k}} T^{0'}_{\mathbb{k}}$, where $T^0_{\mathbb{k}}$ is the primitive period.) The entire contribution should also be divided by $\prod_{\mathbb{k}} n_{\mathbb{k}}$ arising from the monodromy matrix as discussed in Appendix B.4. This last fact is the generalization of the factor of $1/2$ appearing as a prefactor in the second term of Eq. (4.6) for the two-particle case. Therefore, the contribution from a family of dynamical cycles to the oscillatory part of $\mathrm{Tr}(\hat{U}_\tau \hat{G})$ can be written as

$$\tilde{g}^{\mathrm{d}}_\tau(n_\tau, E) = \frac{1}{i\hbar}\frac{1}{(2\pi i\hbar)^{(n_\tau-1)/2}} \left\{ \prod_{\mathbb{k}=1}^{n_\tau} \frac{T^0_{\mathbb{k}}(E_{\mathbb{k}}) \exp\left[i\left(\frac{S_{\mathbb{k}}(E_{\mathbb{k}})}{\hbar} - \sigma_{\mathbb{k}}\frac{\pi}{2}\right)\right]}{\sqrt{\left|\det(\tilde{M}_{\mathbb{k}} - I)\right|}\sqrt{\left|T'_{\mathbb{k}}(E_{\mathbb{k}})\right|}} \right\} \frac{\exp\left(i\delta\frac{\pi}{2}\right)}{\sqrt{\left|\sum_{\mathbb{k}=1}^{n_\tau} \frac{n_{\mathbb{k}}^2}{T'_{\mathbb{k}}(E_{\mathbb{k}})}\right|}}, \tag{4.10}$$

where $\tilde{M}_{\mathbb{k}}$ is the stability matrix for a full cycle $\mathbb{k}$ (see Appendix B.4). Note that the contribution of the group element for which *all* of the particles belong to the same cycle is proportional to $\tilde{\rho}_1(E/N)^3$.

4.3.2 Heterogeneous cycles ((n_s, n_e) HPPOs)

It is also possible that $\mathrm{Tr}(\hat{U}_\tau \hat{G})$ has a contribution from cycles where some particles are fixed (either at extrema of a potential or anywhere in a billiard) while others are evolving dynamically. Let n_s denote the number of cycles that are stationary, and n_e the number of cycles that are evolving dynamically. Then, $n_s + n_e = n_\tau$. To have such a contribution to the oscillating component, group elements must consist of two or more cycles since those that consist of only one $n_{\mathbb{k}}$-cycle will either contribute to Eq. (4.10) if they are dynamical cycles or contribute to the smooth part (see Appendix A.3) if they are stationary cycles. In addition, at least one cycle is required to involve particles that are evolving dynamically ($n_e \geq 1$) *and* at least one cycle must involve particles that are stationary ($n_s \geq 1$). Thus, heterocycles are cycles for which $1 \leq n_e < N$ and $1 \leq n_s < N$.

For potentials, the dimension of a family of orbits is then $(n_e - 1)$ since only the

[3]The division by N of the energy argument simply states that the total energy must be *evenly* divided among all of the particles. The set of orbits corresponding to this cycle is clearly the same as the set of orbits of the one-particle dynamics (almost by definition) and the amplitudes and actions are the same as the one-particle case since the N particles *collectively* execute one complete motion (or a multiple repetition) of the periodic orbit.

generators associated with dynamical cycles generate new orbits. The stationary cycles simply contribute their monodromy matrices and phase indices, and otherwise play no essential role. Equation (4.10) holds for the particles which are evolving dynamically, but n_τ is replaced with n_ϵ and the energy associated with the n_ϵ dynamical cycles, E_{n_ϵ}, is the total energy minus the sum of the potential energies of the stationary particles. For a potential minimum, the contribution of one family of heterocycles [(n_s, n_ϵ) HPPOs] to the oscillatory part of $\mathrm{Tr}(\hat{U}_\tau \hat{G})$ is

$$\tilde{g}_\tau^{\mathrm{h}}(n_\epsilon, n_\tau, E) = \tilde{g}_\tau^{\mathrm{d}}(n_\epsilon, E_{n_\epsilon}) \left\{ \prod_{\mathbb{k}=n_\epsilon+1}^{n_\tau} \frac{\exp\left(-i\frac{\pi d}{2}\right)}{\prod_{j=1}^{d} 2\sin\left(\frac{\omega_{j_\mathbb{k}} T_\mathbb{k}}{2}\right)} \right\}, \tag{4.11}$$

where the $\omega_{j_\mathbb{k}}$ denote the local frequencies around the potential minimum at which the particles of cycle $\mathbb{k}$ reside. If this cycle of particles is actually at a saddle or a maximum, the final factor is modified as in the discussion below Eq. (3.16).

For billiards, the previous relation holds for the dynamical cycles, but the product over stationary cycles is modified. As explained below, the dimension of the orbit families is $[(n_\epsilon - 1) + n_s d]$ since the generators associated with stationary cycles also generate new orbits. If there are n_s stationary 1-cycles, these generators and the conjugate parameters are $\mathbf{J} = (\mathbf{p}_1, \ldots, \mathbf{p}_{n_s})$ and $\mathbf{\Theta} = (\mathbf{q}_1, \ldots, \mathbf{q}_{n_s})$, respectively. (There are $n_s d$ components since both $\mathbf{p}_i$ and $\mathbf{q}_i$ are d-dimensional.) In fact, this is true regardless of the number of particles belonging to the stationary cycle. At first, this may seem incorrect since longer cycles will introduce additional generators because these involve more particles. However, this larger set of generators is not an independent set. To see this, recall that the particles involved in a stationary cycle can be anywhere in the billiard. If the cycle is not a 1-cycle, but rather an $n_\mathbb{k}$-cycle, the combined operations of time evolution and particle exchange will not restore the initial configuration unless all the particles involved in this cycle possess the same phase space coordinates. More formally, a stationary $n_\mathbb{k}$-cycle possesses a set of generators, $\mathbf{J} = (\mathbf{p}_1, \ldots, \mathbf{p}_{n_\mathbb{k}})$ and the conjugate parameters $\mathbf{\Theta} = (\mathbf{q}_1, \ldots, \mathbf{q}_{n_\mathbb{k}})$, where both $\mathbf{p}_i$ and $\mathbf{q}_i$ have d components. However, after the specification of a single $(\mathbf{p}_i, \mathbf{q}_i)$ pair, all others are uniquely determined: $\mathbf{p}_1 = \mathbf{p}_2 = \cdots = \mathbf{p}_{n_\mathbb{k}}$ *and* $\mathbf{q}_1 = \mathbf{q}_2 = \cdots = \mathbf{q}_{n_\mathbb{k}}$. Thus, one independent set of generators is $\mathbf{J} = \mathbf{p}/n_\mathbb{k}$, where $\mathbf{p}$ is the momentum of one particle of the stationary cycle. The factor of $1/n_\mathbb{k}$ comes from the fact that the momentum of the cycle must be equally partitioned among the $n_\mathbb{k}$ particles belonging to this cycle. (It is not necessary for stationary particles of distinct cycles to have the same phase space

coordinates.) Thus, for a d-dimensional billiard, the contribution to the oscillatory part of $\mathrm{Tr}(\hat{U}_\tau \hat{G})$ from a family of heterocycles [(n_s, n_e) HPPOs] is

$$\tilde{g}_\tau^{\mathrm{h}}(n_e, n_\tau, E) = \tilde{g}_\tau^{\mathrm{d}}(n_e, E) \left\{ \prod_{\mathbb{k}=n_e+1}^{n_\tau} \frac{\Omega_d \exp\left(-i\frac{\pi d}{4}\right)}{\left(\frac{2\pi\hbar n_{\mathbb{k}} T_{\mathbb{k}}}{m}\right)^{d/2}} \right\}. \tag{4.12}$$

Equations (4.11) and (4.12) are the most general formulas of this chapter. These trace formulas allow for any amount of particle permutation and any number of particles can be evolving while the rest are stationary. Each cycle can involve an arbitrary repetition of the primitive motion. As before, if $n_e = 1$, then $\delta \equiv 0$. Heterocycles in billiards are $O(1/\hbar^{n_s d/2})$ stronger than in smooth potentials. For potentials [billiards], heterocycles are $O(\hbar^{n_s/2})$ weaker [$O(1/\hbar^{(d-1)n_s/2})$ stronger] than dynamical cycles. Thus, the most significant structures are dynamical cycles for smooth potentials and heterocycles for billiards.

4.4 Three Identical Particles in a Cardioid Billiard

In the following subsections, we study the symmetry decomposition of a three-particle system in a cardioid billiard. The contributions of the heterocycles and the dynamical cycles to the symmetrized densities are determined using the results of Sec. 4.3. The numerical analysis in reciprocal L space involves comparing quantum and semiclassical densities that belong to the nontrivial symmetry classes (conjugacy classes) of S_3. These quantities are analogous to the quantum and semiclassical exchange terms studied for the two-particle case in Sec. 4.2. This type of analysis provides an immediate interpretation of the quantum spectra in terms of pseudoperiodic orbits in the classical phase space.

4.4.1 Quantum mechanics

Due to the identical nature of the particles, the eigenstates of $\hat{H}$ can be classified according to the irreps of S_3, the permutation group of three identical particles. Each group element belongs to one of three classes [i.e. $(3,0,0)$,$(1,1,0)$,$(0,0,1)$] based on the cycle structure of the group element. Thus, there are also three irreps. These are the symmetric (trivial) irrep $\mathscr{A}_+$, the antisymmetric irrep $\mathscr{A}_-$, and the two-dimensional mixed-symmetry irrep $\mathscr{E}$. (S_N always possesses exactly two one-dimensional irreps regardless of the size of $N > 1$.) The character table for S_3 is given below. Numbers in front of class labels indicate the number of elements in that class.

The total three-particle density of states can be decomposed into symmetrized densities $\rho_{\mathcal{I}}(E)$, each belonging to an irrep $\mathcal{I}$ of S_3:

$$\rho_3(E) = \rho_+(E) + \rho_-(E) + \rho_{\mathscr{E}}(E). \tag{4.13}$$

Each partial density may be obtained by projection $\rho_{\mathcal{I}}(E) = \mathrm{Tr}(\hat{P}_{\mathcal{I}}\delta(E-\hat{H}))$, where the operator $\hat{P}_{\mathcal{I}}$ projects[4] onto the irrep $\mathcal{I}$. Expressing the trace in the energy eigenbasis as in Eq. (4.3), the symmetrized densities are

$$\rho_\pm(E) = \frac{1}{6}\left[\rho_3(E) \pm \frac{3}{2}\rho_1\left(\frac{E}{2}\right) * \rho_1(E) + \frac{2}{3}\rho_1\left(\frac{E}{3}\right)\right], \tag{4.14}$$

$$\rho_{\mathscr{E}}(E) = \frac{2}{6}\left[2\rho_3(E) - \frac{2}{3}\rho_1\left(\frac{E}{3}\right)\right]. \tag{4.15}$$

To understand how the cross term arises in Eq. (4.14), consider the contribution from $\tau = (a)(bc) \in (1,1,0)$:

$$\begin{aligned}
\sum_{i,j,k}\langle ijk|\hat{U}_\tau\delta(E-\hat{H})|ijk\rangle &= \sum_{i,j,k}\langle ikj|ijk\rangle\delta(E-E_{ijk}) \\
&= \sum_{i,j}\delta(E-E_{ijj}) \\
&= \sum_{i,j}\delta(E-(\varepsilon_i+2\varepsilon_j)) \\
&= \frac{1}{2}\rho_1\left(\frac{E}{2}\right) * \rho_1(E).
\end{aligned} \tag{4.16}$$

The other contributions can be found in a similar manner. We could compute each partial density separately for comparison with the numerics, but it is more illuminating to isolate the contribution from each symmetry class by inverting the above system of equations:

$$\rho_{(1,1,0)}(E) \equiv \rho_+(E) - \rho_-(E) = \frac{1}{2}\rho_1\left(\frac{E}{2}\right) * \rho_1(E), \tag{4.17}$$

$$\rho_{(0,0,1)}(E) \equiv \rho_+(E) + \rho_-(E) - \frac{1}{2}\rho_{\mathscr{E}}(E) = \frac{1}{3}\rho_1\left(\frac{E}{3}\right), \tag{4.18}$$

[4]For a discrete group G, the operator $\hat{P}_{\mathcal{I}}$ that projects onto the irrep $\mathcal{I}$ is $\hat{P}_{\mathcal{I}} = (d_{\mathcal{I}}/|G|)\sum_g \chi_{\mathcal{I}}(g)\hat{U}_g^\dagger$, where the sum is over all group elements $g \in G$, $d_{\mathcal{I}}$ is the dimension of the irrep, $|G|$ is the order of the group, $\chi_{\mathcal{I}}(g)$ is the character of the group element g in the irrep $\mathcal{I}$, and $\hat{U}_g$ is the operator that transforms Ψ as prescribed by the group element $g \in G$. Permutation operators are unitary (S_N is a unitary group). For $\mathscr{A}_\pm$ irreps, this reduces to the operator of Eq. (4.9), and for the irrep $\mathscr{E}$ of S_3, using the information provided in Table 4.2, $\hat{P}_{\mathscr{E}} = \frac{2}{6}(2\hat{I} - \hat{U}_{\tau_1} - \hat{U}_{\tau_2})$, where $\tau_{1/2} \in (0,0,1)$ and $\hat{I}$ denotes the identity operator.

$\mathcal{I}$	$1(3,0,0)$	$3(1,1,0)$	$2(0,0,1)$
$\mathscr{A}_+$	1	1	1
$\mathscr{A}_-$	1	-1	1
$\mathscr{E}$	2	0	-1

Table 4.2: Character table for S_3.

where $\rho_{(1,1,0)}(E)$ and $\rho_{(0,0,1)}(E)$ denote the densities belonging to the class of two-particle and three-particle exchanges, respectively. (The identity class which reproduces the total density of states is ignored here since this was studied in the preceding chapter.) From Eq. (4.18), note that the contribution of the longest cycle is directly related to the one-particle density of states as discussed at the end of Sec. 4.3.1. In the following subsections, we shall examine in detail the semiclassical decomposition of each partial density into smooth and oscillatory components:

$$\rho_{\mathcal{I}}(E) = \bar{\rho}_{\mathcal{I}}(E) + \tilde{\rho}_{\mathcal{I}}(E). \tag{4.19}$$

4.4.2 Stationary cycles

If all particles being permuted are fixed, the cycles are stationary and contribute to $\bar{\rho}_{\mathcal{I}}(E)$. Using the results of Appendix A.3, it can be shown that the smooth densities belonging to each irrep are given by Eqs. (4.14) and (4.15), but with ρ replaced by $\bar{\rho}$. Thus,

$$\begin{aligned}\bar{\rho}_{(1,1,0)}(E) &= \frac{1}{2}\bar{\rho}_1\left(\frac{E}{2}\right) * \bar{\rho}_1(E) \\ &= \frac{1}{2}\left[\frac{\alpha^2\mathcal{A}^2}{16\pi^2}E - \frac{\alpha^{3/2}\mathcal{A}\mathcal{L}(1+\sqrt{2})}{16\pi^2}\sqrt{E} + \frac{\alpha}{4\pi}\left(\frac{\sqrt{2}\mathcal{L}^2}{16} + 3\mathcal{A}\mathcal{K}\right)\right],\end{aligned} \tag{4.20}$$

$$\bar{\rho}_{(0,0,1)}(E) = \frac{1}{3}\bar{\rho}_1\left(\frac{E}{3}\right) = \frac{1}{3}\left[\frac{\alpha\mathcal{A}}{4\pi} - \frac{\sqrt{3\alpha}}{8\pi}\frac{\mathcal{L}}{\sqrt{E}} + 3\mathcal{K}\delta(E)\right]. \tag{4.21}$$

Note that in Eq. (4.20), the terms that are $O(1/\hbar)$ are ignored since some of the contributions at this order cannot be calculated exactly. These terms can be computed numerically, but are insignificant for the analysis.

4.4.3 Heterogeneous cycles

The leading-order cycles are the three 1-cycles of the identity class. If one 1-cycle is stationary and the other two 1-cycles are dynamical ($n_s = 1, n_\ell = 2$), then the result from Eq. (4.12) is identical to $\tilde{\rho}^{\mathrm{h}}_{\Gamma}(2,3,E)$. If instead two 1-cycles are stationary and one 1-cycle is dynamical ($n_s = 2, n_\ell = 1$), then Eq. (4.12) reduces to $\tilde{\rho}^{\mathrm{h}}_{\Gamma}(1,3,E)$. There are three contributions of each type.

The first correction is from permutations $\tau \in (1,1,0)$ that consist of one 1-cycle and one 2-cycle. There are two such contributions. The first one is from heterocycles for which the 1-cycle is stationary and the 2-cycle is dynamical. Using formula (4.12) such that $\mathbb{k} = 1$ is the 1-cycle and $\mathbb{k} = 2$ is the 2-cycle ($n_1 = 1, n_2 = 2, J_2 = 2E_2 = H = E \Rightarrow E_2 = E/2$), the result has the structure of the leading-order term of $\frac{1}{2}\tilde{\rho}_1(E/2) * \bar{\rho}_1(E)$. There is also the situation for which the 2-cycle is stationary and the 1-cycle is dynamical. Using Eq. (4.12) such that $\mathbb{k} = 1$ is the dynamical cycle (just a standard periodic orbit of the one-particle phase space) and $\mathbb{k} = 2$ is the 2-cycle, the result has the structure of the leading-order term of $\frac{1}{2}\bar{\rho}_1(E/2) * \tilde{\rho}_1(E)$. Group elements $\tau \in (0,0,1)$ consist of single 3-cycles. Therefore, there are no contributions from this class. To summarize,

$$\tilde{\rho}^{\mathrm{h}}_{\pm}(E) = \frac{1}{6}\left[3\tilde{\rho}^{\mathrm{h}1}_3(E) + 3\tilde{\rho}^{\mathrm{h}2}_3(E) \pm 3\left(\frac{1}{2}\tilde{\rho}_1\left(\frac{E}{2}\right) * \bar{\rho}_1(E) + \frac{1}{2}\bar{\rho}_1\left(\frac{E}{2}\right) * \tilde{\rho}_1(E)\right)\right], \quad (4.22)$$

$$\tilde{\rho}^{\mathrm{h}}_{\mathscr{E}}(E) = 2\left[\tilde{\rho}^{\mathrm{h}1}_3(E) + \tilde{\rho}^{\mathrm{h}2}_3(E)\right]. \quad (4.23)$$

4.4.4 Dynamical cycles

The leading-order contribution to $\tilde{\rho}^{\mathrm{d}}_{\pm}(E)$ comes from the identity element $\iota = (a)(b)(c)$, which consists of three 1-cycles ($n_\tau = 3; J_1 = h_a, J_2 = h_b, J_3 = h_c; \sum_{\mathbb{k}} J_{\mathbb{k}} = H$). Thus, there are two independent commuting generators other than H and so we expect two-dimensional periodic orbit families. Using Eq. (4.10) and the fact that 1-cycles are equivalent to periodic orbits of the one-particle phase space, we find the leading-order term of $\tilde{\rho}^{\mathrm{d}}_{\pm}(E)$ is $\tilde{\rho}^{\mathrm{d}}_3(E)/6$.

The next contribution is from permutations $\tau \in (1,1,0)$. There are three elements in this class each consisting of one 1-cycle and one 2-cycle ($n_\tau = 2$; $\Bbbk = 1, n_1 = 1$; $\Bbbk = 2, n_2 = 2$). Then, for $\tau = (ab)(c)$, $J_1 = h_c, J_2 = h_a + h_b$ and similarly for the other elements in this class. Thus, there is only one independent generator (other than H) and we expect one-dimensional families. Using Eq. (4.10), we find this contribution has the structure of a two-particle density. The 1-cycles ($\Bbbk = 1$) are assigned to γ_1 and the 2-cycles ($\Bbbk = 2$) to γ_2, where $\gamma_{1/2}$ are any periodic orbits of the one-particle phase space. Then, all cycle properties are those of the corresponding orbit (see the 1-cycle and 2-cycle of Fig. 4.3; note the repetition $l_2/n_2 = 2/2 = 1$, which denotes the case where the particles of the 2-cycle evolve together is not shown). Multiple repetitions of the 2-cycle are either fractions (if l_2 is odd) and correspond to type-1 DPPOs *or* integers (if l_2 is even) and are type-0 DPPOs (recall the classification scheme used in Sec. 4.1.1). The generators $J_1 = n_1 E_1 = E_1$ and $J_2 = n_2 E_2 = 2E_2$ are the energies of the particles involved in the 1-cycle and 2-cycle, respectively (particles of the 2-cycle *each* have energy $E/2$). Thus, the final form is structurally equivalent to $\frac{1}{2}\tilde{\rho}_1(E/2) * \tilde{\rho}_1(E)$.

The two group elements $\tau \in (0,0,1)$ each consist of one 3-cycle ($n_\tau = 1, \Bbbk = 1, n_1 = 3$), which implies there are no generators independent of H and thus the orbits are isolated. As before, cycle properties can be mapped to those of an orbit of the one-particle phase space (see the 3-cycle shown Fig. 4.4; $l_\Bbbk/n_\Bbbk = l_1/n_1 = 1/3, 2/3, 3/3$; higher repetitions $l_1/n_1 = l_1/3$ would have action $l_1 S$, phase index $l_1\sigma$, and stability matrix $\tilde{M}^{l_1}$, where $S, \sigma, \tilde{M}$ are the properties of the primitive orbit to which the cycle is assigned). The energy E_1 in Eq. (4.10) is the energy of each particle involved in the 3-cycle ($\Bbbk = 1$) and since $H = J_1 = 3E_1 = E$, it follows that $E_1 = E/3$. Thus, the result has the structure of a one-particle trace formula, but it is evaluated at $E/3$ and has a cycle structure prefactor of $1/3$. Including the prefactors from the projection operator, we conclude that

$$\tilde{\rho}^{\mathrm{d}}_{\pm}(E) = \frac{1}{6}\left[\tilde{\rho}^{\mathrm{d}}_3(E) \pm \frac{3}{2}\tilde{\rho}_1\left(\frac{E}{2}\right) * \tilde{\rho}_1(E) + \frac{2}{3}\tilde{\rho}_1\left(\frac{E}{3}\right)\right], \tag{4.24}$$

$$\tilde{\rho}^{\mathrm{d}}_{\mathscr{E}}(E) = \frac{2}{6}\left[2\tilde{\rho}^{\mathrm{d}}_3(E) - \frac{2}{3}\tilde{\rho}_1\left(\frac{E}{3}\right)\right]. \tag{4.25}$$

Although the correction terms have structures equivalent to one- and two-particle densities, these are in fact contributions from the dynamical pseudoperiodic orbits of the full three-particle phase space.

4.4.5 Trace formulas for the two symmetry classes

Combining the results of Eqs. (4.22)-(4.25), the fluctuating densities for the two nontrivial symmetry classes are

$$\begin{aligned}\tilde{\rho}_{(1,1,0)}(E) &= \tilde{\rho}_+(E) - \tilde{\rho}_-(E) \\ &= \frac{1}{2}\tilde{\rho}_1\left(\frac{E}{2}\right) * \tilde{\rho}_1(E) + \left[\frac{1}{2}\bar{\rho}_1\left(\frac{E}{2}\right) * \tilde{\rho}_1(E) + \frac{1}{2}\tilde{\rho}_1\left(\frac{E}{2}\right) * \bar{\rho}_1(E)\right] \\ &= \tilde{\rho}^{\mathrm{d}}_{(1,1,0)}(E) + \left[\tilde{\rho}^{\mathrm{h1}}_{(1,1,0)}(E) + \tilde{\rho}^{\mathrm{h2}}_{(1,1,0)}(E)\right] \\ &= \tilde{\rho}^{\mathrm{d}}_{(1,1,0)}(E) + \tilde{\rho}^{\mathrm{h}}_{(1,1,0)}(E), \end{aligned} \tag{4.26}$$

and

$$\tilde{\rho}_{(0,0,1)}(E) = \tilde{\rho}_+(E) + \tilde{\rho}_-(E) - \frac{1}{2}\tilde{\rho}_{\mathscr{E}}(E) = \frac{1}{3}\tilde{\rho}_1\left(\frac{E}{3}\right). \tag{4.27}$$

The leading-order term of $\tilde{\rho}^{\mathrm{h}}_{(1,1,0)}(E)$ is given by

$$\begin{aligned}\tilde{\rho}^{\mathrm{h}}_{(1,1,0)}(E) &= \frac{\alpha\mathcal{A}}{4\pi^2}\sum_{\gamma}\frac{(L^0_\gamma/2L_\gamma)}{\sqrt{\left|\det\left(\tilde{M}_\gamma - I\right)\right|}}\cos\left(\sqrt{\alpha E}L_\gamma - \sigma_\gamma\frac{\pi}{2} - \frac{\pi}{2}\right) \\ &\quad + \left\{L^0_\gamma \to \sqrt{2}L^0_\gamma, L_\gamma \to \frac{L_\gamma}{\sqrt{2}}\right\}. \end{aligned} \tag{4.28}$$

The first term of Eq. (4.28) is the contribution from two particles being stationary at the same point in the billiard (i.e. a stationary 2-cycle) while the third particle evolves on a periodic orbit (i.e. a dynamical 1-cycle). The second term is the contribution from one particle being stationary (i.e. a stationary 1-cycle) while the other two particles evolve on a periodic orbit (i.e. a dynamical 2-cycle). Higher-order contributions from heterocycles can be calculated (see Appendix C.3), and these are included in the numerics. The contribution from the dynamical cycles as determined above can be written as

$$\begin{aligned}\tilde{\rho}^{\mathrm{d}}_{(1,1,0)}(E) &= \frac{\alpha^{3/4}}{(2\pi)^{3/2}E^{1/4}}\sum_{\gamma_1,\gamma_2}\left(\prod_{i=1}^{2}\frac{L^0_{\gamma_i}}{\sqrt{\left|\det\left(\tilde{M}_{\gamma_i} - I\right)\right|}}\right) \\ &\quad \times \left[2(2L^2_{\gamma_1} + L^2_{\gamma_2})\right]^{-1/4}\cos\left[\frac{\sqrt{\alpha E}}{\sqrt{2}}L_{12} - \sigma_{12}\frac{\pi}{2} - \frac{\pi}{4}\right], \end{aligned} \tag{4.29}$$

where $L_{12} = \sqrt{2L^2_{\gamma_1} + L^2_{\gamma_2}}$ and $\sigma_{12} = (\sigma_{\gamma_1} + \sigma_{\gamma_2})$. To understand how this result is obtained, recall the structure of the dynamical cycles in this class. Each full cycle consists of one 1-cycle and one 2-cycle. The total energy is partitioned among the three particles such that

the periods of the cycles are the same. Suppose the 1-cycle and 2-cycle are associated with the orbits γ_1 and γ_2, respectively. The energies E_1, E_2 are determined from the periodicity condition

$$T_{\gamma_1}(E_1) = \frac{1}{2}T_{\gamma_2}(E_2) \equiv T. \tag{4.30}$$

Using the usual relations for actions and periods in a billiard (3.28), it can be shown that

$$E_1 = \left[\frac{2L_{\gamma_1}^2}{2L_{\gamma_1}^2 + L_{\gamma_2}^2}\right] E, \quad E_2 = \left[\frac{(L_{\gamma_2}^2/2)}{2L_{\gamma_1}^2 + L_{\gamma_2}^2}\right] E, \tag{4.31}$$

where E_1 is the energy of the particle of the 1-cycle, $2E_2$ is the total energy of the particles involved in the 2-cycle (each of them has energy E_2 since their energies must be equal), and $E = E_1 + 2E_2$ is the total energy of the three-particle system. The 2-cycles are similar to the DPPOs of a two-particle system and the classification scheme of Sec. 4.1.1 applies to all 2-cycles. The trace formula for $\tilde{\rho}_{(0,0,1)}(E)$ is a one-particle trace formula except that $L_\gamma^0 \to \sqrt{3}L_\gamma^0$ and $L_\gamma \to L_\gamma/\sqrt{3}$.

4.4.6 Numerics

We first consider the class $(1,1,0)$, and compare numerically the length spectrum of the dynamical cycles

$$\tilde{F}^{\rm sc}_{(1,1,0)}(L) = \mathcal{F}\{\tilde{\rho}^{\rm d}_{(1,1,0)}(k)\}, \tag{4.32}$$

with its quantum analog

$$\tilde{F}^{\rm qm}_{(1,1,0)}(L) = \mathcal{F}\{\rho_{(1,1,0)}(k) - \bar{\rho}_{(1,1,0)}(k) - \tilde{\rho}^{\rm h}_{(1,1,0)}(k)\}. \tag{4.33}$$

The first 241 080 levels of $\rho_{(1,1,0)}(k)$ were computed using the first 1000 single-particle energies. The smooth term was computed from Eq. (4.20) using the billiard parameters for the odd spectrum given below Eq. (3.31) and trace formulas were computed using all geometrical orbits with length $L < 10$. The result is shown in Fig. 4.5.

We now examine some of the L-space structures of Fig. 4.5. The first peak ($L \approx 3.18$) is due to DPPOs of the full phase space for which both 1- and 2-cycles are on the primitive orbit $\gamma^0 = \frac{1}{2}(*2a)$. The particle of the 1-cycle completes one full motion on the orbit while the particles of the 2-cycle each traverse half the orbit and are then exchanged. The second peak ($L \approx 4.17$) arises from DPPOs for which the 1- and 2-cycles are on primitive orbits $\gamma_1^0 = \frac{1}{2}(*2a)$ and $\gamma_2^0 = \frac{1}{2}(*4b)$, respectively. For the third peak ($L \approx 4.50$),

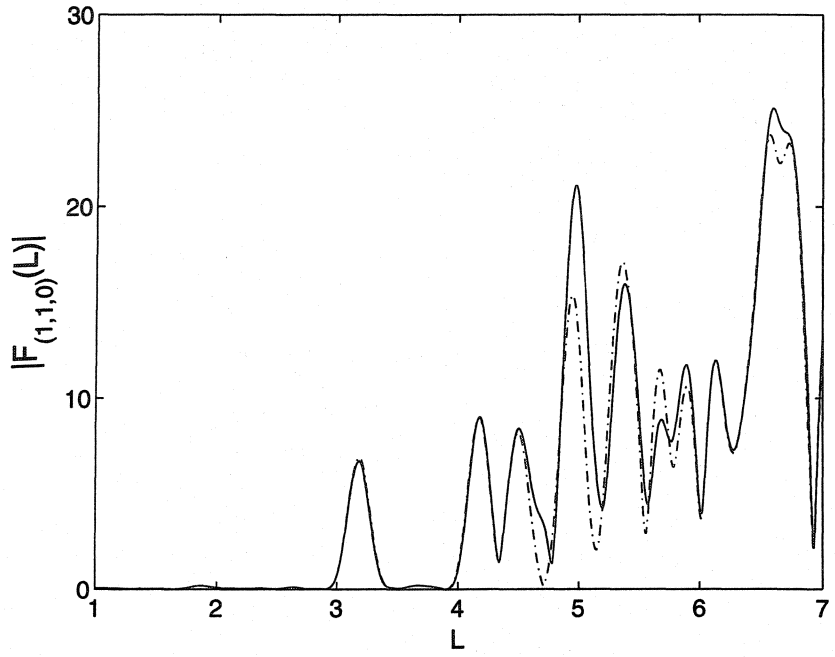

Figure 4.5: Length spectrum for the class $(1,1,0)$. Quantum (solid line) and semiclassical (dashed-dotted line) results for $L < 7$. Each peak is due to a family of dynamical pseudoperiodic orbits in the full three-particle phase space.

the 1-cycle is as in the first case, except that the 2-cycle is type-0. Thus, as the particle of the 1-cycle completes one full motion on $\gamma^0 = \frac{1}{2}(*2a)$, the particles of the 2-cycle each traverse the full orbit and are then exchanged. This is summarized in Table 4.3 where some of the DPPO families in this class are listed. In each case, the energies are divided according to Eq. (4.31). For $L < 7$, there are 27 families of DPPOs. All structures in L space can be accounted for in a similar manner and can be checked systematically by noting that due to the energy division between the particles, peaks are expected at $L = \sqrt{L_{\gamma_1}^2 + (n_{\gamma_2}^{\pm} L_{\gamma_2}^0)^2/2}$. The 2-cycles are type-0 and type-1 for even $(n_{\gamma_2}^+)$ and odd $(n_{\gamma_2}^-)$ integer repetition indices, respectively.

The discrepancies between quantum and semiclassical results are due to the problematic orbits mentioned in the previous chapter. The structure at $L \approx 5$ is poorly reproduced due to the HPPOs involving 1-cycles that are stationary and 2-cycles that are dynamical and evolving on the problematic orbits $\gamma^0 = 4a$ and $\gamma^0 = \frac{1}{2}(*10b)$. (The length spectrum of the HPPOs is shown in Fig. 4.6.) All other discrepancies are due to DPPOs, and these are summarized in Table 4.4.

L	2-cycle type	γ_1	γ_2^0
3.18	1	$\frac{1}{2}$(*2a)	$\frac{1}{2}$(*2a)
4.17	1	$\frac{1}{2}$(*2a)	$\frac{1}{2}$(*4b)
4.50	0	$\frac{1}{2}$(*2a)	$\frac{1}{2}$(*2a)
4.93	1	$\frac{1}{2}$(*2a)	$\frac{1}{2}$(*6b)
4.97	1	$\frac{1}{2}$(*4b)	$\frac{1}{2}$(*2a)
5.51	1	(*2a)	$\frac{1}{2}$(*2a)
5.90	0	$\frac{1}{2}$(*4b)	$\frac{1}{2}$(*2a)
6.09	2(1)	$\frac{1}{2}$(*2a)	$\frac{1}{2}$(*2a)
6.14	1	(*2a)	$\frac{1}{2}$(*4b)
6.20	1	$\frac{1}{2}$(*6b)	$\frac{1}{2}$(*2a)
6.36	0	(*2a)	$\frac{1}{2}$(*2a)

Table 4.3: Some DPPOs of a three-particle system in a cardioid billiard for the class $(1,1,0)$. The first column gives the position of the peak in L space arising from a family of DPPOs; the third and fourth columns specify the orbits on which the 1- and 2-cycles evolve. The second column indicates the type of 2-cycle using the classification scheme of Sec. 4.1.1. The cycle family that produces a peak at $L \approx 6.09$ has a prefactor of 2 with its 2-cycle type indicator to denote that it is the first repetition of a type-1 2-cycle. In this case, each particle involved in the 2-cycle traverses *one and one-half* of the primitive orbit γ_2^0 before particle exchange.

L	γ_1^0	γ_2^0
5.3868	$\frac{1}{2}$(*2a)	$\frac{1}{2}$(*8b)
5.6551	$\frac{1}{2}$(*2a)	4a
5.6560	$\frac{1}{2}$(*2a)	$\frac{1}{2}$(*10b)
6.6031	$\frac{1}{2}$(*4b)	$\frac{1}{2}$(*8b)
6.8237	$\frac{1}{2}$(*4b)	4a
6.8245	$\frac{1}{2}$(*4b)	$\frac{1}{2}$(*10b)
6.9217	$\frac{1}{2}$(*8b)	$\frac{1}{2}$(*2a)

Table 4.4: Some DPPOs of the class $(1, 1, 0)$ that are responsible for numerical discrepancies. The first column gives the position of the peak in L space arising from a family of DPPOs; the second and third columns specify the primitive orbits on which the 1- and 2-cycles evolve.

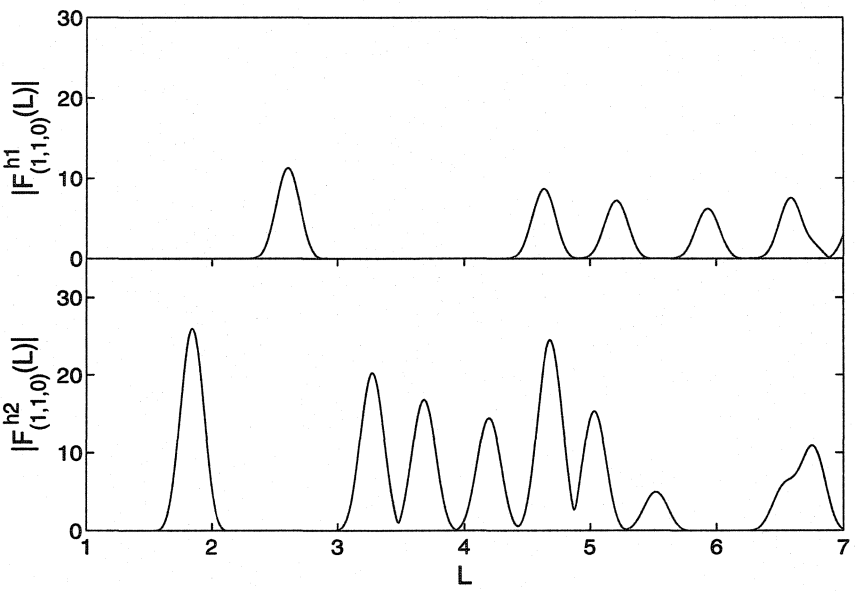

Figure 4.6: Length spectrum of the HPPOs for the class $(1,1,0)$. The upper and lower windows show $\mathcal{F}\left\{\tilde{\rho}^{\mathrm{h1}}_{(1,1,0)}(k)\right\}$ and $\mathcal{F}\left\{\tilde{\rho}^{\mathrm{h2}}_{(1,1,0)}(k)\right\}$, respectively.

We next consider the class $(0,0,1)$, and numerically compare the Fourier transform of the 3-cycle DPPOs

$$\tilde{F}^{\mathrm{sc}}_{(0,0,1)}(L) = \mathcal{F}\{\tilde{\rho}^{\mathrm{d}}_{(0,0,1)}(k)\}, \tag{4.34}$$

with its quantum analog

$$\tilde{F}^{\mathrm{qm}}_{(0,0,1)}(L) = \mathcal{F}\{\rho_{(0,0,1)}(k) - \bar{\rho}_{(0,0,1)}(k)\}. \tag{4.35}$$

The first 1000 energies of $\rho_{(0,0,1)}(k)$ were used. The smooth term was computed from Eq. (4.21) and trace formulas were computed using all geometrical orbits with length $L < 11$. The result is shown in Fig. 4.7. We now identify some of the peak structures with one or several of the orbits listed in Fig. 3.2.

The first peak ($L \approx 1.5$) can be identified with a type-1 3-cycle DPPO consisting of all three particles evolving on the orbit $\gamma^0 = \frac{1}{2}(^*2a)$ with the same energy and exactly $T_\gamma/3$ out of phase. Each of these particles completes one-third of the full motion on the orbit and is then permuted as specified by $\tau = (acb)$ [see Fig. 4.8]. The third peak ($L \approx 3$) is due to a type-2 3-cycle DPPO for which all three particles evolve on the orbit $\gamma^0 = \frac{1}{2}(^*2a)$ as above, except that each particle completes two-thirds of the full motion on the orbit

L	3-cycle type	γ^0
1.50	1	$\frac{1}{2}$(*2a)
2.67	1	$\frac{1}{2}$(*4b)
3.00	2	$\frac{1}{2}$(*2a)
3.42	1	$\frac{1}{2}$(*6b)
3.80	1	3a
3.85	1	$\frac{1}{2}$(*8b)
4.50	0	$\frac{1}{2}$(*2a)
5.33	2	$\frac{1}{2}$(*4b)
5.52	1	$\frac{1}{2}$(*8c)
5.99	1	5a
6.00	2(1)	$\frac{1}{2}$(*2a)
6.05	1	$\frac{1}{2}$(*10h)

Table 4.5: Some 3-cycle DPPOs of a three-particle system in the cardioid billiard. The first column gives the position of the peak in L space arising from the 3-cycle DPPO and the third column specifies the primitive orbit on which the 3-cycle evolves. The second column indicates the type of 3-cycle using the classification scheme of Fig. 4.4. The DPPO that produces a peak at $L = 6.00$ has a prefactor of 2 to denote that it is the first repetition of a type-1 3-cycle. This situation is described further in the text.

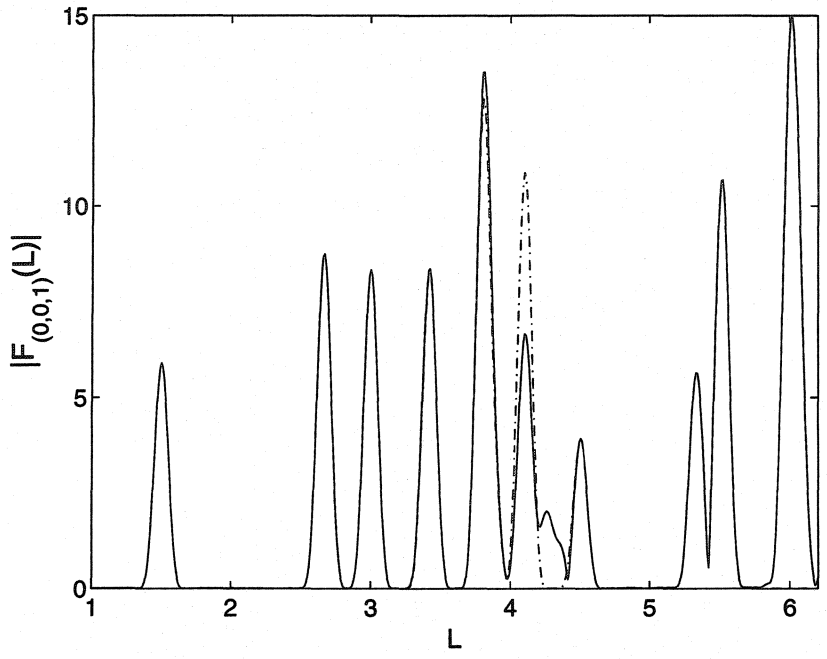

Figure 4.7: Length spectrum for the class $(0,0,1)$. Quantum (solid line) and semiclassical (dashed-dotted line) results for $L < 6.25$. Each peak is due to a 3-cycle DPPO of the full phase space.

before being exchanged according to $\tau = (abc)$ [see Fig. 4.9]. The peak at $L \approx 4.5$ is from a type-0 3-cycle DPPO consisting of all three particles starting and evolving together in phase on $\gamma^0 = \frac{1}{2}(^*2a)$, but each completing one full motion on the orbit and then being trivially exchanged as prescribed by any group element $\tau \in (0,0,1)$. As an example of a higher multiple cycle, consider the first repetition of the type-1 cycle mentioned above. It is the same as before except that each particle completes *one and one-third* of the motion on the orbit before being permuted. This is summarized in Table 4.5 where some of the 3-cycle DPPOs are listed. (The structure at $L \approx 4.3$ arises from a diffractive orbit.) As before, the discrepancy that occurs at $L \approx 4.1$ arises from the two orbits $\gamma^0 = 4a$ and $\gamma^0 = \frac{1}{2}(^*10b)$.

The examples shown in Figs. 4.8 and 4.9 illustrate a general feature of 3-cycle DPPOs. Recall that DPPOs are structures that are periodic under the combined operations of time evolution and particle exchange. Suppose the particles are $T/3$ out of phase at $t = 0$. After time $T/3$, a periodicity can occur only if the particles are subsequently permuted by the group element $\tau = (acb)$, since the other permutation does not restore the initial conditions. (This is a type-1 3-cycle DPPO.) For the same reason, after the particles evolve

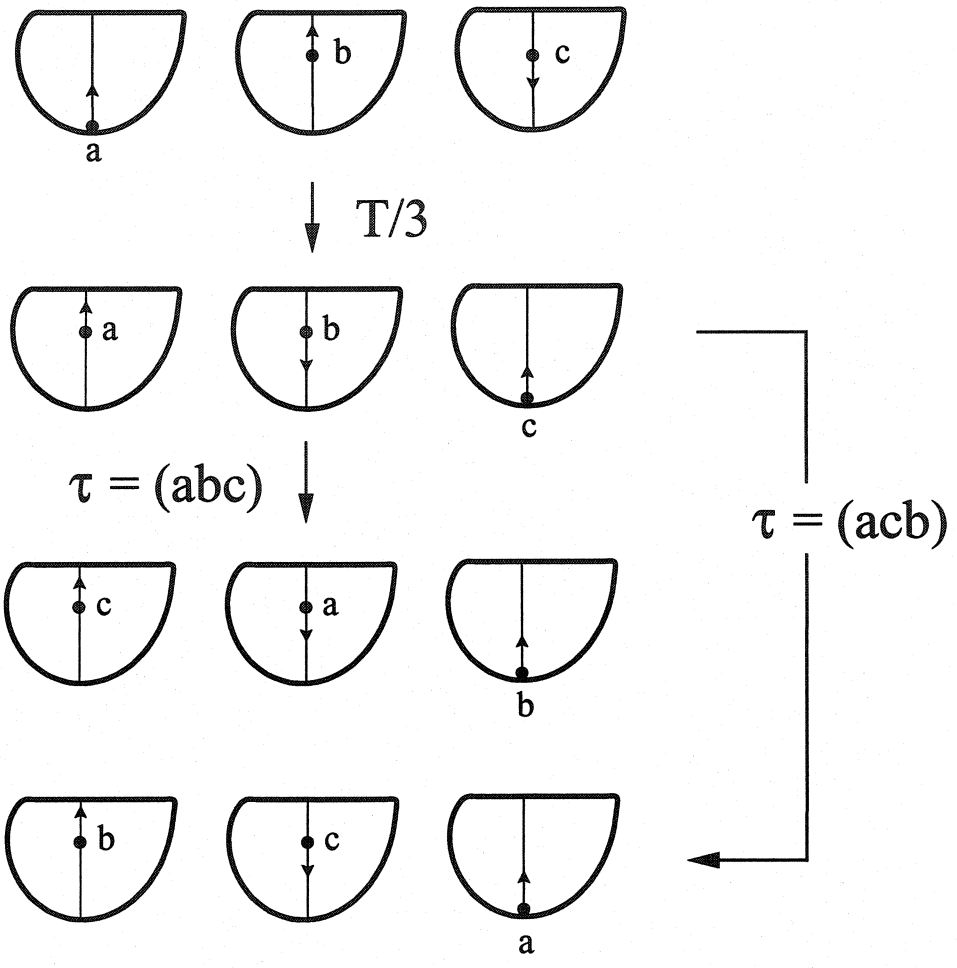

Figure 4.8: A type-1 3-cycle DPPO where all three particles evolve on the orbit $\gamma^0 = \frac{1}{2}(*2a)$. The particles are exactly $T/3$ out of phase at $t = 0$. After time $T/3$, the particles can be exchanged using the two group elements in $(0, 0, 1)$, but only the permutation $\tau = (acb)$ restores the initial conditions.

for time $2T/3$, a periodicity occurs only if the particles are permuted by the group element $\tau = (abc)$. (This is a type-2 3-cycle DPPO.) After evolution for time T, both permutations result in a configuration that differs from the original. But, if the particles have the same initial conditions and evolve in phase for a time T, then any subsequent permutation has no effect and the structure is trivially periodic. (This is a type-0 3-cycle DPPO.)

All structures in L space can be accounted for in a similar manner. As a systematic check, recall that each 3-cycle DPPO can be mapped one-to-one with a periodic orbit γ of the one-particle phase space. If the orbit has length $L_\gamma = n_\gamma L^0_\gamma$, where n_γ is a repetition

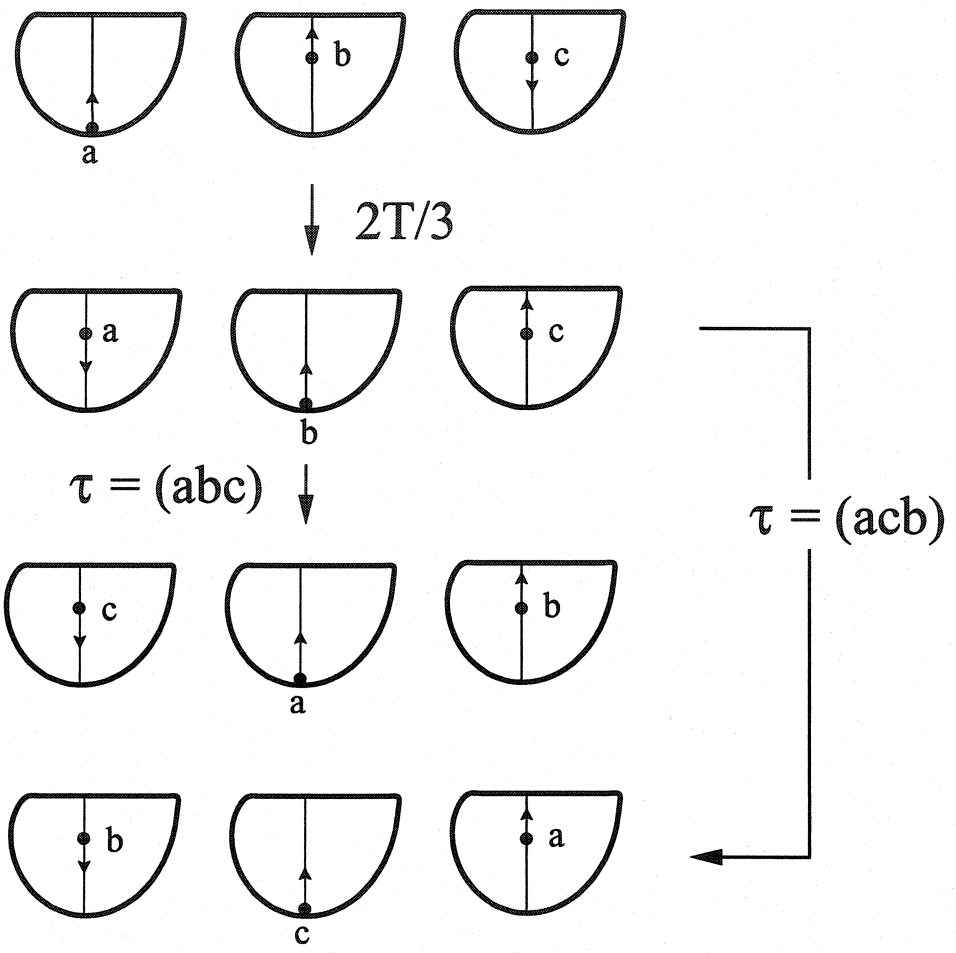

Figure 4.9: A type-2 3-cycle DPPO where all three particles evolve on the orbit $\gamma^0 = \frac{1}{2}(^*2a)$. The particles are exactly $T/3$ out of phase at $t = 0$. After time $2T/3$, the particles can be exchanged using the two group elements in $(0, 0, 1)$, but only the permutation $\tau = (abc)$ restores the initial conditions.

index, it is mapped to a 3-cycle where each particle executes a fraction $n_\gamma/3$ of the full motion on γ. We can then write $n_\gamma/3 = i + j/3$, where $i = \text{int}(n_\gamma/3)$ [i.e. integer part of $n_\gamma/3$] and $j/3$ ($j = 0, 1, 2$) is the remainder. If $j \neq 0$, then the orbit with length L_γ is associated with the ith repetition of a type-j 3-cycle DPPO. If $j = 0$, then it is the $(i-1)$th repetition. To determine peak positions, we recall that all particles of the 3-cycle have the same energy $E/3$ and thus we expect peaks at lengths $L = n_\gamma L^0_\gamma/\sqrt{3}$. (Recall that a billiard orbit with length L_γ has action $S_\gamma(\varepsilon) = \hbar\sqrt{\alpha\varepsilon}L_\gamma$.)

Chapter 5

Weak Interactions

As mentioned above, a major advantage of the formalism presented in Chapter 3 (as compared to the convolution formalism of Ref. [35] and Appendix C) is that it can be extended to include interactions. Any interaction between the particles destroys the periodic orbit families and replaces them by a discrete set of isolated orbits. This is a specific example of the more general situation in which there is a symmetry breaking. There is a substantial literature on symmetry breaking in semiclassical mechanics. In particular, a perturbative theory, which is applicable to any situation where continuous symmetries are broken, has been developed in Ref. [38]. The results of this general theory apply to the special case of weak interactions. Since much of the background theory has been given in Chapter 1, we begin immediately with the analysis for a two-body system.

5.1 Two-Body System

Suppose the full two-body Hamiltonian is

$$H = \frac{\mathbf{p}_a^2}{2m} + \frac{\mathbf{p}_b^2}{2m} + U(\mathbf{q}_a) + U(\mathbf{q}_b) + \epsilon V(\mathbf{z}_a, \mathbf{z}_b), \tag{5.1}$$

where U is a one-body confining potential, and the perturbative term $\epsilon V(\mathbf{z}_a, \mathbf{z}_b)$ is a weak two-body interparticle interaction. The $\mathbf{z}_{a/b}$ are the phase space coordinates of the particles, and ϵ is a continuous parameter.

5.1.1 Dynamical orbit families under perturbation

First, we briefly review the periodic orbit structure for $\epsilon = 0$. If both particles are on periodic orbits, the full phase space periodic orbit is a dynamical periodic orbit. In

that event, there is a second constant of motion in involution with H. This is $J = h(\mathbf{z}_a)$, the single-particle Hamiltonian. It generates time translations of particle a while leaving particle b fixed. There is a corresponding group parameter θ that is conjugate to J and has the dimension of time. For any initial condition on a full phase space periodic orbit, flows generated by H and J map out a two-dimensional torus. This means there is a 1-parameter degenerate family of periodic orbits. For the present, it is assumed that there are no continuous symmetries other than J so that all periodic orbits of the one-particle phase space are isolated. This is the case most applicable to chaotic systems. However, there are integrable systems where this is also true, and one example shall be examined in the following section.

If we consider a typical member of the periodic orbit family Γ specified by the group parameter

θ, it will still be approximately periodic for $\epsilon \neq 0$, but with a modified action. To first order in perturbation theory, the change in action at fixed energy E is (using the results of Ref. [38])

$$\Delta S_\Gamma(\theta; E, \epsilon) \approx -\epsilon \int_{\Gamma_\theta} V(\mathbf{z}_a(t;\theta), \mathbf{z}_b(t))\mathrm{d}t. \tag{5.2}$$

The interval is over one period of the periodic orbit. The orbit specified by the parameter θ involves a shift of the initial condition of particle a, that is, $\mathbf{z}_a(t;\theta) = \mathbf{z}_a(t+\theta)$. The amplitude of the trace formula is now modified by the "modulation factor", which (again using the results of Ref. [38]) is then given by

$$\mathcal{M}_\Gamma(\epsilon/\hbar, E) = \frac{1}{T}\int \exp\left[i\Delta S_\Gamma(\theta; E, \epsilon)/\hbar\right]\mathrm{d}\theta. \tag{5.3}$$

If the interaction is absent, then ΔS is zero and the modulation factor is unity. On the other hand, if the interaction is sufficiently strong so that $\Delta S \gg \hbar$, then the above integral can be done by stationary phase. Each critical point of the integral is then identified as the initial condition of some isolated orbit in the Gutzwiller limit. For this to be a complete picture, consider that there exists a range of interaction strengths where the perturbation is small enough to justify the use of classical perturbation theory while nevertheless $\Delta S \gg \hbar$. We use the analysis outlined above for small interaction strengths and use the isolated orbit analysis for larger interaction strengths and expect that there is an intermediate regime where these are both valid.

Conceptual example: stable harmonic orbit

Consider the two-dimensional single-particle Hénon-Heiles potential

$$U(x,y) = \frac{1}{2}x^2 + \frac{1}{2}y^2 + x^2y - \frac{1}{3}y^3. \tag{5.4}$$

If $E_p < \frac{1}{6}$, the motion along the x-axis ($y = 0$) is harmonic and stable since slight deviations in the y direction do not get amplified (see Fig. 5.1). As the first example, this potential is populated with two particles, and an initial condition is chosen such that both particles start on the x-axis. The noninteracting system then consists of both particles executing independent single-particle motions on the periodic orbit $x(t) = A\cos t$, where the amplitude A is energy dependent. In general, the particles are initially out of phase. A small harmonic attraction is then introduced between the particles:

$$\epsilon V(\mathbf{z}_a, \mathbf{z}_b) = \frac{\epsilon}{2}(x_a - x_b)^2, \tag{5.5}$$

where x_a and x_b denote the positions of the two particles, and ϵ is a measure of the interaction strength. Using $x_a(t) = A\cos(t+\theta)$ and $x_b(t) = A\cos t$, we find

$$\Delta S_\Gamma(\theta; E, \epsilon) = \frac{-\epsilon T A^2}{2}(1 - \cos\theta), \tag{5.6}$$

where the period $T = 2\pi$. The modulation factor is found by integrating over θ:

$$\begin{aligned} \mathcal{M}_\Gamma(\epsilon/\hbar, E) &= \frac{1}{T}\int_0^T \exp\left[i\left(\frac{-\epsilon T A^2}{2\hbar}\right)(1-\cos\theta)\right] \mathrm{d}\theta \\ &= \exp\left(\frac{-i\epsilon T A^2}{2\hbar}\right) J_0\left(\frac{\epsilon T A^2}{2\hbar}\right), \end{aligned} \tag{5.7}$$

where J_0 is the zero-order Bessel function.

In the limit $\epsilon T A^2/2 \gg \hbar$, the integral can be analyzed by stationary phase. There are two critical points[1]. (The stationary phase analysis is equivalent to using the asymptotic expansion of the Bessel function.) These have phases of $\pm\pi/4$ relative to the noninteracting case and have relative amplitudes $O(\sqrt{\hbar})$. The two stationary phase points $\theta = 0$ and $\theta = \pi = T/2$ correspond physically to situations where the two particles are in phase and $T/2$ out of phase, respectively at $t = 0$ (see Fig. 5.2). For the latter situation, there is a shift in the action by the amount $-2\epsilon T A^2$. As stated above, these contributions give the isolated orbits in the Gutzwiller limit.

[1]The stationary phase point θ^* is obtained from the conditions $\frac{\mathrm{d}}{\mathrm{d}\theta}\left[\Delta S_\Gamma(\theta; E, \epsilon)\right]\Big|_{\theta=\theta^*} = 0$ and $\frac{\mathrm{d}^2}{\mathrm{d}\theta^2}\left[\Delta S_\Gamma(\theta; E, \epsilon)\right]\Big|_{\theta=\theta^*} \neq 0$ for fixed E and ϵ.

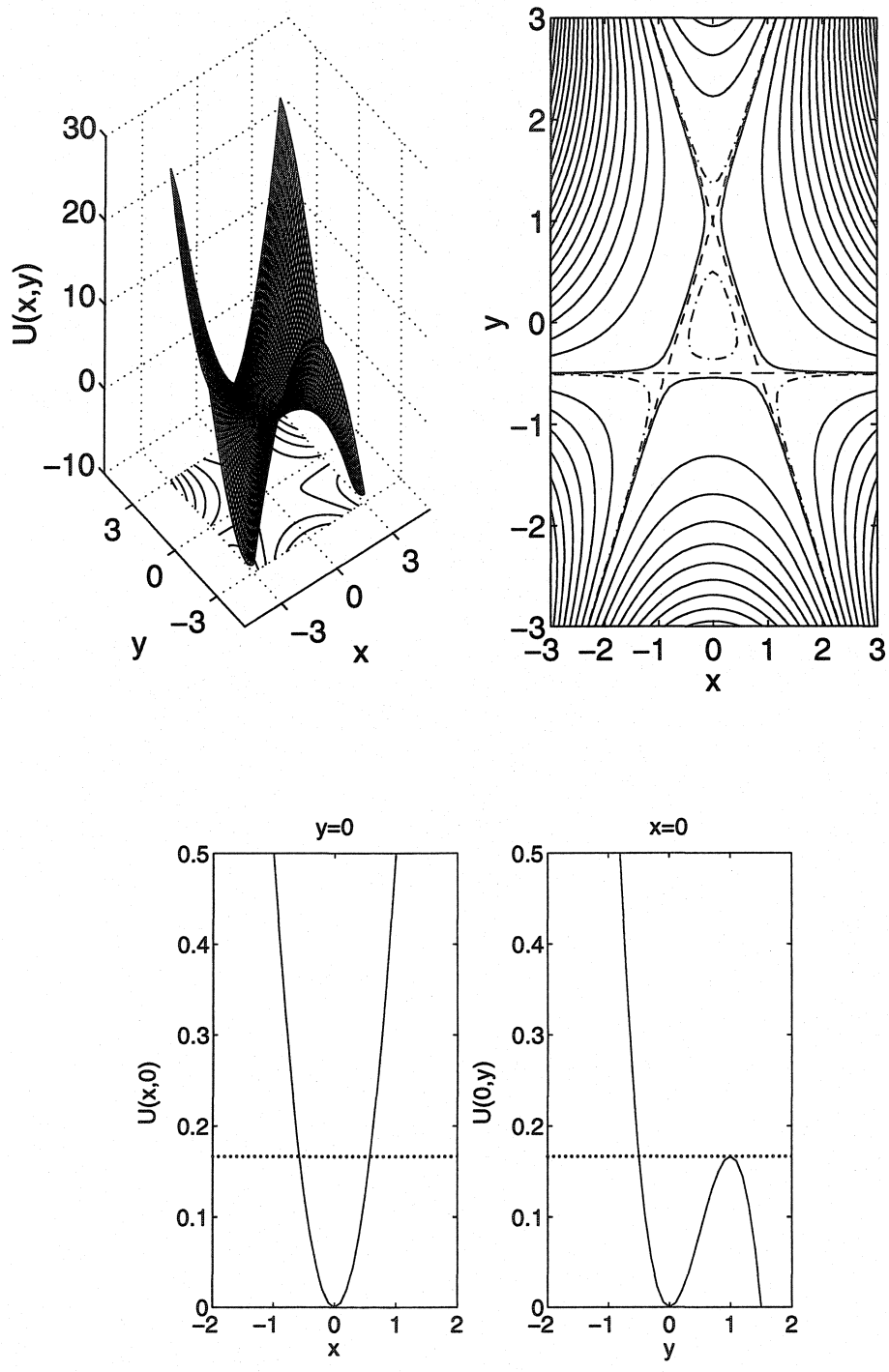

Figure 5.1: The cubic Hénon-Heiles potential. (Top) Surface and contour plots. The three symmetry axes (dashed lines) are lines along which $U(x,y) = \frac{1}{6}$, and the locus of points for which $U(x,y) = \frac{1}{12}$ is shown by dashed-dotted lines. (Bottom) Slices of the potential along $y = 0$ and $x = 0$.

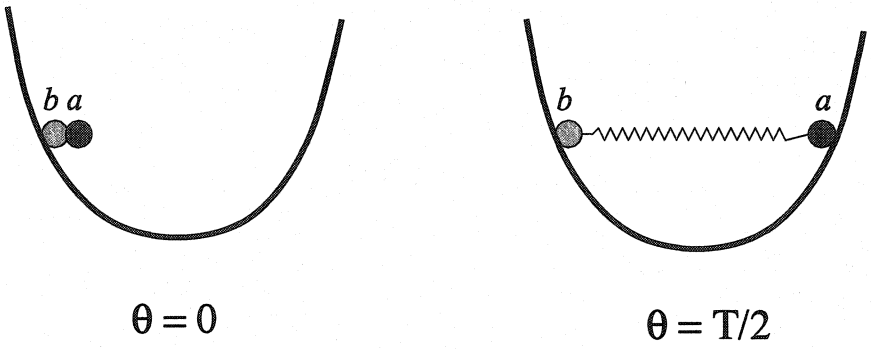

Figure 5.2: The particle configurations at $t = 0$ corresponding to the stationary phase points of the integral in Eq. (5.7). To the left, particles a and b are displayed beside each other, but it should be understood that these are at the same position and actually overlap.

Note that the analysis performed here depends crucially on understanding the geometry of the orbit families in the full phase space and would not have been possible using the formalism of convolutions used in Ref. [35]. This clearly demonstrates the advantages in using the formalism of Chapter 3 for situations which include interactions.

The heterogeneous orbits are isolated even in the absence of interactions. Upon adding an interaction, this fact does not change, however the orbit does change its action smoothly as is usual for any periodic orbit under perturbation. The specific property that one of the particles is stationary while the other evolves with all of the energy will no longer be true, but the Gutzwiller trace formula is still valid.

5.1.2 Heterogeneous orbit families under perturbation

Interactions cause further symmetry breaking in billiard systems. For $\epsilon = 0$, there are also contributions from heterogeneous periodic orbits in the full phase space where one particle executes dynamics while the other particle remains stationary. In particular, suppose that particle a is stationary at some point in phase space and particle b evolves dynamically on a periodic orbit. Although flows generated by $J = h(\mathbf{z}_a)$ do not map out any new orbits, the stationary particle can be anywhere in the billiard, and thus the heterogeneous orbits still occur in continuous families. Of course, for $\epsilon \neq 0$, there are no such orbits (i.e. these orbits are destroyed and replaced by isolated orbits). However, for weak interactions (i.e. $\epsilon \ll 1$), the Gutzwiller amplitudes will again be incorrect and classical perturbation theory should be used to obtain a trace formula with the correct

amplitudes. As before, there will be a regime of interaction strengths where this type of analysis reproduces the results of the Gutzwiller theory.

Consider a d-dimensional billiard. In the unperturbed case, the orbit manifold has the topology of $\mathcal{B} \times \mathcal{S}^1$, where $\mathcal{B}$ denotes the billiard domain, and $\mathcal{S}^1$ is the 1-torus associated with the dynamics of the evolving particle b. In addition to E, there are d independent constants of motion, which (without loss of generality) are $\mathbf{J} = (J_1, J_2, \ldots, J_d) = (p_{q_1}, p_{q_2}, \ldots, p_{q_d})_a = \mathbf{p}_a$, and the conjugate group parameters are $\mathbf{\Theta} = (q_1, q_2, \ldots, q_d)_a = \mathbf{q}_a$. In the presence of a weak interaction, a periodic orbit will have a modified action

$$\Delta S_\Gamma(\mathbf{q}; E, \epsilon) \approx -\epsilon \int_{\Gamma_\mathbf{q}} V(\mathbf{q}, \mathbf{z}_b(t)) \mathrm{d}t. \tag{5.8}$$

As before, we integrate over one full period of the orbit family which is now the period of the orbit γ on which particle b evolves. The orbit specified by $\mathbf{q}$ indicates the position of the stationary particle in the billiard. (The complete phase space coordinates of particle a are not required since it has zero momentum.) The modulation factor is then

$$\mathcal{M}_\Gamma(\epsilon/\hbar, E) = \frac{1}{\Omega_d} \int_\mathcal{B} \exp\left[i \Delta S_\Gamma(\mathbf{q}; E, \epsilon)/\hbar\right] \mathrm{d}\mathbf{q}. \tag{5.9}$$

The group volume $V_G = \int \mathrm{d}\mathbf{q} = \Omega_d$ is the d-dimensional volume of the billiard.

5.2 Two Weakly-Interacting Particles in a Square Well

Consider the one-dimensional single-particle potential

$$U(x) = \begin{cases} 0, & x_1 < x < x_2 \\ \infty, & \text{otherwise.} \end{cases} \tag{5.10}$$

We populate this potential with two particles and introduce an Eckart (Pöschl-Teller) two-body interaction

$$\epsilon V(|x_a - x_b|) = \epsilon V_0 \operatorname{sech}^2 \kappa (x_a - x_b), \tag{5.11}$$

where x_a and x_b denote the positions of the two particles, and ϵ is a measure of the interaction strength. (Hereafter, V_0 shall be absorbed into the definition of ϵ, which then has units of energy and can be positive or negative.) The system will generally have mixed dynamics and may become chaotic for large values of ϵ, and in that case, the standard Gutzwiller

theory can be applied. For small values of ϵ, the Gutzwiller amplitudes become invalid and actually diverge in the limit $\epsilon \to 0$. Although the tori are destroyed for $\epsilon \neq 0$, the periodic orbits are not sufficiently isolated for small values of ϵ since their perturbed actions differ by less than $\hbar$.

5.2.1 Semiclassical analysis

Consider first the noninteracting case ($\epsilon = 0$). The smooth term can be obtained simply from the convolution identity

$$\bar{\rho}_2(E) = (\bar{\rho}_1 * \bar{\rho}_1)(E) = \frac{m\mathcal{L}^2}{2\pi\hbar^2} - \sqrt{\frac{2m}{E}}\frac{\mathcal{L}}{2\pi\hbar} + \frac{1}{4}\delta(E), \tag{5.12}$$

where we have used the formula

$$\bar{\rho}_1(E) = \frac{1}{2}\left[\frac{1}{\sqrt{\mathcal{E}_0 E}} - \delta(E)\right], \tag{5.13}$$

and $\mathcal{E}_0 \equiv \pi^2\hbar^2/2m\mathcal{L}^2$ is the ground state energy of the one-body system. In Eqs. (5.12) and (5.13), the δ-function correction does not actually contribute to the density of states, but rather to any integrated quantity where the density of states is part of the integrand (the most common example is the cumulative density of states $N(E) = \int_0^E \rho(\xi)\mathrm{d}\xi$). This correction has been identified as belonging to the one-particle Weyl expansion (see, for example, Eq. (4.141) of Ref. [7]).

There are two contributions to the oscillatory part of the density of states; the first arises from orbits in the full phase space where both particles evolve on periodic orbits and the second is due to orbits where one particle is stationary inside the well while the other particle evolves on a periodic orbit. As mentioned above, these are called dynamical and heterogeneous periodic orbits, respectively.

Dynamical periodic orbits consist of both particles executing independent single-particle motions on an arbitrary repetition of the primitive periodic orbit. If the initial position is at x_1, and the repetition index of the orbit is n, then the position of a particle as a function of time is

$$x(t;n) = \sum_{j=0}^{(2n-1)} \left[X_j + (-1)^j v\left(t - \frac{jT}{2n}\right)\right] \mathcal{G}_{\frac{T}{2n}}\left(t - \frac{jT}{2n}\right), \tag{5.14}$$

where X_j is x_1 or x_2 when j is even or odd, respectively, v is the speed of the particle, T is

the period of the orbit, and the gate function is defined as

$$\mathcal{G}_\mu(t-\nu) = \begin{cases} 0, & t < \nu \\ 1, & \nu < t < \mu + \nu \\ 0, & t > \mu + \nu. \end{cases} \tag{5.15}$$

Suppose that particles a and b are on the n_ath and n_bth repetition of the primitive orbit. Using the results of Sec. 3.1.3, the contribution of the dynamical periodic orbits to the two-particle resolvant is

$$\tilde{g}_2^{\mathrm{d}}(E) = -i\pi \sum_{n_a=1}^{\infty} \sum_{n_b=1}^{\infty} \frac{\exp i\left(2\pi\sqrt{(n_a^2+n_b^2)E/\mathcal{E}_0} - \frac{\pi}{4}\right)}{\left[\left(n_a^2+n_b^2\right)\mathcal{E}_0^3 E\right]^{1/4}}. \tag{5.16}$$

Now consider the heterogeneous orbits. Since one of the particles is stationary, time-translational symmetry does not exist and the energy can only be partitioned in one way; the evolving particle has all of the energy while the stationary particle has zero energy. However, there is a space-translational symmetry (the stationary particle can be anywhere in the well) that is generated by the momentum. Using the theory of Sec. 3.1.4, heterogeneous orbits make the following contribution to the two-particle resolvant:

$$\tilde{g}_2^{\mathrm{h}}(E) = -i\pi \sum_{n=1}^{\infty} \frac{\exp i\left(2n\pi\sqrt{E/\mathcal{E}_0} - \frac{\pi}{4}\right)}{\left(n^2\mathcal{E}_0^3 E\right)^{1/4}} \tag{5.17}$$

Note that both Eqs. (5.16) and (5.17) are $O(1/\hbar^{3/2})$ and have identical energy prefactors $O(1/E^{1/4})$ which is generally true for orbits that occur in 1-parameter families. The standard semiclassical approximation for the oscillatory part of the resolvant, that is, the leading-order semiclassical trace formula is the sum of Eqs. (5.16) and (5.17). This yields a set of peaks at the positions of the quantum two-particle spectrum and *also* a spurious set of peaks at the positions of the one-particle spectrum. However, there is a "surface correction" to Eq. (5.17) that can be interpreted as coming from *isolated* boundary heterogeneous orbits where one particle is fixed at a *corner* of the well while the other evolves *inside* the well. This term arises most naturally when the trace formulas derived above are obtained from an equivalent semiclassical analysis that involves writing the two-particle density of states as the autoconvolution of the one-particle density of states [35]. The correction for the two-particle system may be obtained from an analysis of the mixed convolution integral $(\bar{\rho}_1 * \tilde{\rho}_1)(E)$. There are two contributions; the first reproduces Eq. (5.17), and the second

is the corner correction term of the full two-particle trace formula and is $O(1/\hbar)$. As expected, the latter term is identical to the boundary correction term for the two-dimensional square billiard (see Eq. (2.187) of Ref. [7]). The corner correction when subtracted from the leading-order term exactly cancels the spurious peaks mentioned above. A similar situation occurs in the case of one particle in an equilateral triangle billiard (see Sec. 6.1.2 of Ref. [7]).

We now examine each contribution to the semiclassical density of states for $\epsilon \neq 0$. The Thomas-Fermi term, that is, the leading-order term of the average density of states can be computed from the inverse Laplace transform of the classical partition function $Z_2^{\rm cl}(\beta) = \frac{1}{2(2\pi\hbar)^2} \int {\rm d}\mathbf{p} \int {\rm d}\mathbf{q} \exp\left[-\beta H\left(\mathbf{q},\mathbf{p}\right)\right]$. The integral over momentum $\mathbf{p} = (p_{x_a}, p_{x_b})$ is trivial and the remaining integral over the coordinates $\mathbf{q} = (x_a, x_b)$ can be transformed to a one-dimensional integral after a change of variables to center-of-mass and relative coordinates: $X = (x_a + x_b)/2$, $x = x_a - x_b$. Under the inverse Laplace transform, this reduces to

$$\bar{\rho}_2(E;\epsilon) = \frac{m\mathcal{L}}{2\pi\hbar^2} \int_0^{\mathcal{L}} \Theta\left(E - \epsilon\, {\rm sech}^2 \kappa x\right) {\rm d}x, \tag{5.18}$$

where $\Theta(\cdots)$ in Eq. (5.18) is a step function. Due to the properties of the integrand, the Thomas-Fermi term is a constant, $m\mathcal{L}^2/2\pi\hbar^2$ for $E > \epsilon$, and zero otherwise.

For the oscillatory part of the density of states, we must determine the perturbed actions for each family of *unperturbed* orbits. For dynamical orbits, in general, the particles are out of phase, and the unperturbed orbits are $x_a(t;\theta) = x(t+\theta; n_a)$ and $x_b(t) = x(t; n_b)$. Then,

$$\Delta S_\Gamma(\theta; E, \epsilon) \approx -\epsilon \int_{\Gamma_\theta} V(x_a(t;\theta), x_b(t)) {\rm d}t = -\epsilon \int_0^{T_\Gamma} {\rm sech}^2 \kappa \left[x_a(t;\theta) - x_b(t)\right] {\rm d}t. \tag{5.19}$$

The above integral splits into $2(n_a + n_b)$ intervals, each of which must be evaluated separately. To evaluate the integral, the distance function $\mathscr{D}_{ab}(t;\theta) = x_a(t;\theta) - x_b(t)$ should be calculated on θ-intervals of size $T/2n_an_b$; the reason is that particle a reverses direction at $j_aT/2n_a$ ($j_a = 1, 2, 3, \ldots, 2n_a$), whereas particle b reverses direction at $j_bT/2n_b$ ($j_b = 1, 2, 3, \ldots, 2n_b$), and thus the distance function changes discontinuously at values of θ that are integer multiples of $\min\{|j_aT/2n_a - j_bT/2n_b| : j_an_b - j_bn_a \neq 0\} = T/2n_an_b$, or more precisely $\mathscr{D}_{ab}(t;\theta)$ changes discontinuously at $\theta_j = jT/2n_an_b$, where $j = 1, 2, 3, \ldots 2n_an_b$. After careful integration of Eq. (5.19) using Eq. (5.14) in the argument of the secant func-

tions, we find, by induction,

$$\frac{\Delta S_\Gamma(\theta;E,\epsilon)}{\hbar} = -\frac{2\epsilon v_a}{\hbar\kappa\left(v_a^2-v_b^2\right)}\sum_{j=0}^{(n_a-1)}\left[\tanh\kappa\left(v_b\theta+\frac{j\mathcal{L}}{n_a}\right)\right.$$
$$\left.+\tanh\kappa\left(-v_b\theta+\frac{(j+1)\mathcal{L}}{n_a}\right)\right]+\{a\leftrightarrow b\} \tag{5.20}$$

for $0\leq\theta\leq T/2n_an_b$, where $v_{a/b}=\sqrt{2E_{a/b}/m}$. The energies of the particles are such that the periods of the orbits are the same: $E_{a/b}=n_{a/b}^2E/(n_a^2+n_b^2)$. (Of course, $E_a+E_b=E$.) As mentioned above, the distance function has a different functional form for values of θ in each of the $2n_an_b$ intervals. We should calculate $\Delta S_\Gamma(\theta)$ for each of these intervals. However, the range of the action shifts is identical for all intervals. Thus, it is sufficient to compute the action shift for one interval (for instance, the first interval) and then use the multiplicative factor $2n_an_b$ when computing the modulation $\mathcal{M}_\Gamma$, which is then found by integrating over θ:

$$\mathcal{M}_\Gamma(\epsilon/\hbar,E)=\frac{2n_an_b}{T_\Gamma}\int_0^{\frac{T_\Gamma}{2n_an_b}}\exp\left[i\Delta S_\Gamma(\theta;E,\epsilon)/\hbar\right]\mathrm{d}\theta, \tag{5.21}$$

where $\Gamma=(n_a,n_b)$, $\Delta S_\Gamma(\theta)$ is given by Eq. (5.20), and the common period $T_\Gamma=T_{n_a}(E_a)=T_{n_b}(E_b)\equiv T(E)=\pi\hbar\sqrt{\left(n_a^2+n_b^2\right)/\mathcal{E}_0E}$.

If the particles are on the same orbit ($n_a=n_b=n$), the distance function changes discontinuously at integer multiples of $T/2n$. Then, the integral in Eq. (5.19) splits into $4n$ intervals and again using Eq. (5.14) in the argument of the secant function, we find, by induction,

$$\frac{\Delta S_\Gamma(\theta;E,\epsilon)}{\hbar}=-\frac{2n\epsilon}{\hbar}\left[\left(\frac{T_\Gamma}{2n}-\theta\right)\mathrm{sech}^2(\kappa v\theta)+\frac{1}{\kappa v}\tanh(\kappa v\theta)\right] \tag{5.22}$$

for $0\leq\theta\leq T_\Gamma/2n$, where $v=\sqrt{E/m}$. Similarly, for the other θ intervals. The complete modulation factor is then

$$\mathcal{M}_\Gamma(\epsilon/\hbar,E)=\frac{2n}{T_\Gamma}\int_0^{\frac{T_\Gamma}{2n}}\exp\left[i\Delta S_\Gamma(\theta;E,\epsilon)/\hbar\right]\mathrm{d}\theta, \tag{5.23}$$

where $\Gamma=(n,n)$, the common period $T_\Gamma=T_n(E_a)=T_n(E_b)\equiv T(E)=n\pi\hbar\sqrt{2/\mathcal{E}_0E}$, and $\Delta S_\Gamma(\theta)$ is as given in Eq. (5.22). The appropriate modulation [Eq. (5.21) or Eq. (5.23)] is then inserted as a multiplicative factor under the summation of Eq. (5.16). Finally, the

contribution of the dynamical orbits to the oscillatory part of the density of states is,

$$\begin{aligned}\tilde{\rho}_2^{\rm d}(E;\epsilon) &= -\frac{1}{\pi}{\rm Im}\left\{\tilde{g}_2^{\rm d}(E;\epsilon)\right\} \\ &= \sum_{n_a=1}^{\infty}\sum_{n_b=1}^{\infty}\frac{1}{\left[n_\Gamma^2 \mathcal{L}_0^3 E\right]^{1/4}}\left[{\rm Re}\left\{\mathcal{M}_\Gamma\left(\frac{\epsilon}{\hbar},E\right)\right\}\cos\left(S_\Gamma(E)-\frac{\pi}{4}\right)\right. \\ &\qquad \left. + {\rm Im}\left\{\mathcal{M}_\Gamma\left(\frac{\epsilon}{\hbar},E\right)\right\}\sin\left(S_\Gamma(E)-\frac{\pi}{4}\right)\right],\end{aligned} \tag{5.24}$$

where $\Gamma = (n_a, n_b)$, $n_\Gamma^2 = (n_a^2 + n_b^2)$, and $S_\Gamma(E) = 2\pi\sqrt{n_\Gamma^2 E/\mathcal{L}_0}$.

In the limit $\epsilon \gg \hbar$, we can analyze the modulation integrals by stationary phase. As examples, consider $\Gamma = (1,1)$ and $\Gamma = (2,1)$. In the former, using the modulation factor (5.23), there are two contributions. These have phases of $\pm\pi/4$ relative to the noninteracting case and have relative amplitudes $O(\sqrt{\hbar})$. The two stationary phase points $\theta = 0$ and $\theta = T/2$ correspond physically to the situations where the two particles are in phase and half-a-period out of phase, respectively. (For $T/2 \le \theta \le T$, there are also two critical points $\theta = T/2$ and $\theta = T$, but these physically describe situations similar to those described before in the sense that $\theta = 0$ and $\theta = T$ indicate that both particles are initially at x_1.) The corresponding shifts in the action are $\Delta S(0) = -\epsilon T$ and $\Delta S(T/2) = -\epsilon T \tanh(\kappa\mathcal{L})/\kappa\mathcal{L}$, respectively. For $\Gamma = (2,1)$, using Eq. (5.21), there are 9 critical points $\theta_k = kT/8$, $k = 0, 1, 2, \ldots, 8$. The stationary points correspond physically to one of three situations: both particles are initially at x_1 *or* one particle is at x_1 while the other is at the center of the well (i.e. the particles are separated by a distance $\mathcal{L}/2$), *or* the particles are on opposite sides of the well (separated by a distance $\mathcal{L}$). As stated above, these contributions reproduce the Gutzwiller formula appropriate for isolated orbits.

More generally, if $n_a \neq n_b$, there are $(4n_a n_b + 1)$ critical points $\theta_k = kT/(4n_a n_b)$, where $k = 0, 1, 2, \ldots, 4n_a n_b$. These correspond physically to situations where the particles are initially separated by integer multiples of $\mathcal{L}/n_a n_b$. If $n_a = n_b = n$, there are $(2n+1)$ critical points $\theta_k = kT/(2n)$, where $k = 0, 1, 2, \ldots, 2n$. These critical points describe the physical situations where the particles either both begin at x_1 or begin at opposite sides of the square well. In all cases, the action shifts are obtained by substituting each critical point into Eqs. (5.20) and (5.22). Note that the number of critical points increases with the length of the orbits. This implies that families having smaller actions break into relatively fewer isolated orbits than families having larger actions which are replaced by many more isolated orbits.

For heterogeneous orbits, upon adding an interaction, the specific property that one of the particles is stationary while the other evolves with all of the energy will no longer be true, but it is still necessary to smoothly interpolate between the cases when the space-translational symmetry exists and the case for which this symmetry is destroyed. Consider a typical member of the heterogeneous orbit family Γ_x, specified by the group parameter x. To first order in perturbation theory, the modified action at fixed energy E is

$$\Delta S_\Gamma(x;E,\epsilon) \approx -\epsilon \int_{\Gamma_x} V(x, x_b(t))\mathrm{d}t. \tag{5.25}$$

As before, we integrate over one period of the orbit family. In this case, this is the period of the evolving particle T. If the evolving particle is on the nth repetition of the primitive orbit, then the shift in the action is

$$\Delta S_n(x;E,\epsilon) = -\frac{2n\epsilon}{\kappa v}\left[\tanh\kappa\left(x-x_1\right)+\tanh\kappa\left(x_2-x\right)\right], \tag{5.26}$$

where $v=\sqrt{2E/m}$. The modulation factor for heterogeneous orbits is then

$$\mathcal{M}_n(\epsilon/\hbar,E) = \frac{1}{\mathcal{L}}\int_{x_1}^{x_2} \exp\left[i\Delta S_n(x;E,\epsilon)/\hbar\right]\mathrm{d}x. \tag{5.27}$$

(Note the group volume $V_G=\int_{x_1}^{x_2}\mathrm{d}x=(x_2-x_1)\equiv\mathcal{L}$.) The modulation factor in Eq. (5.27) is now included as a multiplicative factor under the summation of Eq. (5.17). Thus, the contribution of the heterogeneous orbits to the oscillatory part of the density of states is $\tilde{\rho}_2^{\mathrm{h}}(E;\epsilon) = -\frac{1}{\pi}\mathrm{Im}\left\{\tilde{g}_2^{\mathrm{h}}(E;\epsilon)\right\}$, that is,

$$\begin{aligned}\tilde{\rho}_2^{\mathrm{h}}(E;\epsilon) = \sum_{n=1}^{\infty}\frac{1}{\left(n^2\mathcal{L}_0^3E\right)^{1/4}}\Bigg[&\mathrm{Re}\left\{\mathcal{M}_n\left(\frac{\epsilon}{\hbar},E\right)\right\}\cos\left(S_n(E)-\frac{\pi}{4}\right)\\ &+\mathrm{Im}\left\{\mathcal{M}_n\left(\frac{\epsilon}{\hbar},E\right)\right\}\sin\left(S_n(E)-\frac{\pi}{4}\right)\Bigg],\end{aligned} \tag{5.28}$$

where $S_n(E)=2n\pi\sqrt{E/\mathcal{L}_0}$.

For large values of ϵ, we can again determine the integral by stationary phase. In this case, we get only one contribution since there is only one stationary phase point $x=(x_1+x_2)/2$, which is at the center of the well. Thus, after the interaction is turned on, each heterogeneous orbit family is destroyed and replaced by a single isolated orbit.

The boundary heterogeneous orbits are isolated even in the absence of interactions. Upon adding an interaction, this fact does not change, however the orbits do change their action smoothly as is usual for any periodic orbit under a perturbation. The actual change

in the action is given by Eq. (5.26) with $x = x_1$ or $x = x_2$. The periods are also modified and can be obtained from the energy derivative of the new action. The corner correction is not generally important for quantization. It's main role is the removal of spurious levels, and it is numerically insignificant otherwise. Including this term is crucial only if we are interested in perturbed levels of the two-particle system whose unperturbed counterparts coincide with a level of the one-particle spectrum. However, these degeneracies are rare (for example, for $E < 1000$, this happens only 10 times), and unless the entire spectrum ($E < E_{\max}$) is desired, the leading-order semiclassical trace formulas are sufficient. Therefore,

$$\tilde{\rho}_2(E;\epsilon) = \tilde{\rho}_2^{\mathrm{h}}(E;\epsilon) + \tilde{\rho}_2^{\mathrm{d}}(E;\epsilon). \tag{5.29}$$

5.2.2 Numerics

For numerical comparisons, only the evolution of the singlet states will be considered, that is, the states that are nondegenerate even for $\epsilon = 0$. (Note that the singlet states are symmetric under space reflection *and* particle exchange.) From quantum mechanical perturbation theory, we know the energies of these states are simply shifted away from their unperturbed values for $\epsilon \neq 0$. Semiclassically, we should observe the same behavior as a result of the action shifts discussed above. This is now tested numerically. For the following numerical calculations, $\mathcal{L} = \pi, m = \frac{1}{2}, \hbar = 1, x_1 = 0, x_2 = \pi$ so that $\mathcal{E}_0 = 1$.

For the noninteracting case ($\epsilon = 0$), the shorter orbits have larger amplitudes than the longer orbits since the length dependence of the amplitudes in Eqs. (5.16) and (5.17) is $1/\sqrt{L_\Gamma}$. Hence, length truncation of the sums gives optimal convergence. If $\epsilon \neq 0$, it is not obvious what kind of ordering of the terms is optimal. The exact amplitude behavior is difficult to characterize since the modulation factor is a complicated oscillatory function that depends on the orbit parameters and energy. (Incidentally, for $\epsilon = 0$, the energy dependence can be separated out from the dependence on the orbit parameters.) Nevertheless, length truncation shall be used for the modulated ($\epsilon \neq 0$) sums although this procedure may not be the most efficient.

The semiclassical perturbed energies can be *estimated* numerically using the Gaussian sum rule

$$\tilde{\rho}_\sigma(E;\epsilon) = \sum_\Gamma \exp\left[\frac{-2\sigma^2 T_\Gamma^2(E)}{4\hbar^2}\right] A_\Gamma(E)\ \mathrm{Im}\left\{\mathcal{M}_\Gamma\left(\frac{\epsilon}{\hbar}, E\right) \exp\left[i\left(S_\Gamma(E) - \frac{\pi}{4}\right)\right]\right\}, \tag{5.30}$$

which (upon adding the smooth part $\bar{\rho}_\sigma(E;\epsilon)$) absolutely converges to a Gaussian coarse-grained level density

$$\rho_\sigma(E;\epsilon) = \rho_2(E;\epsilon) * G_\sigma(E) = \sum_n \exp\left[-\frac{(E-E_n)^2}{2\sigma^2}\right]. \tag{5.31}$$

The sum rule in Eq. (5.30) arises from convolving the trace formulas with a Gaussian response function $G_\sigma(E)$, and is the generalization of the sum rule obtained in Chapter 2. The convergence of the sums in Eqs. (5.24) and (5.28) is enforced through an additional exponential damping factor $\exp\left(-\sigma^2\alpha L_\Gamma^2/8E\right)$ in the amplitude. Each peak generated by the sum rule has a Gaussian shape whose maximum (center) occurs at a position along the energy axis that is to be identified with a semiclassical energy. The parameter σ is the variance of the Gaussian[2], $\alpha = 2m/\hbar^2$, and L_Γ is the length of the *unperturbed* periodic orbit family Γ. If all orbits with length $L < L_{\max}$ are included, then there exists a set of values $E < E_{\max}$ for which the exponential factor falls below some threshold parameter δ. This condition immediately gives a simple relation between all the relevant parameters:

$$L_{\max} = \frac{2\sqrt{-2E_{\max}\ln(\delta)}}{\sigma\sqrt{\alpha}}. \tag{5.32}$$

For $L_\Gamma > L_{\max}$ and $E \leq E_{\max}$, all terms are exponentially smaller than δ, and are thus numerically insignificant. The parameter δ is an amplitude cutoff, and for the following calculations, $\delta = 10^{-10}$. The largest errors are in the vicinity of $E_{\max}$ where there are contributions $O(\delta)$ that have been excluded. For all other values of $E < E_{\max}$, the excluded terms are exponentially smaller than δ.

As discussed above, we use a standard length truncation and include all orbits with length $L < L_{\max}$. We first specify $E_{\max}$, σ, and δ, and $L_{\max}$ is then determined from the condition that all orbits with length $L > L_{\max}$ have amplitudes smaller than δ [Eq. (5.32)]. (The parameters could be selected in a different order, but the point is that these quantities are not independent.) The convergence can be checked by including many orbits with length greater than $L_{\max}$ and verifying that the position of the peak maximum does not change

[2]The peak width could be interpreted as a measure of the uncertainty in the semiclassical energy. If so, then a peak maximum that occurs at $\mathcal{E}$ gives a semiclassical energy $\mathcal{E} \pm \sqrt{2}\sigma$. However, to compare with the exact quantum mechanical energies, we are then forced to use small values for σ (for example, 10^{-3}), which as explained later increases the numerical error associated with the sum rule. A semiclassical energy shall be identified with the position of a peak maximum and no further interpretation of the peak width will be assigned here. Generally speaking, the only restriction is that σ be small enough so that individual levels can be resolved. However, this is not a concern here since the singlet states are sufficiently isolated.

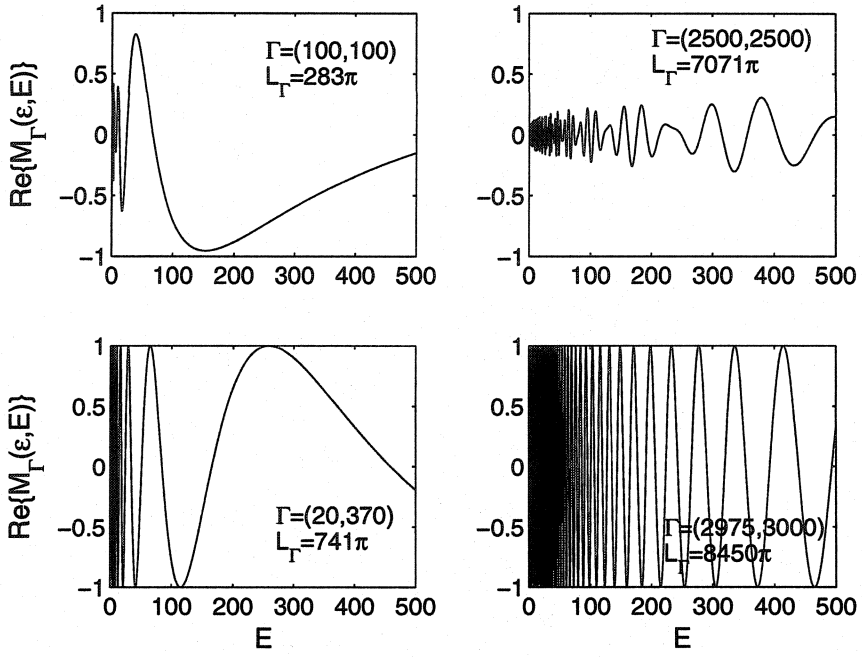

Figure 5.3: The real part of the modulation factor [Eq. (5.21) or Eq. (5.23)] for orbit families $\Gamma = (n_a, n_b)$ perturbed by a long-range repulsive interaction ($\epsilon = 0.1$ and $\kappa = 1/\mathcal{L} = 1/\pi$).

within the specified accuracy[3]. The semiclassical energies can be computed to a specified accuracy by evaluating the sums on energy windows of appropriate size. We start with a window that encloses the entire peak of interest and then systematically refine the size of the window until the position of the peak maximum has been located to the desired accuracy. (It could be argued that this is not an efficient procedure for extracting the energies, but there is little alternative. Unfortunately, the technique of harmonic inversion which has proven to be a powerful tool for extracting eigenvalues from periodic orbit expansions is not applicable to this system since the perturbed Hamiltonian is nonscaling.) The numerical results will be given to $O(10^{-5})$.

The trace formulas are exact for $\epsilon = 0$ and any numerical errors arise exclusively from the approximations made in obtaining the sum rule (5.30). The analysis of the singlet peaks for $\epsilon = 0$ reveals that errors inherent in the sum rule are $O(10^{-4})$ for $\sigma = 0.1$ and

[3]Although the sums are then numerically converged in the sense that adding longer orbits will have no numerical effect, the exact positions of peak maxima will generally depend on the specific choice of the parameter σ. The relative importance of the Thomas-Fermi term also depends on the specific choice of σ. The smaller the value of σ, the less important $\bar{\rho}_2(E;\epsilon)$ becomes and vice-versa. However, the leading-order smooth term only affects the height of the peak maximum and not its position along the energy axis.

$O(10^{-6})$ for $\sigma = 0.01$. In this case, when $\sigma \to 0$ and $L_{\max} \to \infty$, the sum converges to the quantum result. A similar analysis for $\epsilon \neq 0$ reveals that smaller values of σ yield less accurate results. Although we have complete freedom in specifying the variance σ, it should not be chosen too small since this will require that $L_{\max}$ must be quite large. The breakdown of semiclassical perturbation theory for long orbits is discussed in Ref. [38]. However, the errors introduced by including long orbits does not arise from the semiclassical approximation alone. The sum rule itself becomes less accurate when longer orbits are included. The reason is that the modulation factor of long orbits is highly oscillatory for lower values of E (see, for example, Figs. 5.3 and 5.4). The asymptotic analysis of the convolution integral that yields the sum rule assumes that the amplitude of the trace formula is a smooth slowly-varying function of E. To leading order, the amplitude can then be taken outside the integral since it is approximately constant on an interval of size $\sim \sigma$. If the modulation factor is oscillating rapidly (as it does for long orbits), this assumption is no longer valid. However, the interest here is not in how the perturbative procedure breaks down when longer orbits are included nor in the precise value of the perturbed energies. If we were interested in the latter, then we could do the convolution integral exactly (numerically). The important point is that the $\epsilon \neq 0$ sum rule does not converge to the exact quantum coarse-grained level density. Nevertheless, we can still choose a moderate value for σ and obtain an estimate of the energy shift. This itself is a very useful test of the theory. Note that the variance σ must still be small enough to resolve individual levels. For the analysis of the singlet states, the value $\sigma = 0.1$ is a good compromise that satisfies both requirements. As mentioned above, the $\epsilon = 0$ sum rule does converge to the quantum result. In the unperturbed case, the amplitude $A_\Gamma(E) \sim E^{-1/4}\ \forall\, \Gamma$, which is approximately constant on intervals of size σ for $E \gtrsim 1$. Since all orbit families have this energy dependence in their amplitudes, the analysis is accurate for all orbits, and becomes more accurate as $\sigma \to 0$.

It should be emphasized that corrections to the Thomas-Fermi term are not negligible and these introduce an additional error. (To the level of precision of interest here, the smooth term does change across the width of a peak even if that peak is narrow.) A precise determination of this error requires a separate numerical study of the smooth term[4], but since the interest here is only to estimate the energy shift, further analysis of the smooth

[4]We would have to use the Strutinsky method (see Ref. [7]); no other method is applicable to this mixed potential system, which has both a smooth interaction potential and a discontinuous confining potential.

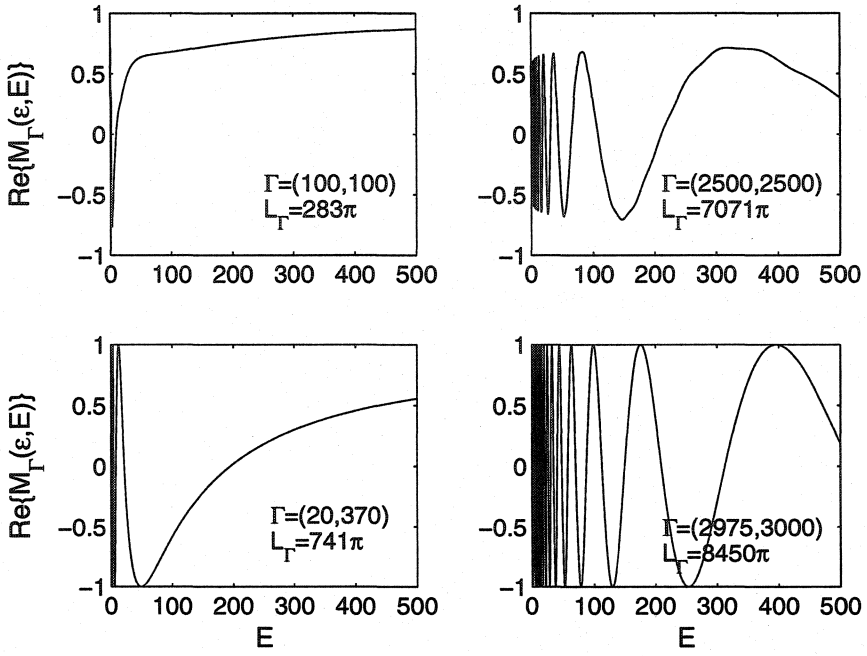

Figure 5.4: Same as Fig. 5.3, except the orbit families $\Gamma = (n_a, n_b)$ are perturbed by a short-range repulsive interaction ($\epsilon = 0.1$ and $\kappa = \mathcal{L} = \pi$).

term will not be considered. A measure of the error can be gleaned from the unperturbed case, where the "surface correction" causes changes in the smooth term of $O(10^{-4})$ across energy windows of size $\sigma \sim 0.1$ for $10 \lesssim E \lesssim 100$ and of $O(10^{-5})$ or less for $E \gtrsim 100$. This suggests that for the perturbed case we should expect errors of at least the same order from neglected corrections to the Thomas-Fermi term.

In Tables 5.1-5.4, numerical results for $\epsilon = \pm 0.1$ are given. In each case, the data were generated using $L_{\max} = 1000\mathcal{L}$ and $\sigma = 0.1$. The number of dynamical orbit families $N_{\rm d} = 98\ 095$ and the number of heterogeneous orbit families $N_{\rm h} = 500$. A consistent length truncation requires that both trace formulas include only orbits with length $L \leq L_{\max}$. It is incorrect to simply specify an upper truncation limit for the sums. Since the dynamical orbits proliferate much more rapidly than the heterogeneous orbits, that is, $N_{\rm d}(L) \ggg N_{\rm h}(L)$, many more of the former must be included in the truncated sums. For large L, the role of the heterogeneous orbits is relatively minor, but still nevertheless important since their contribution ensures the peaks have the correct shape.

As the numerics demonstrate, the sum rule gives estimates of the shifts accurate to $O(10^{-3})$ for long-range interactions, and to $O(10^{-2})$ for short-range interactions. We

n	$E_n^{(0)}$	E_n	E_n^{qm}	E_n^{sc}	Δ_n^{sc}
7	32	32.08709	32.08713	32.08664	0.00045
15	72	72.08689	72.08692	72.08664	0.00025
20	98	98.08684	98.08688	98.08664	0.00020
26	128	128.08681	128.08685	128.08664	0.00017
33	162	162.08679	162.08683	162.08664	0.00015
102	512	512.08674	512.08678	512.08664	0.00010

Table 5.1: Perturbed energies for six singlet states of the unperturbed two-particle system. The parameters $\epsilon = 0.1$, $\kappa = 1/\mathcal{L} = 1/\pi$. This choice of κ corresponds to a repulsive interaction that is long-range with respect to the size of the well. The first column specifies the quantum numbers of states that belong to the symmetric irrep, and the second and third columns give the exact unperturbed and perturbed quantum energies, respectively. The forth and fifth columns are the energies obtained from quantum and semiclassical perturbation theory. The difference between the quantum and estimated semiclassical values is given in the last column. The difference between exact and quantum perturbation theory $\Delta_n^{\mathrm{qm}} = E_n - E_n^{\mathrm{qm}} = 0.00003$ for each given n. For comparison, if $\sigma = 0.05$ (so that longer orbits are less suppressed), then $E_{20}^{\mathrm{sc}} = 98.08657$; the semiclassical error ($\Delta_{20}^{\mathrm{sc}} = 0.00027$) is larger, but the energy shift is unchanged to $O(10^{-4})$.

n	$E_n^{(0)}$	E_n	$E_n^{\rm qm}$	$E_n^{\rm sc}$	$\Delta_n^{\rm sc}$
7	32	32.02094	32.02104	32.01798	0.00296
15	72	72.01940	72.01949	72.01794	0.00146
20	98	98.01913	98.01922	98.01794	0.00119
26	128	128.01899	128.01908	128.01794	0.00105
33	162	162.01891	162.01901	162.01794	0.00097
102	512	512.01879	512.01888	512.01792	0.00087

Table 5.2: Same as Table 5.1 except that $\kappa = \mathcal{L} = \pi$ which corresponds to a short-range repulsive interaction. For each given excited state n, the error $\Delta_n^{\rm qm} = E_n - E_n^{\rm qm} = 0.00009$. For comparison, if $\sigma = 0.05$, then $E_{20}^{\rm sc} = 98.01764$; the error $\Delta_{20}^{\rm sc} = 0.00149$, but the energy shift is unchanged to $O(10^{-3})$.

expect errors of at least $O(10^{-4})$ due to the approximate evaluation of the convolution integral (i.e. the sum rule) and of at least the same order from neglected corrections to the leading-order smooth term. Clearly, however, the semiclassical approximation is more accurate for long-range interactions. This is due to the fact that corrections to the Thomas-Fermi term are much more significant for short-range interactions.

For long-range interactions, the perturbation is somewhat flat on the scale of the dimensions of the well. Generally speaking, from quantum mechanics, we know that a flat perturbation causes all the levels to shift by the same amount. Thus, the quantum energy shifts are expected to be quite similar for all levels in this case. We also expect the approximate semiclassics to give accurate energy shifts for large quantum numbers. It is typical for semiclassics to become more accurate at larger energies and clearly this characteristic is found in the data, but it is because both the Thomas-Fermi term and the sum rule become more accurate for large energies. Since all levels are shifted by similar amounts and the approximate semiclassics more accurately reproduce the energy shifts for large energies, there is generally better agreement between quantum and semiclassical

results in the case of long-range interactions. For short-range interactions, there is more variation in the amount by which the low-lying levels are shifted and for higher energies the quantum shifts again become similar. Thus, the discrepancies are quite large for low energies, but are reduced as the energy increases.

Note that *both* quantum *and* semiclassical perturbation theory are more accurate for long-range interactions. Furthermore, when the interaction is repulsive, $\Delta_{\rm qm}^{\rm SR}/\Delta_{\rm qm}^{\rm LR} \sim 3$, whereas $\Delta_{\rm sc}^{\rm SR}/\Delta_{\rm sc}^{\rm LR} \sim 6$. The error in the smooth term should account for the factor of 2. Finally, a close inspection of the quantum data to $O(10^{-8})$ reveals that the error from quantum perturbation theory slowly falls as the quantum number is increased when the interaction is short-range, but steadily grows when the interaction is long-range. (This is true regardless of whether the interaction is attractive or repulsive.) There is no such distinction for the leading-order semiclassical approximation; it simply improves at higher energies if the interaction is repulsive or becomes worse at higher energies if the interaction is attractive.

The results for attractive interactions seem counterintuitive. For small energies ($E \lesssim 100$), the estimated semiclassical energy shifts are an order of magnitude better for attractive interactions as compared to repulsive interactions. (This is reminiscent of the results of a previous study[5].) There is no obvious reason to expect that the formalism of Sec. 5.1 should be more accurate for attractive interactions ($\epsilon < 0$) than for repulsive interactions ($\epsilon > 0$). There is another anomaly for attractive interactions; for moderate to large energies ($E \gtrsim 100$), the semiclassical error increases. This is unexpected since the sum rule is, in general, more accurate for large energies. (For repulsive interactions, the estimated semiclassical energy shifts are more accurate for high quantum numbers precisely due to the fact that the sum rule is more accurate at large energies.) One possible explanation is that corrections to the Thomas-Fermi term are more significant at large energies when the interaction is attractive.

After the interaction is turned on, the energy levels that were degenerate for $\epsilon = 0$ split. For $\epsilon \ll 1$, the spacing between these levels is very small, in fact, most of them are still degenerate to the numerical precision considered here. (For $\epsilon \gtrsim 1$, the splittings become larger, but the semiclassical analysis is expected to fail in this case.) We could try

[5]The average density of states for a system of interacting fermions in one dimension was briefly considered in Ref. [106], where it was found that the semiclassical approximation is quite accurate for attractive interactions, but largely overestimates the cumulative density of states when there are repulsive interactions.

n	$E_n^{(0)}$	E_n	$E_n^{\rm qm}$	$E_n^{\rm sc}$	$\Delta_n^{\rm sc}$
7	32	31.91284	31.91287	31.91313	0.00029
15	72	71.91305	71.91308	71.91313	0.00008
20	98	97.91309	97.91312	97.91312	0.00003
26	128	127.91312	127.91315	127.91312	$O(10^{-6})$
33	162	161.91314	161.91317	161.91313	0.00001
102	512	511.91319	511.91322	511.91312	0.00007

Table 5.3: Same as Table 5.1 except that $\epsilon = -0.1$ which corresponds to a long-range attractive interaction. The error $\Delta_n^{\rm qm} = E_n - E_n^{\rm qm} = 0.00003$ for each given state n.

to study these level splittings semiclassically. Of course, this would require that we use very small variances, but this is computationally expensive, and it does not seem worth the effort to do this kind of precision test of the perturbed trace formulas. (There is also the fact that the numerical procedure used above becomes less accurate if orbits with large actions are included in the sums.) The same problems arise if the particles are nonidentical. Although there are no degeneracies when $\epsilon = 0$, there are still many near degeneracies, a characteristic of the fact that the unperturbed system is integrable.

5.3 Other Continuous Symmetries

We have assumed that the one-particle dynamics is free of any continuous symmetry[6]. In general, if there are other continuous symmetries, then these must be properly accounted for in the analysis. The theory of Ref. [38] can still be applied if there are no continuous symmetries after perturbation. For example, suppose there are two particles confined in a two-dimensional rectangular billiard. In the absence of interactions, there

[6]Strictly speaking, the analysis of Sec. 5.1 can also be applied to isolated periodic orbits in systems where there are coexisting isolated and nonisolated families of periodic orbits. Two examples would be the isolated orbit of the equilateral triangle billiard, and the isolated diameter orbits of the elliptic billiard.

n	$E_n^{(0)}$	E_n	$E_n^{\rm qm}$	$E_n^{\rm sc}$	$\Delta_n^{\rm sc}$
7	32	31.97887	31.97896	31.98075	0.00188
15	72	71.98041	71.98051	71.98071	0.00030
20	98	97.98068	97.98078	97.98071	0.00003
26	128	127.98082	127.98092	127.98070	0.00012
33	162	161.98090	161.98099	161.98070	0.00020
102	512	511.98103	511.98112	511.98069	0.00034

Table 5.4: Same as Table 5.2 except that $\epsilon = -0.1$ which corresponds to a short-range attractive interaction. For $n = 26, 33, 102$, the error $\Delta_n^{\rm qm} = E_n - E_n^{\rm qm} = 0.00009$, whereas for $n = 7, 15, 20$, the error $\Delta_n^{\rm qm} = 0.0001$.

are four independent constants of the motion: any two of $\{E, E_a, E_b\}$, and any two of $\{|p_x|_a, |p_y|_a, |p_x|_b, |p_y|_b\}$. Without loss of generality, we can choose the four constants to be E and $\mathbf{J} = (E_a, |p_y|_a, |p_y|_b)$. The corresponding conjugate parameters are $\mathbf{\Theta} = (\theta_a, \phi_a, \phi_b)$, where the latter two parameters have dimensions of length. Thus, there are 3-parameter families of periodic orbits. After the interaction is turned on, there are no constants of motion, except E. The families are destroyed, but we can still use the theory of Ref. [38]) to describe the transition. In this specific example, the leading-order change in the action is

$$\Delta S_\Gamma(\mathbf{\Theta}; E, \epsilon) \approx -\epsilon \int_{\Gamma_\Theta} V(\mathbf{z}_a(t; \theta_a, \phi_a), \mathbf{z}_b(t; \phi_b)) \mathrm{d}t. \tag{5.33}$$

The orbit specified by the parameters $\mathbf{\Theta}$ involves time translation of particle a and spatial translations in the y component of both particles: $\mathbf{z}_a(0; \theta_a, \phi_a) = (x_a(\theta_a), y_a(\theta_a; \phi_a), \mathbf{p}_a(\theta_a))$ [where $y_a(0; \phi_a) = \phi_a$], and $\mathbf{z}_b(0; \phi_b) = (x_b(0), \phi_b, \mathbf{p}_b(0))$. The modulation factor is then

$$\mathcal{M}_\Gamma(\epsilon/\hbar, E) = \frac{1}{T} \int \exp\left[i \Delta S_\Gamma(\mathbf{\Theta}; E, \epsilon)/\hbar\right] \mathrm{d}\mathbf{\Theta}. \tag{5.34}$$

5.4 Few-Body System

A perturbation will generically transform families of orbits to a discrete set of isolated orbits as it is turned on. For large particle numbers, there are high-dimensional families. (In general, there are orbit families of arbitrary dimensionality.) Regardless, the prescription is the same; we integrate the perturbed action over the family manifold to determine the perturbed contribution. The asymptotic behavior of the modulation factor will then be such as to absorb the $1/\hbar^{f/2}$ prefactor in the amplitude (where f is the dimensionality of the periodic orbit family) and give all orbits the same generic $1/\hbar$ prefactor.

We next consider a three-particle system. For the classical Hamiltonian

$$H(\mathbf{z}_a, \mathbf{z}_b, \mathbf{z}_c) = H_0(\mathbf{z}_a, \mathbf{z}_b, \mathbf{z}_c) + \epsilon V(\mathbf{z}_a, \mathbf{z}_b, \mathbf{z}_c), \tag{5.35}$$

where H_0 is the Hamiltonian in the absence of interactions, the leading-order change in the action is

$$\Delta S_\Gamma(\theta_a, \theta_b; E, \epsilon) \approx -\epsilon \int_{\Gamma_{(\theta_a,\theta_b)}} V(\mathbf{z}_a(t;\theta_a), \mathbf{z}_b(t;\theta_b), \mathbf{z}_c(t))\mathrm{d}t. \tag{5.36}$$

The periodic orbit specified by the symmetry parameters θ_a and θ_b involves a shift of the initial conditions of particles a and b relative to particle c, that is, $\mathbf{z}_a(t;\theta_a) = \mathbf{z}_a(t+\theta_a)$ and $\mathbf{z}_b(t;\theta_b) = \mathbf{z}_b(t+\theta_b)$.

We revisit the single-particle Hénon-Heiles potential (5.4), and now populate it with three particles, placing them all on the x-axis. There is a family of three-particle periodic orbits consisting of all three particles independently executing the same single-particle motion on the same stable harmonic periodic orbit, but with a phase difference between them. Let $x_a(t) = A\cos(t+\theta_a)$, $x_b(t) = A\cos(t+\theta_b)$, and $x_c(t) = A\cos t$ denote the positions of the three particles. Adding a weak harmonic interaction among the particles

$$\epsilon V(\mathbf{z}_a, \mathbf{z}_b, \mathbf{z}_c) = \frac{\epsilon}{2}\left[(x_a - x_b)^2 + (x_a - x_c)^2 + (x_b - x_c)^2\right] \tag{5.37}$$

changes the action by the amount

$$\Delta S_\Gamma(\theta_a, \theta_b; E, \epsilon) = \frac{-\epsilon T A^2}{2}\left[3 - (\cos\theta_a + \cos(\theta_a - \theta_b) + \cos\theta_b)\right]. \tag{5.38}$$

The modulation factor for this family of orbits becomes

$$\mathcal{M}_\Gamma(\epsilon/\hbar, E) = \frac{\exp\left[-i\left(\frac{3\epsilon T A^2}{2\hbar}\right)\right]}{(2\pi)^2}\int_0^{2\pi}\int_0^{2\pi}\exp\left[i\left(\frac{\epsilon T A^2}{2\hbar}\right)F(\theta_a, \theta_b)\right]\mathrm{d}\theta_a\mathrm{d}\theta_b, \tag{5.39}$$

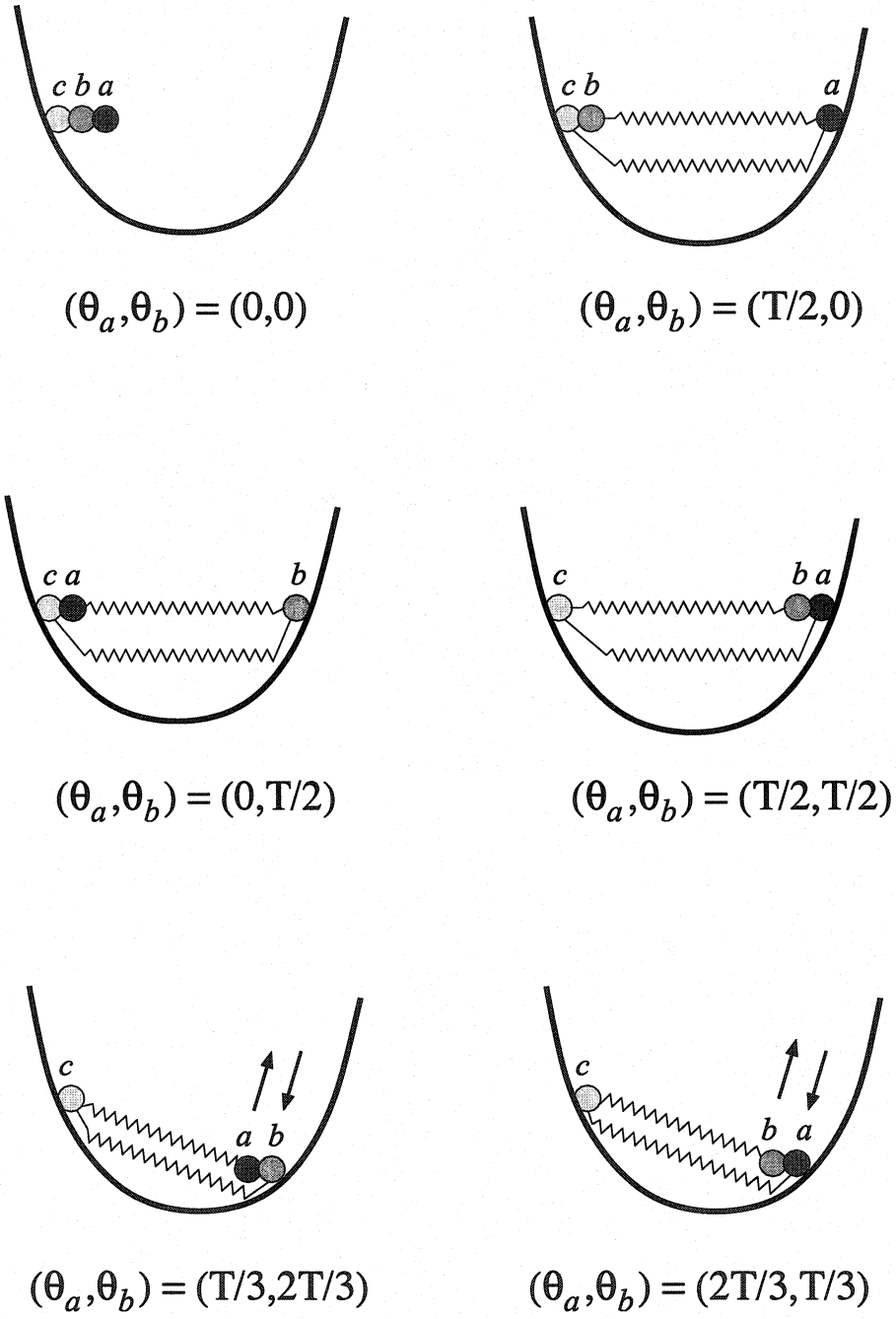

Figure 5.5: The particle configurations at $t = 0$ corresponding to the six stationary phase points of the integral in Eq. (5.39). In the bottom panel, the directions in which particles a and b are traveling are indicated by arrows.

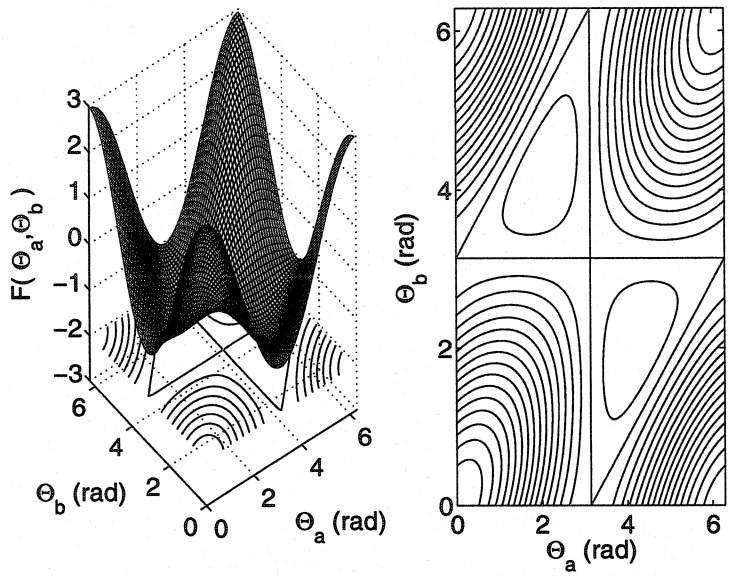

Figure 5.6: The function $F(\theta_a, \theta_b) = \cos\theta_a + \cos(\theta_a - \theta_b) + \cos\theta_b$ on the 2-torus. The six stationary phase points are visible on the right.

where $F(\theta_a, \theta_b) = \cos\theta_a + \cos(\theta_a - \theta_b) + \cos\theta_b$.

In the limit $\epsilon T A^2/2 \gg \hbar$, the integral can again be analyzed by stationary phase. In this example, there are six contributions. These have phases of $\pm\pi/2$ relative to the noninteracting case, and have relative amplitudes $O(\hbar)$ since this is a two-dimensional stationary phase problem. For the following discussion, it is helpful to consider the function $F(\theta_a, \theta_b)$ on the 2-torus. Let $\mathscr{H}_F(\theta_a, \theta_b)$ denote the Hessian matrix of F. The first stationary phase point $(\theta_a, \theta_b) = (0, 0)$ corresponds to the three particles being in phase, and is a maximum of F such that $\det[\mathscr{H}_F(0,0)] = 3$. The three stationary phase points $(\theta_a, \theta_b) = (0, \pi)$, $(\pi, 0)$, and (π, π) correspond to two of the particles being $T/2$ out of phase with the third (see Fig. 5.5). These are saddle points of F at which $\det[\mathscr{H}_F] = -1$. The last two stationary phase points $(\theta_a, \theta_b) = (2\pi/3, 4\pi/3), (4\pi/3, 2\pi/3)$ correspond to all three particles being $T/3$ out of phase (Fig. 5.5), and are minima of F at which $\det[\mathscr{H}_F] = 3/4$ (see also Fig. 5.6). Notice the parallel with the group elements of S_3; this is due to all three particles executing identical motions. When all three particles are in phase, there is no shift in the action [i.e. $\Delta S(0,0) = 0$]. There is a shift in the action by the amount $-2\epsilon T A^2$ whenever any subset of the particles is $T/2$ out of phase with the remaining particle(s), that is, $\Delta S(0,\pi) = \Delta S(\pi,0) = \Delta S(\pi,\pi) = -2\epsilon T A^2$. When all three particles are $T/3$ out of phase with each other, there is a shift $\Delta S(2\pi/3, 4\pi/3) = \Delta S(4\pi/3, 2\pi/3) = -9\epsilon T A^2/4$.

Chapter 6

Conclusion

The unsymmetrized noninteracting many-body problem was studied in Chapter 3. It was explained how time-translational symmetry leads to families of periodic orbits in the full phase space, and using the formalism of Creagh and Littlejohn [33], trace formulas were derived for the many-body resolvant. Heterogeneous periodic orbits in the full phase space were introduced, and there was a discussion on how the structure of these orbits is different in billiards and in analytic potentials, and the explicit contribution of such orbits to the many-body resolvant was determined. The theoretical results were applied to systems of two or three noninteracting particles in a two-dimensional cardioid billiard. The semiclassical formalism correctly reproduced the quantum results, and it was explained how these results were correlated with the periodic orbit families in the full phase space. The classical-quantum correspondence was deduced from the Fourier transform of the quantum spectrum, which is (through the various trace formulas) directly related to the action spectrum of the periodic orbits. It was also shown how degenerate periodic orbit families are destroyed if particle symmetry is broken.

The formalism developed in Chapter 3 yielded results that are consistent with those of the convolution formalism for two- and three-body systems (see Ref. [35] and Appendix C). The convolution formalism involves the tedious and nontrivial asymptotic analysis of many convolution integrals, and the further issue of spurious contributions from these integrals. It is not straightforward to immediately generalize the convolution results for a few-body system to a many-body system. The formalism of Chapter 3, on the other hand, easily generalizes to a many-particle system. It is also more fundamental and conceptually superior to the convolution formalism since it reveals the underlying structure of the periodic orbit families. (The useful feature of the convolution approach is that significant higher-

order corrections from heterogeneous orbits in billiards can be explicitly calculated (see Appendix C.3). The most important difference is that the convolution formalism cannot be used if there are interactions, and it is then necessary to use the full phase space formalism of Chapter 3.

The symmetrized noninteracting many-body problem was then analyzed in Chapter 4. The symmetrized densities of states for two-particle systems (see also Appendix A.2) were first considered. Dynamical pseudoperiodic orbits (DPPOs) were defined and it was shown that their contribution to the symmetrized densities of states has the form of a one-particle trace formula. The symmetrized resolvant for many noninteracting identical particles can be expressed as a sum of resolvants ("exchange terms"), one for each element of the permutation group. The oscillatory components of these exchange terms can be expressed in terms of heterogeneous and dynamical pseudoperiodic orbits (HPPOs and DPPOs), which are structures in phase space that are periodic under time evolution and particle permutation. Since each permutation can be decomposed into cycles, it was shown that the trace formulas for each exchange term could be written as a product over cycles, where each cycle is assigned to a periodic orbit of the one-particle phase space. The theoretical results were again applied to systems of two and three noninteracting identical particles in a cardioid billiard. The trace formulas correctly reproduced the quantum results, and it was explained how these results were correlated with the pseudoperiodic orbits in the full phase space. In this case, the correspondence was deduced from the Fourier transform of the symmetry-reduced density of states belonging to a particular conjugacy class of the permutation group, which is (through the various trace formulas) directly related to the action spectrum of the pseudoperiodic orbits.

The unsymmetrized few-body problem in the limit of weak interactions was studied in Chapter 5. Any weak interparticle coupling can be thought of as a symmetry-breaking perturbation, and it is then possible to apply the results of the perturbative theory introduced by Creagh [38]. Some simple conceptual examples were given to illustrate the general procedure. A system of two weakly-interacting particles in a square well was used as the main example. The foremost reason for choosing a one-dimensional billiard as the confining potential is that $\hbar$-corrections are not required for the analysis. This system may have seemed somewhat trivial. On the contrary, the problem is nonintegrable and involves a nonscaling interaction, and the analysis of this problem adequately illustrates many generic aspects of a calculation in higher dimensions. In fact, precisely the same analysis would

apply to the diameter orbits of the elliptic billiard, for instance, regardless of the stability of the orbit. The perturbed contributions of all the nonprimitive heterogeneous and dynamical orbits were calculated, and it was possible to obtain a closed form for all the action shifts.

The fact that the perturbed contributions could be computed for all nonprimitive orbits is quite significant from the perspective of semiclassical quantization. At present, the quantization of nonintegrable systems is not viable. Actually, Creagh's method cannot generally be used for the purposes of full quantization, but an approximate quantization was achieved from summing the Gaussian-convolved perturbed trace formulas (Gaussian sum rule) and identifying the center of the Gaussian line to a specified accuracy. The numerical results allow for some general conclusions to be made regarding the accuracy of the leading-order semiclassical approximation: (i) it is more accurate for long-range interactions since corrections to the Thomas-Fermi term are much more important for short-range interactions; (ii) it is more accurate for attractive interactions at low energies; (iii) For repulsive interactions, the semiclassical estimates monotonically improve as the energy increases, whereas for attractive interactions, the semiclassical estimates improve for the low-lying excited states, but then become less accurate for higher quantum numbers. The last property is quite surprising since the sum rule itself is more accurate at higher energies. However, it is possible that corrections to the Thomas-Fermi term are more significant at higher energies for attractive interactions (see, for example, Ref. [99]), but further analysis of attractive interactions is required to understand why the semiclassical analysis is better for attractive interactions (for small to moderate quantum numbers) and why the semiclassical approximation slowly becomes worse for higher quantum numbers.

It was noted after doing an asymptotic analysis of the modulation integrals that the number of critical points increases with the length of the dynamical orbits. This implies that families with small actions break into relatively few isolated orbits, whereas families having larger actions are destroyed and replaced by many more isolated orbits. Although the longer nonprimitive dynamical orbits do break up into many more isolated periodic orbits, it is likely that these orbits are degenerate, that is, the orbits are different, but their classical invariants (actions, stabilities, and phase indices) are the same. However, further analysis is required to verify this statement. In contrast, the asymptotic analysis of the modulation factor for the heterogeneous orbits yields exactly one critical point. Therefore, as the interaction is turned on, each nonprimitive heterogeneous family is broken up and replaced by a single isolated periodic orbit. It would be interesting to understand the

reasons for this dichotomy between the heterogeneous orbits and the dynamical orbits. Intuitively, we do not expect such a qualitative difference since both types of orbits have equal degeneracy before the interaction is turned on.

The $\hbar$ dependence of the many-body trace formulas immediately implies the amplitude of the level density oscillations (and therefore the strength of the shell effects) grows with the size of a noninteracting many-body system. (Recall the degeneracy of the periodic orbit families $f \geq (N-1)$, where N is the number of particles.) Interactions are a symmetry-breaking phenomenon and reduce this degeneracy or destroy it altogether. Hence, interactions reduce the amplitude of level density oscillations, and therefore reduce the strength of shell effects in a many-body system. This is a generic property of interactions; the shell effects are reduced regardless of the specific form of the interaction. The classical-quantum correspondence is as follows: as more particles are introduced into the system, the quantum degeneracy increases, and this degeneracy is also present in the underlying classical dynamics since the degeneracy of the periodic orbit families increases as the size of the system grows. Interactions destroy quantum degeneracies, and this is manifested classically also since interactions reduce the dimensionality (degeneracy) of the periodic orbit families or destroy them altogether. This correspondence is valid regardless of whether there is an exact quantum degeneracy (i.e. whether there is particle symmetry) since shell effects are expected to be more pronounced for noninteracting systems with more particles and to be reduced in the presence of interactions. If particle symmetry is broken, then spectral degeneracies are destroyed in quantum mechanics, and this is exhibited classically also since degenerate periodic orbit structures are also destroyed after particle symmetry is removed.

Future Work

Noninteracting systems

For completeness, it remains to work out the contribution of the heterogeneous orbits in smooth potentials for $d > 1$ using the convolution formalism (the $d = 1$ case is analyzed in Appendix C.2). It is not immediately obvious how from the point of view of convolutions the commensurate or incommensurate nature of the frequencies associated with potential extrema are subsumed in the final expressions. The situation in which the denominator vanishes and the conditions that lead to this divergence should also be explored.

Generally speaking, it would be worthwhile to examine the significance[1] of heterogeneous orbits in some concrete examples, and in general determine the accuracy of the trace formulas (3.15) and (3.26). A good candidate smooth potential is the family of quartic potentials, which are scaling, and exhibit the full range of dynamics.

The single-particle dynamics were assumed to be free of any continuous symmetry. If there are additional symmetries, then these must be properly accounted for in the theory. If the additional symmetries are Abelian, then $\mathbf{J}$ and $\boldsymbol{\Theta}$ become higher dimensional. An example is two particles in a disk billiard. In this case, there are four independent constants of the motion (any two of $\{E, E_a, E_b\}$ and any two of $\{L_z, L_{z_a}, L_{z_b}\}$), and the periodic orbits occur in 3-parameter families. In principle, the extension of the formalism in Chapter 3 to include additional Abelian symmetries is straightforward.

If the additional symmetries are non-Abelian, then the modifications may be nontrivial. The mixture of Abelian (time-translational) symmetries and non-Abelian symmetries is presumably not an issue for the hydrogen atom (i.e. the Coulomb problem), which has $O(4)$ symmetry, or the three-dimensional spherical billiard, which has $SO(3)$ symmetry. On the contrary, the theory requires a major revision for harmonic oscillator (HO) potentials, which have $SU(d)$ symmetry in d dimensions. Note that the anholonomy term vanishes for harmonic oscillators, and that both the formalism of Ref. [35] and Chapter 3 are thus invalid. This failure is due to the intrinsic non-Abelian symmetry. For example, two identical particles in a one-dimensional HO is formally equivalent to an isotropic two-dimensional HO, which has $SU(2)$ symmetry.

Equations (3.15) and (3.26), which give the contribution from the heterogeneous orbits also fail for identical particles in a HO since the denominators are zero in this case. However, these formulas do apply to nonidentical particles. Consider the simplest case: two nonidentical particles in a one-dimensional HO. This system is formally equivalent to an anisotropic two-dimensional HO, and for incommensurate deformations, there is no continuous symmetry. To clarify this further, suppose the two particles have masses such that ω_a/ω_b is irrational. If the particles are placed in a one-dimensional HO, the particles are always on distinct periodic orbits (γ_a and γ_b), and due to their differing masses $T_{\gamma_a}(E_a) \neq T_{\gamma_b}(E_b)$, regardless of the particle energies E_a and E_b. In that event, there are no dynamical periodic orbits. Nonetheless, there are heterogeneous orbits, and their contributions are

[1] As explained in Chapter 3, if the potential is analytic, then the contributions of the heterogeneous orbits are higher order in $\hbar$ than those of the dynamical orbits.

given exactly by Eq. (3.15). Combining the contributions reproduces the trace formula for an anisotropic two-dimensional HO. This can also be understood from the fact that in an anisotropic two-dimensional HO, the dynamics in the two transverse directions are completely decoupled so that the system is formally the same as if there were two distinct particles executing these motions. The analogous formula [Eq. (3.26)] applies to nonidentical many-particle systems in a HO potential, but there is only *one* type of heterogeneous orbit for nonidentical particles in a HO when the masses are incommensurate.

Anyway, there is the important problem of isotropic or commensurate harmonic oscillator potentials. Of course, an exact convolution analysis could be done (although this is not a trivial calculation in general), but this approach would be useless for studying interactions or developing uniform approximations. To study interactions, it would be necessary to first revise the formalism of Chapter 3. Such a project would require using the theory of Ref. [34], which derives trace formulas for systems with more general symmetries including non-Abelian cases. The results would extend the work of Ref. [40], and would be of interest for semiclassical analyses of few-electron quantum dots where the confining potential is typically parabolic [101].

Interactions

The correspondence between classical and quantum perturbation theory in the context of the semiclassical many-body problem can be summarized as follows: Quantum perturbation theory predicts shifts in energy after an interaction is turned on, and in classical perturbation theory, these shifts are due to the action shifts of the periodic orbits. The quantum theory uses only unperturbed quantum information (i.e. the unperturbed eigenstates), and the classical theory uses only unperturbed classical information (i.e. the unperturbed periodic orbits).

An immediate extension to the problem studied in Chapter 5 is to do an exact calculation of the smooth term and also evaluate the convolution integrals exactly (numerically). Exact numerics would actually provide a meaningful comparison between quantum and classical perturbation theory. It would also be possible to then study precisely how and when the semiclassical theory breaks down for long orbits, and whether this breakdown of the theory for the long-term dynamics is a worthwhile consideration at all with respect to approximate quantization. A complete analysis would also involve an investigation of the

Gutzwiller limit ($\epsilon \gg 1$), and an estimation of the range of interactions strengths for which the Gutzwiller theory and the theory of Chapter 5 yield similar results. Another interesting idea is to use a different interaction and determine whether the asymptotic analysis yields the same critical points. If so, this would imply that the specific form of the interaction is not important, but rather that the structure of the unperturbed orbit (and therefore the unperturbed dynamics) is the fundamental property. The asymptotic analysis should also be supported with numerics, and a possibility is to make use of the Gabor transform [60]. It would also be worthwhile to consider the three-body version of the problem since this would require analyzing other types of orbits that can arise and undergo symmetry breaking. Another immediate extension is to study the symmetry decomposition in the presence of interactions. For this problem, it is a matter of understanding how the dynamical pseudoperiodic orbits (DPPOs) are affected by interactions. In the two-body problem, these orbits are isolated, and so the theory of Refs. [36] (see also Refs. [100]) applies. Note the discrete symmetry must still be accounted for in the calculation and so the theory of Ref. [30] must also be used. For three or more particles, a perturbative analysis for the various families of HPPOs and DPPOs is required.

A major research initiative is to apply the theory of Chapter 5 to higher-dimensional systems. The choice of system and interaction depends on the motivation. (The main interest in Chapter 5 was to test the formalism, and so it sufficed to use a mathematical model.) An important extension is to study two or more weakly-interacting particles in a d-dimensional billiard[2] ($d > 1$). The choice of billiard is not too important, but the advantage of a chaotic billiard is that there are no other continuous symmetries and so the semiclassical analysis is simpler than for an integrable billiard where there are other symmetries. However, the quantum spectra used for numerical comparisons would be harder to obtain for a chaotic billiard. Regardless, if an interaction that preserved scaling was introduced, a standard Fourier transform analysis in reciprocal space could be used. However, it is most likely that the symmetry breaking could not be observed directly, that is, we could not observe the expected peak splitting in reciprocal space since the resolution ultimately depends on the size of the quantum spectrum used for comparisons. However, the idea in this case is to rather observe the change in peak amplitude (as the interaction

[2]This requires a knowledge of the higher-order $\hbar$-corrections from the heterogeneous orbits (for example, see Ref. [35] and Appendix C.3), and these corrections must be understood from a full phase space analysis in order to study interactions. A complete analysis would also include corrections to the one-particle Gutzwiller trace formula.

strength is varied), and verify whether semiclassical perturbation theory can accurately reproduce it. Similar kinds of analyses have been used in studies of atoms in external fields [102]. A better method is to exploit specialized high-resolution spectral techniques such as harmonic inversion, which has proved to be an immensely valuable tool in numerical semiclassics [103]. For interactions which destroy all scaling properties of the Hamiltonian, we could, in principle, apply the Gabor transform technique introduced to study periodic orbit structures in the quantum spectra of nonscaling Hamiltonians [60]. In this case, we are again confronted with the finite resolution of the transformation. Another alternative is to perform an $\hbar$-quantization at a specified energy. Generally speaking, since interactions are a symmetry-breaking phenomenon, resolution is a critical issue, and therefore high-resolution spectral analysis (i.e. harmonic inversion) is invaluable. However, for purposes of low-resolution analysis of quantum fluctuations in energy space (rather than action/period reciprocal space), a point of view adopted in Ref. [7], specialized numerical techniques are not necessary.

The formalism of Chapter 5 assumes that *all* of the continuous symmetries are destroyed. In other words, as the interaction is turned on, degenerate f-parameter families of orbits become isolated. The transition $f = 1 \rightarrow f = 0$ was considered in the main example, and in the conceptual example of Sec. 5.3, there were additional symmetries, but these were *all* destroyed once the interaction was turned on ($f = 3 \rightarrow f = 0$). In the event that continuous symmetries persist after the interaction is turned on, families of orbits reduce to lower-dimensional families as the interaction is turned on. Although the formalism of Refs. [33, 34] works in the two limiting cases (with the appropriate family dimensions), a theory is still required to interpolate between them. For example, consider the two-particle disk problem mentioned above. If there are no interactions, there are four constants of the motion: $\{E, E_a, L_{z_a}, L_{z_b}\}$. Thus, there are 3-parameter families of orbits, and the formalism of Ref. [33] applies. After the interaction is turned on, there is only one constant of the motion (other than E), namely $L_z = (L_{z_a} + L_{z_b})$. The system is no longer integrable, but the orbits still occur in 1-parameter families. The remaining rotational symmetry can of course be destroyed by introducing a noncentral (i.e. angle-dependent) interparticle interaction, and in that event, the formalism of Chapter 5 again applies.

Another problem is how to analyze interactions for which the modulation integrals diverge. Such interactions are ubiquitous in applications. One example is the interaction between two electrons confined in two-dimensions in a semiconductor heterostructure,

where short-range interactions are logarithmic and long-range interactions are Coulombic [104]. There are also interactions that do not possess singularities, but nevertheless attain relatively large values at short interparticle distances. An example would be Morse-type interactions, which are used in chemical physics. For such cases, a somewhat different analysis would be required. When the particles are sufficiently close, such interactions can no longer be thought of as perturbations, and must be analyzed using exact quantum mechanics similar to the treatment of channels in the Pullen-Edmonds potential studied in Ref. [46]. When the particles are sufficiently separated, the interaction can again be thought of as a perturbation, and the analysis of Chapter 5 again applies. The two limits must then be matched at the boundaries.

Another type of interaction that would require a different analysis is that of a completely local interaction such as a delta-function potential. In two dimensions, this interaction has been used to describe the behavior of electrons in mesoscopic systems, and in three dimensions to describe effective internucleon interactions. The formalism of Chapter 3 is also the foundation to study (zero-range) point-interactions. These interactions are often considered as corrections to mean-field approximations. Semiclassically, point-interactions can be analyzed using the formalism of diffractive orbits [105]. We can imagine that such interactions leave the periodic orbit families (of the noninteracting system) largely unchanged, but introduce qualitatively new diffractive orbits. The contributions from diffractive orbits which reside on standard geometric orbits simply rescale the existent geometric orbit contribution. To find qualitatively new contributions from diffractive orbits, we must look for diffractive orbits that do not reside on geometric orbits.

Uniform approximations

The ultimate goal is to develop uniform approximations for the few-body problem. For the unsymmetrized problem, this theory would continuously interpolate between the theory of Chapter 3 and the Gutzwiller theory. For the symmetrized problem, this theory would interpolate between the theory of Chapter 4 and the generalization of the Weidenmüller formalism [42].

Appendix A

Thomas-Fermi-Weyl Density of States

A.1 Two-Particle System

We first discuss the smooth two-particle density of states and then its decomposition into bosonic and fermionic densities. Using the identity $\delta[E - h(\mathbf{z}_a) - h(\mathbf{z}_b)] = \int \delta[\varepsilon - h(\mathbf{z}_a)]\delta[E - \varepsilon - h(\mathbf{z}_b)]\mathrm{d}\varepsilon$, we can show that the leading-order smooth term for the two-particle density of states is the autoconvolution of the leading-order smooth term of the one-particle density of states (1.2). We could verify this term-by-term in the expansion of $\bar{\rho}_2(E)$, but we can do it more efficiently for all terms as follows.

We use the partition function $Z(\beta) = \mathrm{Tr}(\exp(-\beta\hat{H}))$, which is the Laplace transform of the density of states. It is convenient to work with the Wigner transform, which is defined for an arbitrary operator $\hat{A}$ as

$$\hat{A}_{\mathrm{W}}(\mathbf{z}) = \int \left\langle \mathbf{q} + \frac{\mathbf{x}}{2} \middle| \hat{A} \middle| \mathbf{q} - \frac{\mathbf{x}}{2} \right\rangle \exp\left(-i\frac{\mathbf{p}\cdot\mathbf{x}}{\hbar}\right) \mathrm{d}\mathbf{x}, \tag{A.1}$$

in terms of which the trace is

$$\mathrm{Tr}\{\hat{A}\} = \frac{1}{(2\pi\hbar)^d} \int \hat{A}_{\mathrm{W}}(\mathbf{z})\mathrm{d}\mathbf{z}. \tag{A.2}$$

The trace of a product of two (but not more) operators is given by

$$\mathrm{Tr}\{\hat{A}\hat{B}\} = \frac{1}{(2\pi\hbar)^d} \int \hat{A}_{\mathrm{W}}(\mathbf{z})\hat{B}_{\mathrm{W}}(\mathbf{z})\mathrm{d}\mathbf{z}. \tag{A.3}$$

The Wigner transform of the evolution operator $\exp(-\beta\hat{H})_{\mathrm{W}}(\mathbf{z})$, can be written as an asymptotic expansion in powers of $\hbar$, the first few terms of which are typically retained and

used as the smooth approximation to the partition function. Taking the inverse Laplace transform then gives the smooth density of states. In particular, the leading-order term of $\exp(-\beta\hat{H})_{\mathrm{W}}(\mathbf{z})$ is $\exp[-\beta\hat{H}_{\mathrm{W}}(\mathbf{z})]$, where the Wigner transform of the quantum Hamiltonian $\hat{H}_{\mathrm{W}}(\mathbf{z})$ is simply the classical Hamiltonian, which is denoted by $H(\mathbf{z})$. (There are corrections to this if the Hamiltonian is not of the kinetic plus potential form.) The inverse Laplace transform of this expression yields the leading-order smooth term (1.2).

For two independent particles, the full quantum Hamiltonian is the sum of one-particle Hamiltonians and since these are functions of independent phase space variables,

$$\exp(-\beta\hat{H})_{\mathrm{W}}(\mathbf{z}) = \exp(-\beta\hat{h})_{\mathrm{W}}(\mathbf{z}_a)\exp(-\beta\hat{h})_{\mathrm{W}}(\mathbf{z}_b). \tag{A.4}$$

Thus, the smoothed two-particle partition function is simply the product of smooth one-particle partition functions. By the Laplace convolution theorem, this implies that the smoothed two-particle density of states is the autoconvolution of the smoothed one-particle density of states. This same argument can be made for the exact density of states as an alternate proof of Eq. (3.5).

A.2 Symmetrization of a Two-Body System

The bosonic and fermionic partition functions are $Z_{\pm}(\beta) = \mathrm{Tr}(\hat{P}_{\pm}\exp(-\beta\hat{H}))$, where $\hat{P}_{\pm}$ are the projection operators defined in Eq. (4.1). The leading-order term is just the two-particle partition function. The next term $\mathrm{Tr}(\hat{U}\exp(-\beta\hat{H}))$ requires slightly more analysis and can be evaluated directly using Eq. (A.3). We begin by finding $\hat{U}_{\mathrm{W}}(\mathbf{z})$.

It is shown in Ref. [98] that for a one-particle system with a symmetry axis through the coordinate $\mathbf{q}$, the Wigner transform of the reflection operator is

$$\left(\hat{\mathcal{R}}\right)_{\mathrm{W}}(\mathbf{z}) = \pi\hbar\delta(\mathbf{q})\delta(\mathbf{p}), \tag{A.5}$$

where $\mathbf{p}$ is the momentum conjugate to $\mathbf{q}$. We map the present problem onto the reflection problem as follows. First, suppose that the one-particle system is one-dimensional and define the Jacobi coordinates: $q = (q_a - q_b)$, $p = (p_a - p_b)/2$, $Q = (q_a + q_b)/2$, and $P = (p_a + p_b)$. Then, exchanging a and b is equivalent to reflecting in q so that the variable q in the above equation is replaced by $(q_a - q_b)$ and p is replaced by the conjugate momentum $(p_a - p_b)/2$. Then, $\hat{U}_{\mathrm{W}}(\mathbf{z}) = 2\pi\hbar\delta(q_a - q_b)\delta(p_a - p_b)$. If the one-particle system is higher dimensional, then $\hat{U}$ is the product of one such inversion in every component. All of them are independent

so that the final result is the product of the individual ones (for the same reason that Eq. (A.4) is multiplicative). The final result is

$$\hat{U}_{\rm W}(\mathbf{z}) = (2\pi\hbar)^d \delta(\mathbf{z}_a - \mathbf{z}_b), \tag{A.6}$$

where the δ function represents the product of all $2d$ δ functions (two for each component). Equivalent results can be found in Ref. [106]. Then,

$$\begin{aligned} \mathrm{Tr}\left(\hat{U}\exp\left(-\beta\hat{H}\right)\right) &= \frac{1}{(2\pi\hbar)^{2d}}\int \hat{U}_{\rm W}(\mathbf{z})\exp\left(-\beta\hat{H}\right)_{\rm W}(\mathbf{z})\mathrm{d}\mathbf{z} \\ &= \frac{1}{(2\pi\hbar)^{d}}\int \exp\left(-2\beta\hat{h}\right)_{\rm W}(\mathbf{z}_a)\mathrm{d}\mathbf{z}_a, \end{aligned} \tag{A.7}$$

where we used the δ functions from $\hat{U}_{\rm W}(\mathbf{z})$ in Eq. (A.6) to do the integrals over the $\mathbf{z}_b$ variables and the multiplicative property of the Wigner functions as in Eq. (A.4). The first few terms of Eq. (A.7) give the smooth approximation to the one-particle partition function evaluated at 2β. Under the inverse Laplace transform, this becomes $\bar{\rho}_1(E/2)/2$ and we conclude

$$\bar{\rho}_{\pm}(E) = \frac{1}{2}\left[\bar{\rho}_2(E) \pm \frac{1}{2}\bar{\rho}_1\left(\frac{E}{2}\right)\right], \tag{A.8}$$

consistent with Eq. (4.4).

A.3 Symmetrization of a Many-Body System

We now discuss the smooth contribution to $\mathrm{Tr}(\hat{U}_\tau\hat{G})$ and we shall evaluate it using Wigner transforms as in Appendix A.2. We need to determine the smooth approximation to the symmetric (antisymmetric) partition function

$$\begin{aligned} Z_{\pm}(\beta) &= \mathrm{Tr}\left(\hat{P}_{\pm}\exp(-\beta\hat{H})\right) \\ &= \frac{1}{N!}\sum_{\tau}(\pm 1)^{s_\tau}\mathrm{Tr}\left(\hat{U}_\tau\exp(-\beta\hat{H})\right) \\ &= \frac{1}{N!}\sum_{\tau}(\pm 1)^{s_\tau}\frac{1}{(2\pi\hbar)^{Nd}}\int (\hat{U}_\tau)_{\rm W}(\mathbf{z})\Big[\exp(-\beta\hat{H})\Big]_{\rm W}(\mathbf{z})\mathrm{d}\mathbf{z}. \end{aligned} \tag{A.9}$$

Since each group element can be decomposed into independent cycles,

$$(\hat{U}_\tau)_{\rm W}(\mathbf{z}) = \prod_{\mathbb{k}} f_{\mathbb{k}}(\mathbf{z}_{\mathbb{k}}), \tag{A.10}$$

where $\mathbb{k}$ indicates the different cycles comprising the group element τ, $f_{\mathbb{k}}$ is a function discussed below, and $\mathbf{z}_{\mathbb{k}}$ denotes the phase space coordinates of the $n_{\mathbb{k}}$ particles being

permuted by these cycles. (For each group element, the unique decomposition into cycles also provides a unique decomposition of the phase space into the subspaces corresponding to the cycles.) The function $f_{\mathbb{k}}$ can be specified without loss of generality by choosing to label the particles being permuted by the cycle as $1, 2, \ldots, n_{\mathbb{k}}$ (i.e. $1 \to 2$, $2 \to 3$, $\ldots, n_{\mathbb{k}} \to 1$) and to leading order in $\hbar$ [106, 98],

$$f_{\mathbb{k}}(\mathbf{z}_{\mathbb{k}}) \approx (2\pi\hbar)^{(n_{\mathbb{k}}-1)d}\delta(\mathbf{z}_1 - \mathbf{z}_2)\delta(\mathbf{z}_2 - \mathbf{z}_3)\cdots\delta(\mathbf{z}_{n_{\mathbb{k}}-1} - \mathbf{z}_{n_{\mathbb{k}}}). \tag{A.11}$$

The first group element of the sum in Eq. (A.9) is the identity element for which the decomposition is into cycles where each particle is in a cycle by itself so that all of the $f_{\mathbb{k}}$ are identically unity. Integrating the smooth approximation to the Wigner function of $e^{-\beta\hat{H}}$ yields the smooth N-particle partition function. Using the generalization of property (A.4), we observe that the leading-order term of $\bar{Z}_{\pm}(\beta)$ is just the Nth power of the single-particle smooth partition function $\bar{Z}_1(\beta)^N$ and under the inverse Laplace transform, this is just the $(N-1)$-fold convolution integral of the single-particle smooth density of states. The prefactor of $1/N!$ comes from the projection operator (4.9) and we conclude that the identity term is $O(1/N!\hbar^{Nd})$. The first correction will come from group elements that consist of one 2-cycle and $(N-2)$ 1-cycles. The contribution from this class will have the form $\bar{Z}_1(\beta)^{N-2}\bar{Z}_1(2\beta)$. Compared to the leading-order term, this class contributes to the density of states with relative order $O(N\hbar^d/2)$. The factor of N is due to the fact that this class has $N(N-1)/2$ members and these all contribute identically. The factor of 2 comes from the inverse Laplace transform since the argument of one of the single-particle partition functions is 2β. The general structure then emerges. For an arbitrary group element, the contribution to the smooth partition function is $\prod_{\mathbb{k}} \bar{Z}_1(n_{\mathbb{k}}\beta)$. It contributes to the smooth density of states with relative order $O(\hbar^{(N-n_\tau)d}w_\tau)$, where n_τ is the number of independent cycles in the decomposition of τ. The factor w_τ is the size of the class (a combinatoric factor which can be found from Eq. (1-27) of Ref. [97]) divided by a factor arising from the inverse Laplace transform, which equals $\prod_{\mathbb{k}} n_{\mathbb{k}}$.

As a formal expansion in powers of $\hbar$, this may be inconsistent since some of the neglected corrections from the first few group elements may be of more significant order than the leading-order contributions of later group elements. However, for large N, we could easily imagine that the combinatoric factor w_τ offsets this effect. Keeping the leading-order $\hbar$ term of all the group elements then guarantees that we have a good approximation regardless of the relative sizes of $1/\hbar$ and N.

Appendix B

Stability Matrix Identities

B.1 Monodromy Matrix of a Harmonic Oscillator

For heterogeneous orbits in smooth potentials, the stationary particle resides at an equilibrium point of the potential and its perturbed motion is harmonic. In the neighborhood of a minimum, the potential is like a stable harmonic oscillator $m/2(\omega_x^2 x^2 + \omega_y^2 y^2)$ for which Hamilton's equations can be written in matrix form as

$$\begin{pmatrix} \dot{x} \\ \dot{p_x} \\ \dot{y} \\ \dot{p_y} \end{pmatrix} = \begin{pmatrix} 0 & 1/m & & \\ -m\omega_x^2 & 0 & \mathbf{0} & \\ & & 0 & 1/m \\ \mathbf{0} & & -m\omega_y^2 & 0 \end{pmatrix} \begin{pmatrix} x \\ p_x \\ y \\ p_y \end{pmatrix}. \tag{B.1}$$

Let A_x and A_y denote the 2×2 matrix blocks of the x and y motions, respectively. Then, the fundamental matrix of this linear system is given by

$$F(t) = \begin{pmatrix} \exp(A_x t) & \mathbf{0} \\ \mathbf{0} & \exp(A_y t) \end{pmatrix} = \begin{pmatrix} X(t) & \mathbf{0} \\ \mathbf{0} & Y(t) \end{pmatrix}, \tag{B.2}$$

where

$$X(t) = \begin{pmatrix} \cos(\omega_x t) & \frac{1}{m\omega_x}\sin(\omega_x t) \\ -m\omega_x \sin(\omega_x t) & \cos(\omega_x t) \end{pmatrix}, \tag{B.3}$$

and similarly for $Y(t)$, where $x \to y$. The monodromy matrix is obtained by evaluating the fundamental matrix $F(t)$ at the period. There are *two* fundamental periods, one for each harmonic motion: $T_{x/y} = \frac{2\pi}{\omega_{x/y}}$. The monodromy and stability matrices are $M_{x/y}$ and $\tilde{M}_{x/y}$, respectively, where

$$M_x = F\left(T_x\right) = \begin{pmatrix} I & \mathbf{0} \\ \mathbf{0} & \tilde{M}_x \end{pmatrix} = \begin{pmatrix} I & \mathbf{0} \\ \mathbf{0} & Y(T_x) \end{pmatrix}, \tag{B.4a}$$

$$M_y = F(T_y) = \begin{pmatrix} \tilde{M}_y & \mathbf{0} \\ \mathbf{0} & I \end{pmatrix} = \begin{pmatrix} X(T_y) & \mathbf{0} \\ \mathbf{0} & I \end{pmatrix}. \tag{B.4b}$$

Near a saddle point, the potential is like an unstable harmonic oscillator $m/2(\omega_x^2 x^2 - \omega_y^2 y^2)$. In this case, $X(t)$ is unchanged, but, the trigonometric functions in $Y(t)$ are replaced by hyperbolic functions and there is no minus sign in the lower left matrix element.

The important result is that the stability matrix for a primitive orbit *along* the x-axis is

$$\tilde{M}_x = \begin{pmatrix} \cos(\omega_y T_x) & \frac{1}{m\omega_y}\sin(\omega_y T_x) \\ -m\omega_y \sin(\omega_y T_x) & \cos(\omega_y T_x) \end{pmatrix}, \tag{B.5}$$

where ω_y is the frequency of the *transverse* y-motion and $T_x = 2\pi/\omega_x$ is the period of the x-motion. It is straightforward to show that $\sqrt{|\det(\tilde{M}_x - I)|} = 2\sin(\omega_y T_x/2)$. In higher dimensions, the monodromy matrix is simply block diagonal so that $\sqrt{|\det(\tilde{M}_x - I)|} = \prod_j 2\sin(\omega_j T_x/2)$, where the product is over directions other than x.

B.2 Monodromy Matrix of a Heterogeneous Orbit

For the analysis of heterogeneous orbits, we require the stability of a harmonic oscillator (the perturbed motion of the stationary particle a), which evolves for some fixed amount of time T_γ (the period of the orbit γ on which particle b evolves). This period is not related to the harmonic frequencies associated with potential extrema.

The only role played by the x variable above was to specify the time of evolution in the arguments of the sinusoids. It was not important that it be a harmonic motion, it is enough that it be periodic. These results apply for *any* periodic orbit γ with period T_γ as long as the *transverse* motion is harmonic. This exactly describes a heterogeneous orbit and justifies the amplitude factor in the denominator of Eq. (3.15) for $d = 1$. In higher dimensions, the stability is given by both the one-particle monodromy matrix of the evolving particle (M_γ) and the one-particle monodromy matrix for the harmonic motion of the stationary particle about its potential minimum (M_a) (Each of the these is a $2d \times 2d$ matrix). But, these motions are uncoupled and so are simply multiplicative in their

combined contribution to the amplitude:

$$M_\Gamma = \begin{pmatrix} M_a & \mathbf{0} \\ \mathbf{0} & M_\gamma \end{pmatrix} = \begin{pmatrix} M_a & \mathbf{0} \\ \mathbf{0} & \begin{pmatrix} I_2 & \mathbf{0} \\ \mathbf{0} & \tilde{M}_\gamma \end{pmatrix} \end{pmatrix}, \tag{B.6}$$

where $\tilde{M}_\Gamma$ is the $(4d-2)\times(4d-2)$ stability matrix of the full heterogeneous orbit, M_a is the $2d\times 2d$ stability matrix of particle a and $\tilde{M}_\gamma$ is the $(2d-2)\times(2d-2)$ stability matrix of particle b on γ. Hence, $\det(\tilde{M}_\Gamma - I) = \det(M_a - I)\det(\tilde{M}_\gamma - I)$. For example, if $d=2$, then

$$\begin{aligned} \det(M_a - I) &= \det\left[X(T_\gamma) - I\right]\det\left[Y(T_\gamma) - I\right] \\ &= \left[4\sin^2(\omega_x T_\gamma/2)\right]\left[4\sin^2(\omega_y T_\gamma/2)\right]. \end{aligned} \tag{B.7}$$

If there is a local maximum in one of the directions, this corresponds to the case of an unstable harmonic oscillator. Suppose the maximum is along the y-axis with a harmonic frequency ω_y. Then,

$$\begin{aligned} \det(M_a - I) &= \det\left[X(T_\gamma) - I\right]\det\left[Y(T_\gamma) - I\right] \\ &= \left[4\sin^2(\omega_x T_\gamma/2)\right]\left[4\sinh^2(\omega_y T_\gamma/2)\right]. \end{aligned} \tag{B.8}$$

B.3 Phase Index of a Heterogeneous Orbit

The phase factor can be determined in an analogous manner from the exact harmonic oscillator trace formula. The phase index is 3 for a primitive orbit of a stable harmonic oscillator. A factor of 2 arises from the two turning points experienced by the orbit in traversing its motion independent of the harmonic motion transverse to the orbit. The remaining factor of 1 can be attributed to the transverse harmonic motion and is related to the sign of the determinant of the monodromy matrix. For heterogeneous orbits, this means that we should simply include a phase factor of $-\pi/2$ for a transverse harmonic motion in addition to any phase factors that arise from the one-particle motion associated with the periodic orbit γ. In higher dimensions, each transverse direction is independent and the phase index is additive. This accounts for the phase factor of $-d\pi/2$ in Eq. (3.15). The fact that all transverse harmonic directions are decoupled from each other as well as from the one-particle dynamics transverse to the periodic orbit γ allows us to simply multiply the amplitudes and add the phase factors.

Finally, if the equilibrium point of the potential is a local maximum in one of the directions (the case of an unstable harmonic oscillator), then its phase index is trivially zero since an unstable periodic orbit on a ridge introduces no caustics in phase space. This fact is also consistent with the trace formula for an unstable harmonic oscillator (see Ref. [7]). In higher dimensions with a mixture of stable and unstable directions, we continue to multiply the amplitude factors and add the phase indices of the separate directions. This fully accounts for the modifications described immediately below Eq. (3.16).

B.4 Stability Matrix of Pseudoperiodic Orbits

We first prove that $\det(\tilde{M}_{\gamma'} - I) = 4\det(\tilde{M}_\gamma - I)$, where $\tilde{M}_{\gamma'}$ is the stability matrix of a pseudoperiodic orbit γ' of the full two-particle phase space and $\tilde{M}_\gamma$ is the stability matrix of the corresponding periodic orbit γ in the one-particle phase space. This admits various generalizations which are used in the main discussion. We shall focus on the type-1 DPPO, but the type-0 DPPO can be similarly analyzed. The (type-1) dynamical pseudoperiodic orbit (DPPO) consists of both particles evolving for half of the single-particle period $T_\gamma/2$ followed by the symplectic mapping u that exchanges the two particles.

The coordinates are defined as follows (see Fig. B.1). For particle a, an initial section Σ_a is defined such that the phase space flow is transverse to it and all points on the section are at equal energy. Another coordinate is defined pointing along the orbit η_a. Without loss of generality, we can take $\partial\eta_a/\partial t \equiv 1$. A coordinate κ_a can also be defined that is transverse to the constant h_a surface (but in the phase space of particle a). If this coordinate takes the values of h_a, then it is canonically conjugate to η_a and has zero time derivative under the flow since h_a is conserved. The remaining $(2d-2)$ coordinates for particle a lie on the section Σ_a and will be collectively denoted by ξ_a. As the flow evolves, changes in the ξ_a coordinates are described by the $(2d-2)\times(2d-2)$ symplectic stability matrix (for the one-particle dynamics) $\tilde{N}_a$. Similarly, we define Σ_b, η_b, κ_b, ξ_b, and $\tilde{N}_b$ for particle b. The coordinates on Σ_a are connected by parallel transport to those on Σ_b so that, for example, the stable and unstable manifolds are mapped onto each other.

We start by defining the symplectic transformation

$$\begin{aligned} \eta &= \frac{\eta_a + \eta_b}{2}, \qquad & \kappa &= \kappa_a + \kappa_b, \\ \upsilon &= \eta_a - \eta_b, \qquad & \zeta &= \frac{\kappa_a - \kappa_b}{2}. \end{aligned} \tag{B.9}$$

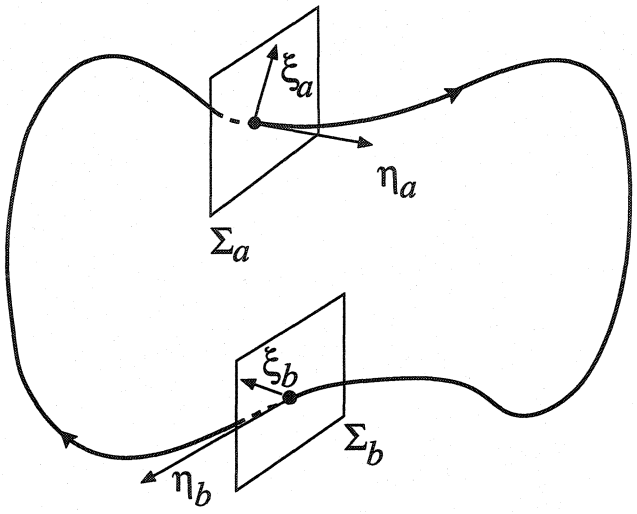

Figure B.1: The coordinates of particles a and b on a (type-1) dynamical pseudoperiodic orbit γ' of the full phase space (which can be mapped one-to-one to an orbit γ of the one-particle phase space). Σ_a denotes an initial section for particle a, η_a is the coordinate along the orbit (the coordinate transverse to the h_a surface denoted by κ_a is not shown) and ξ_a are the $(2d-2)$ remaining coordinates for particle a which lie on Σ_a. (All points on Σ_a are at equal energy.) Similarly, for particle b.

The monodromy matrix $M_{\gamma'}$ describes the linearized motion of small perturbations around a DPPO γ' of the full phase space. In particular, if $\boldsymbol{\Upsilon} = (\kappa, \eta, \upsilon, \zeta, \xi_a, \xi_b)$, then $\delta\boldsymbol{\Upsilon} = M_{\gamma'}\delta\boldsymbol{\Upsilon}_0$. Consider an initial slight change in η by the amount $\delta\eta_0$ while keeping all other coordinates constant. This implies that both η_a and η_b increase by $\delta\eta_0$. After time evolution for $T_\gamma/2$ and particle exchange, $\delta\eta = \delta\eta_0$ while all other coordinates are unchanged (in particular, the transverse coordinates are unaffected). Now consider an initial small change in κ by the amount $\delta\kappa_0$. This implies that κ_a and κ_b change by $\delta\kappa_0/2$. After integrating for time $T_\gamma/2$ and interchanging the particles, we observe that $\delta\kappa = \delta\kappa_0$. However, this change of value in κ does affect the η coordinate. Under this change, the period of the orbit γ also changes; let T'_γ denote the derivative of this period with respect to the single-particle energy. Since we are only integrating for half of the period, and the single-particle energies are changed by $\delta\kappa_0/2$, we find that $\delta\eta = -T'_\gamma\delta\kappa_0/4$. (The minus sign indicates that if the period increases and we integrate for the same amount of time as before, then the particles will fail to execute a complete loop, corresponding to a negative value of η.) Thus, the

monodromy matrix of the pseudoperiodic orbit γ' in the full phase space has the form

$$M_{\gamma'} = \begin{pmatrix} \begin{pmatrix} 1 & 0 \\ -\frac{T'_\gamma}{4} & 1 \end{pmatrix} & \mathbf{0} \\ \mathbf{0} & \tilde{M}_{\gamma'} \end{pmatrix}. \tag{B.10}$$

We are interested in calculating $\det(\tilde{M}_{\gamma'} - I)$ to evaluate the Gutzwiller amplitude. Note that the matrix $\tilde{M}_{\gamma'}$ involves only the $(4d-2)$ phase space coordinates other than η and κ. We can understand the calculation up to now as follows. The transformation (B.9) can be thought of as a transformation to center-of-mass coordinates. We have removed the center-of-mass coordinates η and κ from consideration, and are only left with the relative coordinates υ and ζ (as well as all the transverse coordinates ξ_a and ξ_b.) It is reasonable that only the relative coordinates are important for determining the stability.

The next two coordinates we consider are υ and ζ. Let us start with υ. A small initial change in υ by the amount $\delta\upsilon_0$ implies that η_a changes by $\delta\upsilon_0/2$ while η_b changes by $-\delta\upsilon_0/2$. After integrating for time $T_\gamma/2$, this remains unchanged, but after particle exchange, the final values of $\delta\eta_a$ and $\delta\eta_b$ are changed in sign so that the corresponding diagonal matrix element of $\tilde{M}_{\gamma'}$ is -1. Similarly, the diagonal matrix element corresponding to the ζ coordinate is also -1. As before, an infinitesimal change in ζ implies an infinitesimal change in υ. In this case, the corresponding matrix element is T'_γ. Therefore, we can write

$$\tilde{M}_{\gamma'} = \begin{pmatrix} \begin{pmatrix} -1 & 0 \\ T'_\gamma & -1 \end{pmatrix} & \mathbf{0} \\ \mathbf{0} & \tilde{N} \end{pmatrix}. \tag{B.11}$$

Then, $\det(\tilde{M}_{\gamma'} - I) = 4\det(\tilde{N} - I)$, where we use appropriately dimensioned identity matrices on each side of the equality. It remains to calculate the determinant of the $(4d-4)\times(4d-4)$ matrix $\tilde{N} - I$. The matrix $\tilde{N}$ involves only the coordinates ξ_a and ξ_b. Since these two sets of coordinates live on different sections, we cannot immediately define a mapping between them. To do so, note that we have defined coordinates on the two sections so that the exchange operation is a simple mapping of the form

$$\tilde{E} = \begin{pmatrix} \mathbf{0} & I \\ I & \mathbf{0} \end{pmatrix}, \tag{B.12}$$

where I is a $(2d-2)\times(2d-2)$ identity matrix. In terms of these coordinates, the one-particle stability matrices $\tilde{N}_a$ and $\tilde{N}_b$ are such that $\tilde{N}_a\tilde{N}_b = \tilde{M}_\gamma$, which is the stability matrix of

the full periodic orbit for the one-particle dynamics. The combined operations of flow and exchange give

$$\tilde{N} = \begin{pmatrix} \mathbf{0} & \tilde{N}_b \\ \tilde{N}_a & \mathbf{0} \end{pmatrix} \tag{B.13}$$

and

$$\det(\tilde{N} - I) = \det \begin{pmatrix} -I & \tilde{N}_b \\ \tilde{N}_a & -I \end{pmatrix} = \det \begin{pmatrix} \tilde{N}_a & -I \\ -I & \tilde{N}_b \end{pmatrix} = \det(\tilde{M}_\gamma - I), \tag{B.14}$$

where after the second equality, we interchanged rows to put the matrix into a more useful form. (The matrix has even dimension so there is no sign introduced as a result of this interchange.) The final equality of Eq. (B.14) requires the following identity. If a matrix C has the form

$$C = \begin{pmatrix} A & -I \\ -I & B \end{pmatrix}, \tag{B.15}$$

then $\det(C) = \det(AB - I)$. This can be shown by multiplying C by the matrix

$$C' = \begin{pmatrix} B & I \\ I & A \end{pmatrix}. \tag{B.16}$$

After multiplying them together, the product is block-diagonal with $(AB - I)$ in one block and $(BA - I)$ in the other. These have equal determinants. Since C' has the same determinant as C, it follows that $[\det(C)]^2 = [\det(AB - I)]^2$ and thus we have identified the two determinants within a sign. The sign follows from the fact that the contribution to the determinant of the fully diagonal term $\prod A_{ii}B_{ii}$ should be positive. Thus, we conclude that $\det(\tilde{M}_{\gamma'} - I) = 4\det(\tilde{M}_\gamma - I)$.

It is a straightforward extension to generalize this result to a cycle with n particles on an orbit. We first have to find some appropriate set of variables so that an upper-left block of the monodromy matrix can be separated out in analogy to Eq. (B.11). This comes from the $2n$ coordinates η and κ. As in the previous case, we separate the variables into center-of-mass coordinates (which subsequently play no role) and a set of relative (Jacobi) coordinates. Using similar arguments to the $n = 2$ case, the determinant of the upper-left block is then n^2. The contribution from the rest of the matrix (i.e. the lower-right block) comes from the transverse coordinates. In terms of these transverse coordinates, the single-particle stability matrices $\tilde{N}_a, \tilde{N}_b, \ldots, \tilde{N}_n$ are such that $\tilde{N}_a\tilde{N}_b \cdots \tilde{N}_n = \tilde{M}_\gamma$, which

is the stability matrix of the full periodic orbit for the one-particle dynamics. Through a sequence of manipulations and transpositions similar to the $n = 2$ case, the determinant of this lower-right block (i.e. $\det(\tilde{N} - I)$) can then be reduced to the form

$$\det \begin{pmatrix} \tilde{N}_a & -I & 0 & \cdots & 0 & 0 \\ 0 & \tilde{N}_b & -I & \cdots & 0 & 0 \\ \vdots & \vdots & \vdots & \ddots & \vdots & \vdots \\ 0 & 0 & 0 & \cdots & \tilde{N}_{n-1} & -I \\ -I & 0 & 0 & \cdots & 0 & \tilde{N}_n \end{pmatrix}, \tag{B.17}$$

which is a generalization of the $n = 2$ case. It can be shown that $\det(\tilde{N} - I) = \det(\tilde{M}_\gamma - I)$ and thus, $\det(\tilde{M}_{\gamma'} - I) = n^2 \det(\tilde{M}_\gamma - I)$. If the orbit is not primitive, but is a repetition of some simpler orbit, then we can absorb this into the definitions of the single-particle stability matrices and carry through all of the manipulations as before. The result is unchanged.

Appendix C

Convolution Formalism

C.1 Nonidentical Particles in a 1D Harmonic Oscillator

If the single-particle density is decomposed into its smooth and oscillatory components as in Eq. (1.1), this gives a decomposition of the two-particle density of states into four distinct contributions,

$$\rho_2(E) = \bar{\rho}_{1a} * \bar{\rho}_{1b}(E) + \bar{\rho}_{1a} * \tilde{\rho}_{1b}(E) + \tilde{\rho}_{1a} * \bar{\rho}_{1b}(E) + \tilde{\rho}_{1a} * \tilde{\rho}_{1b}(E), \tag{C.1}$$

where the indices a and b refer to the two distinct particles and the indices 1 and 2 still refer to one- or two-particle densities of states. Each convolution integral can be calculated asymptotically in the case where the periods and actions are not known analytically since we can then use the general trace formula in the integrand [35]. However, if all the classical properties are known analytically as a function of energy, an equivalent approach is to do the convolution integrals exactly and then replace the resulting functions with their asymptotic values. Each term of Eq. (C.1) can be interpreted semiclassically as follows: the first term does not depend on dynamics and corresponds to the Weyl formula in the full two-particle space; the mixed terms depend only on one-particle dynamics and correspond to the situation where one particle is stationary and the other particle evolves dynamically on a periodic orbit; the last term (with only oscillating one-particle densities) involves two-particle dynamics and corresponds to the situation where both particles evolve dynamically on distinct periodic orbits. Thus, the mixed convolution terms and the unmixed oscillating term should reproduce the contributions from heterogeneous orbits and dynamical orbits, respectively. This is the generic connection and was demonstrated in Chapter 3. The purpose of this section is to show how this association fails for nonidentical particles in

a harmonic oscillator. The specific case of two nonidentical particles in a 1D harmonic oscillator where the particle masses are incommensurate is considered here[1].

It is instructive to first illustrate the generic scenario using a simple concrete example. Consider two nonidentical particles in a 1D infinite square well of length $\mathcal{L}$. The one-particle densities for the nonidentical particles a and b are given by

$$\rho_{1a/1b}(E) = \frac{1}{2\sqrt{E^0_{a/b}E}}\left[1 + 2\sum_{n_{a/b}=1}^{\infty}\cos\left(2\pi n_{a/b}\sqrt{\frac{E}{E^0_{a/b}}}\right)\right], \tag{C.2}$$

where the single-particle ground-state energies $E^0_{a/b} = \pi^2\hbar^2/2m_{a/b}\mathcal{L}^2$. The decomposition (C.1) is

$$\begin{aligned}\rho_{1a}(E) * \rho_{1b}(E) &= \int_0^E \rho_{1a}(\varepsilon)\rho_{1b}(E-\varepsilon)\mathrm{d}\varepsilon \\ &= \frac{1}{4\sqrt{E^0_a E^0_b}}\left[\pi + 2\sum_{n_b=1}^{\infty}\int_0^E \frac{1}{\sqrt{\varepsilon(E-\varepsilon)}}\cos\left(2\pi n_b\sqrt{\frac{\varepsilon}{E^0_b}}\right)\mathrm{d}\varepsilon + \{b\to a\}\right. \\ &\left. + 4\sum_{n_a=1}^{\infty}\sum_{n_b=1}^{\infty}\int_0^E \frac{1}{\sqrt{\varepsilon(E-\varepsilon)}}\cos\left(2\pi n_a\sqrt{\frac{\varepsilon}{E^0_a}}\right)\cos\left(2\pi n_b\sqrt{\frac{(E-\varepsilon)}{E^0_b}}\right)\mathrm{d}\varepsilon\right].\end{aligned} \tag{C.3}$$

All convolution integrals can be evaluated analytically after a change of variable to $u = \sqrt{E-\varepsilon}$ (the details will be omitted here). The final result is

$$\begin{aligned}\rho_2(E) = \frac{\pi}{4\sqrt{E^0_a E^0_b}}&\left[1 + 2\sum_{n_b=1}^{\infty} J_0\left(2\pi n_b\sqrt{\frac{E}{E^0_b}}\right) + \{b\to a\}\right. \\ &\left. + 4\sum_{n_a=1}^{\infty}\sum_{n_b=1}^{\infty} J_0\left(2\pi\sqrt{\left[\frac{n_a^2}{E^0_a} + \frac{n_b^2}{E^0_b}\right]E}\right)\right].\end{aligned} \tag{C.4}$$

If the zero-order Bessel function $J_0(x)$ is replaced by its asymptotic value[2], then the semiclassical approximation to the two-particle density of states $\rho_2^{\mathrm{sc}}(E)$ is obtained. The mixed terms and the unmixed term then reproduce the contributions from the heterogeneous and dynamical orbits, respectively, and therefore the correspondence is as described in Chapter 3. In general, it is possible that the asymptotic values of the oscillatory terms involve nonsinusoidal functions of E (for example, see Appendix B of Ref. [35]). Such contributions have

[1] The situation where the masses are commensurate could also be analyzed, but the full phase analysis considered in Chapter 3 is not applicable since this system has a non-Abelian $SU(2)$ symmetry. See also the comments on harmonic oscillator potentials in Chapter 6.

[2] $J_0(x) \sim \sqrt{2/\pi x}\,\cos(x-\pi/4)$

the same asymptotic structure as $\bar{\rho}_{1a} * \bar{\rho}_{1b}(E)$. However, the smooth term $\bar{\rho}_{1a} * \bar{\rho}_{1b}(E)$ itself already completely describes the average behavior of the two-particle density of states and so any smooth contributions arising from the oscillatory terms should be regarded as spurious. It is also possible that the asymptotic evaluation of the unmixed convolution integral gives some contributions that are sinusoidal functions of E, but depend on properties of only *one* of the orbits (and therefore depend only on one-particle dynamics). These contributions have the same asymptotic structure as $\bar{\rho}_{1a} * \tilde{\rho}_{1b}(E) + \tilde{\rho}_{1a} * \bar{\rho}_{1b}(E)$. However, the mixed terms alone give all contributions that arise from one-particle dynamics and any further contributions with the same structure should also be regarded as spurious. As mentioned above, evaluating the integrals exactly and then replacing the resulting functions with their asymptotic values is equivalent to a direct asymptotic analysis of the convolution integrals [35]. An endpoint analysis of the mixed convolution integrals ignoring the endpoint contribution that corresponds to using the trace formula at zero energy gives all contributions associated with one-particle dynamics. A stationary phase analysis of the unmixed convolution integral yields the only contribution associated with two-particle dynamics. We could also do a local asymptotic calculation for each of the endpoints of the unmixed convolution integral, but the same spurious structure described above emerges.

Using this correspondence between the convolution and full phase space formalisms, we expect $\tilde{\rho}_{1a} * \tilde{\rho}_{1b}(E) = 0$, since there are no dynamical orbits[3]. The unmixed convolution integral has no stationary phase point so it will have the same structure as the mixed terms, but this contribution should be regarded as spurious since the mixed terms should already reproduce the contribution from the heterogeneous orbits. Thus, we expect $\tilde{\rho}_2(E) = \tilde{\rho}_2^{\mathrm{h}}(E) = \bar{\rho}_{1a} * \tilde{\rho}_{1b}(E) + \tilde{\rho}_{1a} * \bar{\rho}_{1b}(E)$. However, as shown below, $\tilde{\rho}_2(E)$ actually arises from a combination of the mixed and unmixed convolution integrals.

Consider two nonidentical particles in a one-dimensional harmonic oscillator. The one-particle densities for the nonidentical particles a and b are given by

$$\rho_{1a/1b}(E) = \frac{1}{\hbar\omega_{a/b}}\left[1 + 2\sum_{n_{a/b}=1}^{\infty}(-1)^{n_{a/b}}\cos\left(\frac{2\pi n_{a/b}E}{\hbar\omega_{a/b}}\right)\right]. \tag{C.5}$$

[3]The condition for a dynamical periodic orbit is $T_a(E_a) = T_b(E_b) \Longleftrightarrow \frac{n_a}{n_b} = \frac{\omega_a}{\omega_b}$. This condition can never be fulfilled since $\frac{n_a}{n_b} \in \mathbb{Q}$, whereas $\frac{\omega_a}{\omega_b} \notin \mathbb{Q}$. Hence, there are no globally periodic orbits that involve both particles evolving dynamically on distinct periodic orbits of the same period, regardless of how the total energy is partitioned between the two particles.

The decomposition (C.1) is

$$\begin{aligned}\rho_{1a}(E) * \rho_{1b}(E) &= \int_0^E \rho_{1a}(\varepsilon)\rho_{1b}(E-\varepsilon)\mathrm{d}\varepsilon \\ &= \frac{1}{\hbar^2\omega_a\omega_b}\left[E + 2\sum_{n_b=1}^{\infty}(-1)^{n_b}\int_0^E \cos\left(\frac{2\pi n_b\varepsilon}{\hbar\omega_b}\right)\mathrm{d}\varepsilon + \{b\to a\}\right. \\ &\left. + 4\sum_{n_a=1}^{\infty}\sum_{n_b=1}^{\infty}(-1)^{n_a+n_b}\int_0^E \cos\left(\frac{2\pi n_a\varepsilon}{\hbar\omega_a}\right)\cos\left(\frac{2\pi n_b(E-\varepsilon)}{\hbar\omega_b}\right)\mathrm{d}\varepsilon\right]. \qquad \text{(C.6)}\end{aligned}$$

The mixed convolution integrals can be evaluated immediately and are

$$\bar{\rho}_{1a} * \tilde{\rho}_{1b}(E) + \tilde{\rho}_{1a} * \bar{\rho}_{1b}(E) = \frac{1}{\pi\hbar\omega_a}\sum_{n_b=1}^{\infty}\frac{(-1)^{n_b}}{n_b}\sin\left(\frac{2\pi n_b E}{\hbar\omega_b}\right) + \{b\leftrightarrow a\}. \qquad \text{(C.7)}$$

The unmixed oscillating term is (after use of trigonometric identities and some algebra),

$$\begin{aligned}\tilde{\rho}_{1a} * \tilde{\rho}_{1b}(E) &= \frac{2}{\pi\hbar}\sum_{n_a=1}^{\infty}\sum_{n_b=1}^{\infty}(-1)^{n_a+n_b}\left(\frac{n_a\omega_b}{n_a^2\omega_b^2 - n_b^2\omega_a^2}\right)\sin\left(\frac{2\pi n_a E}{\hbar\omega_a}\right) + \{a\leftrightarrow b\} \\ &= \frac{2}{\pi\hbar\omega_a}\sum_{n_a=1}^{\infty}(-1)^{n_a}\sin\left(\frac{2\pi n_a E}{\hbar\omega_a}\right)\left[\sum_{n_b=1}^{\infty}\frac{(-1)^{n_b}\kappa_a}{\kappa_a^2 - n_b^2}\right] + \{a\leftrightarrow b\}, \qquad \text{(C.8)}\end{aligned}$$

where $\kappa_a = (\omega_b/\omega_a)n_a$. The quantity in square brackets is the series expansion[4] for $\csc(\pi\kappa_a)$:

$$\frac{\pi}{2}\left(2\pi\kappa_a\sum_{n_b=1}^{\infty}\frac{(-1)^{n_b}}{\pi^2\kappa_a^2 - n_b^2\pi^2}\right) = \frac{\pi}{2}\left(\frac{1}{\sin\left(n_a\pi\frac{\omega_b}{\omega_a}\right)} - \frac{1}{n_a\pi\frac{\omega_b}{\omega_a}}\right).$$

Note the restriction $\kappa_a \neq n_b \in \mathbb{N}$, which is satisfied since the particle masses are incommensurate. If the particle masses are commensurate $[(\frac{\omega_a}{\omega_b}) \in \mathbb{Q}]$, then the restriction is equivalent to $n_a \neq \ell\omega_a$, where $\ell \in \mathbb{N}$. Therefore,

$$\begin{aligned}\tilde{\rho}_{1a} * \tilde{\rho}_{1b}(E) &= \frac{1}{\hbar\omega_a}\sum_{n_a=1}^{\infty}\frac{(-1)^{n_a}\sin\left(\frac{2\pi n_a E}{\hbar\omega_a}\right)}{\sin\left(n_a\pi\frac{\omega_b}{\omega_a}\right)} - \tilde{\rho}_{1a} * \bar{\rho}_{1b}(E) \\ &+ \frac{1}{\hbar\omega_b}\sum_{n_b=1}^{\infty}\frac{(-1)^{n_b}\sin\left(\frac{2\pi n_b E}{\hbar\omega_b}\right)}{\sin\left(n_b\pi\frac{\omega_a}{\omega_b}\right)} - \bar{\rho}_{1a} * \tilde{\rho}_{1b}(E). \qquad \text{(C.9)}\end{aligned}$$

The mixed oscillating terms are exactly canceled and the final result is

$$\rho_2(E) = \frac{E}{\hbar^2\omega_a\omega_b} + \frac{1}{\hbar\omega_a}\sum_{n_a=1}^{\infty}\frac{(-1)^{n_a}\sin\left(\frac{2\pi n_a E}{\hbar\omega_a}\right)}{\sin\left(n_a\pi\frac{\omega_b}{\omega_a}\right)} + \frac{1}{\hbar\omega_b}\sum_{n_b=1}^{\infty}\frac{(-1)^{n_b}\sin\left(\frac{2\pi n_b E}{\hbar\omega_b}\right)}{\sin\left(n_b\pi\frac{\omega_a}{\omega_b}\right)}. \qquad \text{(C.10)}$$

[4] $2z\sum_{n=1}^{\infty}\frac{(-1)^n}{z^2-n^2\pi^2} = \frac{1}{\sin(z)} - \frac{1}{z}$, where $z \neq n\pi$.

Therefore, to summarize, $\tilde{\rho}_2(E) = \tilde{\rho}_2^{\rm h}(E) = \bar{\rho}_{1a} * \tilde{\rho}_{1b}(E) + \tilde{\rho}_{1a} * \bar{\rho}_{1b}(E) + \tilde{\rho}_{1a} * \tilde{\rho}_{1b}(E)$, contrary to the generic correspondence between the convolution and full phase space formalisms.

C.2 Heterogeneous Periodic Orbits in Smooth Potentials

We obtain the contribution from a single family of heterogeneous orbits [Eq. (3.15)] for the special case $d = 1$ using the convolution method. The convolution integral is given by

$$(\rho_{\rm h} * \tilde{\rho}_\gamma)(E) = \int_0^E \rho_{\rm h}(\varepsilon)\tilde{\rho}_\gamma(E-\varepsilon){\rm d}\varepsilon, \tag{C.11}$$

where we assume the motion about the potential minimum is locally harmonic with a frequency ω so that (see [7])

$$\rho_{\rm h}(\varepsilon) = \frac{1}{\hbar\omega}\sum_n (-1)^n e^{i2\pi n\varepsilon/\hbar\omega}. \tag{C.12}$$

Here, the sum is over all integers; the zero term in the sum being the Thomas-Fermi term. For the other term in the convolution integrand, we use the oscillating density of states [Eq. (1.5)] at finite energy $(E-\varepsilon)$. Then,

$$(\rho_{\rm h} * \tilde{\rho}_\gamma)(E) = \frac{i\hbar}{(\hbar\omega)(2\pi\hbar)}\sum_n (-1)^n \mathcal{I}_n(E), \tag{C.13}$$

where

$$\mathcal{I}_n(E) = \int_0^E A_\gamma(E-\varepsilon)e^{i2\pi n\varepsilon/\hbar\omega}\left[e^{i(S_\gamma(E-\varepsilon)/\hbar - \sigma_\gamma\pi/2)} + c.c.\right]{\rm d}\varepsilon. \tag{C.14}$$

Since we include only the lower endpoint contribution (the upper endpoint is spurious [45, 35]), we can use an expansion of $\tilde{\rho}_\gamma(E-\varepsilon)$ valid near $\varepsilon = 0$. Hence, to leading order, we may remove the amplitude factor from inside the integral, Taylor expand the argument of the exponential and extend the upper limit to infinity. Then,

$$\mathcal{I}_n(E) \approx A_\gamma(E)\int_0^\infty e^{i2\pi n\varepsilon/\hbar\omega}\left[e^{i(S_\gamma(E)/\hbar - \sigma_\gamma\pi/2)}e^{-iT_\gamma(E)\varepsilon/\hbar} + c.c.\right]{\rm d}\varepsilon, \tag{C.15}$$

where we have Taylor expanded the action and used

$$\left.\frac{{\rm d}S_\gamma(E-\varepsilon)}{{\rm d}\varepsilon}\right|_{\varepsilon=0} = -\left.T_\gamma(E-\varepsilon)\right|_{\varepsilon=0} = -T_\gamma(E). \tag{C.16}$$

If we combine the results for positive and negative n in Eq. (C.13), we can write

$$(\rho_{\rm h} * \tilde{\rho}_\gamma)(E) \approx \frac{i\hbar}{2\pi\hbar}A_\gamma(E)\cos\left(\frac{S_\gamma(E)}{\hbar} - \sigma_\gamma\frac{\pi}{2} - \frac{\pi}{2}\right)\left[\frac{1}{z} + 2z\sum_{n=1}^\infty (-1)^n\frac{1}{z^2-\pi^2n^2}\right], \tag{C.17}$$

where $z = \omega T_\gamma(E)/2$. We identify the quantity in square brackets as an expansion of $1/\sin(z)$ [108] so that

$$(\rho_{\rm h} * \tilde{\rho}_\gamma)(E) \approx \frac{1}{\pi\hbar}\frac{T_\gamma^0(E)}{2\sin(\omega T_\gamma(E)/2)}\cos\left(\frac{S_\gamma(E)}{\hbar} - \sigma_\gamma\frac{\pi}{2} - \frac{\pi}{2}\right). \tag{C.18}$$

This agrees with Eq. (3.15) for the special case $d = 1$. Note that this is just the contribution from the lower endpoint of the integral; stationary phase points are accounted for in Ref. [35]. We can also think of this term as actually arising from the combination of two distinct endpoint contributions from the $(\bar{\rho}_{\rm h} * \tilde{\rho}_\gamma)(E)$ integral and the $(\tilde{\rho}_{\rm h} * \tilde{\rho}_\gamma)(E)$ integral. Note that there is a factor of 2 in front of the mixed term in Eq. (3.8b) so that the contribution from heterogeneous orbits in the convolution picture comes with an additional factor of 2. This fact is implicit in Eq. (3.15) since either particle a or particle b can be stationary. This convolution analysis can be extended to more particles. For example, for $N = 3$, if we convolve the $\rho_{\rm h}$ of Eq. (C.12) with the $(\tilde{\rho}_{\gamma_a} * \tilde{\rho}_{\gamma_b})(E)$ term obtained from Eq. (3.14) or $\rho_{\rm h}$ with $(\rho_{\rm h} * \tilde{\rho}_\gamma)(E)$ of Eq. (C.18), this yields formulas consistent with the special cases $N = 3, M = 2$ of Eq. (3.26) and $N = 3, M = 1$ of Eq. (3.26), respectively. The extension to higher dimensions will be considered elsewhere.

C.3 Three-Particle Heterogeneous Orbits in Plane Billiards

In this thesis, the focus is on the leading-order contributions to the oscillatory part of the many-body density of states. (The oscillatory component is an asymptotic series in powers of $\hbar$.) For billiards, heterogeneous orbits generally occur in higher dimensional families than dynamical orbits, and the $\hbar$-corrections from the former are important. Consider the three-particle density of states

$$\rho_3(E) = \bar{\rho}_3(E) + \tilde{\rho}_3^{\rm h}(E) + \tilde{\rho}_3^{\rm d}(E). \tag{C.19}$$

The Thomas-Fermi term is $O(1/\hbar^6)$, and the leading-order contributions of the heterogeneous and dynamical terms are $O(1/\hbar^3)$ and $O(1/\hbar^2)$, respectively. Since the highest-order contribution (from the dynamical orbits) is $O(1/\hbar^2)$, we require the complete asymptotic series for $\bar{\rho}_3(E)$ and $\tilde{\rho}_3^{\rm h}(E)$ up to $O(1/\hbar^2)$. We now calculate the corrections for $\tilde{\rho}_3^{\rm h}(E)$ [up to $O(1/\hbar^{3/2})$] using the convolution formalism. The first few terms of the asymptotic series can be determined by convolving the Weyl expansion (1.3) term-by-term with a two-particle trace formula. As a formal expansion in powers of $\hbar$, this is inconsistent since corrections

to the one-particle trace formula (1.5) itself are excluded. However, the numerics indicate that corrections to the Gutzwiller trace formula are negligible for isolated periodic orbits in billiard systems, otherwise the quantum results could not be reproduced with the accuracy obtained above.

The contribution from the first type of heterogeneous orbit where one particle evolves while the others are stationary is calculated from

$$\tilde{\rho}_3^{\rm h1}(E) = \bar{\rho}_1(E) * (\bar{\rho}_1 * \tilde{\rho}_1)(E) = \int_0^E \bar{\rho}_1(\varepsilon)(\bar{\rho}_1 * \tilde{\rho}_1)(E-\varepsilon)\mathrm{d}\varepsilon. \tag{C.20}$$

After convolving Eq. (1.3) with the oscillatory function $(\bar{\rho}_1 * \tilde{\rho}_1)(E)$ (which has been calculated in Ref. [35]), we find that there are nine integrals to do, but three of these are trivial because of a δ function in the integrand. The remaining six integrals require careful analysis. As an example, we derive the asymptotic expansion of one integral. The others are calculated in the same manner, but the details will not be given here. The first correction to the leading-order result (3.32) comes from two terms; the first (second) is the convolution of the area (perimeter) term of $\bar{\rho}_1(E)$ with the perimeter (area) term of $(\bar{\rho}_1 * \tilde{\rho}_1)(E)$. The integral involved in the first term is

$$I_{\mathcal{AL}}(E) = \int_0^E (E-\varepsilon)^{-1/4} \cos\left(a\sqrt{E-\varepsilon}+b\right) \mathrm{d}\varepsilon, \tag{C.21}$$

where $a = \sqrt{\alpha}L_\gamma$ and $b = -\sigma_\gamma\pi/2 - \pi/4$. We want to perform a local analysis about $\varepsilon = 0$. The reason for this is that small ε corresponds physically to the situation where the stationary particles have little energy and most of the energy belongs to the dynamically evolving particle. For $\varepsilon \approx E$, it is the opposite situation, which does not make sense physically. We first make several changes of variable to simplify the calculation. A first change of variable $u = (E-\varepsilon)^{1/2}$ removes the square root in the argument of the sinusoid. Next, we need the Taylor series expansion about the point $u = \sqrt{E}$ and to facilitate this, we make a second change of variable $x = \sqrt{E} - u$. The integral then becomes

$$\begin{aligned} I_{\mathcal{AL}}(E) &= 2\int_0^{\sqrt{E}} (\sqrt{E}-x)^{1/2} \cos\left(a(\sqrt{E}-x)+b\right) \mathrm{d}x \\ &\approx 2\,\mathrm{Re}\left\{ e^{ia\sqrt{E}+b} \int_0^\infty (\sqrt{E}-x)^{1/2} e^{-iax}\mathrm{d}x \right\}. \end{aligned} \tag{C.22}$$

The integral $\int_0^{\sqrt{E}}(\cdots) = \int_0^\infty(\cdots) - \int_{\sqrt{E}}^\infty(\cdots)$; the second integral is an endpoint correction, but asymptotic in E, this correction is negligible. Thus, we are justified in replacing $\sqrt{E}$

by ∞ in the second line above. At this point, we obtain the Taylor expansion of $f(x) = (\sqrt{E}-x)^{1/2}$ about $x = 0$:

$$f(x) = E^{1/4} - \frac{1}{2}E^{-1/4}x - \frac{1}{8}E^{-3/4}x^2 + \ldots. \tag{C.23}$$

Since the final correction $[I_{\mathcal{KL}}(E)]$ in the expansion (C.20) is $O(E^{-1/4})$, it is only necessary to include terms in the Taylor series to $O(E^{-1/4})$. Thus,

$$\begin{aligned}\int_0^\infty (\sqrt{E}-x)^{1/2}e^{-iax}\mathrm{d}x &\approx E^{1/4}\int_0^\infty e^{-iax}\mathrm{d}x - \frac{1}{2}E^{-1/4}\int_0^\infty xe^{-iax}\mathrm{d}x \\ &= E^{1/4}\left(-\frac{i}{a}\right) - \frac{1}{2}E^{-1/4}\left(-\frac{1}{a^2}\right),\end{aligned} \tag{C.24}$$

(note that a has a small imaginary part for the integration) and asymptotically,

$$I_{\mathcal{AL}}(E) \sim \tfrac{2}{a}\left\{E^{1/4}\cos\left(a\sqrt{E}+b-\tfrac{\pi}{2}\right) + \tfrac{E^{-1/4}}{2a}\cos\left(a\sqrt{E}+b\right)\right\}. \tag{C.25}$$

An equivalent approach is to evaluate the integral exactly and then replace the resulting functions with their asymptotic forms. Evaluating the integral (C.21) at the upper limit using this method then corresponds to the situation where one of the stationary particles has all of the energy while the dynamically evolving particle has no energy. Physically, this does not make sense and this is evident mathematically since the contribution that comes from evaluating the integral at the upper endpoint is a smooth function of E and is therefore spurious in the sense discussed in Refs. [45, 35]. The result is only meaningful if we drop this smooth contribution. This is justified since we know that any smooth contribution to the density of states is already contained in the $\bar{\rho}_3(E)$ term. This is completely equivalent to what is done above [the spurious smooth contribution above is the endpoint correction that was dropped in the second line of Eq. (C.22)]. All six convolution integrals can be analyzed in this way. Collecting the contributions from all six integrals, the expansion up to $O(1/\hbar^{3/2})$ is

$$\begin{aligned}\tilde{\rho}_3^{\mathrm{h1}}(E) = \sum_\gamma \frac{L_\gamma^0}{\sqrt{\left|\det\left(\tilde{M}_\gamma - I\right)\right|}}\Bigg[&-\frac{\alpha^{3/2}\mathcal{A}^2E^{1/2}}{8\pi^3L_\gamma^2}\cos\left(\Phi\right) - \frac{\alpha^{5/4}\mathcal{AL}E^{1/4}}{8\sqrt{2}\pi^{5/2}L_\gamma^{3/2}}\cos\left(\Phi-\frac{3\pi}{4}\right) \\ &+ \frac{\alpha}{2\pi^2L_\gamma}\left(\frac{\mathcal{A}^2}{4\pi L_\gamma^2}+\frac{\mathcal{L}^2}{32}+\mathcal{AK}\right)\cos\left(\Phi-\frac{\pi}{2}\right) - \frac{\alpha^{3/4}\mathcal{L}E^{-1/4}}{8\sqrt{2}\pi^{3/2}L_\gamma^{1/2}}\left(\frac{3\mathcal{A}}{8\pi L_\gamma^2}+\mathcal{K}\right)\cos\left(\Phi-\frac{\pi}{4}\right)\Bigg],\end{aligned} \tag{C.26}$$

where $\Phi = \sqrt{\alpha E} L_\gamma - \sigma_\gamma \pi/2$. The contribution from the second type of heterogeneous orbit where one particle is stationary while the others evolve is calculated from

$$\tilde{\rho}_3^{\mathrm{h}2}(E) = \bar{\rho}_1(E) * (\tilde{\rho}_1 * \tilde{\rho}_1)(E) = \int_0^E \bar{\rho}_1(\varepsilon)(\tilde{\rho}_1 * \tilde{\rho}_1)(E-\varepsilon)\mathrm{d}\varepsilon. \tag{C.27}$$

After convolving Eq. (1.3) with the formula for $(\tilde{\rho}_1 * \tilde{\rho}_1)(E)$ (which has been calculated in Ref. [35] using stationary phase asymptotics), we find that there are only two convolution integrals that require analysis. These are evaluated asymptotically using the same technique as above. The final result [up to $O(1/\hbar^{3/2})$] is

$$\begin{aligned}\tilde{\rho}_3^{\mathrm{h}2}(E) = \sum_{\gamma_1,\gamma_2} \frac{L^0_{\gamma_1} L^0_{\gamma_2} \left(L^2_{\gamma_1} + L^2_{\gamma_2}\right)^{-1/4}}{\sqrt{\left|\det(\tilde{M}_{\gamma_1} - I)\right|}\sqrt{\left|\det(\tilde{M}_{\gamma_2} - I)\right|}} \Bigg[\frac{\alpha^{5/4}\mathcal{A}E^{1/4}}{(2\pi)^{5/2}L_{12}} \cos\left(\Phi_{12} - \frac{3\pi}{4}\right) \\ - \frac{\alpha\mathcal{L}}{16\pi^2 L_{12}^{1/2}} \cos\left(\Phi_{12} - \frac{\pi}{2}\right) + \frac{\alpha^{3/4}E^{-1/4}}{(2\pi)^{3/2}} \left(\frac{\mathcal{A}}{4\pi L_{12}^2} + \mathcal{K}\right) \cos\left(\Phi_{12} - \frac{\pi}{4}\right) \Bigg],\end{aligned} \tag{C.28}$$

where $L_{12} = \sqrt{L^2_{\gamma_1} + L^2_{\gamma_2}}$, $\sigma_{12} = \sigma_{\gamma_1} + \sigma_{\gamma_2}$, and $\Phi_{12} = \sqrt{\alpha E} L_{12} - \sigma_{12}\pi/2$.

Heterogeneous cycles

The higher-order contributions from heterocycles for the class of two-particle exchanges $(1,1,0)$ can be obtained from calculations similar to those found in Ref. [35]. It is shown there that the mixed convolution integral

$$\bar{\rho}_1(E) * \tilde{\rho}_1(E) = \tilde{\rho}_{\mathcal{A}}(E) + \tilde{\rho}_{\mathcal{L}}(E) + \tilde{\rho}_{\mathcal{K}}(E), \tag{C.29}$$

where for an isolated billiard orbit γ,

$$\tilde{\rho}_{\mathcal{A}}(E) = \frac{\alpha\mathcal{A}}{4\pi^2} \sum_\gamma \frac{C^0_\gamma}{L_\gamma} \cos\left(\Phi_\gamma - \frac{\pi}{2}\right), \tag{C.30a}$$

$$\tilde{\rho}_{\mathcal{L}}(E) = -\frac{\alpha^{3/4}\mathcal{L}}{4(2\pi)^{3/2}E^{1/4}} \sum_\gamma \frac{C^0_\gamma}{\sqrt{L_\gamma}} \cos\left(\Phi_\gamma - \frac{\pi}{4}\right), \tag{C.30b}$$

$$\tilde{\rho}_{\mathcal{K}}(E) = \frac{\sqrt{\alpha}\mathcal{K}}{2\pi\sqrt{E}} \sum_\gamma C^0_\gamma \cos\left(\Phi_\gamma\right), \tag{C.30c}$$

where $\Phi_\gamma = \sqrt{\alpha E} L_\gamma - \sigma_\gamma \pi/2$, and $C^0_\gamma = L^0_\gamma / \sqrt{|\det(\tilde{M}_\gamma - I)|}$. (Note that this is an expansion in powers of $\sqrt{\hbar}$.) The convolution calculation that lead to these results can be repeated

with appropriate changes of the energy arguments to give the heterocycle contributions. Using relations (C.30), the result can be written as

$$\tilde{\rho}^{\mathrm{h1}}_{(1,1,0)}(E) = \frac{1}{2}\bar{\rho}_1\left(\frac{E}{2}\right) * \tilde{\rho}_1(E) = \frac{1}{2}\left[\tilde{\rho}_{\mathcal{A}}(E) + \sqrt{2}\tilde{\rho}_{\mathcal{L}}(E) + 2\tilde{\rho}_{\mathcal{K}}(E)\right], \quad \text{(C.31a)}$$

$$\tilde{\rho}^{\mathrm{h2}}_{(1,1,0)}(E) = \frac{1}{2}\tilde{\rho}_1\left(\frac{E}{2}\right) * \bar{\rho}_1(E) = \frac{1}{2}\left[2\tilde{\rho}_{\mathcal{A}}\left(\frac{E}{2}\right) + \sqrt{2}\tilde{\rho}_{\mathcal{L}}\left(\frac{E}{2}\right) + \tilde{\rho}_{\mathcal{K}}\left(\frac{E}{2}\right)\right]. \quad \text{(C.31b)}$$

C.4 Three-Particle Dynamical Orbits

It is shown in Ref. [35] that the convolution of two trace formulas

$$\begin{aligned}\tilde{\rho}(E) * \tilde{\rho}(E) = {} & \frac{2}{(2\pi\hbar)^{3/2}} \sum_{\Gamma_1,\Gamma_2} \frac{A_{\Gamma_1}(E_1)A_{\Gamma_2}(E_2)}{\sqrt{|\Upsilon(\Gamma_1,\Gamma_2,E)|}} \\ & \times \cos\left[\frac{1}{\hbar}\left[S_{\Gamma_1}(E_1) + S_{\Gamma_2}(E_2)\right] - (\sigma_{\Gamma_1} + \sigma_{\Gamma_2})\frac{\pi}{2} + \nu\frac{\pi}{4}\right],\end{aligned} \quad \text{(C.32)}$$

where

$$\begin{aligned}\Upsilon(\Gamma_1,\Gamma_2,E) &= \left(\frac{\mathrm{d}^2 S_{\Gamma_1}(\xi)}{\mathrm{d}\xi^2} + \frac{\mathrm{d}^2 S_{\Gamma_2}(E-\xi)}{\mathrm{d}\xi^2}\right)\Bigg|_{E_1}, \\ \nu &= \mathrm{sign}\left[\Upsilon(\Gamma_1,\Gamma_2,E)\right],\end{aligned}$$

and the particle energies E_1 and $E_2 = (E - E_1)$ are determined from the condition

$$T_{\Gamma_1}(E_1) = T_{\Gamma_2}(E_2). \quad \text{(C.34)}$$

(Note that the amplitudes $A_\Gamma(\xi)$ contain no further $\hbar$ dependence for isolated orbits.) The solutions of Eq. (C.34) are functions of the total energy E: $E_1 = f_1(E)$ and $E_2 = f_2(E)$. This result was understood to be the leading-order contribution of the dynamical periodic orbits in the two-particle phase space obtained from the convolution of two trace formulas, each involving orbits Γ_1, Γ_2, belonging to a one-particle phase space. However, for the present discussion, assume that Γ_1 is an orbit of a one-particle phase space with period T_{Γ_1}, and Γ_2 is an orbit of a two-particle phase space with period T_{Γ_2}. The dynamical contribution for a three-body system can now be determined as follows. The procedure is to convolve the composite orbits Γ_2 (of the two-particle phase space) with periodic orbits of the one-particle phase space using the general formula above for the convolution of two trace formulas [Eq. (C.32)]. The two-particle trace formula has the form

$$(\tilde{\rho}_1 * \tilde{\rho}_1)(\varepsilon) = \frac{1}{\pi\hbar}\sum_{\Gamma_2} A_{\Gamma_2}(\varepsilon)\cos\left[\frac{1}{\hbar}S_{\Gamma_2}(\varepsilon) - \sigma_{\Gamma_2}\frac{\pi}{2}\right], \quad \text{(C.35)}$$

where

$$\begin{aligned}
\Gamma_2 &= (\gamma_a, \gamma_b) \Rightarrow \sum_{\Gamma_2} \equiv \sum_{\gamma_a, \gamma_b}, \\
A_{\Gamma_2}(\varepsilon) &= \frac{1}{(2\pi\hbar)^{1/2}} \frac{A_{\gamma_a}(\varepsilon_a) A_{\gamma_b}(\varepsilon_b)}{\sqrt{\left|T'_{\gamma_a}(\varepsilon_a) + T'_{\gamma_b}(\varepsilon_b)\right|}}, \\
S_{\Gamma_2}(\varepsilon) &= S_{\gamma_a}(\varepsilon_a) + S_{\gamma_b}(\varepsilon_b), \\
\sigma_{\Gamma_2} &= \sigma_{\gamma_a} + \sigma_{\gamma_b} - \frac{\nu}{2}.
\end{aligned}$$

In the denominator of the amplitude factor $A_{\Gamma_2}(\varepsilon)$, primes denote differentiation with respect to energy ξ. The differentiated functions are then evaluated at the respective particle energies $\varepsilon_a = f_a(\varepsilon)$ and $\varepsilon_b = f_b(\varepsilon)$. The convolution over orbits $\Gamma_2 = (\gamma_a, \gamma_b)$ and $\Gamma_1 = \gamma_c$ using Eq. (C.32) is

$$\begin{aligned}
(\tilde{\rho}_1 * \tilde{\rho}_1)(E) * \tilde{\rho}_1(E) = \frac{2}{(2\pi\hbar)^2} \sum_{\gamma_a, \gamma_b, \gamma_c} \frac{A_{\gamma_a}(E_a) A_{\gamma_b}(E_b) A_{\gamma_c}(E_c)}{\sqrt{\left|T'_{\gamma_a}(E_a) + T'_{\gamma_b}(E_b)\right|} \sqrt{\left|\Xi(\gamma_a, \gamma_b, \gamma_c, E)\right|}} \\
\times \cos\left[\frac{1}{\hbar}\left[S_{\gamma_a}(E_a) + S_{\gamma_b}(E_b) + S_{\gamma_c}(E_c)\right] - \left(\sigma_{\gamma_a} + \sigma_{\gamma_b} + \sigma_{\gamma_c}\right)\frac{\pi}{2} + (\nu + \mu)\frac{\pi}{4}\right],
\end{aligned} \tag{C.36}$$

where

$$\Xi(\gamma_a, \gamma_b, \gamma_c, E) = \left(\frac{\mathrm{d}^2 \mathcal{S}(\varepsilon)}{\mathrm{d}\varepsilon^2} + \frac{\mathrm{d}^2 S_{\gamma_c}(E - \varepsilon)}{\mathrm{d}\varepsilon^2}\right)\Bigg|_{\varepsilon = \varepsilon^*} = \left(\frac{\mathrm{d}\mathcal{T}(\varepsilon)}{\mathrm{d}\varepsilon} - \frac{\mathrm{d}T_{\gamma_c}(E - \varepsilon)}{\mathrm{d}\varepsilon}\right)\Bigg|_{\varepsilon = \varepsilon^*} \tag{C.37}$$

and the phase factors

$$\nu = \mathrm{sign}\left[T'_{\gamma_a}(E_a) + T'_{\gamma_b}(E_b)\right], \tag{C.38a}$$

$$\mu = \mathrm{sign}\left[\Xi(\gamma_a, \gamma_b, \gamma_c, E)\right]. \tag{C.38b}$$

The particle energies E_a, E_b, E_c are determined from the condition

$$T_{\gamma_a}(E_a) = T_{\gamma_b}(E_b) = T_{\gamma_c}(E_c), \tag{C.39}$$

and as before the solutions can be expressed as functions of the total energy: $E_a = F_a(E)$, $E_b = F_b(E)$, and $E_c = F_c(E)$. [The stationary phase point ε^* is determined from the stationary phase condition $T_{\gamma_a}(f_a(\varepsilon^*)) = T_{\gamma_b}(f_b(\varepsilon^*)) = T_{\gamma_c}(E - \varepsilon^*) \equiv T(E)$ so that the energies of the three-particle system are $E_a = f_a(\varepsilon^*)$, $E_b = f_b(\varepsilon^*)$ and $E_c = (E - \varepsilon^*)$, and $E_a + E_b + E_c = E$.] The amplitude $(2\pi\hbar)^{1/2} A_{\Gamma_2}(\varepsilon^*) = A_{\gamma_a}(E_a) A_{\gamma_b}(E_b) / \sqrt{\left|T'_{\gamma_a}(E_a) + T'_{\gamma_b}(E_b)\right|}$, where $T'_{\gamma_a/\gamma_b}(E_{a/b}) = (\mathrm{d}T_{\gamma_a/\gamma_b}(\xi)/\mathrm{d}\xi)|_{\xi = E_{a/b}}$.

The function $(\mathrm{d}\mathcal{T}(\varepsilon)/\mathrm{d}\varepsilon)|_{\varepsilon=\varepsilon^*}$ involves the periods of both orbits γ_a and γ_b, and the differentiation is with respect to the two-particle energy variable ε. This function is determined more explicitly as follows. Recall that $T_{\gamma_a}(\varepsilon_a) = T_{\gamma_b}(\varepsilon_b) \equiv \mathcal{T}(\varepsilon)$, and that $\varepsilon_a = f_a(\varepsilon)$, $\varepsilon_b = f_b(\varepsilon)$, $\varepsilon_a + \varepsilon_b = \varepsilon$. (Let $\mathcal{T}'$ denote $\mathrm{d}\mathcal{T}(\varepsilon)/\mathrm{d}\varepsilon$.) Suppose ε is changed to $\varepsilon + \mathrm{d}\varepsilon$ (and $\varepsilon_{a/b} \to \varepsilon_{a/b} + \mathrm{d}\varepsilon_{a/b}$), then the problem is to determine how $\mathcal{T}$ changes. First, note that the periods must remain equal (at the new energy), that is,

$$T_{\gamma_a}(\varepsilon_a + \mathrm{d}\varepsilon_a) = T_{\gamma_b}(\varepsilon_b + \mathrm{d}\varepsilon_b), \tag{C.40}$$

and since the periods are the same at the old energies

$$T'_{\gamma_a}(\varepsilon_a)\mathrm{d}\varepsilon_a = T'_{\gamma_b}(\varepsilon_b)\mathrm{d}\varepsilon_b \equiv \mathcal{T}'\mathrm{d}\varepsilon. \tag{C.41}$$

Then, using the fact that $\mathrm{d}\varepsilon = \mathrm{d}\varepsilon_a + \mathrm{d}\varepsilon_b$, we solve for $\mathrm{d}\varepsilon_a$:

$$\mathrm{d}\varepsilon_a = \frac{T'_{\gamma_b}(\varepsilon_b)}{\left[T'_{\gamma_a}(\varepsilon_a) + T'_{\gamma_b}(\varepsilon_b)\right]}\mathrm{d}\varepsilon, \tag{C.42}$$

and similarly solve for $\mathrm{d}\varepsilon_b$, which can be shown to be the same as Eq. (C.42) except that $a \leftrightarrow b$. Using Eqs. (C.41) and (C.42) immediately gives

$$\mathcal{T}'(\varepsilon) = \frac{\mathrm{d}\mathcal{T}(\varepsilon)}{\mathrm{d}\varepsilon} = \frac{T'_{\gamma_a}(\varepsilon_a)T'_{\gamma_b}(\varepsilon_b)}{\left[T'_{\gamma_a}(\varepsilon_a) + T'_{\gamma_b}(\varepsilon_b)\right]} = \frac{T'_{\gamma_a}\left(f_a(\varepsilon)\right)T'_{\gamma_b}\left(f_b(\varepsilon)\right)}{\left[T'_{\gamma_a}\left(f_a(\varepsilon)\right) + T'_{\gamma_b}\left(f_b(\varepsilon)\right)\right]}. \tag{C.43}$$

and therefore

$$\mathcal{T}'(\varepsilon^*) = \frac{T'_{\gamma_a}(E_a)T'_{\gamma_b}(E_b)}{\left[T'_{\gamma_a}(E_a) + T'_{\gamma_b}(E_b)\right]}. \tag{C.44}$$

Furthermore,

$$-\left.\frac{\mathrm{d}T_{\gamma_c}(E-\varepsilon)}{\mathrm{d}\varepsilon}\right|_{\varepsilon=\varepsilon^*} = \left.\frac{\mathrm{d}T_{\gamma_c}(\xi)}{\mathrm{d}\xi}\right|_{\xi=(E-\varepsilon^*)=E_c} = T'_{\gamma_c}(E_c). \tag{C.45}$$

The denominator of the amplitude factor in Eq. (C.36) is then

$$\sqrt{\left|T'_{\gamma_a}(E_a)T'_{\gamma_b}(E_b) + T'_{\gamma_a}(E_a)T'_{\gamma_c}(E_c) + T'_{\gamma_b}(E_b)T'_{\gamma_c}(E_c)\right|},$$

which is consistent with Eq. (3.24) for $N = 3$.

Finally, note that the phase factors ν and μ of Eq. (C.36) are defined differently than the phase δ of Eq. (3.25). However, $(\nu + \mu) = \{-2, 0, 2\} \Rightarrow (\nu + \mu)\frac{\pi}{4} = \{-\frac{\pi}{2}, 0, \frac{\pi}{2}\}$, whereas $\delta = \{0, 1, 2\} \Rightarrow (\delta - 1)\frac{\pi}{2} = \{-\frac{\pi}{2}, 0, \frac{\pi}{2}\}$, so that the phases are consistent in the two formulas.

Billiard orbits

For an orbit γ in a billiard system, $T_\gamma(\xi) = \frac{\hbar\sqrt{\alpha}L_\gamma}{2\sqrt{\xi}}$. The condition $T_{\gamma_a}(\varepsilon_a) = T_{\gamma_b}(\varepsilon_b)$ gives

$$\varepsilon_{a/b} = f_{a/b}(\varepsilon) = \left(\frac{L^2_{\gamma_a/\gamma_b}}{L^2_{\gamma_a} + L^2_{\gamma_b}}\right)\varepsilon, \tag{C.46}$$

so that

$$T_{\gamma_a}(\varepsilon_a) = T_{\gamma_b}(\varepsilon_b) = (\hbar/2)\sqrt{\alpha\left(L^2_{\gamma_a} + L^2_{\gamma_b}\right)/\varepsilon} \equiv \mathcal{T}(\varepsilon). \tag{C.47}$$

The condition $T_{\gamma_a}(f_a(\varepsilon^*)) = T_{\gamma_b}(f_b(\varepsilon^*)) = T_{\gamma_c}(E - \varepsilon^*)$ gives the stationary phase energy

$$\varepsilon^* = \left(\frac{L^2_{\gamma_a} + L^2_{\gamma_b}}{L^2_{\gamma_a} + L^2_{\gamma_b} + L^2_{\gamma_c}}\right)E. \tag{C.48}$$

The three-particle energies are then

$$E_{a/b} = f_{a/b}(\varepsilon^*) = \left(\frac{L^2_{\gamma_a/\gamma_b}}{L^2_{\gamma_a} + L^2_{\gamma_b} + L^2_{\gamma_c}}\right)E, \tag{C.49a}$$

$$E_c = (E - \varepsilon^*) = \left(\frac{L^2_{\gamma_c}}{L^2_{\gamma_a} + L^2_{\gamma_b} + L^2_{\gamma_c}}\right)E. \tag{C.49b}$$

Using Eqs. (C.44) and (C.49a) [or Eqs. (C.47) and (C.48)],

$$\mathcal{T}'(\varepsilon^*) = -\frac{\hbar\sqrt{\alpha}\left(L^2_{\gamma_a} + L^2_{\gamma_b} + L^2_{\gamma_c}\right)^{3/2}}{4\left(L^2_{\gamma_a} + L^2_{\gamma_b}\right)E^{3/2}}. \tag{C.50}$$

References

[1] E. J. Heller, S. Tomsovic, and M. Sepulveda, Chaos **2**, 105 (1992); S. Tomsovic and E. J. Heller, Phys. Rev. E **41**, 282 (1993); *ibid.* **68**, 038201 (2003).

[2] M. C. Gutzwiller, J. Math. Phys. **8**, 1979 (1967); *ibid.* **10**, 1004 (1969); *ibid.* **11**, 1791 (1970); *ibid.* **12**, 343 (1971).

[3] R. Balian and C. Bloch, Ann. Phys. (N.Y.) **60**, 401 (1970); *ibid.* **63**, 592 (1971); *ibid.* **69**, 76 (1972); *ibid.* **85**, 514 (1974).

[4] V. M. Strutinsky, Nukleonika **20**, 679 (1975); V. M. Strutinsky and A. G. Magner, Sov. J. Part. Nucl. **7**, 138 (1976).

[5] M. V. Berry and M. Tabor, Proc. R. Soc. London A **349**, 101 (1976); J. Phys. A **10**, 371 (1977).

[6] Chaos **2**, (1992), focus issue on *Periodic Orbit Theory in Classical and Quantum Mechanics*, edited by P. Cvitanović.

[7] M. Brack and R. K. Bhaduri, *Semiclassical Physics* (Addison-Wesley, Reading, MA, 1997).

[8] M. C. Gutzwiller, Am. J. Phys. **66**, 304 (1998).

[9] M. C. Gutzwiller, *Chaos in Classical and Quantum Mechanics* (Springer-Verlag, New York, 1990); H.-J. Stöckmann, *Quantum Chaos: An Introduction* (Cambridge University Press, Cambridge, 1999).

[10] P. Cvitanović *et al.*, *Classical and Quantum Chaos: A Cyclist Treatise* (Niels Bohr Institute, Copenhagen, 2000). (`www.nbi.dk/ChaosBook/`)

[11] V. M. Strutinsky *et al.*, Z. Phys. A **283**, 269 (1977).

[12] H. Frisk, Nucl. Phys. A **511**, 309 (1990); A. G. Magner *et al.*, Ann. Phys. (Leipzig) **6**, 555 (1997); M. Brack, S. M. Reimann, and M. Sieber, Phys. Rev. Lett. **79**, 1817 (1997).

[13] H. Friedrich and D. Wintgen, Phys. Rep. **183**, 37 (1989).

[14] G. Tanner and D. Wintgen, Chaos **2**, 53 (1992).

[15] H. Nishioka, K. Hansen, and B. R. Mottelson, Phys. Rev. B **42**, 9377 (1990); H. Nishioka, Z. Phys. D **19**, 19 (1991).

[16] E. Koch, Phys. Rev. Lett. **76**, 2678 (1996); Phys. Rev. B **58**, 2329 (1998).

[17] D. C. Rouben and G. S. Ezra, J. Chem. Phys. **103**, 1375 (1995); G. S. Ezra, *ibid.* **104**, 26 (1996).

[18] R. Prosmiti and S. C. Farantos, J. Chem. Phys. **103**, 3299 (1995); R. Prosmiti *et al.*, *ibid.* **104**, 2921 (1996).

[19] P. A. Houle, N.-G. Zhang, and C. L. Henley, Phys. Rev. B **60**, 15 179 (1999).

[20] M. Schaden and L. Spruch, Phys. Rev. A **58**, 935 (1998).

[21] *Tunneling in Complex Systems*, edited by S. Tomsovic (World Scientific, Singapore, 1998).

[22] K. Richter, *Semiclassical Theory of Mesoscopic Quantum Systems* (Springer-Verlag, New York, 2000); U. Smilansky, in *Mesoscopic Quantum Physics*, edited by E. Akkermans, G. Montambaux, and J. L. Pichard (Elsevier, Amsterdam, 1995).

[23] *Supersymmetry and Trace Formulae: Chaos and Disorder*, edited by I. V. Lerner, J. P. Keating, and D. E. Khmelnitskii (Plenum Press, New York, 1999).

[24] D. M. Brink, A. Dellafiore, and M. Di Toro, Nucl. Phys. A **456**, 205 (1986); A. Dellafiore, F. Matera, and D. M. Brink, Phys. Rev. A **51**, 914 (1995).

[25] P. Gaspard and S. R. Jain, Pramana-J. Phys. **48**, 503 (1997).

[26] G. S. Ezra *et al.*, J. Phys. B **24**, L413 (1991); D. Wintgen, K. Richter, and G. Tanner, Chaos **2**, 19 (1992); G. Tanner, K. Richter, and J.-M. Rost, Rev. Mod. Phys. **72**, 497 (2000).

[27] *Classical, Semiclassical and Quantum Dynamics in Atoms*, edited by H. Friedrich and B. Eckardt (Springer, Berlin, 1997).

[28] T. Papenbrock and T. H. Seligman, Phys. Lett. A **218**, 229 (1996).

[29] M. C. Gutzwiller, Phys. Rev. Lett. **45**, 150 (1980); Physica D **5**, 183 (1982).

[30] J. M. Robbins, Phys. Rev. A **40**, 2128 (1989).

[31] B. Lauritzen, Phys. Rev. A **43**, 603 (1991).

[32] T. H. Seligman and H. A. Weidenmüller, J. Phys. A **27**, 7915 (1994).

[33] S. C. Creagh and R. G. Littlejohn, Phys. Rev. A **44**, 836 (1991).

[34] S. C. Creagh and R. G. Littlejohn, J. Phys. A **25**, 1643 (1992).

[35] J. Sakhr and N. D. Whelan, Phys. Rev. A **62**, 042109 (2000).

[36] A. M. Ozorio de Almeida, in *Quantum Chaos and Statistical Nuclear Physics*, edited by T. H. Seligman and H. Nishioka, Lecture Notes in Physics Vol. 263 (Springer, Berlin, 1986); A. M. Ozorio de Almeida, *Hamiltonian Systems: Chaos and Quantization* (Cambridge University Press, Cambridge, 1988).

[37] S. Tomsovic, M. Grinberg, and D. Ullmo, Phys. Rev. Lett. **75**, 4346 (1995); Phys. Rev. E **54**, 136 (1996).

[38] S. C. Creagh, Ann. Phys. (N.Y.) **248**, 1 (1996).

[39] M. Brack, S. C. Creagh, and J. Law, Phys. Rev. A **57**, 788 (1998).

[40] M. Brack, P. Meier, and K. Tanaka, J. Phys. A **32**, 331 (1999).

[41] P. Cvitanović, Chaos **2**, 1 (1992).

[42] H. A. Weidenmüller, Phys. Rev. A **48**, 1819 (1993).

[43] M. V. Berry and C. J. Howls, Proc. R. Soc. London A **447**, 527 (1994).

[44] C. J. Howls and S. A. Trasler, J. Phys. A **31**, 1911 (1998); *ibid.* **32**, 1487 (1999).

[45] R. K. Bhaduri *et al.*, Phys. Rev. A **59**, R911 (1999).

[46] S. Tomsovic, J. Phys. A **24**, L733 (1991).

[47] N. D. Whelan, J. Phys. A **30**, 533 (1997).

[48] K. Stewartson and R. T. Waechter, Proc. Camb. Phil. Soc. **69**, 353 (1971).

[49] S. C. Creagh, J. M. Robbins, and R. G. Littlejohn, Phys. Rev. A **42**, 1907 (1990); J. M. Robbins, Nonlinearity **4**, 343 (1991).

[50] P. Gaspard and D. Alonso, Phys. Rev. A **47**, R3468 (1993); P. Gaspard, D. Alonso, and I. Burghardt, Adv. Chem. Phys. **90**, 105 (1995).

[51] B. Grémaud, Phys. Rev. E **65**, 056207 (2002).

[52] G. Vattay, Phys. Rev. Lett. **76**, 1059 (1996); H. Schomerus and M. Sieber, J. Phys. A **30**, 4537 (1997).

[53] A. M. Ozorio de Almeida and J. H. Hannay, J. Phys. A **20**, 5873 (1987); M. Kus, F. Haake, and D. Delande, Phys. Rev. Lett. **71**, 2167 (1993); M. W. Biems and G. Alber, Phys. Rev. A **48**, 3123 (1993); K. M. Atkins and G. S. Ezra, *ibid.* **50**, 93 (1994).

[54] M. Sieber and F. Steiner, Physica D **44**, 248 (1990); Phys. Lett. A **144**, 159 (1990); *ibid.* **148**, 415 (1990); M. Sieber, Chaos **2**, 35 (1992).

[55] B. Eckhardt, G. Hose, and E. Pollack, Phys. Rev. A **39**, 3776 (1989); O. Bohigas, S. Tomsovic, and D. Ullmo, Phys. Rep. **223**, 43 (1993); G. G. de Polavieja, F. Borondo, and R. M. Benito, Phys. Rev. Lett. **73**, 1613 (1994); K. M. Atkins and G. S. Ezra, Phys. Rev. E **51**, 1822 (1995).

[56] A. Holle *et al.*, Phys. Rev. Lett. **56**, 2594 (1986); *ibid.* **57**, 2789 (1986); *ibid.* **61**, 161 (1988).

[57] J. Main *et al.*, Phys. Rev. A **49**, 847 (1994); D. Delande *et al.*, J. Phys. B **27**, 2771 (1994); M. Courtney *et al.*, Phys. Rev. A **51**, 3604 (1995).

[58] D. Provost and M. Baranger, Phys. Rev. Lett. **71**, 662 (1993); D. Provost, Phys. Rev. E **51**, R841 (1995); *ibid.* **51**, 5396 (1995).

[59] B. Lauritzen and N. D. Whelan, Ann. Phys. (N.Y.) **244**, 112 (1995); M. Brack *et al.*, Phys. Rev. Lett. **70**, 568 (1993); Chaos **5**, 317 (1995); *ibid.* **5**, 707 (1995).

[60] M. Baranger *et al.*, Chaos **5**, 261 (1995).

[61] S. C. Creagh, J. Phys. A **26**, 95 (1993).

[62] M. V. Berry and J. P. Keating, J. Phys. A **23**, 4839 (1990).

[63] R. Aurich *et al.*, Phys. Rev. Lett. **61**, 483 (1988); *ibid.* **68**, 1629 (1992).

[64] O. Bohigas, in *Chaos and Quantum Physics*, edited by M.-J. Giannoni, A. Voros, and J. Zinn-Justin (North-Holland, Amsterdam, 1991).

[65] B. Riemann, Monatsber. Akad. Berlin, 671 (1859); the English translation can be found in the appendix of Ref. [66].

[66] H. M. Edwards, *Riemann's Zeta Function* (Academic Press, New York, 1974); Dover Reprint, 2001.

[67] M. V. Berry, in *Quantum Chaos and Statistical Nuclear Physics*, edited by T. H. Seligman and H. Nishioka, Lecture Notes in Physics 263 (Springer-Verlag, Berlin, 1986).

[68] C. Höppler and W. Zwerger, Phys. Rev. B **59**, R7849 (1999).

[69] E. Koch, Phys. Rev. B **58**, 2329 (1998).

[70] S. Frauendorf *et al.*, Phys. Rev. B **58**, 5622 (1998).

[71] E. B. Bogomolny, Nonlinearity **5**, 805 (1992).

[72] T. Szeredi, J. Lefebvre, and D. A. Goodings, Nonlinearity **7**, 1463 (1994); P. A. Boasman, *ibid.* **7**, 485 (1994).

[73] K. Weibert, J. Main, and G. Wunner, Eur. Phys. J. D **12**, 381 (2000).

[74] S. M. Reimann *et al.*, Phys. Rev. A **53**, 39 (1996).

[75] L. S. Schulman, J. Phys. A **27**, 1703 (1994).

[76] P. Cvitanović, Phys. Rev. Lett. **61**, 2729 (1988); P. Cvitanović and B. Eckhardt, *ibid.* **63**, 823 (1989); B. Eckhardt and G. Russberg, Phys. Rev. E **47**, 1578 (1993).

[77] P. Dahlqvist and G. Russberg, J. Phys. A **24**, 4763 (1991); P. Dahlqvist, *ibid.* **27**, 763 (1994).

[78] C. P. Dettmann and G. P. Morriss, Phys. Rev. Lett. **78**, 4201 (1997); C. P. Dettmann and P. Cvitanović, Phys. Rev. E **56**, 6687 (1997); C. P. Dettmann and P. Dahlqvist, *ibid.* **57**, 5303 (1998).

[79] J. Blaschke and M. Brack, Phys. Rev. A **56**, 182 (1997).

[80] R. Balian and C. Bloch, Ann. Phys. (N.Y.) **69**, 76 (1972).

[81] J. P. Keating and N. C. Snaith, Commun. Math. Phys. **214**, 57 (2000).

[82] R. K. Bhaduri *et al.*, Ann. Phys. (N.Y.) **254**, 25 (1997).

[83] G. Tenenbaum and M. M. France, *The Prime Numbers and Their Distributions* (American Mathematical Society, 1999).

[84] C. E. Porter, *Statistical Theories of Spectra : Fluctuations* (Academic Press, New York, 1965).

[85] M. V. Berry and J. P. Keating, SIAM Rev. **41**, 236 (1999).

[86] H. Riesel and G. Göhl, Math. Comput. **24**, 969 (1971).

[87] H. J. Nussbaumer, *Fast Fourier Transform and Convolution Algorithms* (Springer-Verlag, New York, 1982).

[88] R. Aurich, T. Hesse, and F. Steiner, Phys. Rev. Lett. **74**, 4408 (1995); W. Zheng, Phys. Rev. E **60**, 2845 (1999); D. Biswas, *ibid.* **61**, 5129 (2000); D. Biswas, *ibid.* **63**, 016213 (2001).

[89] O. Bohigas, M. J. Giannoni, and C. Schmit, Phys. Rev. Lett. **52**, 1 (1984).

[90] A. M. Odlyzko, Math. Comput. **48**, 273 (1987).

[91] M. L. Mehta, *Random Matrices* (Academic Press, New York, 1991).

[92] J. P. Keating, in *Quantum Chaos: Proceedings of the Enrico Fermi International School of Physics*, edited by G. Casati, I. Guarnieri, and U. Smilansky (Elsevier, Amsterdam, 1993).

[93] J. Sakhr, M.Sc. Thesis, McMaster University, 1999.

[94] H. Bruus and N. D. Whelan, Nonlinearity **9**, 1023 (1996).

[95] A. Bäcker, F. Steiner, and P. Stifter, Phys. Rev. E **52**, 2463 (1995); A. Bäcker and H. R. Dullin, J. Phys. A **30**, 1991 (1997).

[96] F. J. Harris, Proc. IEEE **66**, 51 (1978).

[97] M. Hamermesh, *Group Theory and its Application to Physical Problems* (Dover, New York, 1962).

[98] B. Lauritzen and N. D. Whelan, Ann. Phys. (N.Y.) **244**, 112 (1995).

[99] B. K. Jennings, R. K. Bhaduri, and M. Brack, Phys. Rev. Lett. **34**, 228 (1975).

[100] M. L. Du and J. B. Delos, Phys. Rev. A **38**, 1913 (1988); O. Bohigas *et al.*, Nonlinearity **8**, 203 (1995).

[101] E. Anisimovas and A. Matulis, J. Phys. : Condens. Matter **10**, 601 (1998); G. Lamouche and G. Fishman *ibid.* **10**, 7857 (1998).

[102] C. Neumann *et al.*, Phys. Rev. Lett. **78**, 4705 (1997); N. Spellmeyer *et al.*, *ibid.* **79**, 1650 (1997); M. R. Haggerty *et al.*, *ibid.* **81**, 1592 (1998).

[103] J. Main *et al.*, Phys. Rev. Lett. **79**, 825 (1997); *ibid.* **82**, 3038 (1999); Nonlinearity **11**, 1015 (1998); Phys. Rep. **316**, 233 (1999); Phys. Rev. E **58**, 4436 (1998); *ibid.* **60**, 1630 (1999); T. Bartsch, J. Main, and G. Wunner, *ibid.* **64**, 056705 (2001).

[104] F. C. Zhang and S. Das Sarma, Phys. Rev. B **33**, 2903 (1986).

[105] G. Vattay, A. Wirzba, and P. E. Rosenqvist, Phys. Rev. Lett. **73**, 2304 (1994); N. D. Whelan, *ibid.* **76**, 2605 (1996); N. Pavloff and C. Schmit, *ibid.* **75**, 61 (1995); N. D. Whelan, Phys. Rev. E **51**, 3778 (1995).

[106] H. M. Sommermann and H. A. Weidenmüller, Europhys. Lett. **23**, 79 (1993).

[107] M. Brack and S. R. Jain, Phys. Rev. A **51**, 3462 (1995).

[108] M. Abramowitz and I. A. Stegun, *Handbook of Mathematical Functions* (Dover, New York, 1965).